Local Seismic Response of the Santa Sofia Bell Tower (UNESCO Site) from Advanced Geophysical Investigations

A. Ambrosino[1], S. Sica[1], M.R. Gallipoli[3] and NEW AGE working group

[1]University of Sannio, Benevento (Italy)
[2] National Research Council of Italy, CNR-IMAA (Italy)

The evaluation of local seismic site effects represents a key aspect in the seismic assessment of cultural heritage structures, particularly for UNESCO World Heritage sites where invasive investigations are not permitted. This study addresses the seismic site response at the Santa Sofia bell tower (Benevento, southern Italy), focusing on the role of advanced geophysical investigations in defining subsoil models for local seismic response analyses.

Previous investigations at the site were based on non-invasive and shallow geophysical surveys, providing a simplified characterization of near-surface layers and dominant resonance frequencies. Within the framework of the PRIN 2022 *NEW AGE* "(NEW integrated approach for seismic protection and valorisation of heritAGE buildings on historical soil deposits") project, a new geophysical campaign was conducted using methods with increased depth penetration and resolution. The results confirm the presence of buried historical substructures and identify a significant seismic velocity inversion at depth, related to a soft layer overlying a deeper seismic bedrock. The updated soil model allows the detection of additional amplification peaks in the low-to-intermediate frequency range (approximately 1–10 Hz), which were not identified in the previous investigations. One-dimensional local seismic response analyses were carried out by comparing the seismic response obtained from the shallow model with that derived from the updated stratigraphic configuration. The results show that the inclusion of the soft layer and the deeper bedrock leads to a marked modification of the seismic input motion, resulting in an overall reduction of seismic motion at the foundation level of the bell tower.

The study highlights that site characterization limited to shallow investigations may produce incomplete or misleading estimates of local seismic site effects. The integration of advanced geophysical methods is therefore essential for a reliable evaluation of seismic response in complex and constrained cultural heritage sites.

Corresponding author: anambrosino@unisannio.it

A web platform for crowdsourced building data collection and expert-based validation

Maria Teresa Artese[1], Elisa Varini[1], Chiara Scaini[2], and the SMILE team[3]

[1] Consiglio Nazionale delle Ricerche, Istituto di Matematica Applicata e Tecnologie Informatiche, CNR- IMATI Milano, Italy
[2] OGS, National Institute of Oceanography and Applied Geophysics, Italy
[3] OGS, University Milano-Bicocca, and University of Florence

The SMILE (Statistical MachIne Learning for Exposure development) research project explores the use of machine learning to generate updated building exposure layers by integrating remote sensing imagery, census data, and validated crowdsourced information. Crowdsourced data are collected through targeted initiatives involving trained students and citizens and subsequently verified by experts to ensure reliability.

To support these activities, we developed a web-based multimedia platform capable of guiding users through data collection, managing the data workflow, and storing georeferenced information and images in a structured database. The data collection webform encompasses multiple building characteristics that are deemed relevant for multi-hazard exposure assessment. The database currently holds 4,100 surveys; Fig. 1 shows the distribution of a subsample of surveyed buildings with respect of census areas building density, in the town of Monfalcone (UD), located in a coastal area prone to multiple hazards including floods and earthquakes.

The platform features statistical and GIS-based visualization tools that enable different user groups - policymakers, planners, and citizens - to explore the collected exposure information and assess the quality of collected data. The collected data, once validated, are going to be compared with official datasets (e.g., the ISTAT building census). The collected building data and images have also been used to train machine learning models for the automatic detection of building attributes, such as roof type and number of floors. These models are integrated into the platform to facilitate and streamline future data collection.

Another key objective of the project is to evaluate the reliability of the collected data and determine their potential to update and enrich available building exposure datasets. To this end, the platform offers specific functionalities for the validation of collected data. Experts from the SMILE team reviewed approximately 400 surveys on buildings in Udine, completed by high school students using the SMILE web platform. The expert-validated building sample allowed comparison with student-collected data, enabling identification of potential issues in the web-survey and statistical assessment of the reliability and quality of the collected data.

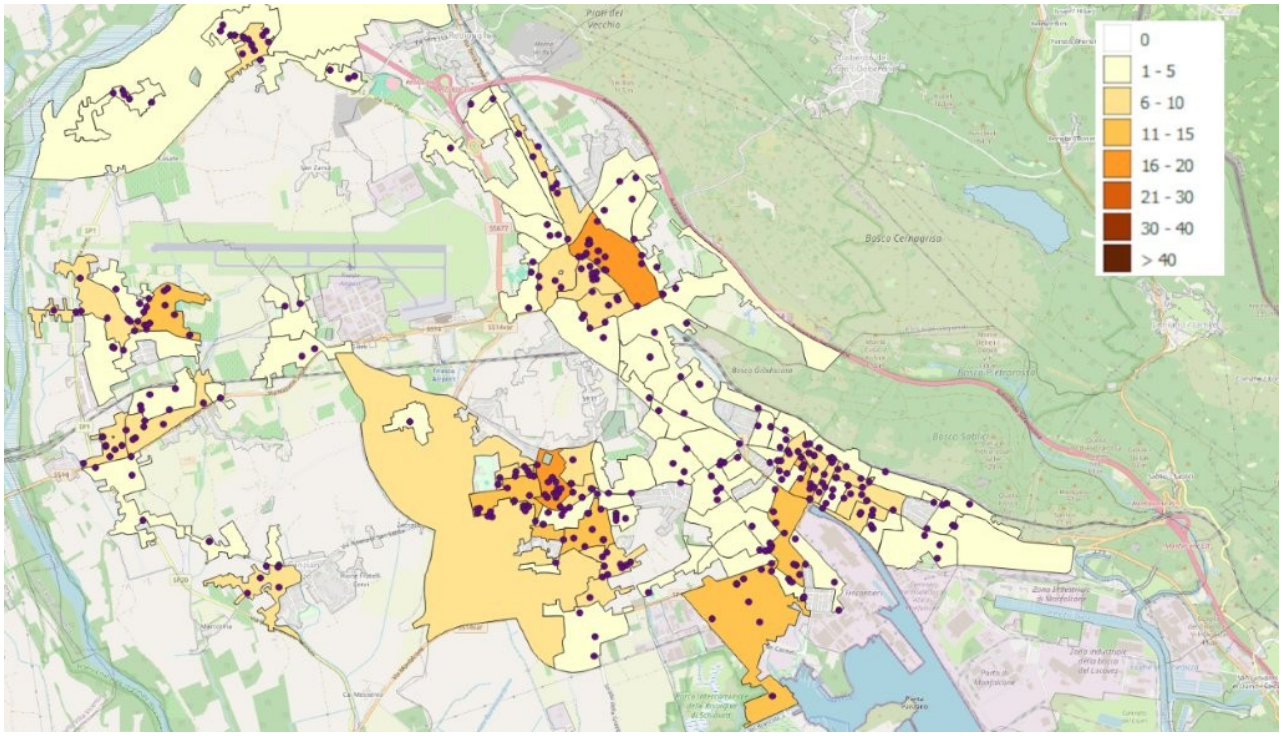

Fig. 1 – Building density by ISTAT census areas in Monfalcone and collected surveys by high school students

Among the broader impacts of this pilot project is also the potential to engage local communities while enhancing existing exposure layers to support risk mitigation and preparedness strategies.

Acknowledgments

This research contributes to the PRIN 2022 PNRR project SMILE "Statistical Machine Learning for Exposure development" (code P202247PK9, CUP B53D23029430001) within the European Union-NextGenerationEU program. We are grateful to the students and teachers at several high schools in the Friuli Venezia Giulia region and to the Università della Terza Età of Trieste for their valuable contribution to data collection. Finally, we warmly acknowledge our colleagues from the SMILE team: Gianluigi Ciocca, Flavio Piccoli, Claudio Rota, and Rajesh Kumar (Univ. Milano-Bicocca); Matteo, Del Soldato, Silvia Bianchini, and Olga Nardini (Univ. Florence); Antonella Peresan, Piero Brondi, Hazem Badreldin, and Hany Mohammed Hassan Elsayed (OGS).

References

SMILE Team; 2025: SMILE building data collection and visualization platform [Web platform]. https://smile.mi.imati.cnr.it

Corresponding author: teresa@mi.imati.cnr.it

NaTech Risk Assessment through 1D and 2D site response analysis in industrial plants

G. Berardo[1], L.M. Giannini[2], A. Marino[3], G. Scarascia Mugnozza[2].

[1] *RINA Consulting S.p.A., Rome, Italy*
[2] *Earth Sciences Department, Sapienza University of Rome, Italy*
[3] *INAIL Department of Technological Innovations and Safety of Plants, Rome, Italy*

Introduction

NaTech events are defined as technological accidents - such as fires, explosions, or the release of toxic substances - that are triggered by natural hazards impacting industrial installations or interconnected lifeline systems (Clerc & Le Claire, 1994; Lindell & Perry, 1996). Historical case studies further emphasise the global relevance of NaTech accidents. The 1999 Kocaeli earthquake in Turkey triggered chemical releases and damage to refineries and pipelines (Tang, 2000). Hurricanes Katrina and Rita in 2005 caused widespread oil spills and hazardous material releases across the Gulf of Mexico. Similarly, the 2008 Wenchuan earthquake in China led to ammonia and sulfuric acid leaks, severe environmental pollution, and the evacuation of over 6,000 residents (Krausmann et al., 2010). One of the most significant examples is the 2011 Great East Japan earthquake and tsunami, which severely impacted the Fukushima powerplant and numerous industrial facilities. In Chiba prefecture, explosions at the Cosmo oil refinery damaged 17 liquefied petroleum gas tanks and forced the evacuation of over 1000 residents (Krausmann & Cruz, 2013).
Among natural hazards, seismic events are recognized as one of the most significant triggers of NaTech disasters worldwide. Earthquakes can damage both structural and non-structural components of industrial facilities, causing roof collapse, loss of containment, fires, and explosions, generating domino effects, where the interconnected systems can enable rapid escalation and the severity of the overall accident.
Risk assessment related to the natural hazard was introduced for the Major-Hazard Industrial Plants (MHIPs) by the Italian Legislative Decree 105/2015, which transposes Directive 2012/18/EU (Seveso III), aimed at the prevention and control of major industrial accidents in industrial plants. This issue is particularly relevant, especially in the Italian context, where a relevant number of Upper-Tier MHIPs are situated in regions exposed to high seismic hazard (Fig. 1).

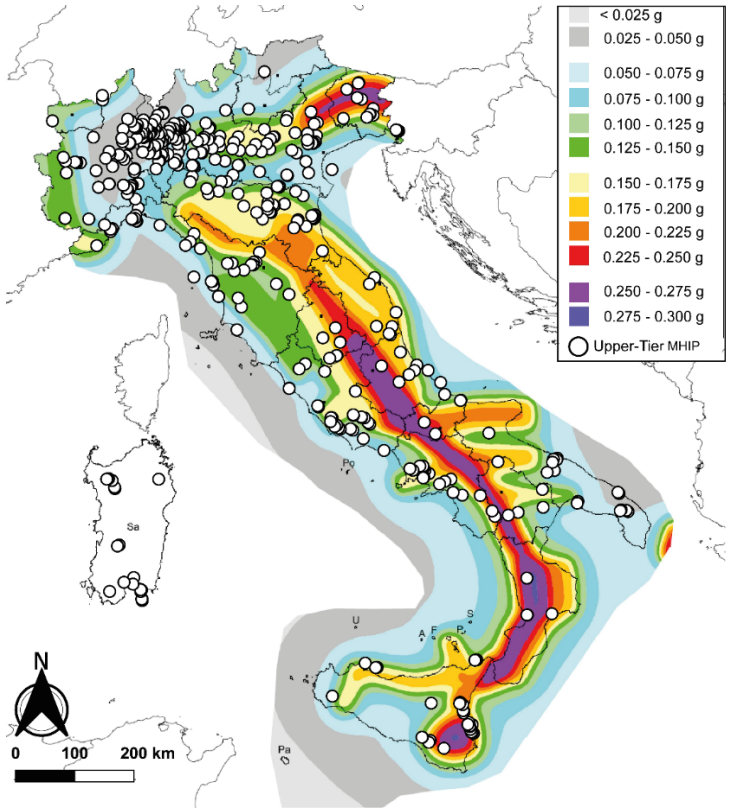

Fig. 1- Distribution of Upper-Tier MHIPs compared with the national seismic hazard map, expressed in terms of peak ground acceleration (PGA) with a 10% probability of exceedance in 50 years, referred to stiff soils, highlighting areas of potential NaTech risk.

Seismic hazard analysis plays a key role in identifying potential NaTech accidents. Among these, seismic hazard encompasses both non-permanent deformation (ground shaking) and permanent deformation (e.g., surface faulting, landslides, liquefaction). This work was focused on ground shaking, which can cause structural and non-structural damage to the MHIPs, potentially triggering cascading effects. The stresses exerted on the facilities and their components during a seismic event may lead to varying degrees of damage, up to collapse. The present study focuses on a representative MHIP located in the Central Apennines, typically characterized by complex geomorphological and geological settings that significantly affect the local seismic response (Lanzo et al., 2011). In particular, the area of interest (AOI) is located within a deep and narrow alluvial valley in one of the most seismically active sectors of the central Mediterranean area (Vannoli et al., 2012). A hypothetical storage tank farm was conceptualized within the AOI, identified as a “test site”. The farm consists of 16 steel storage tanks with varying geometries, each containing hazardous substances at a 50% fill level. The selected substances were chosen as they are widely used across Italy and have the potential to generate toxic clouds or explosions.

The proposed methodology encompasses the assessment of natural and technological hazards, integrating the different fields of expertise required to address such a composite challenge.

The reconstruction of the 3D engineering-geological model of the AOI and its validation through geophysical surveys served as the basis for all follow-up seismic investigations to understand the interplay between seismic and technological hazards for a NaTech overview, converging to generate a potential NaTech event.

Site response analysis: definition of seismic inputs

The most widely adopted approach for the seismic hazard assessment in both engineering and regulatory frameworks is the Probabilistic Seismic Hazard Analysis (PSHA), described by Cornell in 1968. It quantifies, for a given site, the probability distribution of a ground-motion parameter (e.g., PGA, PGV, spectral acceleration Sa) exceeding a certain threshold within a specific time. This approach was applied in the AOI following a systematic characterization of seismogenic sources, active faults, and their seismic history. Seismic hazard assessment allows to define credible accident scenarios within the NaTech risk framework, providing structural design criteria, and supporting emergency preparedness and response planning. Current regulations (e.g., NTC 2018) often rely on simplified approaches that may fail to provide realistic and reliable estimates of a site's seismic response.

In this work, the seismic input analysis is performed using seven natural accelerograms from REXELweb (Iervolino et al., 2010), selected for a reference subsoil condition (rigid subsoil and flat morphology) matching the scenario earthquake parameters identified through the disaggregation map. This selection is based on representative Mw-distance representative criteria targeted for two ultimate limit states: Life Safety (SLS), with a 10% probability of exceedance over a 50-year reference period (return period 975 years), and Collapse (SLC), with a 5% probability of exceedance over the same reference period (return period 1950 years). These seismic records are used as input to simulate the site response of the morpho-stratigraphical configuration of the AOI. To address this, one-dimensional (1D) and two-dimensional (2D) numerical simulations were performed using the equivalent-linear approach (EQL), along three selected points of the 3D engineering-geological model of the AOI, strategically positioned at the two extremities and at the midpoint of the test site (Fig. 2).

The site response within alluvial deep and narrow basin is strongly influenced by 2D phenomena such as basin-edge effects, wave focusing, and lateral trapping of seismic energy. The comparison of 1D and 2D analyses makes it possible to quantify the additional contribution of valley geometry and lateral heterogeneities to site amplification, moving from the simplified framework of 1D simulations to a more realistic representation of seismic wave propagation in complex geological settings. The 2D effects are consistent with physical processes such as edge-generated surface waves, interference, and focusing, which can only be reproduced within a two-dimensional framework, providing the amplification profiles along the investigated geological cross-section for both SLS and SLC conditions. Specifically, the outputs from the three selected points are adopted as representative inputs for the NaTech risk assessment.

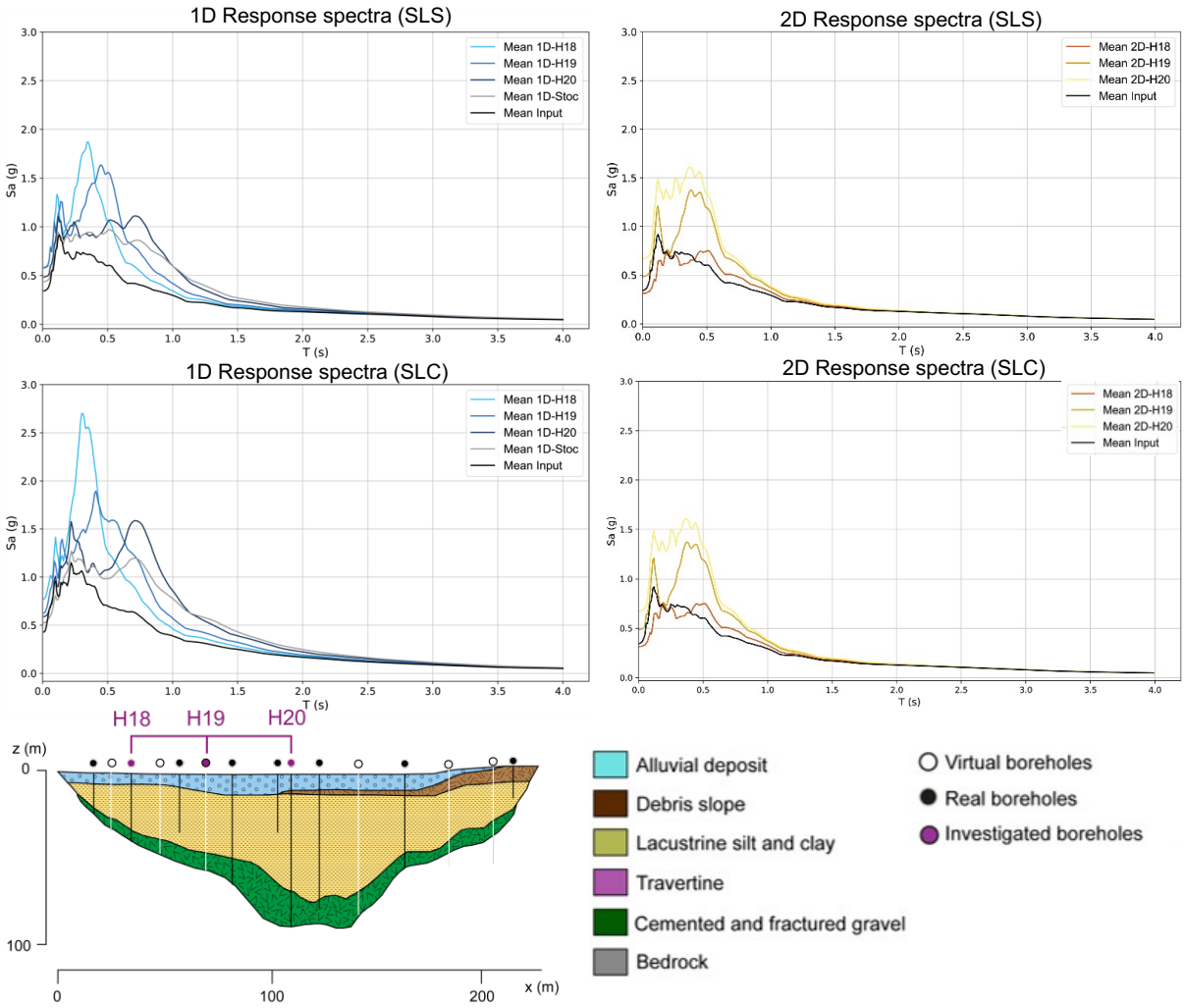

Fig. 2 – Comparison between 1D -1D stochastic - 2D response spectra in the SLS (top) and SLC (bottom) conditions, along the three investigated points of the geological section.

How can a NaTech event be triggered by an earthquake?

Understanding the interaction between seismic events and the storage tanks represents the first step of this study in bridging seismic and technological hazards.
Local seismic response analysis revealed significant PGA variability across the test site, driven by seismo-morpho-tectonic conditions, with values increasing from basin margins toward its center. 2D simulations quantified this variability, providing detailed PGA distributions and amplification factors for both SLS and SLC conditions. Consequently, the PGA values were then linked to storage tanks along the cross-section to estimate damage probabilities based on their configurations and fragility curves. In this way, the integration of the site response analyses with fragility curves enabled a direct link between the seismic hazard of the site and the seismic vulnerability of the storage tanks. Fragility curves are fundamental tools in seismic risk assessments, providing insights into the vulnerability of storage tanks to earthquake-induced damages (Phan et al., 2018). For the purpose of this study, these curves, which plot the probability of a storage tank (anchored and unanchored) exceeding different damage states (DS) at varying PGA levels, are critical for developing effective modification strategies. The damage state spans from DS2, characterized by minor damage without loss of containment, to DS5, involving complete damage with collapse and loss of containment, as determined by the site-specific interaction between seismic hazard and storage tank vulnerability.

It is possible to develop vulnerability maps for different seismic hazards and to delineate the areas of an MHIP most prone to damage for each DS, thus providing a framework for industrial design and maintenance (Fig. 3).

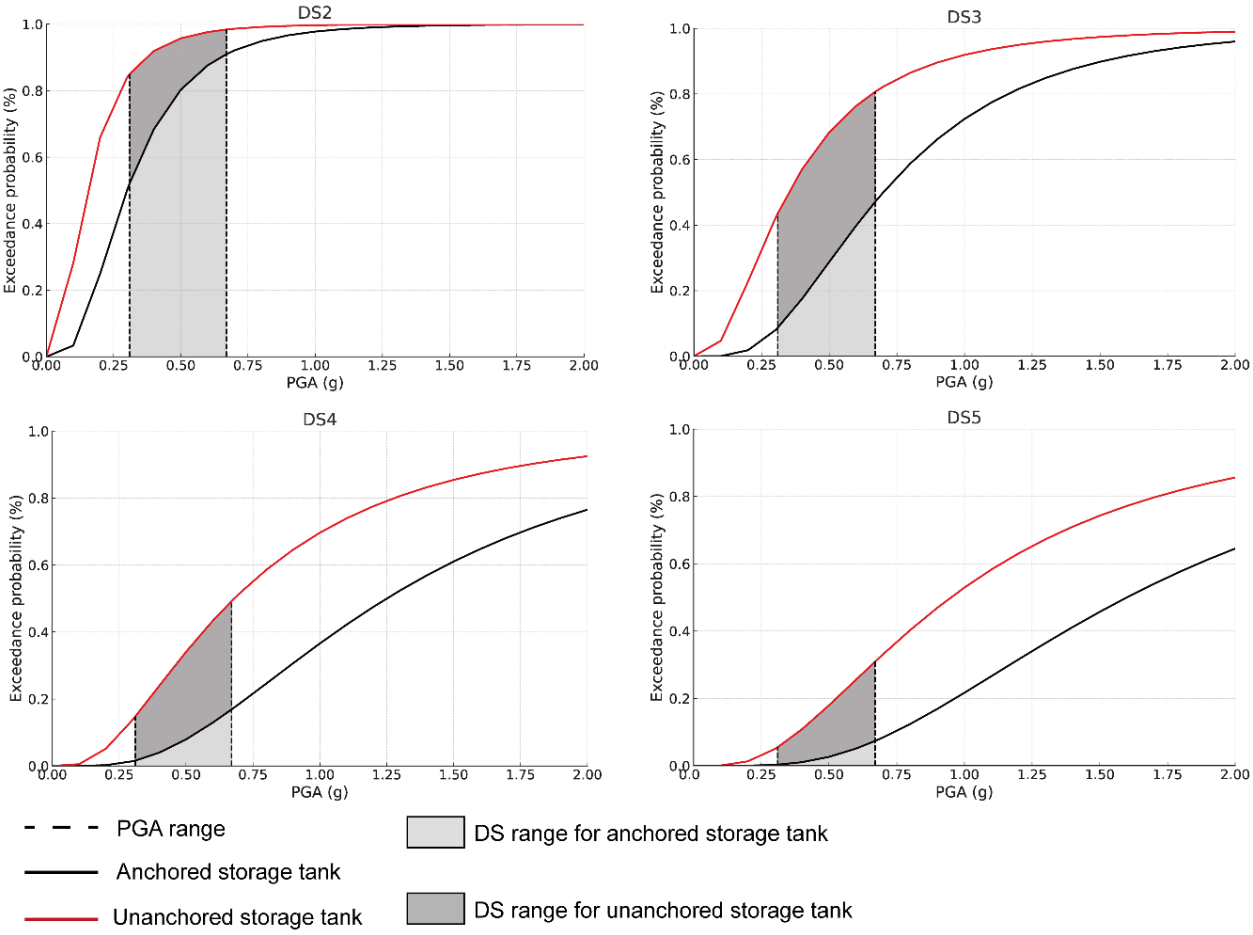

Fig. 3 – Exceedance probability ranges for each DS (from DS2 to DS5) considering both anchored and unanchored steel storage tanks (FEMA, 2010).

The spatial distribution of the amplification factor can serve as a guide for the optimal placement of storage tanks, taking into account their structural characteristics. In addition, the vibration period of each storage tank was plotted on the 2D output response spectra to calculate the amplification factor within its specific period range. This analysis provides a quantitative measure of the site effects and emphasizes how seismic energy transmission varies across different periods of the response spectrum. It was essential to identify the most critical frequency ranges for different storage tank configurations, highlighting the spatial and period variability of seismic amplification across the site, able to generate a NaTech event. In addition, past earthquake events have shown that liquid-filled steel storage tanks are more susceptible to sloshing phenomena and fluid-structure interaction effects, which significantly affect damage and its correlation with ground motion frequency content (Girgin, 2011; Brignone et al., 2025).

From structural damage to the uncontrolled release of toxic substances, these potential failures may ultimately lead to the dispersion of hazardous toxic clouds across the surrounding environment. In this context, a simulation of the toxic clouds generated from the chemical substances of the storage tank of the AOI is developed with their associated threat.

Conclusions

This study offers a scientific contribution towards the development of a multidisciplinary and integrated methodological approach for NaTech risk assessment in seismic areas. The reconstruction of the 3D engineering–geological model and the local seismic response analysis, performed through 1D deterministic, 1D stochastic, and 2D simulations, established a solid basis for the identification of the most amplifying zones within the AOI. These results provide valuable support for the design and planning of seismic risk mitigation strategies. The novelty contribution of this research is the central role assigned to local seismic response studies, which serve as the basis for risk and seismic resilience analyses, enabling the estimation of the domino effects and the recovery time in post-seismic scenarios. This integration enhances the reliability of NaTech risk assessments and establishes a robust and transferable methodological framework, well-suited for application to other MHIP sites situated in geologically complex environments.

References

Brignone, M., Santamato, F., Ravina, M., Busini, V., & Panepinto, D. (2025). NaTech database and methodologies for its risk assessment: A review. Natural Hazards, 121, 19565–19590. https://doi.org/10.1007/s11069-025-07562-z

Clerc A. & Le Claire G. (1994). The environmental impacts of natural and technological (NaTech) disasters. Background paper for the World Conference on Natural Disaster Reduction, Yokohama, Japan.

Cornell C. A. (1968). Engineering seismic risk analysis. Bulletin of the seismological society of America, 58(5), 1583-1606.

FEMA (2010). HAZUS-MH MR5 Technical Manual - Earthquake Model.

Girgin S (2011) The Natech events during the 17 August 1999 Kocaeli earthquake: aftermath and lessons learned. Nat Hazards Earth Syst Sci 11:1129–1140. https://doi.org/10.5194/nhess-11-1129-2011.

Iervolino I., Galasso C., & Cosenza E. (2010). REXEL: Computer-aided record selection for code-based seismic structural analysis. Bulletin of Earthquake Engineering, 8(2), 339–362.

Krausmann E., Cruz A. M. & Affeltranger B. (2010). The impact of the 12 May 2008 Wenchuan earthquake on industrial facilities. Journal of Loss Prevention in the Process Industries, 23(2), 242–248. https://doi.org/10.1016/j.jlp.2009.10.004

Krausmann E. & Cruz A. M. (2013). Impact of the 11 March 2011 Great East Japan earthquake and tsunami on the chemical industry. Natural Hazards, 67(2), 811–828.https://doi.org/10.1007/s11069-013-0607-0

Lanzo G., Silvestri F., Costanzo A., D'Onofrio A., Martelli L., Pagliaroli A., ... & Simonelli A. (2011). Site response studies and seismic microzoning in the Middle Aterno valley (L'Aquila, Central Italy). Bulletin of Earthquake Engineering, 9(5), 1417-1442. https://doi.org/10.1007/s10518-011-9278-y

Lindell M.K. & R.W. Perry. (1996). Identifying and managing conjoint threats: Earthquake induced hazardous materials releases in the US. Journal of Hazardous Materials 50: 1-31.

Phan, H. N., Paolacci, F., Corritore, D., & Alessandri, S. (2018). Seismic vulnerability analysis of storage tanks for oil and gas industry. Pipeline Science and Technology, 2(1), 55–65.

Tang A. K. (2000). Izmit (Kocaeli), Turkey, earthquake of August 17, 1999 including Duzce earthquake of November 12, 1999: Lifeline performance (Vol. 17).

Vannoli P., Burrato P., Fracassi U., & Valensise G. (2012). A fresh look at the seismotectonics of the Abruzzi (Central Apennines) following the 6 April 2009 L'Aquila earthquake (Mw 6.3). Italian Journal of Geosciences, 131(3), 309–329. https://doi.org/10.3301/IJG.2012.03

Corresponding author: giorgia.berardo@rina.org

Seismic fragility curves of existing masonry school buildings in Friuli-Venezia Giulia

I. Boem[1], N. Gattesco[1]

[1] *Department of Engineering and Architecture, University of Trieste, Italy*

Motivation

In Italy, there are approximately 50000 schools, around one fifth are masonry buildings. Around 80% of these were constructed before 1970 and were designed primarily to resist gravitational loads. However, Italy is a seismically active country, and masonry buildings display significant seismic vulnerability. Furthermore, school masonry structures may be even more vulnerable than ordinary build due to function-related architectural features. Given the societal importance of ensuring the safety of school buildings against natural hazards, this study provides a preliminary framework for assessing the seismic vulnerability of existing masonry schools at a regional scale, supporting data-driven decision-making in seismic risk mitigation.

Specifically, seismic fragility curves were derived for a representative dataset of schools in the Friuli-Venezia Giulia region. For each building, capacity curves were obtained using an analytical-mechanical approach based on simplified global pushover analyses. Buildings were then classified into homogeneous sub-categories according to the number of storeys and construction period. Median resisting ground accelerations and associated dispersions were computed for the four EMS98 damage levels to develop the fragility curves.

Reference dataset

The reference dataset comprises 101 unreinforced masonry (URM) school buildings of the Italian Friuli–Venezia Giulia region, representative of the URM school building stock at both the regional and national level (Giusto et al., 2025). For each building, detailed structural information was collected through the analysis of design documentation and on-site surveys, including location, construction age and major interventions, subdivision into structural units, number and height of storeys, masonry and floor typologies, plan layout, and wall thickness.

The sample (Fig.1) is predominantly composed of two-storey buildings (50%) with small plan areas (84% < 1000 m²), large inter-storey heights (median 3.6 m) and wide spacing between walls. The walls are predominately made of solid brick masonry with lime mortar (54%), or hollow brick masonry (25%), or stone masonry (21%); floor systems are mainly of mixed type (>90%, r.c. ribs with hollow clay blocks). The construction ages are approximately evenly distributed among the pre-1970 periods, while URM structures were progressively replaced by r.c. thereafter. The school structures

generally feature squat internal walls with limited openings, whereas the main façades include numerous openings. The plan configuration varies from compact to elongated or irregular layout. Typically, the percentage of load-bearing walls at ground floor increases with the floors number, with median values of 3.5%, 4.6%, and 6.2% for 1, 2, and ≥3 storey buildings, respectively.

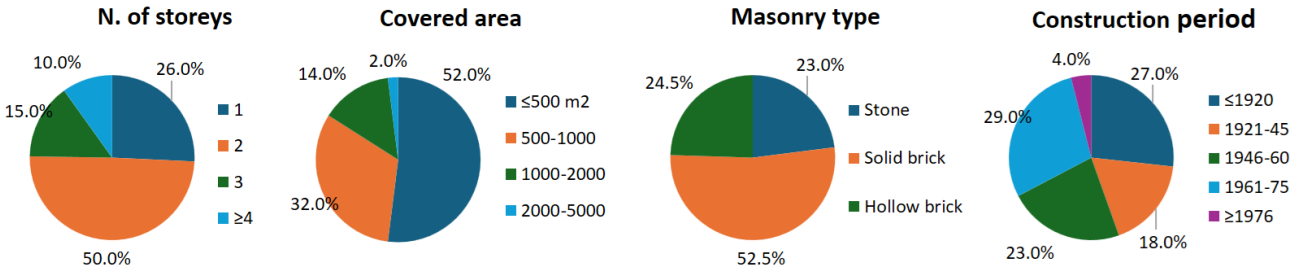

Fig. 1 – Percentage distribution of the FVG school sample, according to the number of storeys (a), plan area (b), masonry typology (c) and construction period (d).

Method

The pushover analyses of each building are performed using the "Firstep-M_PRO" tool. The required input includes the in-plan distribution of shear walls (centroid coordinates, length, and thickness), masonry typology, number of storeys, and floor and roof characteristics. Based on these inputs and predefined parameters (modifiable by the user), the software assigns mechanical properties to each wall (Young's modulus, compressive and shear strength) and evaluates gravitational loads for the seismic combination. Axial stresses in the piers, which significantly affect lateral performance, are computed considering masonry self-weight and floor loads through influence areas.

According to the conventional approach (MIT, 2019), the in-plane response of each pier is idealized as elastic–plastic up to ultimate displacement, possibly with residual strength (Tab.1). Secant stiffness accounts for both flexural and shear deformability, while strength is governed by the weaker mechanism between diagonal shear cracking (according to the Turnšek and Čačović criterion) and bending failure. Ultimate drift limits of 0.5% or 1.0% are adopted, respectively.

Tab. 1– Estimation of resistance, stiffness and ultimate displacement for the simplified elastic-plastic schematization of the in-plane behavior of masonry piers

Resistance	**Stiffness**	
$V_{P,max} = min(V_{P,d}; V_{P,fl})$ Shear failure $V_{P,d(URM)} = \frac{1.5\tau_0}{\beta} b \cdot t \sqrt{1 + \frac{\sigma_o}{1.5\tau_0}}$ Bending failure $V_{P,fl} = \frac{M_P}{h_0}$ *with* $M_P = \frac{\sigma_o b^2 t}{2}\left(1 - \frac{\sigma_o}{0.85 f_m}\right)$	$K_e = \left(\frac{h^3}{\eta J E} + \frac{1.2h}{Gbt}\right)^{-1}$ **Ultimate displacement** $d_{ult} = \theta_{lim} * h$ θ_{lim} = 0.005 shear = 0.01 bending	*h pier height* *b pier width* *t pier thickness* *J 2nd moment of area* *E Young modulus* *G shear modulus* σ_0 *axial stress* f_m *compressive strength* τ_0 *shear strength* h_0 *effective shear span*

Since the pier capacity is strongly influenced by its effective height and boundary conditions - related to the coupling action of spandrels – these aspects must be properly accounted for, to ensure reliable predictions. Based on detailed numerical investigations on several case study schools, the effective pier height was set equal to 0.85 times the inter-storey height. A shear-type behavior was

assumed for single-storey buildings (strong spandrels), while a mixed behavior between shear-type and cantilever mechanisms was considered for multi-storey buildings (partially effective spandrels).

The Firstep-M_PRO approach considers a global structural behavior, assuming sufficiently stiff and well-connected floors. Once the control displacement at the floor mass center is defined, displacements and internal forces of individual piers are computed (Fig.2a). Initial centers of mass and rigidity are estimated to account for both translational and torsional effects due to plan eccentricity. Separate analyses are performed along the two principal directions (X and Y). For each direction, the control displacement corresponding to the yielding of the first pier is identified and subsequently increased incrementally. The center of rigidity and floor rotations are updated at each step. The sum of pier forces provides the storey shear, which is converted into base shear using a triangular distribution of lateral forces along the height. This procedure is applied independently to each storey, and the base shear corresponding to the weakest storey(s) governs the global response. The resulting capacity curve is defined in terms of base shear versus global displacement. The Fisrtep-M_PRO simplified procedure was validated against several case studies, by comparing simplified capacity curves with those obtained from detailed pushover analyses carried out on whole buildings through software MidasGEN, modelled by means of the equivalent frame method with lumped plasticity.

Target points corresponding to four damage levels - DL1 (slight), DL2 (moderate), DL3 (heavy), and DL4 (very heavy), according to Grünthal (1998) - are identified on the capacity curve of the multi-degree-of-freedom (MDOF) system. The curve is then transformed into an equivalent single-degree-of-freedom (SDOF) capacity curve, assuming dominance of the first translational mode. Damage levels are defined as follows: DL1, reduction of initial elastic stiffness by at least 30%; DL2, onset of plastic behavior; DL3, attainment of 75% of the displacement at sudden strength degradation or onset of gradual degradation; and DL4, sudden strength loss or gradual degradation of at least 25%.

Ground accelerations associated with each damage level are computed using the Capacity Spectrum Method (MIT, 2019), based on equivalent viscous damping, applied to the SDOF capacity curve (Fig.2b). The elastic response spectrum follows the Italian technical standards (MIT, 2018) for subsoil category A. The damping, ranging form 5% to 20%, follows the formulation proposed by Lagomarsino and Cattari (2014).

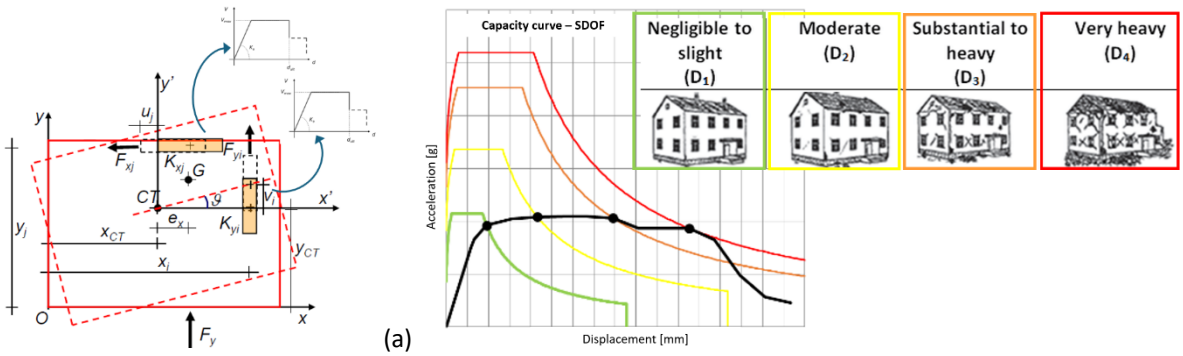

Fig. 2 – Schematization of the step-by-step plan analysis (a) and representation of the Capacity Spectrum Method applied to evaluate the resisting peak ground acceleration associated with the four Damage Levels (b).

The fragility curves are then derived by grouping the resisting ground acceleration values obtained for individual buildings according to the defined sub-typologies and damage levels. Results from both principal directions are included, assuming that the seismic action direction is *a priori* unknown. The median ground acceleration, $a_{g,res}$, and dispersion parameter β (i.e. the standard deviation of the natural logarithms of $a_{g,res}$) are estimated considering a lognormal distribution. It is observed that the analysis accounts explicitly of inter-building variability, considering the architectonic features, geometric characteristics and masonry types of the real scenario. Conversely, intrinsic material variability and uncertainty in seismic demand are not explicitly considered in the adopted approach.

Results and conclusions

Fragility curves (Fig. 3) are grouped by number of storeys and construction period. Although some sub-categories have very limited number of samples and are not statistically representative, some notable observations can be drawn from this study. The seismic vulnerability, for a given DL, significantly increases from single- to multi-storey buildings, while differences between 2- and ≥3-storey structures are generally less relevant. This reflects the higher seismic mass of multi-storey schools, without a sufficient proportional increase in the percentage of resisting masonry; also, single-storey buildings benefit for more compact layouts and effective pier coupling effect of the spandrels. No clear effect is related to the construction period. However, 2-storey schools built after World War II exhibit higher DL3 and DL4 vulnerability, in respect to older ones. This is likely due to more complex layouts and longer spans - increasing seismic demand - without corresponding improvements in material strength or wall thickness. A similar trend emerges in 1-storey schools, but not in ≥3-storey buildings. Within a sub-typology, β tends to decrease for higher DL (values $\beta \leq 0.4$ for DL3-4). It is observed that these results were also compared with an alternative procedure, which produced comparable results (see Giusto et al. 2025 for further details and comparisons).

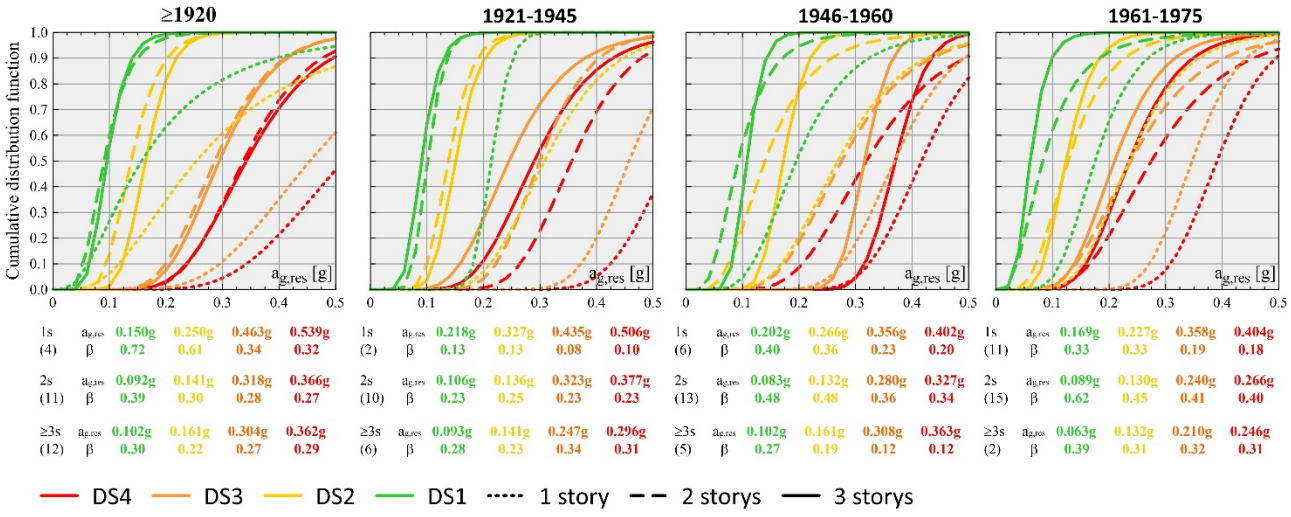

Fig. 3 – Fragility curves for the URM school buildings, for different damage states (DS), varying the construction period and the number of stories. The median values of resisting ground acceleration and dispersions are indicated for each sub-category; the number of school buildings is also reported in round brackets.

Aknowledgments

The financial support of the Italian Department of Civil Protection (IDPC), within the ReLUIS-DPC 2022-2024 Research Project, is gratefully acknowledged.

References

Giusto, S., Boem, I., Alfano, S., Gattesco, N., Cattari, S.; 2025: Derivation of seismic fragility curves through mechanical-analytical approaches: tha case study of the URM school buildings in Friuli-Venezia Giulia region (Italy). Bulletin of Earthquake Engineering, 23, 2611-2646.

Grunthal G. 1998. EMS98 - European Macroseismic Scale 1998. Conseil de l'Europe - Cahiers du Centre Européen de Géodynamique et de Séismologie, Luxemburg.

Lagomarsino, S., Cattari, S.; 2014: Fragility Functions of Masonry Buildings. In: Pitilakism, K., et al. (eds.), SYNER-G: Typology Definition and Fragility Functions for Physical Elements at Seismic Risk, Geotechnical, Geological and Earthquake Engineering, 27.

MIT - Ministero delle Infrastrutture e dei Trasporti; 2018: Aggiornamento delle «Norme tecniche per le costruzioni». Decreto 17 gennaio 2018.

MIT - Ministero delle Infrastrutture e dei Trasporti; 2019: Circolare 21 gennaio 2019, n. 7 C.S.LL.PP.: Istruzioni per l'applicazione dell'«Aggiornamento delle "Norme tecniche per le costruzioni"» di cui al decreto ministeriale 17 gennaio 2018.

Corresponding author: ingrid.boem@dia.units.it

Evaluating the Hybrid Standard Spectral Ratio Method for Seismic Site Response Analysis in the Norcia Sedimentary Basin (Central Italy)

A.M. Borzì[1], R.A. Fard [2], F. Panzera [1] and S. Parolai[2]

[1]Department of Biological, Geological and Environmental Sciences (University of Catania, Catania, Italy);
[2] Department of Mathematics, Informatics and Geosciences (University of Trieste, Trieste, Italy)

Seismic site response plays a crucial role in seismic hazard and risk assessment, particularly in areas characterized by thick sedimentary deposits, where local geological conditions can strongly amplify ground motion. Several methods are commonly used to estimate site response, including the standard spectral ratio (SSR) method applied to earthquake recordings and its counterpart based on seismic ambient noise (SSRn). While both approaches are widely adopted, they present limitations related to data availability and source characteristics.

In this study, we assess the performance of the hybrid standard spectral ratio method (SSRh) for site response estimation in the Norcia sedimentary basin, located in central Italy. The Norcia basin is characterized by a complex sedimentary basins exceeding 200 m in thickness and reaching up to approximately 600 m in its central sector, making it a suitable natural laboratory for testing site-response techniques. The SSR method estimates local amplification by comparing earthquake recordings at basin stations with those at nearby rock reference sites, assuming that spectral differences mainly reflect local site effects. However, this approach requires a sufficiently large dataset of high-quality seismic events. The SSRn method applies a similar concept to ambient seismic noise, but its reliability strongly depends on the spatial distribution of noise sources and on the distance between reference and target stations.

To overcome these limitations, the SSRh method combines earthquake-based SSR and noise-based SSRn approaches. In this framework, SSR is first used to define the relative site response between a rock reference station and a basin station, which is then adopted as a basin reference. Subsequently, SSRn is applied within the basin to characterize spatial variations in site response relative to this internal reference.

Seismic data recorded by a set of stations deployed within and around the Norcia basin were analyzed using the SSR, SSRn, and SSRh methods. Site response functions were derived using earthquake recordings, ambient noise, and their combination. The results show that the SSRh method reproduces the main features of the site response obtained from the classical SSR approach.

Although the overall spectral shapes are consistent, SSRh generally shows slightly higher amplification values, particularly in areas characterized by greater sediment thickness.

These results indicate that the SSRh method provides a reliable alternative for site-response estimation in sedimentary basins where the availability of earthquake recordings is limited. The approach appears particularly suitable for characterizing spatial variations of site effects within complex basins, although further applications are required to fully assess its robustness under different geological and noise conditions.

Acknowledgments

We would like to acknowledge the project “MODERN” (Advanced Seismic lnterferOmetry MethoDs and TechnologiEs for EngineeRiNg Seismology), CUP- J93C24000230001.

Corresponding author: alfiomarco.borzi@unict.it

Rapid Generation of Reports on Post-Seismic Events with gmProcess: A Case Study for A Dense Accelerometric Network in Veneto (NE Italy).

G. Capotosti[1], C. Scaini[1], P.L. Bragato[1], L. Cataldi[1], M. Picozzi[1], P. Comelli[1]

[1] *Center for Seismological Research - National Institute of Oceanography and Applied Geophysics - OGS, Italy*

In recent years, the increasing availability of dense urban accelerometric networks has enabled progressively more detailed characterization of ground shaking at the local scale, while simultaneously introducing significant challenges in data management, processing, and rapid dissemination of large volumes of information. Within this framework, the Dense Accelerometric Network in Veneto (RAD), designed and implemented by the National Institute of Oceanography and Applied Geophysics (OGS) from 2020 to 2022, represents one of the most extensive urban accelerometric infrastructures in Italy and the largest at the scale of a single region. The network currently comprises more than 350 sensors installed at the base of public and private buildings, covering over 50% of the municipalities in the Veneto region (Fig. 1).

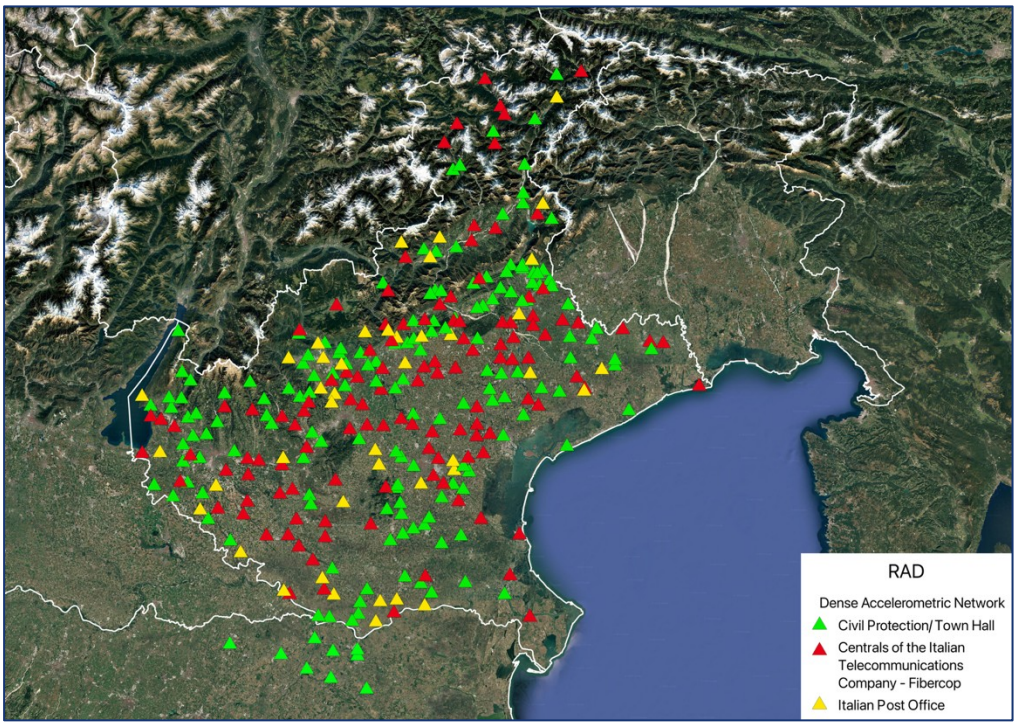

Fig. 1 – The accelerometric network in Veneto.

As described by Bragato et al. (2023, 2025), the primary objective of RAD is to support civil protection activities by providing, in near real time, reliable measurements of ground shaking together with standardized, station-level post-event reports conceived as immediately usable operational tools for rapid earthquake impact assessment. To address these operational requirements, a fully automated data acquisition and processing workflow has been developed based on gmProcess, an open-source software package developed by the U.S. Geological Survey for standardized ground-motion processing (Thompson et al., 2024). Although gmProcess provides a robust framework for computing key engineering parameters, its original architecture designed for smaller networks and largely based on serial execution proved inadequate for managing a very high-density urban network such as RAD. The codebase has therefore been extensively reorganized and adapted to the operational needs of the Center for Seismological Research - OGS, introducing new modules, revising existing components, and integrating the software into a fully automated processing chain specifically aimed at the systematic generation of station-level post-seismic reports, as detailed by Capotosti et al. (2025). A central element of this development is the redesign of the *summary_plots.py* module, which now generates complete station-level reports that integrate, within a single document, accelerometric waveforms, pseudo-spectral acceleration (PSA) response spectra, Peak Ground Acceleration (PGA) tables, and synthetic graphical representations of the recorded ground shaking. The report layout has been optimized for automated production and rapid reading, ensuring that key information is immediately accessible to non-specialist users (Fig. 2). In parallel, the Italian seismic code NTC 2018 has been incorporated into the workflow, enabling the computation of design spectra for soil classes A–E and their direct comparison with observed spectra, thereby making the reports suitable for both engineering applications and post-event technical evaluations (Capotosti et al., 2025).

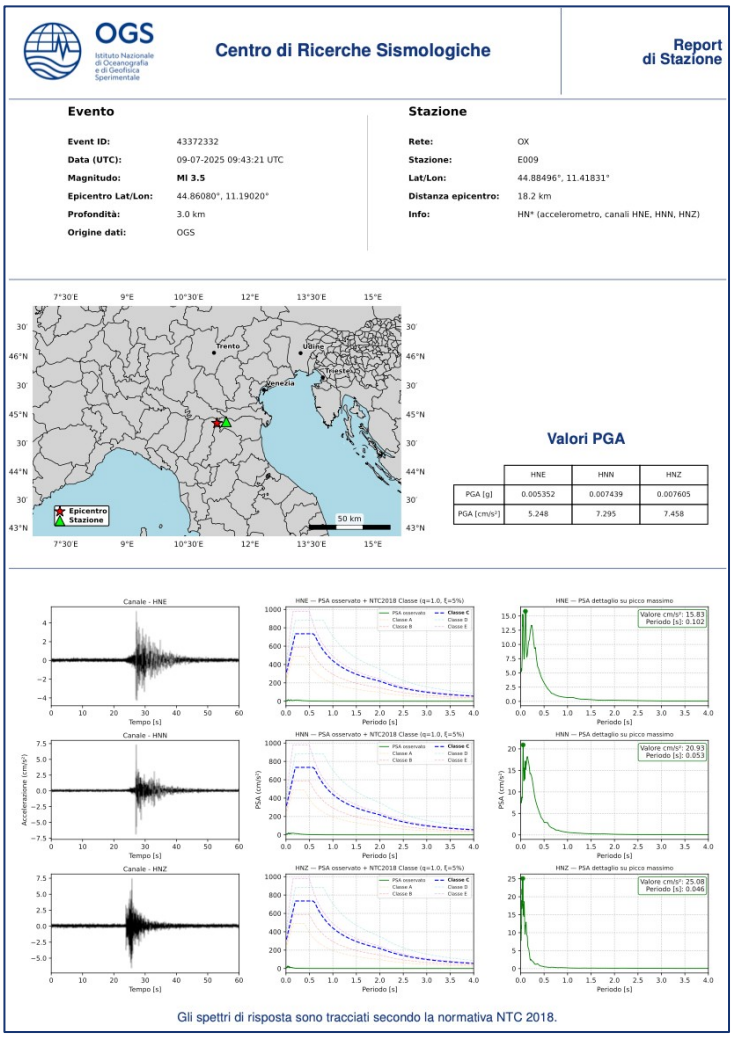

Fig. 2 – Automatically generated station-level post-event report summarizing ground-motion recordings, response spectra, PGA values, and comparison with NTC 2018 design spectra

Additional developments include the introduction of dedicated subcommands for the automatic generation of station- and network-scale maps embedded in the reports, and the transformation of the former *export_metrics* module into *export_pga*, providing PGA values directly compatible with the ShakeMap system (Fig. 3).

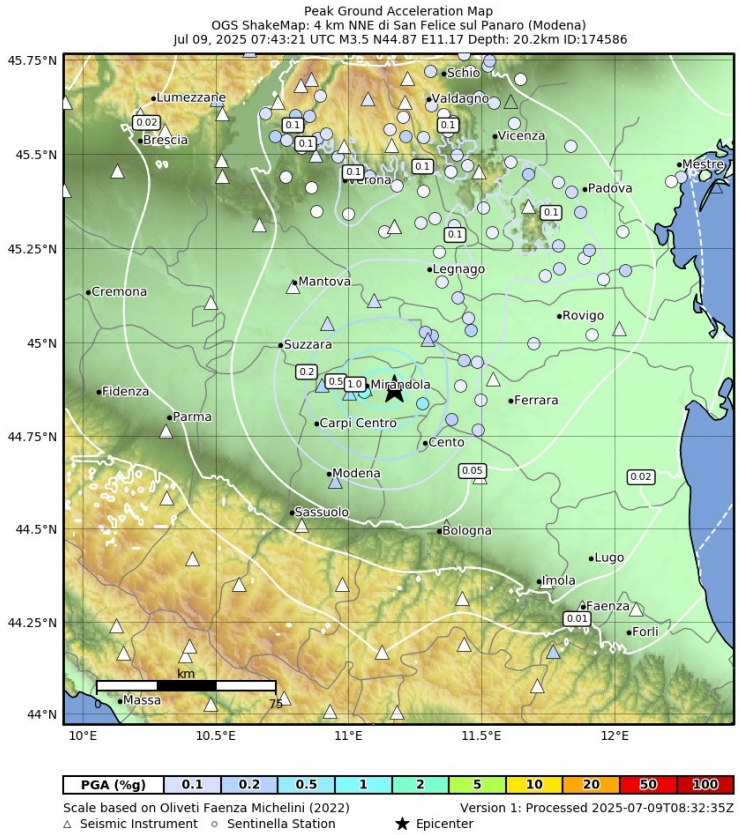

Fig. 3 – ShakeMap generated by the internal system using PGA values obtained from the gmProcess-based workflow (new export_pga module) for the Dense Accelerometric Network in Veneto (RAD).

Given the large number of channels and the need to deliver complete reports within minutes after an earthquake, computational efficiency is a critical aspect of the system. Several components of the workflow have therefore been rewritten to support true multi-core parallelization, with dynamic workload distribution based on the volume of waveform data to be processed. Integration with the high-performance computing resources provided by the TeRABIT infrastructure has enabled full exploitation of these optimizations, resulting in a substantial reduction in processing times. Operational tests show that, despite the introduction of additional computationally demanding steps such as the automatic generation of maps and detailed station reports, the total execution time for hundreds of channels is significantly lower than that of the original serial workflow, in agreement with the results discussed by Capotosti et al. (2025). The automatic station-level reporting system, now fully operational, represents a central tool for rapid post-earthquake documentation and decision support for civil protection authorities, enabling immediate and homogeneous interpretation of recorded ground shaking across the regional territory. The experience gained within the Veneto Dense Accelerometric Network demonstrates that the combination of a dense monitoring infrastructure, appropriately adapted open-source software, and advanced HPC resources constitutes an efficient, scalable, and replicable model for modern seismic monitoring, significantly enhancing post-seismic response capabilities and emergency management.

Acknowledgments

Rapid generation of reports on post-seismic events with gmProcess: a case study for a dense accelerometric network in Veneto (NE Italy) was supported by the National Recovery and Resilience Plan project TeRABIT (Terabit network for Research and Academic Big data in Italy - IR0000022 - PNRR Missione 4, Componente 2, Investimento 3.1 CUP I53C21000370006) in the frame of the European Union - NextGenerationEU funding.

References

Bragato, P.L., Boaga, J., Capotosti, G., Comelli, P., Parolai, S., Rossi, G., Siracusa, H., Ziani, P. and Zuliani, D.; 2025: Implementing a dense accelerometer network in Veneto (NE Italy): a support for rapid earthquake impact assessment. Bull Earthquake Eng 23, 1859–1884. https://doi.org/10.1007/s10518-025-02133-w

Capotosti, G., Bragato, P.L., Scaini, C., Comelli, P.; 2025: Near real-time acquisition and processing of seismological data from dense accelerometric networks with gmProcess. Report interno https://hdl.handle.net/20.500.14083/43583

Thompson, Eric M., Hearne, M., Aagaard, B.T., Rekoske, J.M., Worden, C.B., Moschetti, M.P ., Hunsinger, H.E., Ferragut, G.C., Parker, G.A., Smith, J.A., Smith, K.K., and Kottke, A.R.; 2025: Automated, Near Real-Time Ground-Motion Processing at the U.S. Geological Survey (USGS) - Seismological Research Letters 96 (1): 538–553. https://doi.org/10.1785/0220240021

Bragato, P.L., Boaga, J., Capotosti, G., Comelli P., Parolai, S., Rossi, G., Siracusa, H., Ziani, P. and Zuliani D.; 2023: Relazione Tecnica e Scientifica sull'attuazione dell'Azione 5.3.1 del POR FESR Regione del Veneto 2014-2020. Relazione Interna OGS 2023/30 https://hdl.handle.net/20.500.14083/17342

Corresponding author: gcapotosti@ogs.it

Record selection for seismic microzonation studies in Campi Flegrei area: local ground motion features and analysis challenges

T. Castelbarco[1], G. Lanzano[1], L. Nardone[2], S. Sgobba[1], D. Galluzzo[2], V. Convertito[2], MA. Di vito[2], F. Pacor[1].

[1] *Istituto Nazionale di Geofisica e Vulcanologia, Sezione di Milano.*
[2] *Istituto Nazionale di Geofisica e Vulcanologia, Sezione Osservatorio Vesuviano, Naples, Italy.*

This study outlines methodology and results achieved in selecting accelerograms for seismic site response analysis in the Campi Flegrei area, as part of the activities of the Level III Microzonation Plan for three municipalities (Pozzuoli, Bacoli and eastern Naples). The area has rather complex seismotectonic characteristics, as highlighted by many studies in literature, including recent ones (Scotto di Uccio et al., 2024). The spatial distribution of seismicity in the caldera (Fig. 1) shows two distinct patterns: shallower seismic events on land (hypocentral depths < 5 km), in the Pozzuoli and Bagnoli municipal areas, and deeper offshore events in the western area of the Gulf of Pozzuoli, near Bacoli and Baia. Ground motion observations in the area highlight significant differences compared to crustal seismicity, showing a strong high-frequency content of the signal near the source (within 1-2 km), with high PGA values, and a very rapid attenuation with distance, within the first 4-5 km from the epicentre.

One of the main challenges of the recording selection is the lack of an integrated seismic hazard model that adequately considers both active crustal and volcanic seismicity. The MPS04 model, adopted as the reference model for NTC18, cannot adequately represent the spectral characteristics of local earthquakes. In fact, near the source, the amplitudes observed systematically exceed the regulatory spectrum at short periods and are drastically lower at intermediate and long periods.

For the purposes of this study, the area has been initially divided into three main sectors (Figure 1): a) the Pozzuoli area, with most events occurring on land, and at a maximum depth of approximately 3 km; b) the Bagnoli area, with similar characteristics of the area a; c) the Municipality of Bacoli, which shows peculiar seismic behavior, with a distribution of epicenters mainly offshore or along the coast. The events of sector c are mainly located in the area between Capo Miseno, Baia, and the Gulf of Pozzuoli, with hypocenters deeper than those of Pozzuoli, but with lower frequency of occurrence.

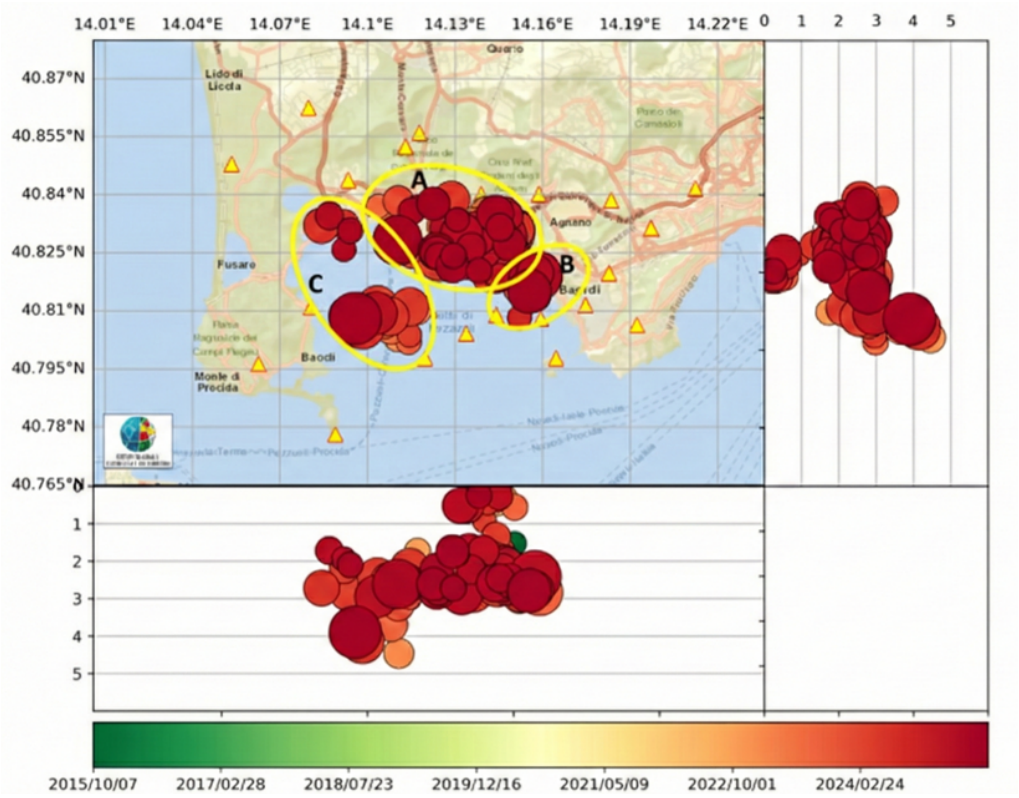

Figure 1. Location of events recorded in the Campi Flegrei area: Md > 2.5 and subdivision (yellow ellipses marked with the letters A, B, and C) into the three municipal areas.

To define the scenario spectrum, we selected empirical ground motion models (GMMs) specific for volcanic areas available in the literature. In particular, we considered the very recent predictive model by Scala et al. (2025), calibrated with recently available data on earthquakes that occurred in the Campi Flegrei. In order to define the reference site conditions for record selection, compatible with the bedrock condition of 1D analysis, Neapolitan Yellow Tuff is the best candidate rock formation, thanks to its relative homogeneity in the area. The typical values of shear wave velocity (Vs) for this lithotype vary between 500 and 1200 m/s, depending on depth and level of alteration (Licata et al. 2019, Nardone et al., 2020, Maresca et al., 2014). These values generally place it in the subsoil category B of the NTC18 standard ($V_{s,eq}$ between 360 and 800 m/s).

Selection of accelerograms

The analyses for identifying spectrum-compatible natural accelerograms were conducted using the REXELweb code (see data and resources; Sgobba et al., 2019; Iervolino et al., 2009). REXELweb was designed to query, integrate, and select signals present in various archives: the Engineering Strong Motion (ESM) database (Luzi et al., 2020), the ITalian ACcelerometric Archive (ITACA) (Felicetta et al., 2023), and the NESS2.0 flatfile (Sgobba et al., 2021). Based on the spatial variability of seismic ground motion, two sets of waveforms, each consisting of seven unscaled accelerograms, were selected to match the different target spectra:

- **SET-1:** The target spectrum adopted was defined using the median scenario prediction from the Scala et al. (2025) model. To determine the representative spectrum for the selection of

accelerograms, we chose a scenario compatible with the maximum expected earthquake in the area, in the range Mw 4.4 - 5.1, according to Scotto di Uccio et al. (2024). The scenario considers a moment magnitude Mw=4.7 and an epicentral distance Repi=2km, focal depth h=2km and subsoil category B. The predictions for the reference scenario have been also compared with the available recordings in the area for a further check.

- **SET-2:** The target spectrum adopted is the design elastic spectrum according to NTC18 for the Campi Flegrei area, corresponding to Tr=475 years, subsoil category B and topographical class T1.

Figure 2 shows the response spectra of the selected accelerograms for SET-1, their average, and the target scenario spectrum. Almost all the selected accelerograms were recorded within 7 km of the epicenter, and only one between 10 and 15 km, confirming that these spectral shapes are mainly observed at sites very close to the source.

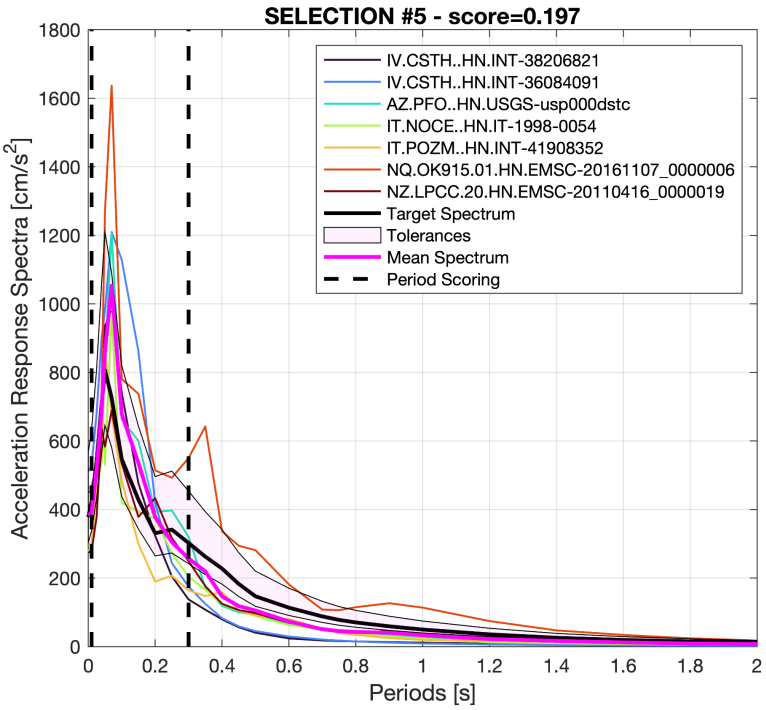

Figure 2. Acceleration response spectra obtained using RexelWEB (Sgobba et al., 2019) with a target scenario spectrum obtained from the median prediction of the SCALA25 model (Scala et al. 2025) for moment magnitude Mw=4.7, epicentral distance Repi=2km, focal depth h=2km and subsoil category EC8-B.

In the case of SET-2 (not shown here), most of the selected accelerograms relate to tectonic earthquakes, except for the waveforms from the UWE station and the Hawaii HV network relate to two volcanic earthquakes.

Based on this study, the joint use of SET-1 and SET-2 for the Pozzuoli and Bagnoli areas (a and b sectors) is recommended for local seismic response based on 1D numerical analyses. This choice is beneficial in terms of safety, since SET-1 reflects the characteristics of seismic motion very close to the source in the areas of interest, while SET-2 ensures that, at intermediate and long periods, the

reference spectrum has amplitudes comparable to the regulatory spectrum. For the Bacoli area, we propose the use of the SET-2 obtained from the NTC18 regulatory spectrum. In fact, the ground motion predicted by an earthquake scenario compatible with seismicity in sector c, which involves greater distances and depths than sectors a and b (in this case, the earthquakes are located at sea), is systematically lower than that obtained from the regulatory spectrum. The use of SET-2 alone simplifies the analysis, while maintaining safety requirements.

References

Felicetta C., Russo E., D'Amico M., Sgobba S., Lanzano G., Mascandola C., Pacor F., Luzi L.; 2023: Italian Accelerometric Archive v4.0 - Istituto Nazionale di Geofisica e Vulcanologia, Dipartimento della Protezione Civile Nazionale. doi: 10.13127/itaca.4.0.

Iervolino I., Galasso C., Cosenza E.; 2009: REXEL: computer aided record selection for code-based seismic structural analysis. Bulletin of Earthquake Engineering, 8:339-362. DOI 10.1007/ s10518-009-9146-1.

Iervolino, I., Cito, P., De Falco, M., Festa, G., Herrmann, M., Lomax, A., ... & Zollo, A.; 2024: Seismic risk mitigation at Campi Flegrei in volcanic unrest. Nature Communications, 15(1), 1-14.

Iervolino, I., Galasso, C., & Cosenza, E.; 2010: REXEL: computer aided record selection for code-based seismic structural analysis. Bulletin of earthquake engineering, 8(2), 339-362.

Lanzano G., Luzi L.; 2020: A ground motion model for volcanic areas in Italy. Bull. Earthq. Eng., 18, 57–76, doi: 10.1007/s10518-019-00735-9

Lanzano G., Felicetta C., Pacor F., Spallarossa D., Traversa P.; 2022b: Generic-To-Reference Rock Scaling Factors for Seismic Ground Motion in Italy. Bulletin of the Seismological Society of America 2022; 112 (3): 1583–1606. doi: https://doi.org/10.1785/0120210063

Licata, V., Forte, G., d'Onofrio, A., Santo, A., & Silvestri, F.; 2019: A multi-level study for the seismic microzonation of the Western area of Naples (Italy). Bulletin of Earthquake Engineering, 17(9), 4711-4741.

Luzi L., Lanzano G., Felicetta C., D'Amico M. C., Russo E., Sgobba S., Pacor, F., & ORFEUS Working Group 5; 2020: Engineering Strong Motion Database (ESM) (Version 2.0). Istituto Nazionale di Geofisica e Vulcanologia (INGV). https://doi.org/10.13127/ESM.2

Maresca, R., Damiano N., Nardone L., Di Vito M. A. and Bianco F.; 2013: A comparison of surface and underground array measurements of ambient noise recorded in Naples (Italy). J. Seismol., 18, 385–400.

Ramadan, F., Lanzano, G., & Sgobba, S.; 2023: Vertical seismic ground shaking in the volcanic areas of Italy: prediction equations and PSHA examples. Soil Dynamics and Earthquake Engineering, 175, 108228.

Ricciolino P., Lo Bascio D., Esposito R.; 2024: GOSSIP - Database sismologico Pubblico INGV-Osservatorio Vesuviano. Istituto Nazionale di Geofisica e Vulcanologia (INGV). https://doi.org/10.13127/gossip

Scala, A., Strumia, C., Cito, P., di Uccio, F. S., Festa, G., Iervolino, I., ... & Iaccarino, A. G.; 2025: Ground Motion Prediction Equations for Campi Flegrei (Italy). Bulletin of Earthquake Engineering (submitted).

Scotto di Uccio, F., Lomax, A., Natale, J., Muzellec, T., Festa, G., Nazeri, S., ... & Zollo, A.; 2024: Delineation and fine-scale structure of fault zones activated during the 2014–2024 unrest at the Campi Flegrei caldera (Southern Italy) from high-precision earthquake locations. Geophysical Research Letters, 51(12), e2023GL107680.

Sgobba, S., Puglia, R., Pacor, F., Luzi, L., Russo, E., Felicetta, C., ... & Iervolino, I.; 2019: REXELweb: A tool for selection of ground-motion records from the Engineering Strong Motion database (ESM). In Earthquake Geotechnical Engineering for Protection and Development of Environment and Constructions (pp. 4947-4953). CRC Press.

Sgobba, S., Pacor, F., Felicetta, C., Lanzano, G., D'Amico, M. C., Russo, E., & Luzi, L.; 2021: NEar-Source Strong-motion flatfile (NESS), version 2.0 (Version 2.0) [Data set]. Istituto Nazionale di Geofisica e Vulcanologia (INGV). https://doi.org/10.13127/NESS.2.0

Corresponding author:

Tommaso Castelbarco

tommaso.castelbarco@ingv.it

The “reference stratigraphic matrix”: a new tool to support the Seismic Microzonation Studies in Italy

S. Catalano[1,3], A. Porchia[1,3], G. Tortorici[2,3]

[1] Department of Biological, Geological and Environmental Sciences (DBGES) – Section of Earth Science, University of Catania, Catania, Italy
[2] Institute of Environmental Geology and Geoengineering of the Italian National Research Council, Monterotondo, Italy
[3] Center for Seismic Microzonation and its applications_c/o Institute of Environmental Geology and Geoengineering of the Italian National Research Council, Monterotondo, Italy

Seismic Microzonation (SM) studies in Italy consist of assigning local values of ground-motion amplification to stratigraphically homogeneous portions of the territory, using 1D numerical models of their representative stratigraphic columns. The meaning of these columns is completely different from that of the stratigraphic logs modeled for the seismic site response analyses. These latter, as well as the Italian seismic code, refer to the precise layering drilled in a specific site, to reproduce the behavior of the very local subsoil volumes. In this case, a precise correlation links geophysical measurements to the stratigraphic horizons, resulting in well-constrained numerical models. On the contrary, the stratigraphic columns modelled in MS studies are physical abstractions representative of an areal domain rather than of a site-specific condition, representative, within admitted variability ranges, the possible topological configurations of large, almost homogeneous ground volumes.

The SM studies in Italy benefit from a standardized methodology, which starts from the construction of the engineering-geological model (SM-Level 1) and completes with numerical modeling of a derivative geotechnical model (SM-Level 2/SM-Level 3) (SM Working Group, 2008). The reliability of the first stage is crucial to ensure the successful outcome of the successive stages. The collection of large number of available subsurface data is the cornerstone to convert rather complex subsurface settings into simplified configurations suitable for numerical modeling, in a cost-effective and time-saving perspective. The second core issue is to provide good parameterization of those subsurface units, which are significant in terms of local seismic response. Usually, geophysical and geotechnical collected data are sorted by engineering geological units (EGUs), as classified in the SM national standard (Technical Commission for Seismic Microzonation, 2020), thus forming heterogeneous statistical populations, regardless the mutual specific stratigraphic location of units. This is irrelevant in very simple subsurface settings, as those showing a single typology of cover unit directly on the geological substratum, where attribution of

the measured physical parameters to the correlative stratigraphic horizon is quite unambiguous. In more complex settings, the experience of the last decade of studies (e.g. Central Italy, Mt. Etna, Phlegrean Fields) teaches us that large numbers of subsurface information actually serves only if adequately elaborated before the final archiving in the SM study perspective. The quality and the usability of the geological subsurface data may vary based on the year of acquisition, the scope of the investigation and the details of the reported descriptions.

This is particularly true for all the case histories regarding areas where the near-surface stratigraphy, relevant in terms of ground-motion modifications, is essentially composed of very thick cover terrains, with frequent lateral and vertical lithological discontinuities, as the volcanic areas. In such conditions, the same EGU could repeatedly occur at different stratigraphic positions in the layering, showing different mechanic behavior with depth. We here discuss the methodology we use on the volcanic areas of southern Italy for the parametrization of the near surface layering by means of available subsurface investigation. The method aims to recognize and parameterize the distinct engineering-geological horizons, with their lateral variation in terms of EGU, which could compose the near-surface stratigraphy. This goal is achieved through the construction of a “reference stratigraphic matrix,” at the end of the accurate revision of the entire set of available geological data. The matrix is compiled ordering, from the surface, all the units that have been detected in the study area, through geological mapping or well drilling, assigning them a specific lithology and stratigraphic position. When finalized, the matrix provides a unique reference codification to classify all the subsurface information sorted by single possible engineering-geological horizons. They constitute the elementary components, better constrained than generic EGUs, for the modular composition of all stratigraphic configurations necessary to reproduce the variability of the subsurface volumes, determining the microzonation at the surface. This would substantially reduce uncertainties in the subsequent numerical modelling, resulting in a more reliable prediction of the local ground-motion amplification.

References

SM Working Group 2008: Guidelines for Seismic Microzonation, Conference of Regions and Autonomous Provinces of Italy-Civil Protection Department. 3 vol. and DVD. English edition published online in 2015. Rome. https://www.centromicrozonazionesismica.it/it/strumenti/linee-guida-ms/

Technical Commission for Seismic Microzonation 2020: Graphic and data archiving standards. Version 4.2. Department of Civil Protection of the Presidency of the Council of Ministers. Rome.

Corresponding author: catalano@unict.it

Ground motion models for Arias intensity and significant duration at Campi Flegrei: preliminary results

P. Cito[1], A. Grella[1], I. Iervolino[1,2,3]

[1] *Università degli Studi di Napoli Federico II, Italy*
[2] *Università degli Studi di Pavia, Italy*
[3] *Istituto Nazionale di Geofisica e Vulcanologia, Italy*

This contribution presents GMMs for the Campi Flegrei volcanic area (near the city of Naples, southern Italy) derived for the largest horizontal component of Arias intensity (I_a) and 5-95 significant duration (D_{5-95}). GMMs were calibrated using about one thousand ground motion records from more than ninety earthquakes with duration magnitude (M_d) in the range (2.5,4.6) which had been recorded between March 2022 and late 2025. For almost all earthquakes, records made available by the *Rete Accelerometrica Nazionale* (RAN) portal (https://ran.protezionecivile.it/IT) were considered. For six events for which RAN does not give records, data provided by *Istituto Nazionale di Goefisica e Vulcanologia* were used. Accelerometric records, response spectra, Husid plot and metadata for all recorded earthquakes, including the I_a and D_{5-95} values used to fit GMMs, are publicly available at http://wpage.unina.it/iuniervo/CampiFlegrei_EQ_Records/. Records featuring peak ground acceleration lower than 0.001 g were excluded, along with those that appeared to include ground motion from multiple events. For each earthquake in the dataset, M_d was converted to moment magnitude (M_w) — the magnitude metric adopted for the GMMs — according to Iervolino et al. (2024), while distance metric used is the epicentral distance (R_{epi}). The soil site conditions at the recording stations are the Eurocode 8 or EC8 (CEN, 2004) classes as provided by RAN or, when not available, by Forte et al. (2019). Mixed-effect regressions were performed to account for both inter- and intra-event variability in the recorded I_a and D_{5-95} observations. Regressions were carried out over the range of M_w from 2.3 to 4, using records with $R_{epi} < 40 km$ and grouping EC8 classes A and B as stiff sites and classes C and D as soft sites.

References

CEN; 2004: Eurocode 8: design provisions for earthquake resistance of structures, Part 1.1: general rules, seismic actions and rules for buildings. PrEN 1998-1, European Committee for Standardisation, Brussels, Belgium

Forte, G., Chioccarelli, E., De Falco, M., Cito, P., Santo, A., & Iervolino, I; 2019: Seismic soil classification of Italy based on surface geology and shear-wave velocity measurements. Soil

Dynamics and Earthquake Engineering Vol. 122, pp. 79-93, https://doi.org/10.1016/j.soildyn.2019.04.002

Iervolino, I., Cito, P., De Falco, M., Festa, G., Herrmann, M., Lomax, A., Marzocchi, W., Santo, A., Strumia, C., Massaro, L., Scala, A., Scotto di Uccio, F. & Zollo, A.; 2024: Seismic risk mitigation at Campi Flegrei in volcanic unrest. Nature communications Vol. 15, n.1, pp. 1-14, https://doi.org/10.1038/s41467-024-55023-1

Corresponding author: pasquale.cito@unina.it

Machine Learning Seismic Analysis to Support SISMIKO Emergency Network Optimization

A. Costanzo[1], S. Falcone[1], A. La Regina[1], A. Ruffo[1], M. Pastori[1] and SISMIKO *Working Group*

[1] *Istituto Nazionale di Geofisica e Vulcanologia, Osservatorio Nazionale Terremoti, Italy*

The Istituto Nazionale di Geofisica e Vulcanologia (INGV) is responsible for seismic surveillance in Italy within the national Civil Protection system, operating the permanent National Seismic Network (RSN; INGV Seismological Data Centre, 2006) and deploying temporary seismic networks during seismic emergencies.

Within this framework, SISMIKO, one of the six INGV operational groups, is dedicated to the rapid deployment of temporary seismic stations following earthquakes with M_L≥5.0 or during prolonged seismic sequences. Its main objective is to enhance RSN performance in epicentral areas by increasing station density, improving azimuthal coverage, and reducing hypocentral uncertainty during the early phases of seismic activity.

SISMIKO operates through a structured organizational model articulated into thematic working groups, ensuring rapid activation and integration of temporary stations into the national monitoring system, typically within 24 hours of an event (Moretti et al., 2023). Over time, SISMIKO has developed standardized procedures and operational tools for the rapid planning and management of emergency monitoring networks, including GIS-based applications and automated workflows that support station deployment, data sharing, and operational reporting (Pastori et al., 2025).

While this technological framework effectively supports network planning and deployment logistics, it does not currently provide a rapid and systematic analysis of the space–time evolution of seismic sequences from continuously acquired waveform data. Consequently, the evaluation of potential modifications or optimizations of network geometry during ongoing sequence remains largely qualitative and is not directly supported by high-resolution seismic catalogues.

To address this limitation, a machine learning (ML)-based seismic processing workflow has been developed. This workflow integrates automatic phase picking, phase association, and probabilistic earthquakes relocation to generate high-resolution event catalogues from continuous waveform data (Figure 1). By quantifying event locations, uncertainties, and network performance, this approach provides a reproducible framework for evaluating the effectiveness of temporary network deployments.

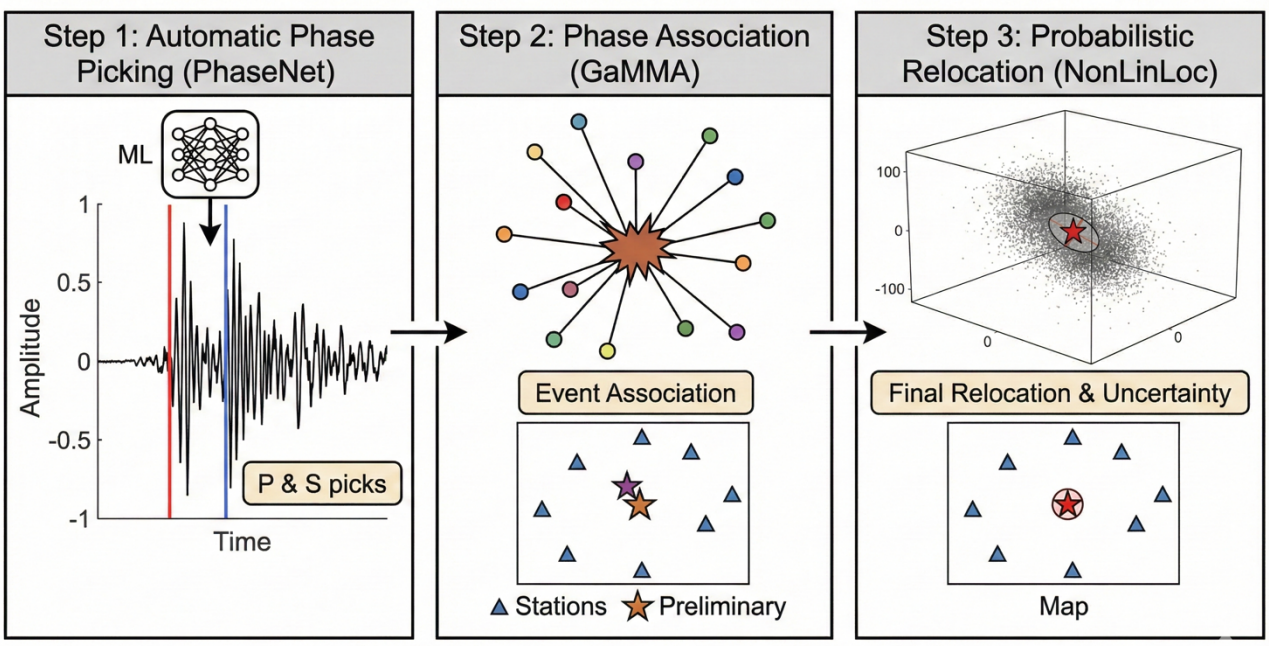

Fig. 1 – ML-based seismic processing workflow, from waveform to high-resolution catalogue.

The workflow was tested through subsequent analyses of two key seismic emergencies monitored by SISMIKO: the 2022 Adriatic Offshore Seismic Sequence (Costanzo, 2025) and the 2024 Pietrapaola Seismic Swarms (Costanzo et al., 2025). Results demonstrate its potential for near-real-time application, providing quantitative basis for assessing network performance and guiding data-driven optimization of temporary station geometry during the emergency phase.

For the 2022 Adriatic deployment (Figure 2) (Y1 network code; D'Alema et al., 2022), ML-based analysis could have systematically identified areas with poor hypocentral resolution or high noise impact, supporting the strategic relocation of stations, i.e. T1711, or the addition of new stations to address coverage gaps.

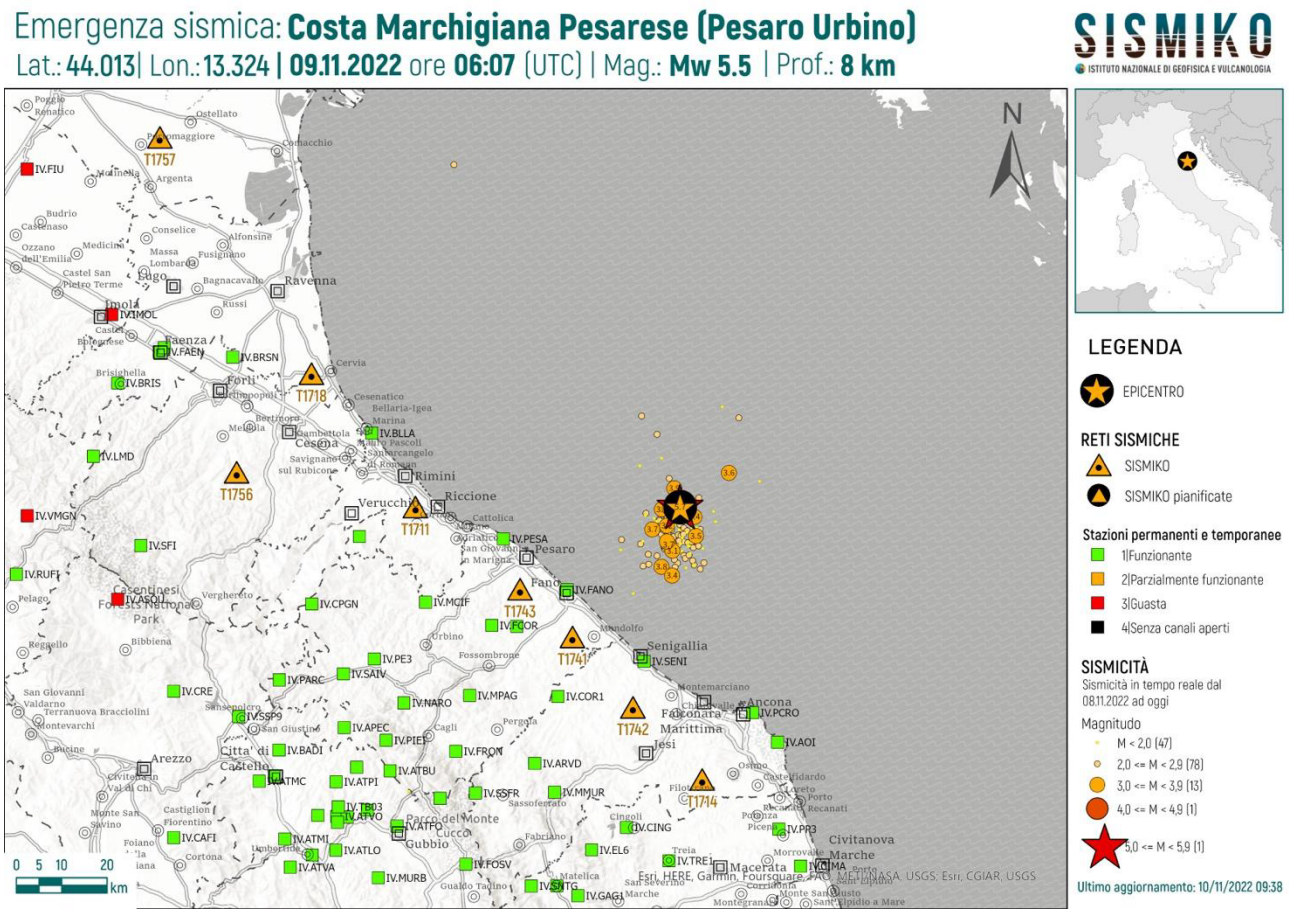

Fig. 2 – Cartographic report illustrating the distribution of seismic stations and recorded seismicity after 24h from the Mw 5.5 mainshock (orange star on black background) occurred on November 09, 2022. The map shows the stations of the Italian National Seismic Network operated by INGV (RSN; squares color-coded by operational status), and the installed SISMIKO temporary seismic stations (orange triangles).

For the 2024 Pietrapaola emergency (Figure 3) (3Q network code; Costanzo et al., 2024), high-resolution event mapping and associated location uncertainties could enable accurate tracking of swarm migration, allowing SISMIKO to focus resources on the most active areas and optimize station density where evolving seismicity is most critical.

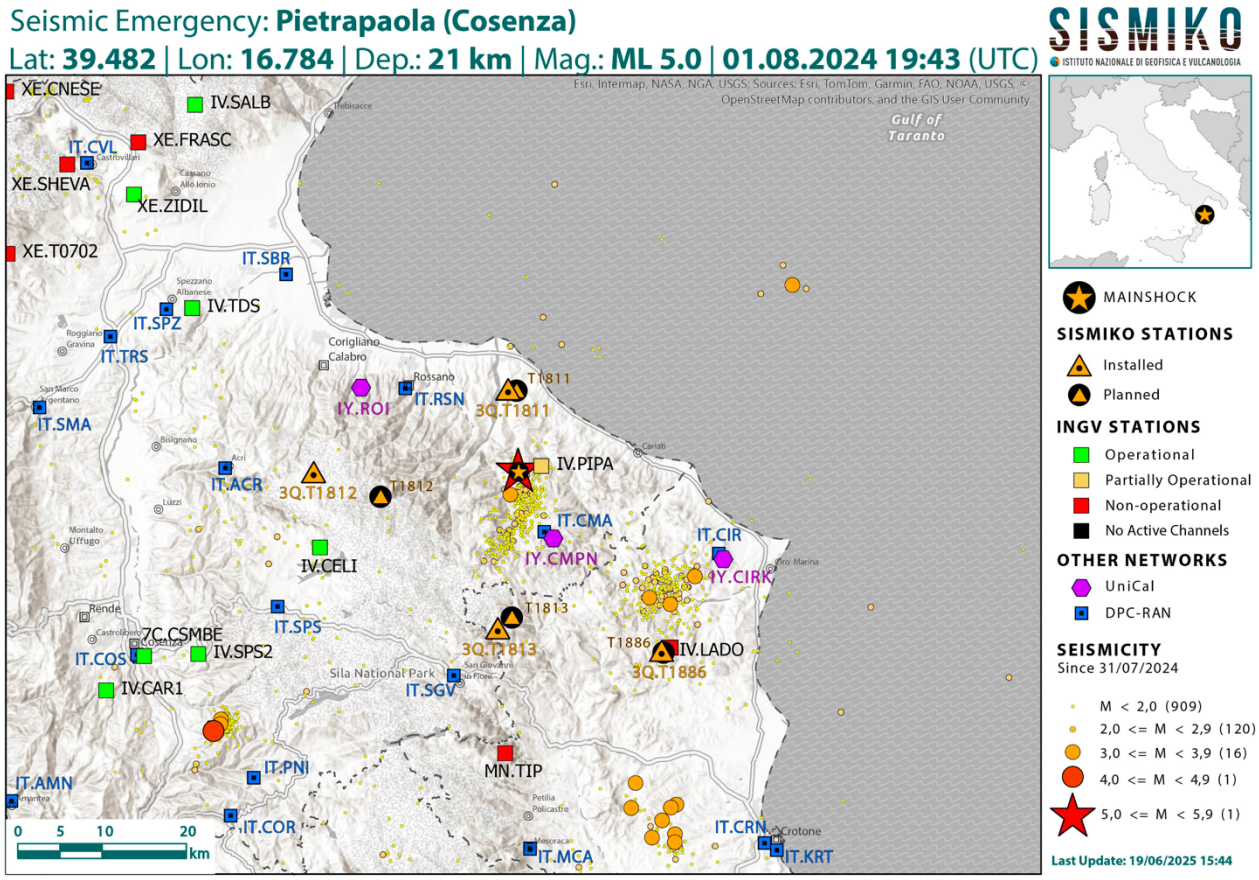

Fig. 3 – Cartographic report illustrating the distribution of seismic stations and recorded seismicity between 31 July 2024 and 19 June 2025. The map shows the epicenter of the mainshock (red star), the stations of the Italian National Seismic Network operated by INGV (RSN; squares color-coded by operational status), the stations of the National Accelerometric Network managed by the Italian Civil Protection Department (RAN; blue squares), those operated by the University of Calabria (purple hexagons), and the SISMIKO temporary seismic stations, both installed (orange triangles) and planned (orange triangles on a black background).

In summary, the implementation of this workflow facilitates a transition towards adaptive seismic monitoring strategies, in which the configuration and geometry of the seismic network are continuously and dynamically optimized in response to the spatiotemporal evolution of the ongoing seismic sequence. Such adaptability enables the network to maintain optimal station coverage as seismicity migrates or clusters, thereby enhancing the robustness and precision of hypocentral parameter estimation. Moreover, by improving detection capabilities and location accuracy in real-time, this approach contributes to increased catalogue completeness and reliability, providing a more comprehensive characterization of seismic processes.

References

Costanzo, A., Pastori, M., Cavaliere, A., D'Alema, E., Margheriti, L., Marzorati, S., Moretti, M., Piccinini, D., Anselmi, M., Bagh, S., Colasanti, M., Criscuoli, F., Falcone, S., Gervasi, A., La Regina, A., Migliari, M., Ruffo, A., Carluccio, I., & Locati, M.; 2025. The SISMIKO Monitoring Network and Insights into the 2024 Seismic Swarms on the Ionian Side of the Calabrian Arc. *Geosciences*, *15*(11), 436. https://doi.org/10.3390/geosciences15110436

Costanzo, A.; 2025. A New Catalogue and Insights into the 2022 Adriatic Offshore Seismic Sequence Using a Machine Learning-Based Procedure. Sensors 2025, 25, 82.https://doi.org/10.3390/s25010082

Costanzo, A., Pastori, M., Cavaliere, A., D'Alema, E., Margheriti, L., Marzorati, S., Moretti, M., Piccinini, D., Anselmi, M., Bagh, S., Colasanti, M., Criscuoli, F., Falcone, S., Gervasi, A., Migliari, M., Ruffo, A., Carluccio, I., & Locati, M.; 2024. INGV SISMIKO Emergency Seismic Network for Pietrapaola Sequence 2024 (Southern Italy) [Data set]. Istituto Nazionale di Geofisica e Vulcanologia (INGV). https://doi.org/10.13127/SD/O5PHM7WPKO

D'Alema, E., Alparone, S., Augliera, P., Biagini, D., Calamita, C., Castagnozzi, A., Cavaliere, A., Costanzo, A., Della Bina, E., Farroni, S., Galluzzo, D., Gasparini, A., Ladina, C., Lauciani, V., Mandiello, A. G., Margheriti, L., Marzorati, S., Moretti, M., Pantaleo, D., … Zuccarello, L. (2022). Seismic Data acquired by the SISMIKO Emergency Group - Northern Marche Coast - Italy 2022 - T17 [Data set]. Istituto Nazionale di Geofisica e Vulcanologia (INGV). https://doi.org/10.13127/SD/TBLKBA-3U6

INGV Seismological Data Centre; 2006. Rete Sismica Nazionale (RSN). Istituto Nazionale di Geofisica e Vulcanologia (INGV). Italy. doi:10.13127/sd/x0fxnh7qfy.

Moretti M., Margheriti L., D'Alema E. and Piccinini D.; 2023. SISMIKO: INGV operational task force for rapid deployment of seismic network during earthquake emergencies. Frontiers Earth Science 11:1146579. doi: 10.3389/feart.2023.1146579.

Pastori, M.; Falcone, S.; Moschillo, R.; Cavaliere, A.; Nardone, L.; D'Ambrosio, M.; 2025. SISMIKO: Strumenti operativi per la gestione delle emergenze sismiche sviluppati in ARCGIS. Rapp. Tec. INGV 2025, 499, 1–30. http://dx.doi.org/10.13127/rpt/499.

Corresponding author: marina.pastori@ingv.it

Dense seismic array in the Campi Flegrei (Italy) volcanic area for Seismic Microzonation purposes

G. Cultrera[1], L. Nardone[1], M. Vassallo[1], M. Carandente[1], S. Madonna[1], D. Galluzzo[1], G. Di Giulio [1], G. Riccio[1], S. Pucillo[1], D. Galluzzo[1], INGV team[1] (A. Bobbio, G. Brandi, G. Brunelli, F. Cara, A. Fedele, G. Gaudiosi, S. Hailemikael, A. Iorio, G. Lanzano, A. Mercuri, G. Milana, L. Minarelli, G. Soldati, M. G. Soldovieri, L. Valoroso)

[1] *Istituto Nazionale di Geofisica e Vulcanologia (Italy)*

Seismological measurements, especially those required for seismic microzonation, are inherently challenging to conduct in heavily urbanized areas. This difficulty is further amplified when the area in question is the Campi Flegrei (Italy), one of the world's most active and intensively studied volcanic regions. The area is defined by a large caldera, a formation resulting from massive prehistoric explosions. Over recent decades, this region has exhibited increasing seismic activity and bradyseism, and nowadays is characterized by an acceleration in both seismic tremors and the rate of ground uplift (Astort et al., 2024).

The Extraordinary Plan for urgent measures to prevent seismic risk releted to the bradyseism phenomenon in the Campi Flegrei area (as per decree-law no. 140 of 12 October 2023, converted into law no. 183 of 7 December 2023) led to a collaboration agreement between Istituto Nazionale di Geofisica e Vulcanologia (INGV) and the Department of Civil Protection (DPC). Within this framework, the INGV-CNR Geophysical Prospecting Unit (UR2) has been tasked with the objective of assessing the subsoil characteristics and the propagation velocities of seismic waves in the region.

The INGV addressed this issue through a major seismic measurement campaign in the municipalities of Pozzuoli, Bacoli, and Naples (Italy). A temporary seismic network, consisting of 60 nodes, was deployed approximately for one month from February 25 to March 28, 2025. Each node was equipped with a triaxial geophone (GS-ONE-LF, 4.5 Hz) and a 24-bit digitizer (GSB) with an integrated battery and GPS. Additionally, five seismic arrays were installed to determine shear-wave velocity profiles at the selected sites. Station placement (shown in Fig. 1) prioritized network geometry and accessibility, utilizing public spaces (e.g., schools, municipal offices, police stations, archaeological areas) and private areas.

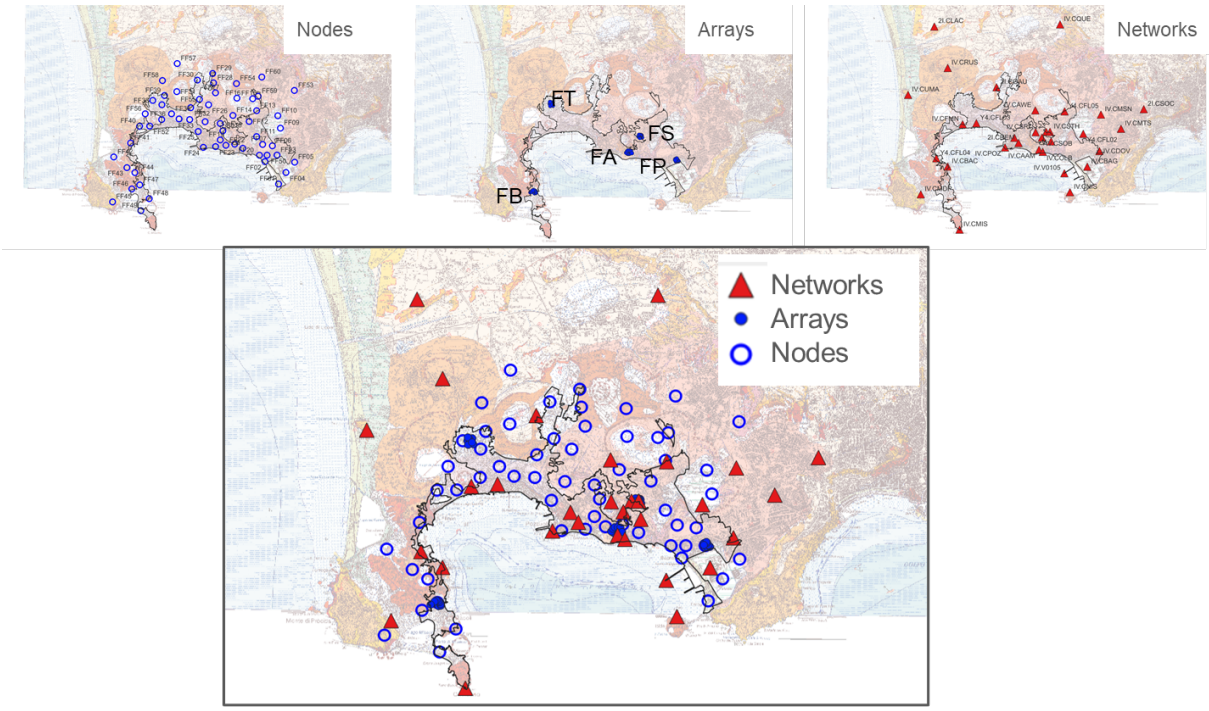

Fig. 1. Location of the 60 seismic nodes installed by INGV (Nodes) and the 5 arrays for the measurement of Vs profiles (Arrays). Also shown are the seismic stations of the permanent IV network (INGV, 2005) and the temporary networks (Galluzzo et al. 2024; https://www.fdsn.org/networks/detail/Y4_2024) present in the area (Networks) whose data were used in the analysis.

During this operation period, the seismic stations recorded over 380 earthquakes with duration magnitude (Md) ranging from values very close to zero to 4.6, the latter for the event of 13-03-2025 at 00:25:02 UTC. However, the observed noise levels were high, as expected in an urban context, similar to or slightly exceeding Peterson's High Noise Level (Peterson, 1993). Spectrograms and averaged values indicated day/night variations for periods shorter than 1 second (frequencies > 1 Hz), which are attributable to local anthropogenic sources. For longer periods (periods > 1 s; frequencies between 0.3 and 1 Hz), time variability was less regular and may be linked to meteorological conditions like wind and rain, or to coastal wave motion.

The continuous recordings from the 60 seismic nodes, along with 31 seismometers from temporary and permanent networks in the area (totaling 151 measurement points), were processed using the HVNEA software (Vassallo et al., 2022). This software automatically calculates the horizontal-to-vertical spectral ratios of the Fourier transform (H/V) using both earthquake or ambient noise data from continuous recordings. As already suggested by Nardone et al. (2025), preliminary findings concerning the fundamental resonance and predominant frequencies (the latter corresponding to the maximum H/V ratio amplitude) indicate that the lowest resonance frequencies, at about 0.3 Hz, are concentrated in the central portion of the caldera, while frequencies greater than 0.3 Hz characterize its edges.

References

Astort A., Trasatti E., Caricchi L. et al.; 2024: Tracking the 2007–2023 magma-driven unrest at Campi Flegrei caldera (Italy). Commun Earth Environ 5, 506. https://doi.org/10.1038/s43247-024-01665-4

Nardone L., Morelli R.S., Gaudiosi G., Liguoro F., Galluzzo D., Orazi M.; 2025: First Steps Towards Site Characterization Activities at the CSTH Broad-Band Station of the Campi Flegrei's Seismic Monitoring Network (Italy). Sensors, 25, 4787. https://doi.org/10.3390/s25154787

Peterson J.; 1993: Observation and modeling of seismic background noise. Open-File Rept. 93-322. U.S. Geological Survey, 94.

Vassallo M., G. Riccio, A. Mercuri, G. Cultrera, G. Di Giulio; 2022: HV Noise and Earthquake Automatic Analysis (HVNEA). Seismological Research Letters. https://doi.org/10.1785/0220220115 e https://github.com/INGV/hvnea

Corresponding author: giovanna.cultrera@ingv.it

Assessment of earthquake-induced road interruption in a virtual testbed

M. Di Domenico[1], P. Ricci[1], G.M. Verderame[1]

[1] *Department of Structures for Engineering and Architecture, University of Naples Federico II, Naples, Italy*

Introduction

In post-earthquake emergency management, roads play a crucial role, both in the immediate phase for population evacuation and in the subsequent phase for the circulation of emergency vehicles. Therefore, the development of tools aimed at predicting the probability that roads are obstructed under a given seismic scenario—based on refined structural analyses but sufficiently simple to be applied in large-scale risk assessments, even when limited data are available—is of great interest for several stakeholders, especially public authorities.

In a recent study (Di Domenico et al., 2025), a tool was developed, based on the results of nonlinear dynamic analyses performed on existing reinforced concrete buildings, to predict the probabilistic distribution of the amount of debris generated by out-of-plane collapse of infill walls for a given seismic intensity. In addition, the same tool allows the evaluation of the probabilistic distribution of the distance from the building façade at which such debris is deposited.

In the present study, this tool is applied, together with other methods available in the literature, to predict the probability of road obstruction in a virtual test site, considering both vehicular and pedestrian traffic.

Virtual Testbed and seismic scenario

Within the framework of the RETURN Project, a Virtual Testbed named *Returnland* has been defined. Within Returnland, two “imaginary” cities, referred to as *Returnville 1* and *Returnville 2*, have been developed.

Returnland is a virtual environment (Virtual Test Bed) that simulates a realistic but non-real ecosystem, designed to test and improve multi-risk analysis tools. It is constructed through the assembly of portions of the Italian territory and is characterized by heterogeneous morphologies and geological phenomena, including a submerged component along both coastlines. The territory

extends from coast to coast, featuring a central mountain range and two Returnville: one coastal and one inland. The coastal Returnville, exposed to hydraulic and marine hazards (floods, landslides, tsunamis, volcanic products), is located near a volcanic edifice. The inland Returnville, situated in an intramontane plain, is exposed to seismicity, ashfall, liquefaction, and debris flows. Returnland does not reproduce historical events; rather, it enables the application of tools within a coherent synthetic territory, allowing multi-hazard simulations in complex urban contexts.

The main objective is the development of a virtual demonstrator for the application and testing of analysis tools. The two Returnville have been designed in accordance with the morphology of Returnland, and the considered hazards are consistent with the geology of the same context. The relationship between Returnville and Returnland is not merely spatial: Returnland does not act as a simple urban container, but rather represents a landscape that generates complex physical phenomena, from which hazard and vulnerability conditions emerge. For this reason, during the construction of the Returnville it was not possible to directly import the real morphology of existing cities; instead, selected urban fragments were adapted to the geological and morphological context of the land, while preserving coherence and functionality.

The Returnville are composed of the aggregation of urban portions and city districts characterized by different geomorphological, demographic, and infrastructural conditions. They may also include infrastructure and functional networks (e.g. water supply systems, main road networks, urban drainage systems), and in the future they can be integrated with additional relevant elements such as schools, hospitals, industrial facilities, or cultural heritage assets. Infrastructure networks can be derived from benchmark networks already tested in previous studies and adapted to the morphology of the Returnville through the definition of demand nodes and functional constraints. This approach allows the simulation, through fragility and vulnerability models, of the impacts of natural or anthropogenic events (e.g. floods, earthquakes, industrial accidents), and the evaluation of metrics such as downtime and the propagation of effects on buildings and services.

The inland Returnville is located in the central-eastern sector of Returnland, within an intramontane plain crossed by a river and a railway line. In this case, the selection of urban portions was guided by the aim of representing settlements exposed to significant seismic risk. Reference cities include Rieti (historic city), Ascoli Piceno, Benevento, and Avellino (consolidated cities), as well as Gemona del Friuli and Pistoia (examples of dispersed urban systems). The estimated total population is approximately 38,000 inhabitants, with a building stock of about 4,000 buildings, evenly distributed between masonry and reinforced concrete structures. Also in this case, the DEM was adapted to ensure morphological continuity and coherence among the urban portions, while preserving the main characteristics of the original landscape.

Both Returnville are conceived as virtual environments suitable for hosting multi-hazard simulations. The present application in developed in Inland Returnville, where a seismic scenario is assumed with PGA ranging from 0.30 to 0.55 g.

Methodology

For the evaluation of the probabilistic distribution of the volume of infill debris projected onto the roadway from reinforced concrete buildings, reference was made to the vulnerability model proposed by Di Domenico et al. (2025) and developed within the RETURN project. Based on the results of nonlinear dynamic analyses performed on existing reinforced concrete (RC) buildings, in which infill walls are explicitly modelled by accounting for their response and potential out-of-plane expulsion, the model allows the estimation, for RC buildings of different construction periods and number of storeys, of the probabilistic distribution of both the volume of generated debris and its ejection distance, based on the scheme shown in Fig. 1.

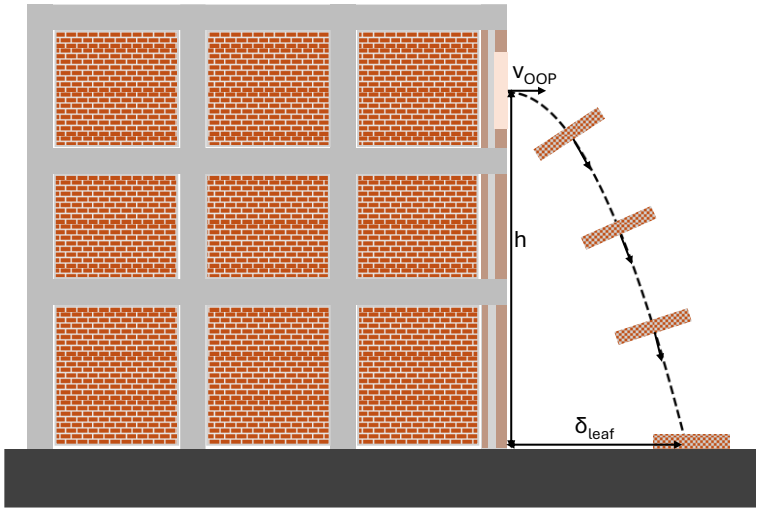

Fig. 1 – Schematic representation of the assumed mechanism of infill walls projection on the road.

The study focuses on reinforced concrete frame buildings subjected to seismic action. Through nonlinear dynamic analyses, both the expected volume of debris originating from infill walls and the corresponding projection distance from the building façade were estimated as a function of increasing seismic intensity.

Six buildings representative of existing Italian structures designed according to outdated seismic codes were modelled, varying construction age, number of storeys, and infill configurations. The results show that, with increasing seismic intensity, both the debris volume and the projection distance increase, but tend to reach a saturation level due to the nonlinear behaviour of the load-bearing structure, which limits the accelerations transmitted to the infill walls.

Key results include:

- The debris volume does not exceed 30% of the total infill volume in older buildings and 20% in more recent ones.

- The projection distance typically reaches up to 10% of the building height for older buildings and up to 25% for more recent ones.
- At the 84th percentile, these values can increase up to 50%.
- No debris generation is expected for PGA values lower than 0.10 g.

By normalizing the results with respect to the total infill volume and the building height, no clear trends related to the number of storeys or to the presence or opening ratio of infill walls emerge. These findings are particularly relevant for the assessment of road usability in emergency conditions, as even limited amounts of debris can significantly hinder evacuation and rescue operations.

Based on these results, a simplified predictive tool was developed to rapidly estimate debris volume and projection distance as a function of seismic intensity and construction age.

However, road interruption may be induced also by the collapse of masonry buildings. For the assessment of the probability of collapse of masonry buildings, fragility curves from the literature relating this probability to PGA for different typological classes were adopted. In particular, the fragility curves proposed by Rota et al. (2008) were used.

With reference to the masonry buildings surveyed in RV1 on the basis of ISTAT data, typological classes IMA2 and IMA6 (irregular layout and deformable diaphragms without ties) were assigned to all masonry buildings constructed before 1919; classes RMA2 and RMA6 (regular layout with deformable diaphragms without ties) were assigned to buildings dating from the 1919–1946 period; and classes RMA3 and RMA7 (regular layout with rigid diaphragms and/or ties) were assigned to buildings constructed after 1946.

Regarding roads' width, it was assumed that it is equal to 3.5 m in the historic center, 5.6 m in the consolidated city, 7 m in the diffued city. Sidewalks' width is assumed to be equal to 1 m in the historic center and 1.5 m in the consolidated and diffused city.

Based on Domaneschi et al. (2019) roads are assumed as obstructed to vehicles if the volume of debris deposited exceeds 0.24 m^3/m^2. Based on Lu et al. (2019), roads are assumed as obstructed if debris occupy at least the 25% of the road width.

Results

The probability of road interruption to vehicular traffic for the census units of Inland Returnville is shown in Fig. 2, while the proabability of road interruption to pedestrians is shown in Fig. 3.

As shown by the maps, the historic city centre is more sensitive to vehicular obstruction, due to the presence of older and more vulnerable buildings that generate larger amounts of debris. Conversely, the expansion area is more vulnerable to pedestrian obstruction, owing to the presence of taller

and more recent buildings, which produce smaller debris volumes but eject them at greater distances from the building façade, thereby occupying larger portions of the adjacent roadways.

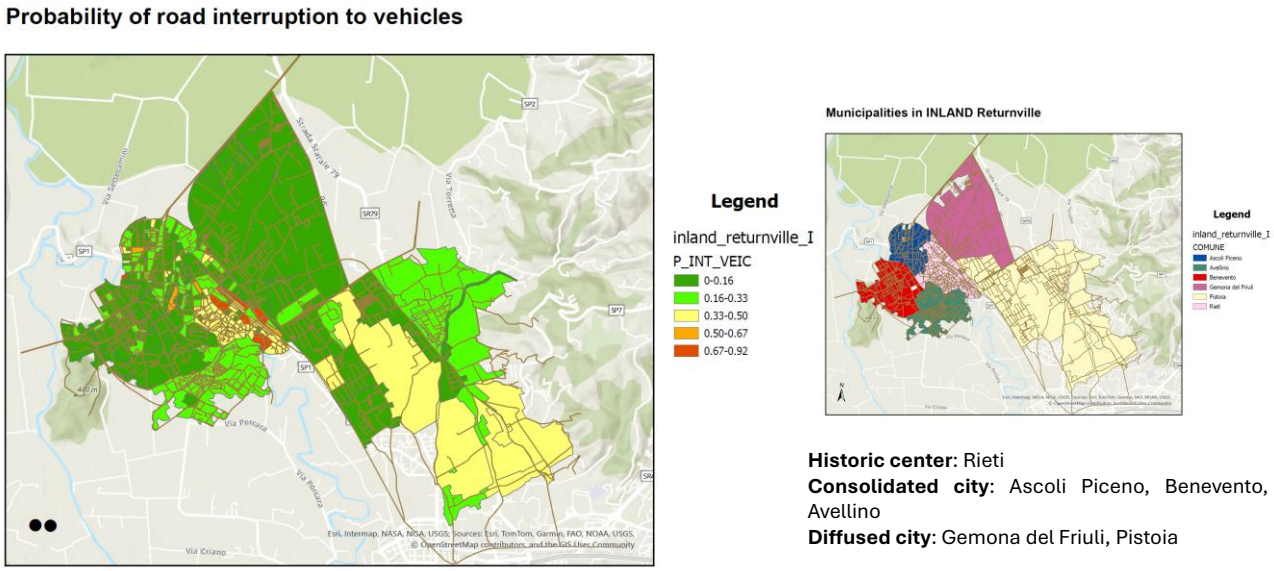

Fig. 2 – Map of probability of road interruption to vehicles in Inland Returnville under the assumed earthquake scenario.

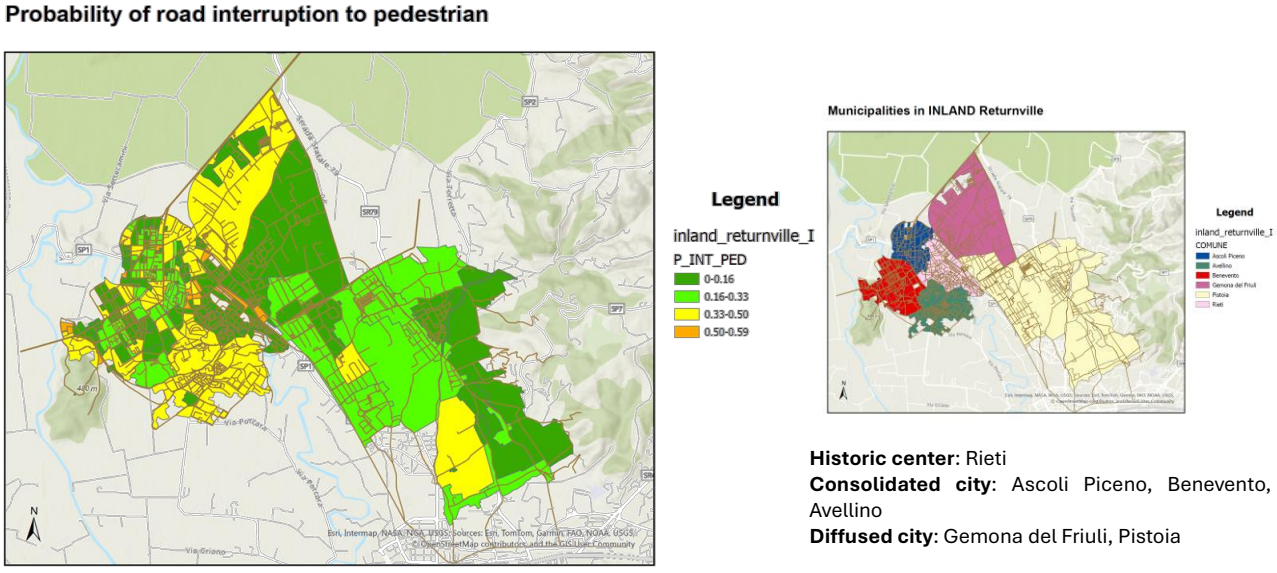

Fig. 3 – Map of probability of road interruption to pedestrians in Inland Returnville under the assumed earthquake scenario.

Acknowledgments

This work was developed under the financial support of RETURN - multi-Risk sciEnce for resilienT commUnities undeR a changiNg climate PE3 (Codice del Progetto di Ricerca approvato nell'ambito del PNRR: PE00000005 Codice Unico di Progetto (CUP): E63C22002000002), financed by European Union – NextGenerationEU within PNRR – MISSIONE 4:

ISTRUZIONE E RICERCA - COMPONENTE 2: DALLA RICERCA ALL'IMPRESA - Investimento 1.3 Creazione di "Partenariati estesi alle università, ai centri di ricerca, alle aziende per il finanziamento di progetti di ricerca di base".

References

Di Domenico, M., Ricci, P., Polese, M., Verderame G.M.; 2025: A tool to assess road interruption due to earthquake-induced collapse of infill walls in RC buildings. International Journal of Disaster Risk Reduction Vol. 128, https://doi.org/10.1016/j.ijdrr.2025.105707

Domaneschi, M., Cimellaro, G.P., Scutiero, G.; 2019: A simplified method to assess generation of seismic debris for masonry structures. Engineering Structures Vol. 186, pp. 306-320, https://doi.org/10.1016/j.engstruct.2019.01.092

Lu, X., Yang, Z., Cimellaro, G.P., Xu, Z.; 2019: Pedestrian evacutation simulation under the scenario with earthquake-induced falling debris. Safety Science Vol. 114, pp. 61-71, https://doi.org/10.1016/j.ssci.2018.12.028

Rota, M., Penna, A., Strobbia, C.L.; 2008: Processing Italian damage data to derive typological fragility curves. Soil Dynamics and Earthquake Engineering Vol. 28, n. 10-11, pp. 933-947, https://doi.org/10.1016/j.soildyn.2007.10.010

Corresponding author: mariano.didomenico@unina.it

Nonlinear static vs. dynamic seismic analysis of masonry aggregates: a case study in Southern Italy

R. Di Chicco[1], A. Formisano[1]

[1] Department of Structures for Engineering and Architecture, University of Naples "Federico II", Italy

Introduction

The seismic vulnerability assessment of historical centres represents a fundamental challenge for structural engineering, particularly when preserving the built heritage of high-seismicity regions like Southern Italy. The urban fabric of these medieval settlements is rarely constituted by isolated structures; rather, it is characterized by building aggregates, complex clusters of structural units that have merged and stratified over centuries. This physical continuity creates a unique structural system where the global seismic response is governed by the interaction between adjacent volumes, often distinguished by different heights, periods of construction, and material properties. In such a heterogeneous context, standard assessment procedures based on simplified assumptions may prove insufficient. While Nonlinear Static analysis is widely adopted in professional practice for its computational efficiency, it relies on invariant lateral load patterns that reduce the dynamic problem to an equivalent static one, potentially neglecting the effects of higher vibration modes and the progressive variation of dynamic properties during the shaking. Consequently, to ensure a rigorous safety evaluation, this study implements a comprehensive validation framework by integrating Nonlinear Dynamic Analysis. This methodology solves the full equations of motion in the time domain, offering a realistic simulation of the structural behaviour under actual ground motions. By explicitly accounting for the accumulation of damage and the hysteretic energy dissipation, the dynamic approach serves as an indispensable benchmark to verify the reliability of static procedures in predicting the seismic response of irregular masonry aggregates. The validation of the structural assessment relies on a synergistic comparison between the two types of analysis, allowing for a mutual verification of the numerical outcomes. Specifically, the time-history analysis is utilized to confirm the suitability of the control node selected for the static procedure, while the pushover curves serve as a benchmark to assess the quality and representativeness of the input seismic signals. This cross- check ensures that the resulting damage patterns are robust, providing a reliable foundation for the definition of targeted retrofitting strategies.

The case study aggregate

The study focuses on a representative masonry aggregate located within the medieval urban sector of Lavello - a small town in the Basilicata region of Italy- and it was selected through the CARTIS inventory tool (DPC-ReLUIS Italian research project) as a significant prototype of the local building stock. The structure exhibits a marked morphological irregularity, featuring a substantial longitudinal extension of approximately 43 meters and a variable elevation profile that ranges from one to three storeys above ground. This configuration is a critical vulnerability factor, as it induces stress concentrations and alters the distribution of seismic forces along the height. Furthermore, the aggregate shows a heterogeneity typical of spontaneous urban evolution: the vertical load-bearing structure combines portions of irregular rough stone masonry, found in the oldest nuclei of the town, with expansions constructed in regular tuff blocks (Figure 1). A distinguishing feature of this case study is the presence of relatively stiff horizontal diaphragms; unlike the flexible timber floors common in many historical centres, the levels here are predominantly composed of steel beams (IPE 140) with a 4 cm concrete topping. On the second and third floors, slabs made of reinforced concrete are also present.

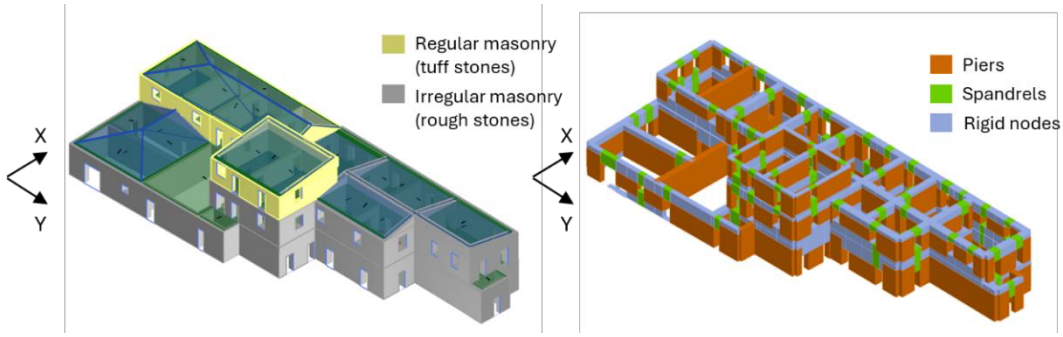

a) b)

Fig. 1 – (a) Three - dimensional model and (b) Macroelement model of the aggregate under study, developed using the 3Muri software.

This detail is pivotal for the numerical modelling, as it ensures a box-like behaviour that effectively redistributes horizontal actions among the shear walls. The structural analysis, performed using the equivalent frame method (3Muri software), highlighted the following dynamic behaviour. The modal analysis revealed a significant decoupling of the principal modes: the first vibration mode is translational in the X-direction, activating 68% of the total mass, while the response in the Y-direction is governed by the third mode, which involves 59% of the total mass. Despite the irregularity in height, the mass participating in the first vibration mode is high, demonstrating the uniform dynamic behaviour of the structure, in which the third-level tower is not characterised by significant local modes.

Seismic assessment: nonlinear static vs. dynamic analysis

The Nonlinear Dynamic Analysis was conducted using a set of 7 spectrum-compatible accelerograms, scaled to match the Life Safety Limit State (SLV) for the site. Moreover, the accuracy of this method relies heavily on the definition of the constitutive law for the masonry macro-elements. The numerical model adopts a sophisticated phenomenological hysteretic model capable

of describing the material's cyclic behaviour beyond the elastic range. Crucially, this model incorporates stiffness degradation as a function of the maximum ductility demand and simulates hysteretic damping through specific unloading and reloading rules (e.g., Takeda-like relationships). This allows the simulation to capture the energy dissipation capacity of the masonry through friction and crack opening, which is the primary mechanism for reducing seismic demand in unreinforced structures. Parallelly, to generate a capacity envelope, 24 Pushover analyses were performed according to NTC2018 standards, utilizing both uniform and static forces load distributions. The design spectrum- for the evaluation of the displacement demand - was defined in accordance with the NTC2018 provisions, accounting for the local site conditions by assuming soil category B and topographic class T1. The validation of the static approach is presented through two key comparisons in terms of seismic demand and seismic capacity. Firstly, the in- plane damage patterns recorded at the maximum displacement (*dmax*) required by the pushover are juxtaposed with that one's corresponding to the peak displacement from the dynamic analyses, revealing a strong consistency in both the location and type of failure mechanisms (Figure 2). It is also important to note that the *dmax* calculated in the non-linear static analysis depends on the control node selected and Pushover analysis applies seismic load distribution separately in the two directions of the structure, while Time history applies accelerograms simultaneously in both directions. Therefore, the control node chosen at the second level of the structure and not below the third-level tower proved to be suitable for capturing the structure's response.

a)

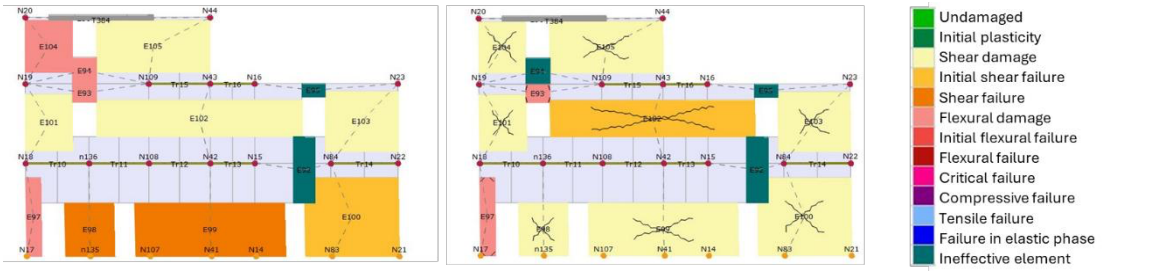

Time history analysis Pushover analysis (X- direction)

b)

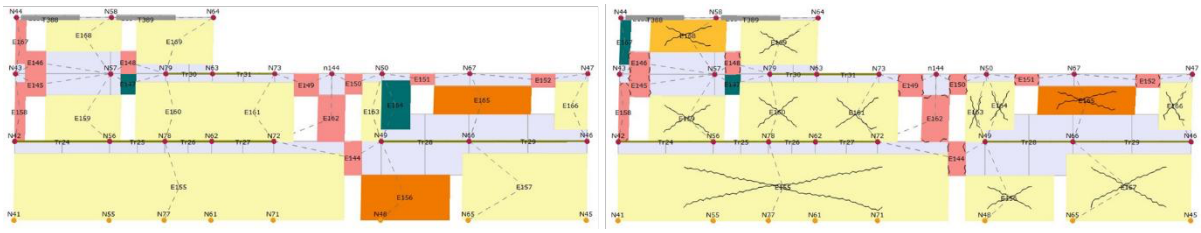

Time history analysis Pushover analysis (Y-direction)

Fig. 2 – Comparison of the in- plane damage mechanisms at demand displacement (*dmax*) between Time history and Pushover analyses: (a) X- direction wall (b) Y-direction wall.

Secondly, the global hysteretic loops obtained from the time-history integration are superimposed onto the static capacity curves. For this purpose, a seismic event representative of the set was

chosen; moreover, the X-direction was chosen for the pushover curves because it governs the structure's first mode. The analysis demonstrates that the static capacity curve effectively envelopes the dynamic hysteretic cycles, acting as a reliable boundary for the structural response, especially in terms of base shear. This confirms that, when the specific hysteretic behaviour of the masonry is adequately modelled, the Pushover analysis provides a robust estimation of the seismic response, mutually validating the results of the more complex dynamic simulations (Figure 3). The comparison also shows slightly how load distribution proportional to static forces is more representative of the behaviour of the structure in the elastic phase, while uniform load distribution is more representative of the deterioration phase. Moreover, especially in the negative direction, the static analysis overestimated the displacement capacity of the aggregate, implying a deformation reserve that does not actually exist under dynamic conditions. This discrepancy is caused by cyclic degradation. While Pushover analysis relies on monotonic loading, Time-History analysis subjects the material to load reversals. Consequently, a masonry wall may fail prematurely due to cumulative damage (or low-cycle fatigue), even before reaching the theoretical ultimate displacement (du) predicted by the static curve.

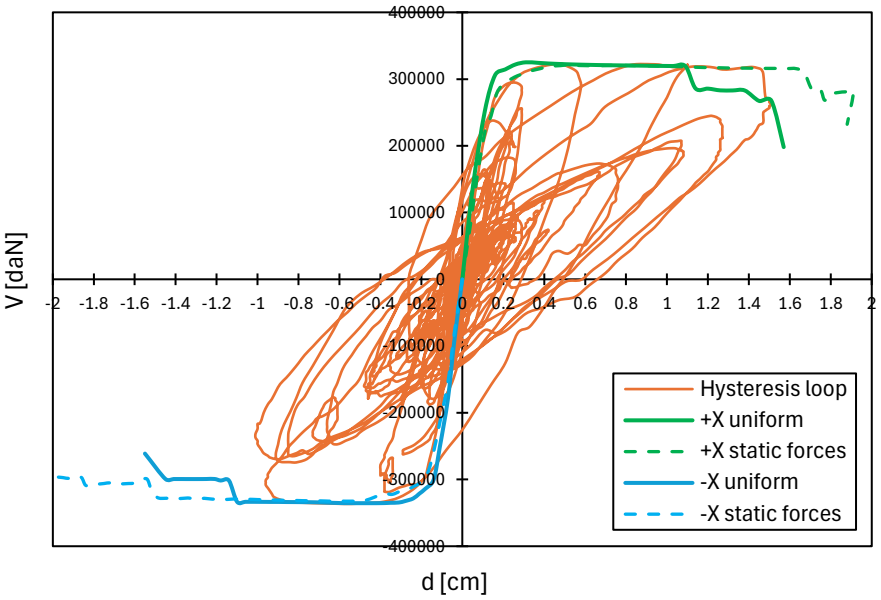

Fig. 3 – Comparison between the capacity curves obtained from pushover analysis (uniform and static load distributions) and the hysteresis loop derived from the time history analysis.

Acknowledgments

The Authors would like to acknowledge the DPC-ReLUIS 2024-2026 research project (WP4 research line) for the financial support to the current research activity.

References

Brando G., Cianchino G., Rapone D., Spacone E., Biondi S.; 2021: A CARTIS-based method for the rapid seismic vulnerability assessment of minor Italian historical centres. Int. J. of Disaster Risk Reduction.

Lagomarsino S., Cattari S., Ottonelli D.; 2021: The heuristic vulnerability model: fragility curves for masonry buildings. Bull. Earthquake Engineering.

Di Trapani, F., Villar, S., Di Benedetto, M., Petracca, M., Camata, G., 2024. Seismic response of unreinforced masonry building aggregates: Investigation on the "aggregate-effect" based on an elementary building aggregate. Engineering Structures 316, 118301.

Pinasco, S., Lagomarsino, S., Cattari, S., 2025. Unreinforced masonry buildings in aggregate of urban settlements: Current approaches and critical issues for the seismic vulnerability assessment. Structures 73,108335.

Angiolilli, M., Lagomarsino, S., Cattari, S., Degli Abbati, S., 2021. Seismic fragility assessment of existing masonry buildings in aggregate. Engineering Structures 247, 113218.

Corresponding author: roberta.dichicco@unina.it

A Harmonized Toolkit for Disaster Preparedness: Simulating Emergency Response System Performance in Cross-Border Urban Areas.

B. Di Napoli[1], S. Cattari[2], M. Lazzati[2], M. Dolšek[3], N. Fazarinc[3], N. Rebora[4], D. Ottonelli[4], B. Borzi[5], M. Faravelli[5], M. Polese[6]

[1] Reluis, Italy
[2] University of Genova, Italy
[3] University of Ljubljana, Slovenia
[4] CIMA Research Foundation, Italy
[5]Eucentre Foundation, Italy
[6] University of Naples Federico II, Italy

Within the BORIS2 project a methodology and tool to for assessing seismic, flood and multi-hazard risk in cross-border areas and referring to different territorial scales (from municipal to sub-municipal) were proposed, with the main aim to support decision-makers in disaster risk management and with a focus on preparedness and planning. This paper describes the operational implementation of the BORIS2 framework, in particular referring to the step 4 of the BORIS2 methodology, allowing the simulation of the Emergency Response System (ERS) to support emergency planning.

The BORIS2 framework: from BORIS to BORIS2

The BORIS2 project (G.A. n. 101140181) is a follow up of the former BORIS project (G.A. n. 101004882 – Polese et al., 2024), which proposed a methodology and a web-platform for harmonized multi-risk assessments and comparison of seismic and flood risks in cross-border regions. While BORIS focused on analysis at municipality scale finalized at multi-risk analysis in large cross-border areas, BORIS2 builds up on BORIS outcomes to develop a methodology and related web-platform that allows to evaluate consequences more relevant for emergency planning, including evaluation of strategic Emergency Management System units (EMS units) such as hospitals and emergency shelters on a municipal or sub-municipal territorial basis towards better planning of emergency response. The methodology provides a structured, four-step procedure that transitions from probabilistic territorial risk assessment to the deterministic simulation of municipal-level emergency response performance.

Overview of the four-steps methodology

In this section, the BORIS2 methodology is briefly synthetised, while a more thorough description may be found in D4.1 (BORIS2, 2025).

The framework integrates exposure, hazard, vulnerability models and consequence functions into an actionable tool to support decision-makers. The methodology is organized in 4 steps (See Fig. 1):

- **STEP 1: Time-based Risk Assessment and Intensity-based Loss Estimation for Residential Buildings.** Utilizing a harmonized 250m x 250m territorial grid, this phase performs risk analyses for seismic, flood and compound hazard. In this phase only residential buildings and population are included in the exposure model. Considering the consequences more relevant for Disaster Risk Management (DRM) – i.e. casualties, potentially injured, homeless people – with either a time-based or intensity-based approach, it is possible to identify "risk-based hotspots" defined as urban areas with the most adverse expected consequences.
- **STEP 2: Definition of Earthquake, Flood and Compound Hazard Scenarios.** Stakeholders define physically plausible events based on target return periods (Approach A) or target consequences (Approach B). This includes single-hazard scenarios and compound (multi-hazard) events, where hazards occur in rapid succession.
- **STEP 3: Scenario-based Loss Estimation for the Affected Area.** The exposure model is expanded to include strategic EMS units (hospitals, emergency shelters, coordination centers) and the risk analysis is performed based on the selection of a specific hazard scenario identified in the previous step. Specialized vulnerability models are introduced to estimate the physical response of the EMS units. Depending on the data availability they can either be developed in customized building-specific fragility models (Fazarinc, 2023) or adopted from models already available in literature, i.e. Cattari et al. (2024), Casotto et al. (2015) and Shooraki et al. (2024) – for seismic assessment – Nirandjan et al. (2024) and FEMA (2013) – for flood assessment.
- **STEP 4: Emergency Response System and Emergency Management System‘s Performance Assessment at the Municipal Level.** This final step allows to evaluate the Emergency Response System (ERS) at the municipal level, allowing for the identification or definition of the best-performing ERS in terms of demand to capacity ratio (e.g. the number of beds required for emergency sheltering, that is the demand, versus the number of beds available for emergency sheltering, that is the capacity). Indeed, based on the results of the scenario analysis performed in step 3 for the selected *hotspot*, the functionality of each element of the ERS can be evaluated and the available capacity to perform the response activity (e.g. the sheltering) can be compared to the effective demand of response. The step 4 is described more in detail in the next paragraph.

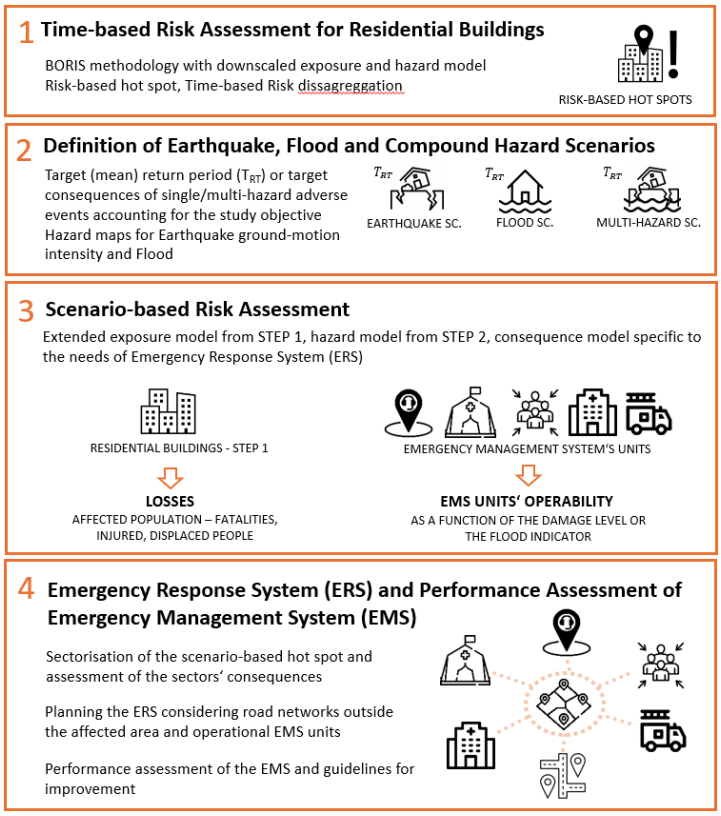

Fig. 1. Overview of the four-step BORIS2 methodology.

STEP 4: Non-mechanistic simulation of the ERS to support emergency planning

Definition of consequence functions

STEP 4 bridges the gap between traditional, methodologically well established, risk analysis results and actionable preparedness strategies. It shifts from mechanistic modelling to a simulation of the ERS, focusing on the interactions between survivors, responders, and infrastructure.

The operativity assessment establishes consequence functions that translate physical damage (derived from STEP 3) into meaningful indicators of usability for emergency purposes. For building-type EMS units, operativity is linked to the Serviceability Limit State, meaning the asset must not experience significant damage or utility interruptions that compromise its function immediately after the event.

To facilitate communication between technical experts and civil protection stakeholders, a traffic-light scale is adopted:

- **Green**: High probability the EMS unit or road is operational;
- **Yellow**: Medium probability the EMS unit or road is operational;
- **Red**: Low probability the EMS unit or road is operational – the asset is likely non-functional due to severe damage or obstruction of the road.

Table 1 – Overview of the damage thresholds adopted for building-type EMS units

Probability of Operability	**Seismic damage threshold (μ_D)**	**Flood damage threshold (DR)**
HIGH (green)	μ_D<0.35	DR<0.15
MEDIUM (yellow)	0.35<μ_D<0.70	0.15<DR<0.40
LOW (red)	μ_D>0.70	DR>0.40

For seismic events, operability is linked to mean damage (μ_D) thresholds computed referring to damage levels graduated according to the EMS-98 scale – Grünthal, 1998 from D0 to D5. For building-type EMS units, a μ_D<0.35 (corresponding to a strong limitation of the probability of exceeding damage D1 and D2) indicates a high probability of operability, whereas μ_D>0.70 signals low operability.

Similarly, for road networks a traffic-light scale was adopted corresponding to a HIGH/MEDIUM/LOW probability of being un-obstructed. For consistency, an approach based on thresholds defined on μ_D for seismic scenarios was adopted. In case of flood scenarios, the traffic-light scale was defined in function of the expected water depth, according with what was proposed by Khalil (2022), setting a 4-meter buffer around each road tract that although not incorporating vulnerability or fragility models it has the advantage of providing differentiated impact levels, similar to seismic risk assessments.

For seismic scenarios, the damage thresholds represent the likelihood of a road tract of being passable considering the damage of the adjacent buildings. Thresholds vary by structural typology to account for different collapse mechanisms. Masonry buildings are assigned higher thresholds (μ_D<2.5 for high operability) because road obstruction usually requires higher damage levels or global collapse. Conversely, reinforced concrete (RC) buildings have more restrictive thresholds (μ_D<1.6) due to the risk of infill wall overturning, which can block narrow streets even at lower global damage states.

Evaluation of functional capacity

Step 4 evaluates whether the capacity of the functional system (e.g., available shelter beds, hospital capacity) can accommodate the needs (e.g., number of displaced or injured persons) generated by the scenario.

Through the interactive use of the platform developed within BORIS2 project, the end-user can cross check the results from the risk assessment coming from the selected scenario in terms of consequence on population who might need assistance and interactively select the relevant and needed EMS structures based also on the information of their expected operability following the same scenario.

Different non-mechanical processes can be modelled:

- PROCESS 1: Focused on unharmed population generally defined as the total displaced people (short-term and long-term) following a hazardous event. This process helps the identification of the gathering areas (GATH) and the shelters (SHEL) based on their functionality check and their maximum capacity. It also provides an insight into the mass transportation units (MASS) implied for transferring healthy displaced people from the scenario-based hotspot to the safe sheltering area. The process is conceptualized in Figure 2, in which the "Total displaced population" is intended to dislocate autonomously to the selected GATH, which should be reached by the MASS originating by the ECC, and be transferred to selected SHEL via multiple repetitions.
- PROCESS 2: Focused on potentially injured population, intended as the sum of the expected injured people and fatalities since, to the ends of emergency planning, also an expected fatality should be considered in need of intervention of search and rescue teams and medical assistance until death declaration. This process helps the identification of hospitals (HOSP) and search and rescue centers (S&R) based on their functionality check and maximum capacity (e.g. number of beds for HOSP and the number of available teams for S&R). It also provides insight into the emergency vehicles for search and rescue (TEAM) or for medical aid (AMB) implied. In Figure 3, a conceptualization of the process is provided, bearing in mind that whenever the number of potentially injured people is higher than zero in the considered sector, this should be considered an "intervention site" which must be reached by the S&R and medical teams. The actual intervention site would be a specific building under a particular damaged condition. Because the analysis does not allow for more refined information and for simplicity reasons, it can be considered the geometrical center of the sector.

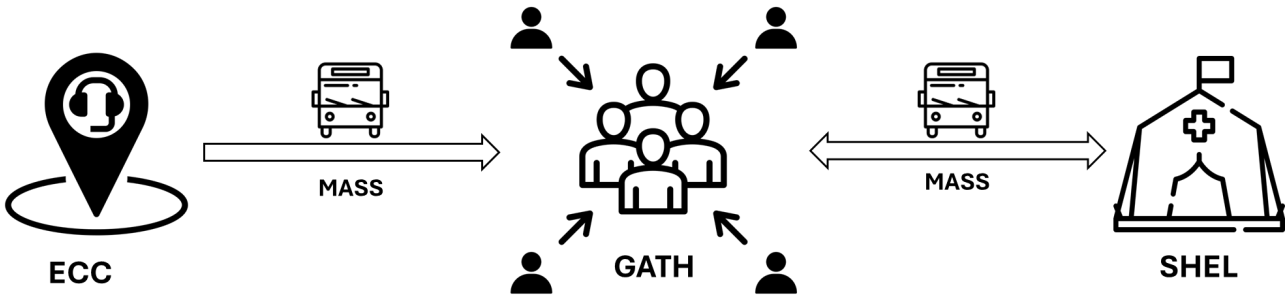

Fig. 2 – Conceptualization of PROCESS 1

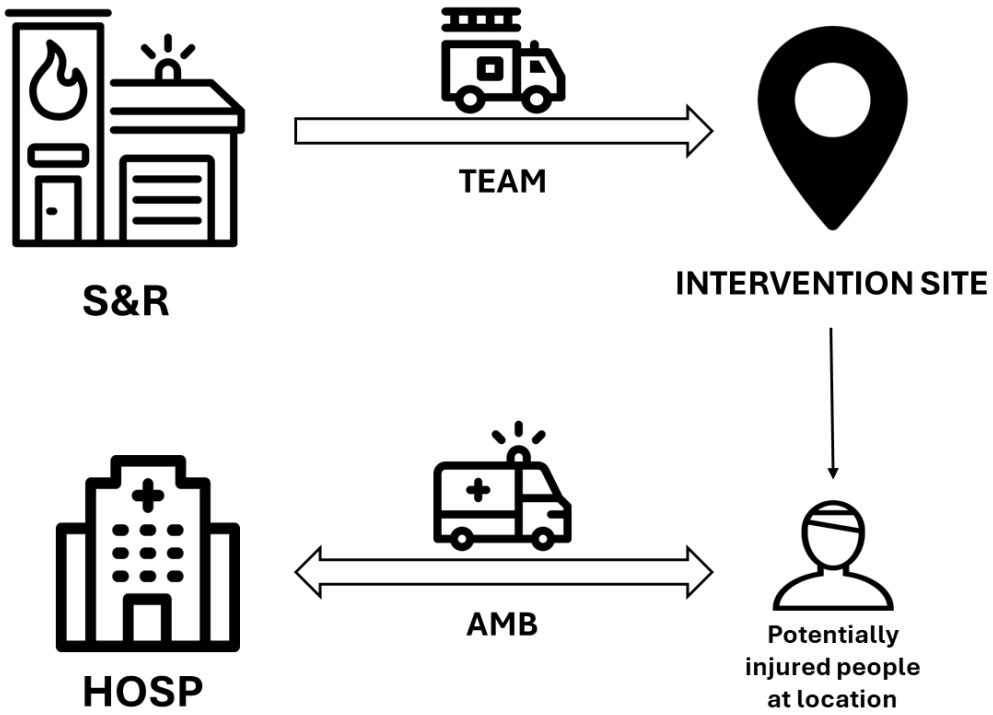

Fig. 3 – Conceptualization of PROCESS 2

The framework acknowledges that structural integrity does not equal functional readiness. Whenever this information is available, the methodology enhances the incorporation of additional information on operational vulnerability – capacity to effectively perform the intended function – such as:

- Redundancy of critical assets such as power generators, water supply, medical gases for hospitals;
- Safety of non-structural elements that also have a role in critical contents (i.e. medical equipment).

Conclusions

Step 4 of the BORIS2 methodology transforms traditional risk assessment techniques into a comprehensive toolkit for civil protection and urban planning. By connecting the expected consequence on population with actual response and operational capacity of the structures intended to provide aid during an emergency phase following an hazardous event, it provides clear guidance for targeted emergency planning and, eventually, mitigation and retrofitting. Ultimately, this framework supports the development of digital models for preparedness, allowing municipalities to simulate and enhance their response capabilities in both single and compound hazard environments.

Acknowledgements

This contribution was performed in the framework of EU project “BORIS2 - Cross Border RISk assessment for increased prevention and preparedness in Europe: way forward” co-funded by the European Union Civil Protection UCPM-2023-KAPP-PV Grant Agreement nr: 101140181.

References

Casotto, C., Silva, V., Crowley, H., Nascimbene, R., & Pinho, R.; 2015: Seismic fragility of Italian RC precast industrial structures. Engineering Structures, vol. 94, pp. 122–136, https://doi.org/10.1016/j.engstruct.2015.02.034

Cattari, S., Alfano, S., Manfredi, V., Borzi, B., Faravelli, M., di Meo, A., da Porto, F., Saler, E., Dall’Asta, A., Gioiella, L., di Ludovico, M., del Vecchio, C., del Gaudio, C., Verderame, G., Gattesco, N., Boem, I., Speranza, E., Dolce, M., Lagomarsino, S., & Masi, A.; 2024: National risk assessment of Italian school buildings: The MARS project experience, International Journal of Disaster Risk Reduction, vol. 113, pp. 104822, https://doi.org/10.1016/j.ijdrr.2024.104822

BORIS2; 2025: Methodology for single risk and multi-risk urban assessment to support emergency condition evaluation, Deliverable 4.1, April 2025, 101140181 — BORIS2 — UCPM-2023-KAPP-PV, Project co-funded by the European Union Civil Protection

Fazarinc, N., Babič, A., & Dolšek, M.; 2023: Parametric pushover curve model for seismic performance assessment of building stock, Bulletin of Earthquake Engineering, https://doi.org/10.1007/s10518-023-01821-9

Grünthal, G.; 1998: “European macroseismic scale 1998 (EMS-98) Europeanseismological commission, sub commission on engineering seismology, working groupmacroseismic scales” in Conseil de l’Europe, Cahiers du Centre Européen deGéodynamique et de Séismologie, vol. 15 (Luxembourg).

Fazarinc, N., Babič, A., & Dolšek, M.; 2023: Parametric pushover curve model for seismic performance assessment of building stock, Bulletin of Earthquake Engineering, https://doi.org/10.1007/s10518-023-01821-9

Khalil, R.; 2022: A new approach to determine the flood hazard impact on road network using 3D city model, Journal of Engineering Sciences, vol. 50(5), pp. 263-275, https://doi.org/10.21608/jesaun.2022.140556.1140

Nirandjan, S., Koks, E. E., Ye, M., Pant, R., Van Ginkel, K. C. H., Aerts, J. C. J. H., Ward, P. J.; 2024: Physical vulnerability database for critical infrastructure hazard risk assessments – a systematic review and data collection, Nat. Hazards Earth Syst. Sci., vol. 24, pp. 4341–4368. https://doi.org/10.5194/nhess-24-4341-2024

Polese, M., Tocchi, G., Babič, A., Dolšek, M., Faravelli, M., Quaroni, D., Borzi, B., Rebora, N., Ottonelli, D., Wernhart, S., Pejovic, J., Serdar, N., Lebar, K., Rusjan, S., Masi, R., Resch, C., Kern, H., Cipranić, I., Ostojic, M., & Prota, A.; 2024: Multi-risk assessment in transboundary areas: A

framework for harmonized evaluation considering seismic and flood risks, International Journal of Disaster Risk Reduction, vol. 101, pp. 104275, https://doi.org/10.1016/j.ijdrr.2024.104275

Shooraki, M. K., Bastami, M., Abbasnejadfard, M., & Motamed, H.; 2024: Development of seismic fragility curves for hospital buildings using empirical damage observations, International Journal of Disaster Risk Reduction, vol. 108, https://doi.org/10.1016/j.ijdrr.2024.104525

Corresponding author: beatrice.dinapoli1992@gmail.com

Assessing the Effectiveness of FinDer-Based Earthquake Early Warning in Northeastern Italy

Fangqing Du[1], Elisa Zuccolo[2], Stefano Parolai[3], Maren Böse[4], Carlo Giovanni Lai[5]

[1] *University School for Advanced Studies IUSS Pavia, Italy*
[2] *National Institute of Oceanography and Applied Geophysics - OGS, Italy*
[3] *Department of Mathematics and Geosciences, University of Trieste, Italy*
[4] *Swiss Seismological Service (SED), ETH Zurich, Switzerland*
[5] *Department of Civil Engineering and Architecture, University of Pavia, Italy*

Effective Earthquake Early Warning (EEW) systems are crucial in earthquake-prone regions to mitigate seismic risk. The Finite fault rupture Detector (FinDer) algorithm (Böse et al., 2012, 2015, 2018, 2023) enables rapid estimation of the location, extent, and orientation of an ongoing earthquake fault rupture by comparing the observed spatial distributions of high-frequency seismic amplitudes with a library of pre-calculated templates derived from empirical ground motion models. Northeastern (NE) Italy—characterised by predominant reverse-faulting setting capable of generating moderate-to-strong seismicity—has been identified as one of the regions with the highest relative feasibility index in Europe (Cremen et al., 2022), thus offering a meaningful and challenging testbed for assessing how well FinDer can support regional EEW.

FinDer's real-time behaviour shows that it can reliably locate events and provide consistent magnitude estimates, while also revealing limitations related to rupture strike determination for small earthquakes ($M_W < 4.5$) and to telemetry latencies in the current seismic station network that can delay alerts.

We also investigate the potential and limitations of a FinDer-based regional EEW system for NE Italy with offline playback tests for moderate-to-large historical events ($5.5 < M_W < 6.7$), exploring the impact of network density and site effects. The results show that FinDer is effective in characterising the extent and location of fault rupture in the offline playback tests, but highlight the need for further improvements in rupture-orientation determination. Moreover, offline test results indicate that increasing station density enhances FinDer's ability to estimate rupture parameters accurately, and underscore the importance of accounting for site effects at least through simplified amplification factor-based adjustments.

Finally, the obtained playback lead times are compared with the expected damage to unreinforced masonry buildings in the main municipalities of NE Italy. For some specific historical earthquake scenarios, FinDer could provide non-negligible lead times before the onset of shaking levels associated with the slight structural damage to typical unreinforced masonry buildings.

In summary, findings in this study suggest that a properly configured FinDer-based EEW system, supported by real-time telemetry, could offer meaningful benefits for seismic-risk mitigation in NE Italy.

References

Böse, M., Heaton, T. H., & Hauksson, E.; 2012: Real-time Finite Fault Rupture Detector (FinDer) for large earthquakes. Geophysical Journal International Vol. 191, n. 2, pp. 803–812, https://doi.org/10.1111/j.1365-246X.2012.05657.x

Böse, M., Felizardo, C., & Heaton, T. H.; 2015: Finite-fault rupture detector (FinDer): Going Real-Time in Californian ShakeAlert Warning System. Seismological Research Letters Vol. 86, n. 6, pp. 1692–1704, https://doi.org/10.1785/0220150154

Böse, M., Smith, D. E., Felizardo, C., Meier, M. A., Heaton, T. H., & Clinton, J. F.; 2018: FinDer v.2: Improved real-time ground-motion predictions for M2–M9 with seismic finite-source characterization. Geophysical Journal International Vol. 212, n. 1, pp. 725–742, https://doi.org/10.1093/GJI/GGX430

Böse, M., Andrews, J., Hartog, R., & Felizardo, C.; 2023: Performance and Next-Generation Development of the Finite-Fault Rupture Detector (FinDer) within the United States West Coast ShakeAlert Warning System. Bulletin of the Seismological Society of America Vol. 113, n.2, pp. 648–663, https://doi.org/10.1785/0120220183

Cremen, G., Galasso, C., & Zuccolo, E.; 2022: Investigating the potential effectiveness of earthquake early warning across Europe. Nature Communications Vol. 13, n. 1, pp. 1–10, https://doi.org/10.1038/s41467-021-27807-2

Corresponding author: fangqing.du@iusspavia.it

Seismic vulnerability of a historic minaret in Old Cairo: an integrated geosciences and earthquake engineering approach

Marco Fasan[1], Hany M. Hassan[2,3], Hesham E. Abdel Hafiez[3], Chiara Bedon[1], Fabio Romanelli[4]

[1] Department of Engineering and Architecture, University of Trieste, Trieste, Italy
[2] Istituto Nazionale di Oceanografia e di Geofisica Sperimentale –OGS Centro di Ricerche Sismologiche, Italy
[3] National Research Institute of Astronomy and Geophysics, Cairo, Egypt
[4] Department of Mathematics, Informatics and Geosciences, University of Trieste, Trieste, Italy

Introduction

Historic masonry structures located in regions characterized by moderate to high seismicity are known to be highly vulnerable to earthquake-induced damage, as demonstrated by recent events in the Mediterranean and Middle Eastern areas. The preservation of such structures represents a major challenge, especially when detailed information on material properties, construction techniques, and seismic input is limited. In many historical urban centres, including Old Cairo, the scarcity of local accelerometric recordings further complicates seismic risk assessment.

Advanced numerical modelling, experimental investigations, and integrated diagnostic approaches are therefore essential to support risk-informed conservation strategies (Masciotta et al. 2017). Within this framework, the Italy–Egypt bilateral project “CoReng” proposes an interdisciplinary methodology that integrates geosciences, earthquake engineering, and structural modelling for the seismic assessment of historic monuments in the Religions Complex in Old Cairo (Hassan et al. 2025). A key aspect of the proposed approach is the use of physics-based ground motion simulations (PBGMS) to define site-specific seismic input in the absence of instrumental data (Vaccari 2025, Chieffo et al. 2021, Panza et al. 2012), , coupled with refined finite element (FE) models calibrated through experimental dynamic identification.

This paper presents the application of the CoReng strategy to the minaret of the Madrasa of Princess Tatar al-Higaziya. The objective is to assess its seismic vulnerability by comparing displacement demand derived from synthetic ground motions with the structural capacity obtained from nonlinear static analyses.

Case-study structure

The investigated minaret is part of a historic complex originally constructed as a mausoleum in 1348 and converted into a madrasa in 1360. The structure rises approximately 24 m and is characterized by a square base transitioning into an octagonal shaft with chamfered corners. The upper termination is missing, likely as a consequence of past seismic events or progressive damage accumulation.

The minaret is not a freestanding structure, as it is partially restrained at its base by adjacent masonry walls. This interaction significantly affects its dynamic behaviour and must be properly accounted for in the structural model. The site is located within a seismically active area and has undergone several restoration campaigns, including interventions following the 1992 Cairo earthquake, during which the minaret exhibited limited damage.

Seismic hazard modelling

Seismic input for the analyses was defined using physics-based ground motion simulations. This approach relies on a kinematic extended source model capable of reproducing rupture processes, directivity effects, and the variability associated with fault mechanics. Synthetic accelerograms were generated through a two-step procedure involving the simulation of fault rupture and the propagation of seismic waves in a layered crustal model.

Four earthquake scenarios were considered, characterized by two moment magnitudes (Mw 5.8 and Mw 6.5) and two focal depths (10 km and 20 km), consistently with previous studies on seismic hazard in the Cairo region (Hassan et al. 2017, 2020). The first two scenarios aim to reproduce the 1992 Cairo earthquake, accounting for uncertainties in focal depth, while the remaining scenarios represent the maximum expected events for the considered seismogenic sources. The location and geometry of the fault planes relative to the minaret site are shown in Fig. 1.

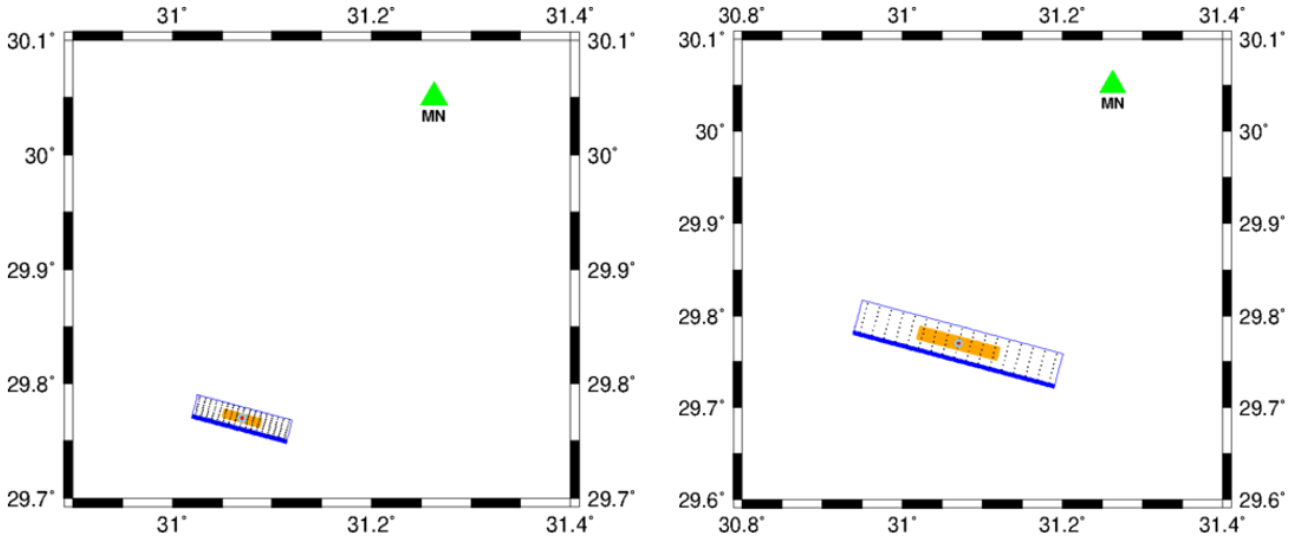

Fig. 1 – Fault location and size, with the minaret's location

For each scenario, multiple rupture realizations were generated using a Monte Carlo approach to account for source variability. Median (50th percentile) response spectra, together with the associated variability, were derived from the synthetic accelerograms and adopted as seismic demand for the structural assessment (Fig. 2).

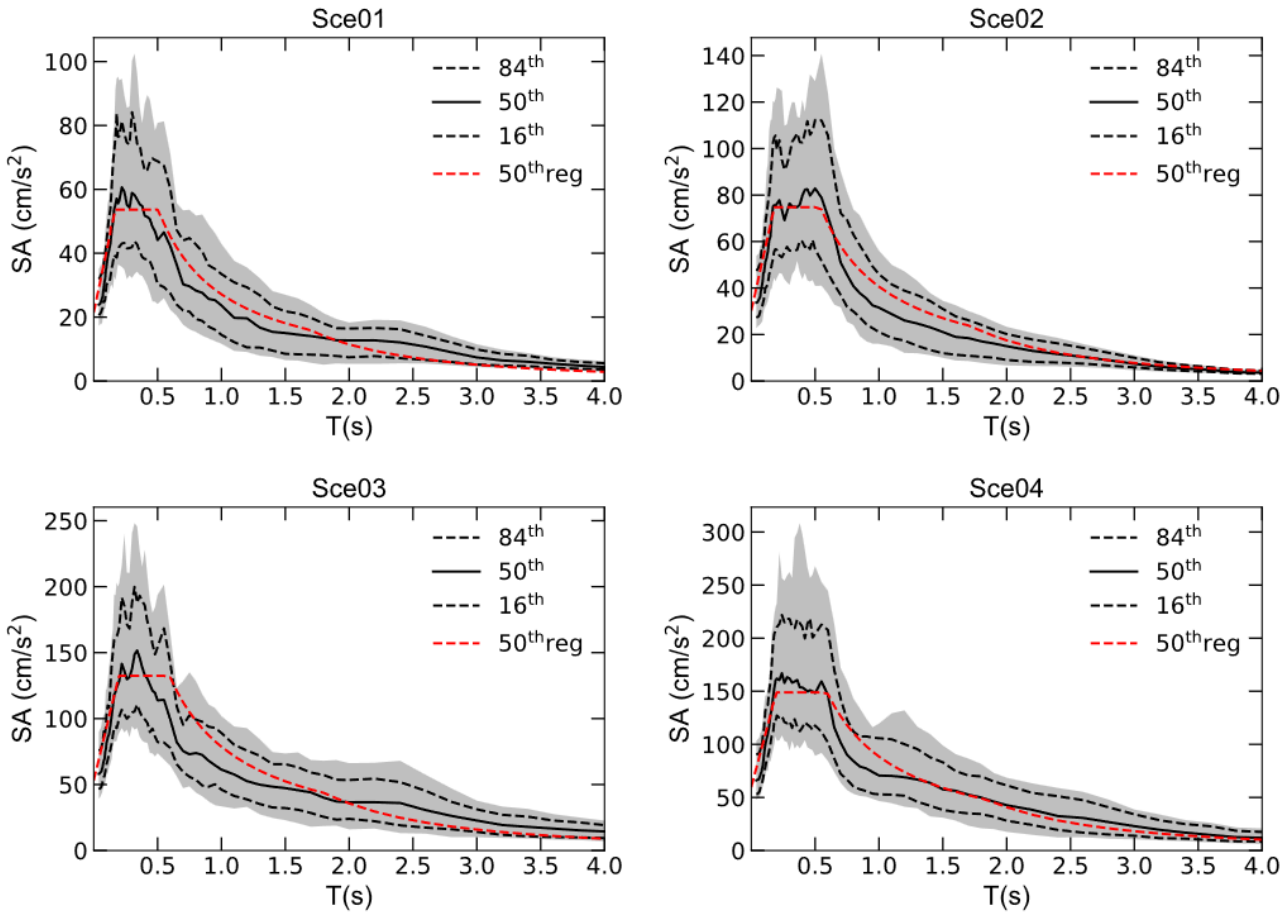

Fig. 2 – Acceleration response spectra from PBGMSs.

Structural modelling and pushover analysis

A three-dimensional geometrical model of the minaret was developed and implemented in a finite element environment. A macro-modelling strategy was adopted, in which the masonry was represented as a homogeneous continuum governed by a concrete damage plasticity (CDP) constitutive law (Fortunato et al. 2017, Funari et al. 2021). This model allows simulation of nonlinear behaviour in both tension and compression, including stiffness degradation due to cracking and crushing.

Material properties were derived from experimental investigations and code-based formulations. The compressive strength of the masonry units was obtained from in situ testing, while mortar properties were conservatively estimated. In accordance with Eurocode 6, characteristic values were adopted without amplification to maintain a safety-oriented modelling approach. Fracture energy parameters were defined following established formulations (Lourenço et al. 2022), ensuring mesh-objective results.

To account for the interaction between the minaret and the surrounding structures, equivalent elastic springs acting only in compression were introduced at the base. Spring stiffness values were calibrated through a trial-and-error procedure aimed at matching the first two experimentally identified natural frequencies of the structure, resulting in satisfactory agreement between numerical and experimental data.

Seismic performance was evaluated through nonlinear static (pushover) analyses performed along the principal horizontal directions of the structure. A mass-proportional load distribution was adopted to represent the inertial forces associated with seismic excitation. The analyses were conducted using an arc-length control strategy to ensure numerical stability under highly nonlinear conditions.

The resulting pushover curves and their bilinear idealization are shown in Fig. 3. Structural capacity was interpreted using the N2 method, which allows comparison between displacement demand derived from response spectra and displacement capacity obtained from pushover curves.

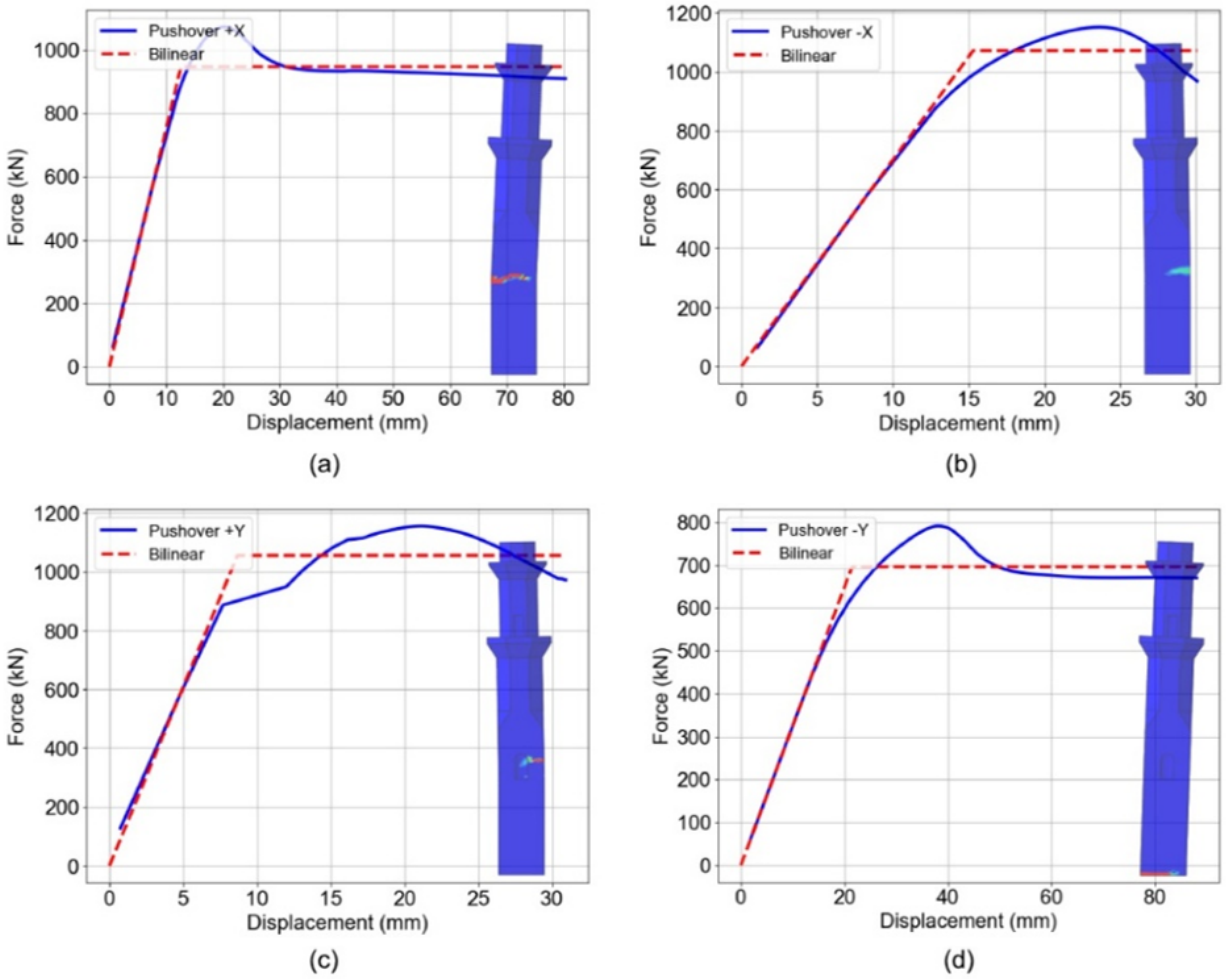

Fig. 2 – Pushover curves and their bi-linearisation.

For each seismic scenario and loading direction, behaviour factors and displacement demand-to-capacity ratios were computed and are summarized in Tab.1

Tab. 1 – Summary of results for the 50th percentile response spectrum

Event id	+X		-X		+Y		-Y	
	q^*	d^*_D/d^*_C	q^*	d^*_D/d^*_C	q^*	d^*_D/d^*_C	q^*	d^*_D/d^*_C
Sce01	1.24	0.29	1.28	0.97	1.18	0.50	1.35	0.48
Sce02	1.74	0.59	1.78	1.88	1.65	1.12	1.88	0.87
Sce03	2.95	1.43	3.03	4.41	2.82	2.84	3.19	1.95
Sce04	3.32	1.67	3.41	5.14	3.17	3.34	3.59	2.26

Results and discussion

The results indicate a satisfactory structural response under the seismic scenario representative of the 1992 Cairo earthquake, with displacement demand remaining below capacity in most directions. This outcome is consistent with the limited damage observed during the historical event and provides validation for both the calibrated FE model and the adopted PBGMS approach.

Conversely, scenarios characterized by higher magnitudes lead to displacement demands exceeding the structural capacity, particularly along one principal direction. These results highlight a significant seismic vulnerability of the minaret under future strong events, despite its apparent past resilience. Damage patterns obtained from the analyses indicate the development of tensile cracking concentrated in the upper shaft, potentially leading to severe structural degradation or collapse.

Conclusions

An integrated methodology combining geoscientific modelling and earthquake engineering tools was applied to the seismic assessment of a historic minaret in Old Cairo. Physics-based ground motion simulations proved effective in defining site-specific seismic demand in the absence of instrumental recordings, while calibrated finite element models enabled a detailed evaluation of structural capacity.

The comparison between demand and capacity confirms the good performance of the minaret during the 1992 Cairo earthquake, while also revealing a high vulnerability under more severe seismic scenarios. The proposed approach provides a robust framework for the seismic assessment and conservation of historic masonry structures and can be extended to other monuments within the Religions Complex in Old Cairo.

Acknowledgements

This study was carried out within the Italy–Egypt bilateral project “CoReng – Conservation of the Religions Complex in Old Cairo through geosciences and earthquake engineering integration”, supported by the Italian Ministry of Foreign Affairs and International Cooperation and by the Science, Technology & Innovation Funding Authority (STDF).

References

Masciotta, M.G.; Ramos, L.F.; Lourenço, P.B.; 2017: The Importance of Structural Moni-toring as a Diagnosis and Control Tool in the Restoration Process of Heritage Struc-tures: A Case Study in Portugal. J Cult Herit, 27, 36–47, doi:10.1016/J.CULHER.2017.04.003

Hassan, H.M.; Abdel Hafiez, H.E.; Sallam, M.A.; Bedon, C.; Fasan, M.; Henaish, A.; 2025: Multidisciplinary Approach of Proactive Preservation of the Religions Complex in Old Cairo - Part 1: Geoscience Aspects. Heritage, 8, 56, doi:10.3390/HERITAGE8020056

Hassan, H.M.; Abdel Hafiez, H.E.; Sallam, M.A.; Bedon, C.; Fasan, M.; Henaish, A.; 2025: Multidisciplinary Approach of Proactive Preservation of the Religions Complex in Old Cairo - Part 2: Structural Challenges. Heritage, 8, 89, doi:10.3390/HERITAGE8030089

Vaccari, F.; 2015: A Web Application Prototype for the Multiscale Modelling of Seismic Input. Earthquakes and Their Impact on Society, 563–584, doi:10.1007/978-3-319-21753-6_23

Chieffo, N.; Fasan, M.; Romanelli, F.; Formisano, A.; Mochi, G.; 2021: Physics-Based Ground Motion Simulations for the Prediction of the Seismic Vulnerability of Ma-sonry Building Compounds in Mirandola (Italy). Buildings, 11, 667, doi:10.3390/buildings11120667

Panza, G.F.; Mura, C. La; Peresan, A.; Romanelli, F.; Vaccari, F.; 2012: Seismic Hazard Scenarios as Preventive Tools for a Disaster Resilient Society. Advances in Geophysics, 53, pp. 93–165, doi: 10.1016/B978-0-12-380938-4.00003-3

Hassan, H.M.; Romanelli, F.; Panza, G.F.; ElGabry, M.N.; Magrin, A.; 2017: Update and Sensitivity Analysis of the Neo-Deterministic Seismic Hazard Assessment for Egypt. Eng Geol, 218, 77–89, doi:10.1016/J.ENGGEO.2017.01.006

Hassan, H.M.; Fasan, M.; Sayed, M.A.; Romanelli, F.; ElGabry, M.N.; Vaccari, F.; Hamed, A.; 2020: Site-Specific Ground Motion Modeling for a Historical Cairo Site as a Step towards Computation of Seismic Input at Cultural Heritage Sites. Eng Geol, 268, 105524, doi:10.1016/j.enggeo.2020.105524

Fortunato, G.; Funari, M.F.; Lonetti, P.; 2017: Survey and Seismic Vulnerability Assess-ment of the Baptistery of San Giovanni in Tumba (Italy). J Cult Herit, 26, 64–78, doi:10.1016/J.CULHER.2017.01.010

Funari, M.F.; Hajjat, A.E.; Masciotta, M.G.; Oliveira, D. V.; Lourenço, P.B.; 2021: A Par-ametric Scan-to-FEM Framework for the Digital Twin Generation of Historic Ma-sonry Structures. Sustainability, 13, 11088, doi:10.3390/SU131911088

Lourenço, P.B.; Gaetani, A.; 2022: Finite Element Analysis for Building Assessment: Ad-vanced Use and Practical Recommendations. Finite Element Analysis for Building Assessment, doi:10.1201/9780429341564

Corresponding author: mfasan@units.it

SIGMA: a new tool for the simulation of spectrum-compatible earthquake ground motions

G. Fiorentino[1], F.Sabetta[1], R. De Risi[2]

[1] Institute of Environmental Geology and Geoengineering, Italian National research Council (CNR-IGAG), Montelibretti, Italy
[2] School of Civil, Aerospace and Design Engineering, University of Bristol, Bristol, UK

Introduction

Ground motion time series provide realistic input for nonlinear dynamic analyses of structures and geotechnical systems, and they are required to verify compliance with seismic-code response spectra. In a hazard-consistent framework, the target spectrum is typically derived from probabilistic seismic hazard assessment (e.g., Uniform Hazard Spectrum) and from scenario information suggested by hazard disaggregation in terms of magnitude, distance, site class and faulting style.

Despite the continuous growth of strong-motion databases, it can still be difficult to find enough natural records that simultaneously satisfy (i) the scenario constraints (magnitude, distance, site conditions, mechanism) and (ii) spectrum-compatibility criteria over the period range of interest. In these situations, the standard practice is to scale the available recordings. However, using large scale factors may undermine consistency with the original seismological features of the records, while modern code-oriented practice typically recommends limiting scaling within moderate bounds (commonly 0.5 to 2) and focusing on the compatibility of the suite mean spectrum with the target.

Ground motion simulation offers a complementary route: instead of searching for scarce recordings, one can generate a pool of accelerograms conditioned on a small set of scenario parameters and then select a subset that best matches the target spectrum. Building on this idea, the present contribution summarizes the workflow of the SIGMA tool (Fiorentino et al. 2025), which combines a non-stationary stochastic simulation model (Sabetta et al. 2021) calibrated on an Italian predictive framework with a genetic-algorithm selection strategy (Mathworks 2023) to efficiently obtain spectrum-compatible suites.

SIGMA simulation procedure

SIGMA (Figure 1) generates one-component accelerograms using a non-stationary stochastic approach calibrated on an Italian ground motion predictive framework, similar to Lanzano et al. (2019), and based on ground motions extracted from the ESM database (https://esm-db.eu/, Luzi et al. 2020). The user defines an earthquake scenario through a limited number of inputs, including moment magnitude, source-to-site distance (with common engineering distance options), site condition via V_{S30}, source depth, and faulting style.

The simulation reproduces the time-varying nature of strong motion by combining an evolving frequency content described through a time-frequency representation with an amplitude modulation that reflects the energy build-up and decay of the record, linked to intensity and duration measures. In practical terms, the procedure produces realistic variability through random phases and by propagating uncertainty in duration and energy-related parameters, enabling the generation of hundreds of candidate accelerograms within user-defined ranges of magnitude, distance, and V_{S30}.

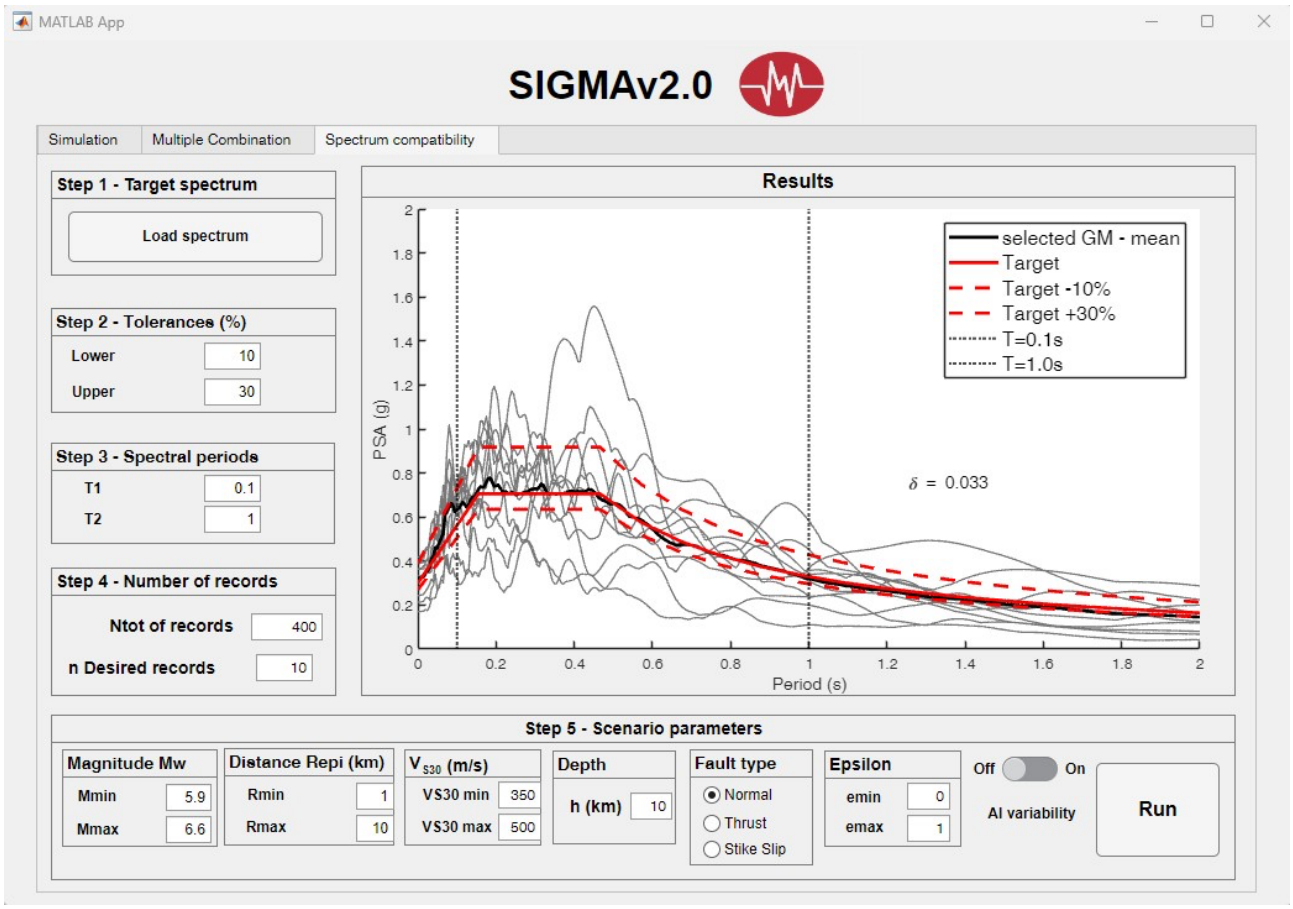

Fig. 1 – GUI of the software to generate simulated ground motions (SIGMA, version 2.0): "Spectrum Compatibility tab": selection of n spectrum-compatible records with a user-defined spectrum. (from Fiorentino et al. 2025)

Spectrum compatibility and selection within SIGMA

Once a pool of simulated records is generated, SIGMA evaluates their response spectra and performs an automated selection aimed at matching a target spectrum in a user-defined period

range and within tolerance bands. The tool searches for a combination of n records whose mean spectrum best fits the target.

This is formulated as an optimization problem solved via a genetic algorithm (GA): each candidate solution is a set of indices identifying records in the simulated pool, and the fitness is based on the mismatch between the mean spectrum and the target spectrum over the selected period range. The GA-driven selection is designed to efficiently explore the combinatorial space and to return suites that achieve strong average compatibility without requiring post-simulation spectral matching of individual time series. Figure 2 shows a set of ten simulated ground motions obtained with SIGMA.

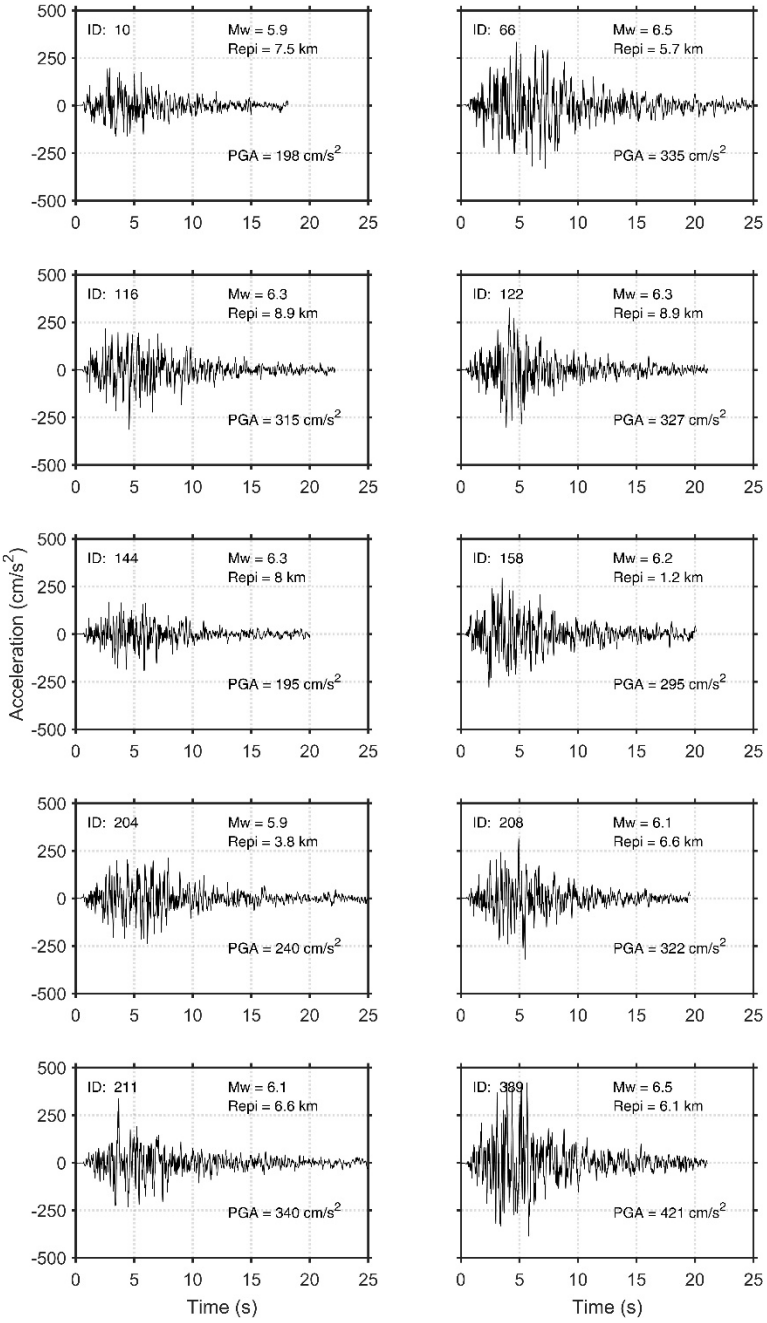

Fig. 2 – Simulated ground motions for Amatrice case study. For each record, the following parameters are reported: ID (identification number), M_w, R_{epi}, PGA. (from Fiorentino et al. 2025)

Conclusions

SIGMA provides a practical and reproducible workflow to generate suites of accelerograms that are both physically plausible for a prescribed earthquake scenario and suitable for code-oriented nonlinear time-history analyses. By combining a non-stationary stochastic simulation model with an optimization-based selection, the tool supports a two-step strategy: first, creating a large pool of candidate records that reflect expected duration, amplitude evolution and non-stationary frequency content; second, extracting from this pool a subset whose mean response spectrum closely matches a target spectrum over a user-defined period range.

A key advantage of the approach is that spectrum compatibility is achieved at the level of the suite, rather than by forcing each individual record to fit the target. This helps preserve record-to-record variability while still meeting engineering requirements on the mean spectrum and tolerance bands. From an operational perspective, the genetic algorithm selection makes the process efficient even for large simulated datasets, and it allows the user to control key choices such as the number of records, the period range of interest and the acceptance criteria.

Overall, SIGMA is intended to facilitate consistent input-motion selection when the analysis requires many spectrum-compatible records and when scenario constraints are important. The workflow can reduce the time and subjectivity typically associated with trial-and-error selection, and it provides a transparent basis for producing suites that can be regenerated and documented within a clear set of input assumptions, making it well suited for both research studies and engineering practice.

Acknowledgements

This work was supported by the Royal Society (RS) and the Consiglio Nazionale delle Ricerche (CNR) through the Joint Bilateral Agreement CNR/RS, Project SIM—Seismic Intelligent Microzonation, Biennial Programme 2025–2026 (CUP: B63C25000450001), IEC\R2\242059 - International Exchanges 2024 Cost Share.

References

Fiorentino, G., Sabetta, F., De Risi; 2025: R. SIGMA: a new tool for the simulation of spectrum-compatible earthquake ground motions. *Nat Hazards* **121**, 15163–15188. https://doi.org/10.1007/s11069-025-07387-w

Lanzano, G., Luzi, L., Pacor, F., Felicetta, C., Puglia, R., Sgobba, S., & D'Amico, M.; 2019: A Revised Ground-Motion Prediction Model for Shallow Crustal Earthquakes in Italy. Bulletin of the Seismological Society of America, 109(2), 525-540.

Luzi L., Lanzano G., Felicetta C., D'Amico M. C., Russo E., Sgobba S., Pacor, F., & ORFEUS Working Group 5; 2020: Engineering Strong Motion Database (ESM) (Version 2.0). Istituto Nazionale di Geofisica e Vulcanologia (INGV). https://doi.org/10.13127/ESM.2

MathWorks; 2023: MATLAB (Version 9.14.0.2206163 R2023a). Natick, Massachusetts: The MathWorks Inc.

Sabetta, F., Pugliese, A., Fiorentino, G. *et al.* ; 2021: Simulation of non-stationary stochastic ground motions based on recent Italian earthquakes. *Bull Earthquake Eng* 19, 3287–3315. https://doi.org/10.1007/s10518-021-01077-1

Corresponding author: gabriele.fiorentino@cnr.it

Assessing Earthquake Early Warning Feasibility at the NITRO Near-Fault Observatory

Simone Francesco Fornasari[1], Giovanni Costa[1]

[1] Department of Mathematics, Informatics, and Geosciences, University of Trieste, Trieste, Italy

Introduction

Earthquake Early Warning Systems (EEWS) aim to provide rapid, actionable information before the arrival of strong shaking, allowing individuals and automated systems to take protective actions (Satriano et al., 2011, Picozzi et al., 2013, Clinton et al., 2016, Rea et al., 2024). Their performance depends critically on network geometry, data transmission latency, algorithmic configuration, and the regional seismotectonic context. This study assesses the feasibility of implementing EEWS within the Northeastern Italy Thrust Faults Observatory (NITRO), a near-fault observatory established to investigate the thrust system responsible for the 1976 Mw 6.4 Friuli earthquake. Although the area is characterised by low-to-moderate seismicity, historical events demonstrate the presence of seismogenic sources capable of producing damaging shaking (Locati et al., 2022).
While EEWS primarily aim to deliver alerts within an actionable timeframe, social studies have shown that the general public, especially when properly trained, tends to respond positively to EEW and that EEW helps foster a culture of preparedness (Allen and Melgar, 2019; Dallo et al., 2022; Orihuela et al., 2023).

Data and Methods

The assessment uses 34 accelerometric stations integrated in the NITRO virtual seismic network, drawing from three regional networks (i.e. RF, University of Trieste, 1993, Costa et al., 2010, Costa et al. 2022; NI, Istituto Nazionale di Oceanografia e di Geofisica Sperimentale and University of Trieste, 2002; and OX, Istituto Nazionale di Oceanografia e di Geofisica Sperimentale and University of Trieste, 2016). A key input to EEWS performance is the real-time telemetry delay: a database of network-wise delay snapshots at the stations has been compiled over six months of continuous monitoring (March-September 2025) and shows that, aside from a few problematic stations, data latencies are stable in the 1.5-3.5 s range. This parameter is essential, as transmission latency directly increases the time of the first alert.
Two complementary datasets describing the regional seismicity were incorporated:

1. the instrumental seismic catalogue by Sugan et al. (2024), enabling spatially realistic source sampling;
2. the Italian Macroseismic Database (DBMI; Locati et al., 2022), containing 3542 intensity observations for 67 earthquakes affecting the NITRO region. Analysis of intensity > 6 (MCS scale) shows that damaging effects are typically confined to within 50 km of the epicentre. This distance is used as a reference for evaluating the performance of early warning systems.

The feasibility analysis has been performed considering PRESTo as EEWS. PRESTo (Satriano et al., 2011) is a network-based EEWS software that estimates location, magnitude, and expected ground motion using only the early P-wave signal. The time of first alert depends on:

- the arrival time of the P-wave at N stations,

- telemetry delays,
- a 2-second P-wave window (at N-1 stations) used to estimate the event magnitude (e.g. Picozzi et al., 2015);
- negligible computational latency (in the order of tens of ms).

Multiple PRESTo configurations were tested, varying the number N of stations required to issue the first alert: varying such parameter trades timeliness of the alert for the reliability of the results.

Numerical simulations were performed for all real events in the catalogue (and synthetic events where seismicity was absent). For each station and each simulation:

- a homogeneous velocity model provided theoretical travel times;
- empirical latencies were added to theoretical P-wave arrival times;
- Gaussian noise (σ = 0.2 s) simulated picking uncertainty;
- a 1s delay was assumed for alert transmission;
- the blind zone radius is computed as the distance travelled by the S-wave until the effective time of first alert;
- simulations were repeated for every latency snapshot in the dataset.

Aggregating the results on a 5 km x 5 km grid, significant statistical metrics have been computed.

To validate numerical results, a 3-station PRESTo configuration was tested on a real event, the 2024 M_w 4.1 Preone (UD) earthquake, replayed 100 times using real measured latencies. The data are fed, with the appropriate delays at each station, to a SeedLink server and consumed by PRESTo as if they were real-time data.

Discussion

Separating the PRESTo runtime from telemetry delays shows that the telemetry delays are spatially stable and largely independent of PRESTo configuration, and PRESTo runtime grows with the number of stations required.
For the 3-station configuration, PRESTo's contribution to alert time has an 89% highest-density interval (HDI) of 3.9–7.6 s (median 5.4 s). The corresponding time of first alert HDI is 6.0–11.0 s (median 8.3 s).

Blind zone radii show clear dependence on network geometry. The region surrounding the 1976 Friuli epicentre exhibits blind-zone radii of 18–25 km (1^{st} to 99^{th} percentile). Within NITRO, the expected variability in the blind zone extent is in the order of 5–15 km (Fig. 2).
Comparable results can be found in the literature for EEWS implemented in other regions: previous studies implementing PRESTo in Italy report blind zones of 19–23 km (Picozzi et al. 2015; Festa et al., 2018), and similar results have been reported for multiple EEWS in Switzerland (Massin et al. 2021).

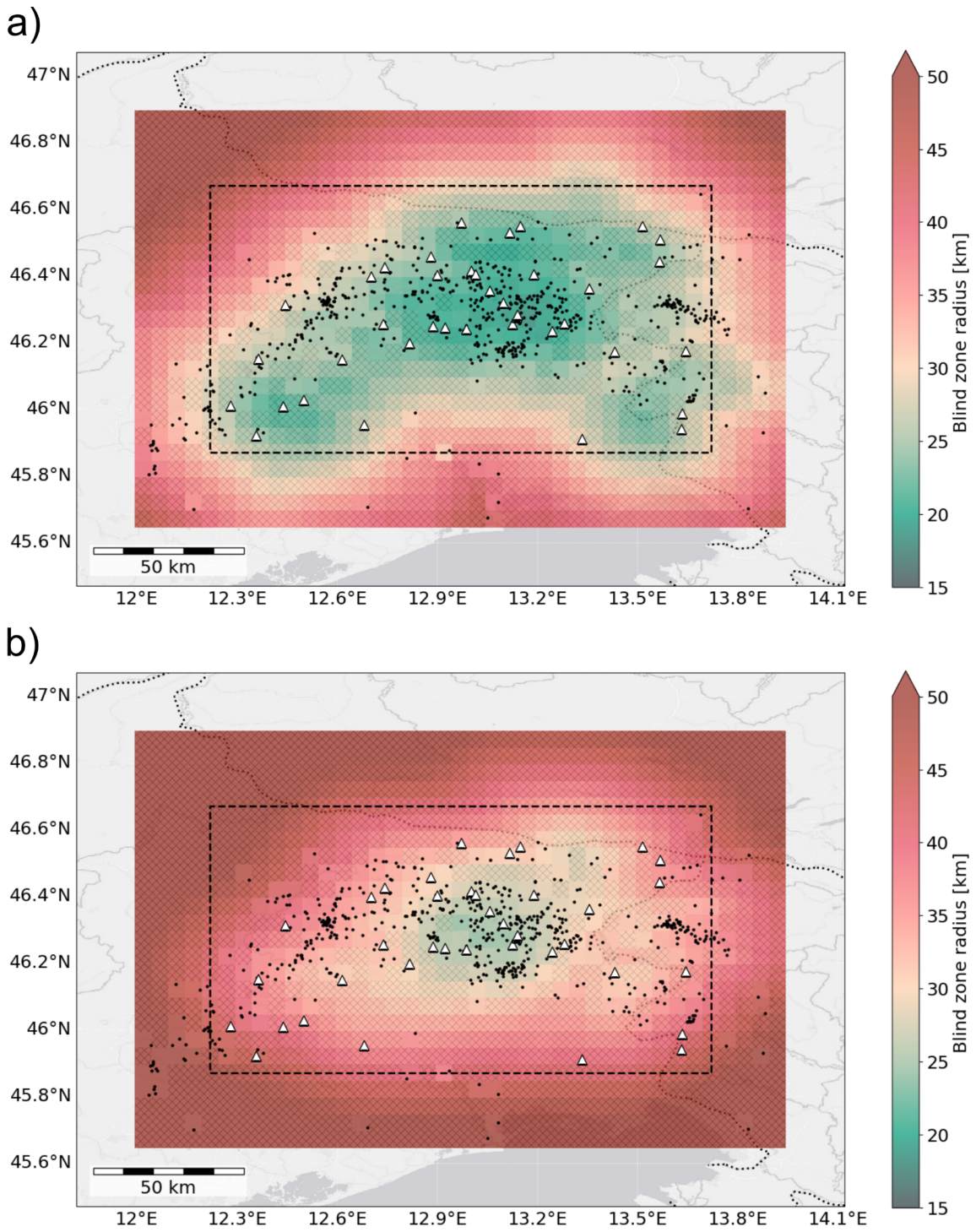

Figure 2: a) 1st percentile and b) 99th percentile of the blind-zone extent obtained from numerical simulations using a 3-station PRESTo configuration. Black dots indicate events from the seismic catalogue; hatched cells denote locations where a synthetic seismic source at 10 km depth was used; white triangles mark the seismic stations included in the simulations.

Repeating the simulations using DBMI macroseismic locations (with intensity ≥VI) as target sites, 60% of damaged locations fell within the blind zone, only 16% of these locations received alerts with a lead time >5 s, and only 5% of these sites would have had a lead time >10 s.

At major settlements within NITRO, lead-time distributions are highly multimodal, reflecting the strong dependence on the epicentral distance for different events (Fig.3).

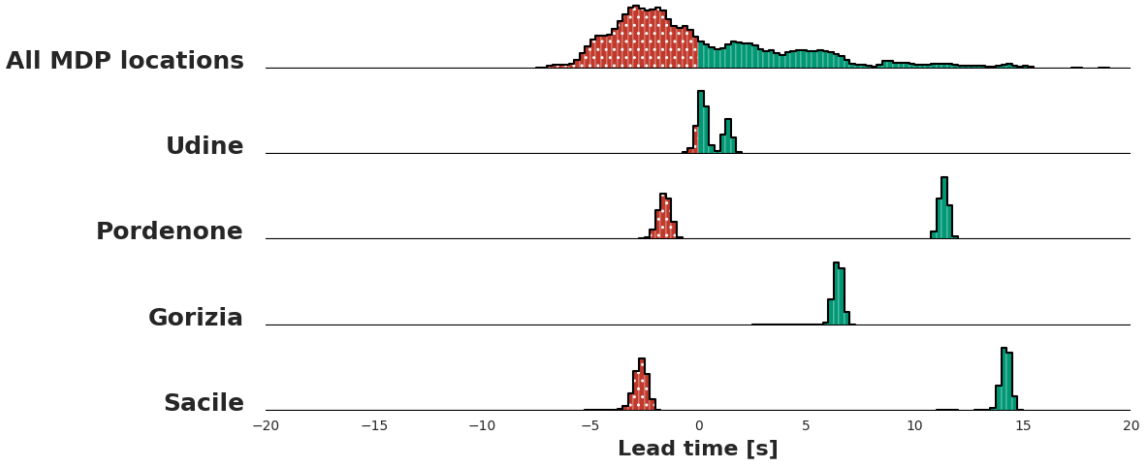

Figure 3: Aggregated simulation results in terms of lead time and distributions of lead time obtained for the largest settlement in the area.

Similarly, the M_w 4.1 Preone offline test confirmed the simulation results (Fig. 4): the distribution of time of first alert is centred around 13 s after origin time; magnitude and location estimates stabilise within 20 s; uncertainty contracts rapidly after the first few iterations.

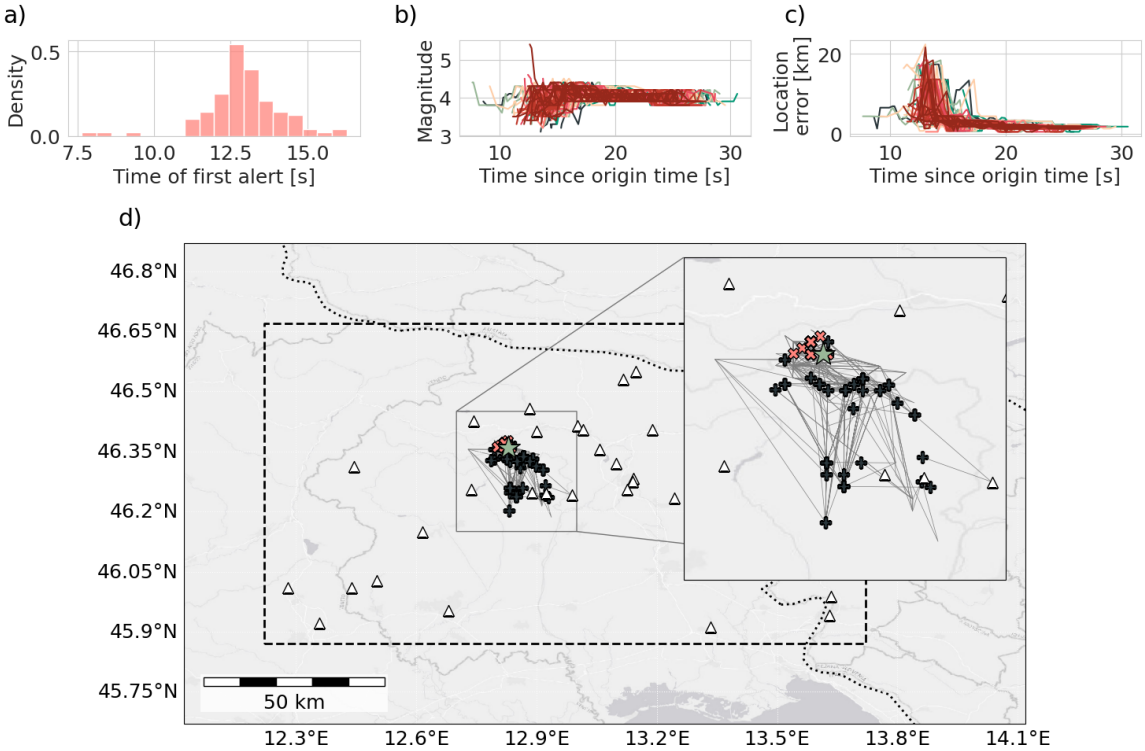

Figure 4: Results from the offline replays of the Preone earthquake: a) distribution of time of first alert for the different scenarios; b) magnitude estimate evolution; c) trend of the epicentre location error over time; d) spatial evolution of the epicentral estimates, with blue and orange markers indicating the initial and final locations, respectively, and grey lines showing the iterative update paths.

Conclusions

Results indicate that with the current network configuration, EEWS at NITRO would provide limited early warning value for locations likely to experience significant shaking. Most of the sites that would experience damage lie too close to epicentral regions for meaningful lead time.
Potential improvements include:

- network densification, particularly through integration of stations from other institutions;
- minor telemetry optimisations, though cost–benefit is small since latency is not the dominant bottleneck;
- installation of EEW-ready seismic sensors (i.e. using direct data transmission with no buffer);
- development of a robust alert dissemination infrastructure;
- consideration of hybrid or on-site EEWS approaches.

Despite limited actionable warning time, EEWS could still serve as a valuable component of a rapid situational-awareness system, supporting emergency response and providing real-time information to Civil Protection and the public.

Acknowledgments
This research was conducted within the framework of the Italian division of the European Plate Observing System (EPOS; EPOS-Italia) and TRANSFORM^2, funded by the European Union within the HORIZON-INFRA-2024-DEV-01-01 call. This research received financial support from the Italian Civil Protection Department - Presidency of the Council of Ministers (DPC) under the agreement between DPC and the University of Trieste for the accelerometric monitoring of the Friuli Venezia Giulia Region.

References

Allen, R. M.; Melgar, D.; 2019: Earthquake Early Warning: Advances, Scientific Challenges, and Societal Needs. Annual Review of Earth and Planetary Sciences Vol. 47, n. 1, pp. 361–388, https://doi.org/10.1146/annurev-earth-053018-060457

Clinton, J.; Zollo, A.; Marmureanu, A.; Zulfikar, C.; Parolai, S.; 2016: State-of-the-art and future of earthquake early warning in the European region. Bulletin of Earthquake Engineering Vol. 14, n. 9, pp. 2441–2458, https://doi.org/10.1007/s10518-016-9922-7

Costa, G.; Moratto, L.; Suhadolc, P.; 2010: The Friuli Venezia Giulia Accelerometric Network: RAF. Bulletin of Earthquake Engineering Vol. 8, n. 5, pp. 1141–1157, https://doi.org/10.1007/s10518-009-9157-y

Costa, G.; Brondi, P.; Cataldi, L.; Cirilli, S.; Cuius, A.; Ertuncay, D.; Falconer, P.; Filippi, L.; Fornasari, S. F.; Pazzi, V.; Turpaud, P.; 2022: Near-Real-Time Strong Motion Acquisition at National Scale and Automatic Analysis. Sensors Vol. 22, n. 15, article 5699, https://doi.org/10.3390/s22155699

Dallo, I.; Marti, M.; Clinton, J.; Böse, M.; Massin, F.; Zaugg, S.; 2022: Earthquake early warning in countries where damaging earthquakes only occur every 50 to 150 years – The societal perspective. International Journal of Disaster Risk Reduction Vol. 83, article 103441, https://doi.org/10.1016/j.ijdrr.2022.103441

Festa, G.; Picozzi, M.; Caruso, A.; Colombelli, S.; Cattaneo, M.; Chiaraluce, L.; Elia, L.; Martino, C.; Marzorati, S.; Supino, M.; Zollo, A.; 2018: Performance of Earthquake Early Warning Systems during

the 2016–2017 Mw 5–6.5 Central Italy Sequence. Seismological Research Letters Vol. 89, n. 1, pp. 1–12, https://doi.org/10.1785/0220170150

Istituto Nazionale di Oceanografia e di Geofisica Sperimentale – OGS; 2016: North-East Italy Seismic Network [SEED data]. FDSN, https://doi.org/10.7914/SN/OX

Istituto Nazionale di Oceanografia e di Geofisica Sperimentale; University of Trieste; 2002: North-East Italy Broadband Network [SEED data]. International Federation of Digital Seismograph Networks, https://doi.org/10.7914/SN/NI

Locati, M.; Camassi, R.; Rovida, A.; Ercolani, E.; Bernardini, F.; Castelli, V.; Caracciolo, C. H.; Tertulliani, A.; Rossi, A.; Azzaro, R.; D'Amico, S.; Antonucci, A.; 2022: Database Macrosismico Italiano (DBMI15), version 4.0. Istituto Nazionale di Geofisica e Vulcanologia (INGV), https://doi.org/10.13127/DBMI/DBMI15.4

Massin, F.; Clinton, J.; Böse, M.; 2021: Status of Earthquake Early Warning in Switzerland. Frontiers in Earth Science Vol. 9, https://doi.org/10.3389/feart.2021.707654

Orihuela, B.; Dallo, I.; Clinton, J.; Strauch, W.; Protti, M.; Yani, R.; Marroquín, G.; Sanchez, J.; Vega, F.; Marti, M.; Massin, F.; Böse, M.; Wiemer, S.; 2023: Earthquake early warning in Central America: The societal perspective. International Journal of Disaster Risk Reduction Vol. 97, article 103982, https://doi.org/10.1016/j.ijdrr.2023.103982

Picozzi, M.; Bindi, D.; Pittore, M.; Kieling, K.; Parolai, S.; 2013: Real-time risk assessment in seismic early warning and rapid response: A feasibility study in Bishkek (Kyrgyzstan). Journal of Seismology Vol. 17, n. 2, pp. 485–505, https://doi.org/10.1007/s10950-012-9332-5

Picozzi, M.; Zollo, A.; Brondi, P.; Colombelli, S.; Elia, L.; Martino, C.; 2015: Exploring the feasibility of a nationwide earthquake early warning system in Italy. Journal of Geophysical Research: Solid Earth Vol. 120, n. 4, pp. 2446–2465, https://doi.org/10.1002/2014JB011669

Rea, R.; Colombelli, S.; Elia, L.; Zollo, A.; 2024: Retrospective performance analysis of a ground shaking early warning system for the 2023 Turkey–Syria earthquake. Communications Earth & Environment Vol. 5, n. 1, https://doi.org/10.1038/s43247-024-01507-3

Satriano, C.; Elia, L.; Martino, C.; Lancieri, M.; Zollo, A.; Iannaccone, G.; 2011: PRESTo, the earthquake early warning system for Southern Italy: Concepts, capabilities and future perspectives. Soil Dynamics and Earthquake Engineering Vol. 31, n. 2, pp. 137–153, https://doi.org/10.1016/j.soildyn.2010.06.008

Sugan, M.; Saraò, A.; Magrin, A.; Snidarcig, A.; Bressan, G.; Renner, G.; Romano, M. A.; Guidarelli, M.; Santulin, M.; Di Bartolomeo, P.; Restivo, A.; 2024: Focal mechanisms of the Southeastern Alps and surroundings (Version 2.0) [Data set]. Zenodo, https://doi.org/10.5281/ZENODO.10853582

University of Trieste; 1993: Friuli Venezia Giulia Accelerometric Network [SEED data]. International Federation of Digital Seismograph Networks, https://doi.org/10.7914/SN/RF

Corresponding author: simonefrancesco.fornasari@units.it

Attenuation of seismic waves in near-surface deposits using borehole-to-surface deconvolution

G. Franceschina[1], A. Tento[2]

[1] *Istituto Nazionale di Geofisica e Vulcanologia – Sezione di Milano, Milano, Italy.*
[2] *Milano – ex Consiglio Nazionale delle Ricerche, Milano, Italy.*

Introduction

The attenuation of seismic waves within near-surface deposits plays a crucial role in the accurate modelling of site effects and the consequent assessment of local seismic hazard. Parolai et al. (2022) provide a comprehensive and in-depth review of the methodologies currently employed for estimating the local-scale S-wave quality factor, *Qs*. Among the approaches relying on passive sources are the evaluation of the high-frequency attenuation parameter *kappa* (Anderson and Hough, 1984) and the deconvolution of borehole seismic recordings with respect to those obtained at the surface (hereinafter referred to as borehole-to-surface deconvolution technique). Recently, Franceschina and Tento (2025) analysed the recordings from station CTL8 (45.28°N, 9.76°E) of the Italian National Seismic Network (INGV, 2005), located near Castelleone (CR) on the thick alluvial deposits typical of the Po Plain (northern Italy). The station is equipped with a surface accelerometric sensor and a borehole velocimetric sensor installed at 162 m depth. Their analysis estimated the attenuation between the borehole and the surface in terms of the difference between the respective *kappa* values ($\Delta\kappa_{162}$) and subsequently derived the corresponding 1D-layered seismic profile. In this study, using the same dataset, we apply the borehole-to-surface deconvolution technique to compare the outcomes of the two approaches.

Borehole-to-surface deconvolution

For borehole recordings obtained at typical depths (up to about hundred metres), it is generally difficult to isolate the incident wavefield from the reflected one due to their mutual interference within the time windows commonly used for analysis. However, in some cases the deconvolution procedure enables this separation. Following Haendel et al. (2019), the method consists of the following steps:

1. computing the spectral ratio between borehole and surface recordings;
2. identifying, in the corresponding time-domain signal, the pulses associated with up-going waves (negative time lag) and down-going waves (positive time lag);
3. computing the spectral ratio between these two pulses (down-going/up-going);

4. estimating *kappa* from the slope of the spectral ratio. It should be noted that the resulting *kappa* value refers to the borehole–surface–borehole path and must therefore be halved to obtain the effective value.

This procedure is strictly valid for a homogeneous half-space, but it can also be applied to layered structures when the first and last pulses can be isolated from intermediate ones. In gradient-like profiles, or in the absence of strong impedance contrasts, these pulses are typically the most energetic and therefore the easiest to identify.

Data

A total of 109 pairs of borehole and surface recordings from station CTL8 were analysed, selected for their high signal-to-noise ratio. The events considered have local magnitudes between 3.0 and 5.8 and epicentral distances between 36 and 256 km. Assuming that wave propagation between the borehole and surface is essentially vertical, identical time windows were selected corresponding to the S-wave portion projected onto the component orthogonal to the source–station azimuth. In order to use the borehole recordings, it was necessary to assess the actual orientation of the sensor using the known orientation of the surface sensor as a reference. Several teleseismic events—e.g., the 23 October 2011 Turkey earthquake (Mw 7.2, epicentral distance 2855 km)—were analysed after correcting for instrumental response and converting into acceleration the borehole waveform. Time windows containing surface waves were selected and then analysed in the highly energetic frequency band 0.05–1.00 Hz. The azimuthal orientation was determined by rotating the surface recording and identifying the angle that maximised its correlation with the borehole components. The resulting estimate indicates that the borehole velocimetric sensor components must be rotated by 144°.

Results

The pulses obtained through deconvolution using the 109 selected events, each of them jointly recorded by the surface and borehole sensor, are shown in Figure 1. Note that the spectra obtained with the borehole velocimeter were not corrected for instrumental response and converted to acceleration. The depth-derived deconvolution signals are therefore the velocity pulses (velocimeter output) that cause a delta-like acceleration pulse at the surface. The figure also reports the mean value of the deconvolution signal and the time-window limits used to identify the up-going and down-going pulses. Figure 2 shows the spectral ratio between these pulses – which is unaffected by the instrumental-response corrections mentioned above – together with the signal-to-noise ratio and the frequency intervals for linear interpolation deemed suitable for estimating $\Delta\kappa_{162}$, which yields: (11.3 **±** 1.1) ms. From Figure 1, the time-average S-wave velocity between the borehole and surface, Vs_{162}, can also be estimated using the time separation between the peaks of the deconvolution pulses. The obtained value, Δt = (890 ± 14) ms, implies Vs_{162} = (364 ± 7) m/s, accounting for an assumed uncertainty of 1.5 m in the borehole sensor depth.

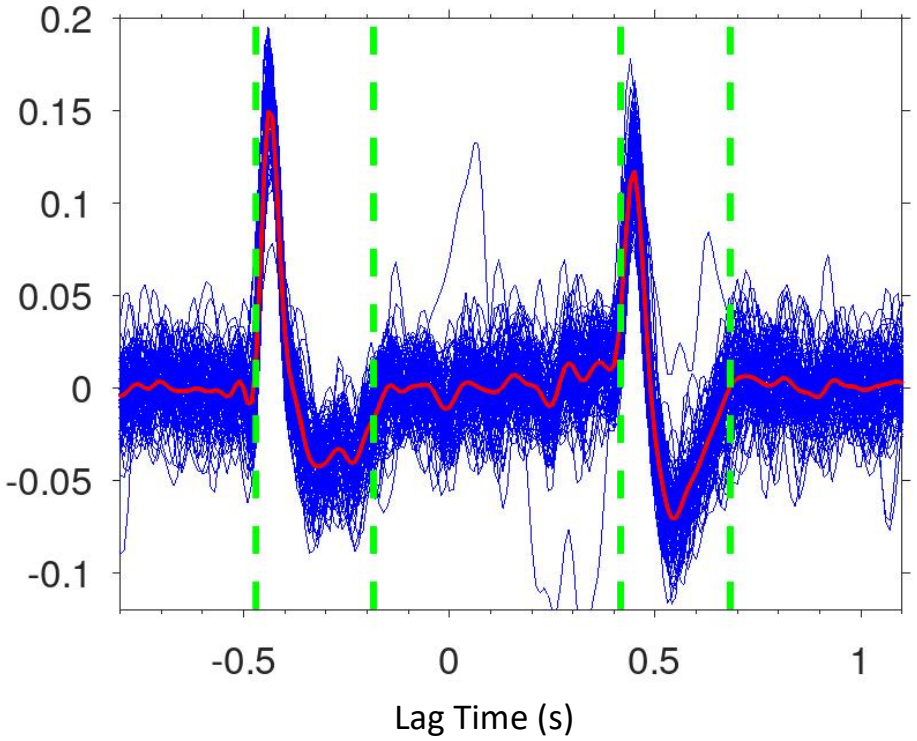

Fig. 1 – Deconvolution pulses obtained with the 109 selected events (blue thin lines); mean deconvolution pulse (red line); time-windows estimated for the up-going and down-going pulses (vertical green dashed lines corresponding to negative and positive time lags, respectively)

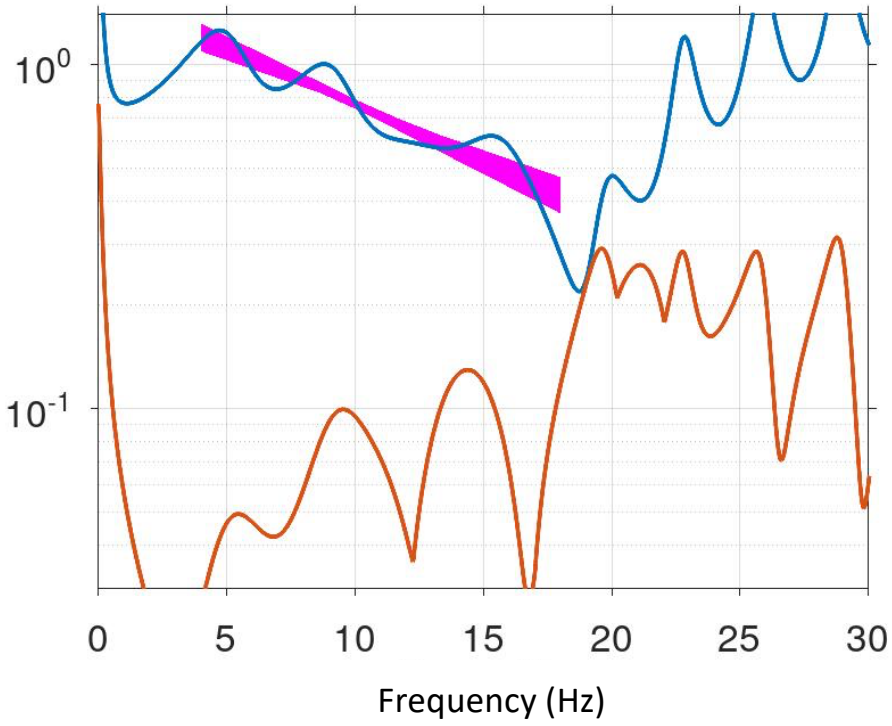

Fig. 2 – Spectral ratio between down-going and up-going pulses (blu line); signal-to-noise spectral ratio (red line); envelope of the linear regression lines deemed suitable for estimating $\Delta\kappa_{162}$ (magenta line). Note that, for each line the obtained slope refers to the borehole-surface-borehole path.

Conclusions

The use of deconvolution to evaluate attenuation and time-average velocity requires several conditions to be satisfied, including vertical S-wave propagation between borehole and surface, the selection of time windows containing only S-waves, and the possibility to clearly isolate the up-going and down-going deconvolution pulses. The latter is the most critical requirement: insufficient borehole depth prevents pulse separation, and strong impedance contrasts may further complicate the process. Among the advantages of this approach are the possibility of using low-magnitude events—provided that the signal-to-noise ratio is adequate—for estimating *kappa*, and the ability to obtain a direct estimate of the average velocity of the near-surface deposits. The results obtained in this study are in good agreement with those derived using standard methodologies by Franceschina and Tento (2025), who also developed a seismic velocity profile for the site. Figure 3 compares the deconvolution signal derived from the data analysed here (see Figure 1) with that computed from the aforementioned velocity profile. We obtain significant agreement between the two signals, although further analysis is needed to refine and fully validate this promising approach.

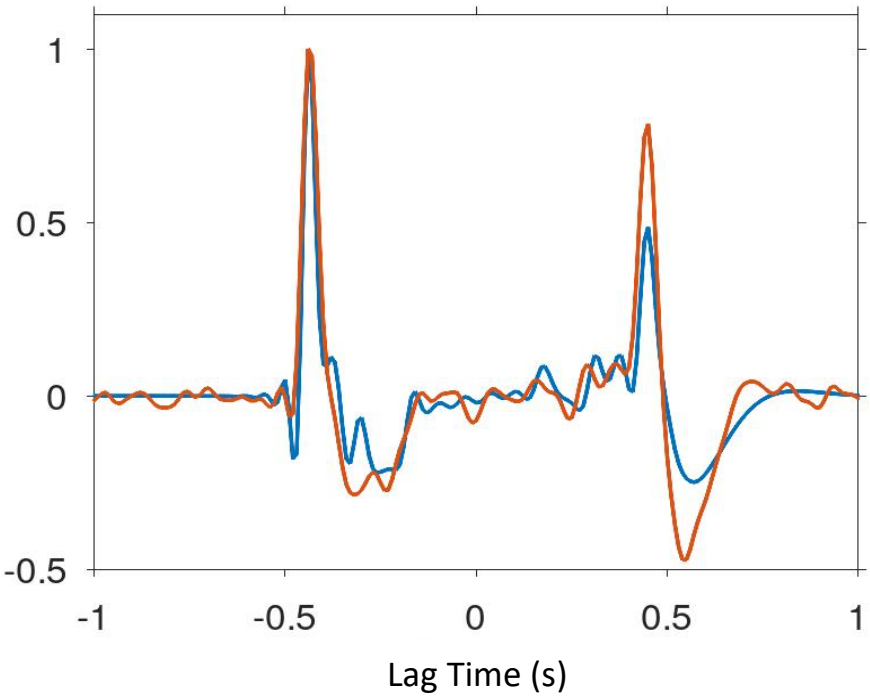

Fig. 3 – Mean deconvolution pulse obtained with the 109 selected events (red line – same line of Figure 1) and deconvolution pulse computed by using the seismic profile obtained by Franceschina and Tento (2025) (blue line). Amplitudes have been normalized.

Acknowledgements

This study received financial support from the Italian municipality of Minerbio under the agreement between 'Comune di Minerbio' and Istituto Nazionale di Geofisica e Vulcanologia: 'Sperimentazione ILG Minerbio stoccaggio' (grant number 0913.010).

References

Anderson J. G., Hough S. E.; 1984: A model for the shape of the Fourier amplitude spectrum of acceleration at high frequencies. Bull. Seismol. Soc. Am., 74(5), 1969-1993. doi: 10.1785/BSSA0740051969.

Franceschina G., Tento A.; 2025: Local seismic response of shallow alluvial deposits in the central Po Plain (northern Italy). Soil Dynam. Earthq. Eng., *under submission*.

Fukushima R., Nakahara H., Nishimura T.; 2016: Estimating S-wave attenuation in sediments by deconvolution analysis of KiK-net borehole seismograms. Bull. Seismol. Soc. Am., 106(2), 552 – 559. doi: 10.1785/0120150059.

Haendel A., Ohrnberger M., Kruger F.; 2019: Frequency-dependent quality factors from the deconvolution of ambient noise recordings in a borehole in West Bohemia/Vogtland. Geophys. J. Int., 216(1), 251 – 260. doi: 10.1093/gji/ggy422.

Istituto Nazionale di Geofisica e Vulcanologia (INGV); 2005: Rete Sismica Nazionale (RSN) [Data set]. Istituto Nazionale di Geofisica e Vulcanologia (INGV). doi: 10.13127/SD/X0FXNH7QFY

Parolai S., Bindi D., Ansal A., Kurtulus A., Strollo A., Zschau J; 2010: Determination of shallow S-wave attenuation by down-hole waveform deconvolution: A case study in Istanbul (Turkey). Geophys. J. Int., 181(2), 1147 – 1158. doi: 10.1111/j.1365-246X.2010.04567.x.

Parolai S., Lai C.G., Dreossi I., Ktenidou O.-J., Yong A.; 2022: A review of near-surface Qs estimation methods using active and passive sources. J. Seismol., 26(4), 823 – 862. doi: 10.1007/s10950-021-10066-5.

Corresponding author: gianlorenzo.franceschina@ingv.it

Exploring Ground-Motion Variability through Synthetic Scenarios in Central Italy

M. Freddi[1], S. Sgobba[2], F. Pacor[2]

[1] *Università degli Studi di Camerino (UNICAM, Italy)*
[2] *Istituto Nazionale di Geofisica e Vulcanologia (INGV, Italy)*

Ground Motion Models (GMMs), usually calibrated by regression of empirical ground-motion data, describe earthquake shaking in terms of a median prediction and a standard deviation in log space, i.e. sigma (σ). This σ has a very strong influence on the results of probabilistic seismic hazard analysis (PSHA) (e.g., Bommer and Abrahamson, 2006), so that a long-standing goal in ground-motion modelling has been to identify ways of reducing its aleatory fraction for example by resolving systematic epistemic contributions to variability (Al-Atik et al., 2010). As the amount and quality of recorded data along with density of seismic networks have increased, it has become possible to relax the ergodic assumption (Anderson and Brune, 1999) and to develop nonergodic models in which part of the total variability is attributed explicitly to source, path and site effects. Despite these advances, important gaps remain, recordings from large earthquakes are still limited in near-source, and stations are often not azimuthally well distributed around faults. One possible strategy to address these limitations is to complement empirical data with synthetic ground-motion data, which allow a controlled exploration of source, path and site parameters and can provide additional insight into ground-motion variability.

In this study, a set of fully simulated ground-motion scenarios developed by Čejka et al. (2025) for a Mw 6.2 normal-faulting event in the central Apennines (Italy) is used to investigate how variability is distributed spatially around the source, for a single-fault/multiple-site configuration. Synthetic ground motions are computed with the broadband Hybrid Integral Composite (HIC) technique of Gallovič and Brokešová (2007), using a source model that combines an integral kinematic representation at low frequencies with a composite high-frequency description, blended in the crossover frequency range. The simulations are defined on a single planar fault with geometry and seismic moment consistent with the 2016 Amatrice mainshock, while the kinematic source variability is explored by systematically varying four key parameters:

- Subsource corner frequencies (*a*), which controls high-frequency energy source radiation
- Rupture velocity (*vr*)
- Slip distribution (*slip*)
- Nucleation point position (*nuc*)

Wave propagation is calculated using 1D crustal velocity models representative of the two main domains in the area, the Amatrice Laga Formation and the Norcia carbonate unit, and the analysis uses the RotD50 (Boore, 2010) spectral acceleration ordinates (SA) at 5% damping in the frequency range 0.1-5 Hz provided for a regular grid of 400 virtual reference-rock receivers (Fig. 1).

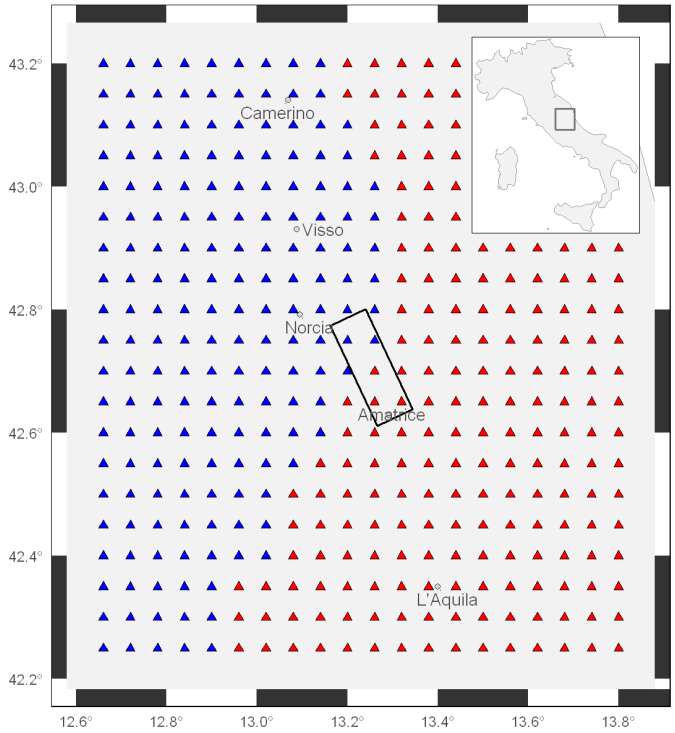

Fig. 1 – Study domain with 400 virtual receivers (triangles coloured blue for the Norcia domain and red for the Amatrice domain) used for ground-motion modelling under variable source scenarios. The black rectangle shows the surface projection of the fault plane, and the top-right inset map indicates the location of the study domain within Italy.

Because all simulations share the same magnitude and focal mechanism, a simplified linear mixed-effects regression is adopted. For each spectral frequency, the median ground motion is described as a function of Joyner-Boore distance through a geometrical spreading plus apparent attenuation term. The total residual ε (with standard deviation σ) is decomposed following the taxonomy of Al-Atik et al. (2010) into a between-scenario term δB_S and a within-scenario term δW_{SS}.

$$\varepsilon = \delta B_S + \delta W_{SS}$$

The between-scenario component is parameterized as the sum of random intercepts associated with the four kinematic parameter groups, plus a small residual scenario term:

$$\delta B_S = \delta_a + \delta_{vr} + \delta_{slip} + \delta_{pnuc} + \delta_0$$

Where δ_a, δ_{vr}, δ_{slip} and δ_{nuc} are the random effects linked to the parameters *a*, *vr*, *slip* and *nuc*, respectively, and δ_0 is the remaining residual term. The corresponding standard deviations τ_a, τ_{vr}, τ_{slip}, τ_{nuc} and τ_0 combine to give the overall between-scenario standard deviation τ_S.

The within-scenario component δW_{SS} is further partitioned into a systematic receiver-to-receiver term δ_{R2R} representing the geometric influence of the receiver positions (relative to the reference rock) with respect to the source, and a scenario- and receiver-corrected residual δW_{SR}^0:

$$\delta W_{SS} = \delta_{R2R} + \delta W_{SR}^{0}$$

with standard deviations φ_{R2R} e φ_0, respectively, whose combination yields the total within-scenario standard deviation φ_{SS}.

In this way, the total standard deviation σ, obtained by combining τ_S and φ_{SS}, can be interpreted as the sum of contributions from explicit kinematic source parameters, systematic receiver-to-receiver variability, and a remaining aleatory residual term that includes other effects not accounted by the model, such as propagation and rupture directivity effects.

The regression is performed at each frequency in the 0.1-5 Hz range, in order to explore the frequency dependence of synthetic ground-motion variability. The analysis shows that this variability can be attributed to different physical effects at different frequencies:

- At low frequencies, the contributions associated with the kinematic parameters are relatively small, each of the order of a few hundredths of logarithmic units, with the nucleation term showing a relatively larger contribution. The receiver-to-receiver term is mainly controlled by finite-fault effects and by the radiation pattern, while the largest share of variability is carried by the scenario- and receiver-corrected residual (i.e. aleatory term). Within this residual, directivity-like effects can be clearly identified.
- At high frequencies, the between-scenario variability becomes much larger and is strongly controlled by the kinematic parametrization, with the dominant contributions coming from the *a* parameter and *vr*. The receiver-to-receiver term is also significant and mainly reflects the contrast between the two crustal models used in the simulations, whereas the scenario- and receiver-corrected residual is still non-negligible but smaller than at low frequencies.

As an illustration of the spatial behaviour of the receiver-to-receiver residual term, Fig. 2 shows the δ_{R2R} at 0.5 Hz and 5 Hz. At low frequency δ_{R2R} exhibits a clear bilobate pattern consistent with the expected S-wave radiation pattern of the normal-fault mechanism, whereas at 5 Hz this pattern disappears and δ_{R2R} mainly reflects the contrast between the two crustal media (i.e. Amatrice and Norcia domains), with positive residuals in the Amatrice Laga domain and negative residuals in the Norcia carbonate domain, reflecting the difference in the average shear wave velocity over the first kilometer in the two domains, i.e. about 1.6 km/s and 2.5 km/s, respectively. In both cases, the remaining δW_{SR}^{0} term stays relatively large, suggesting that it still accommodates directivity-like effects and other source-to-site configuration contributions that are not captured by the explicit kinematic parameters or by the receiver-to-receiver term.

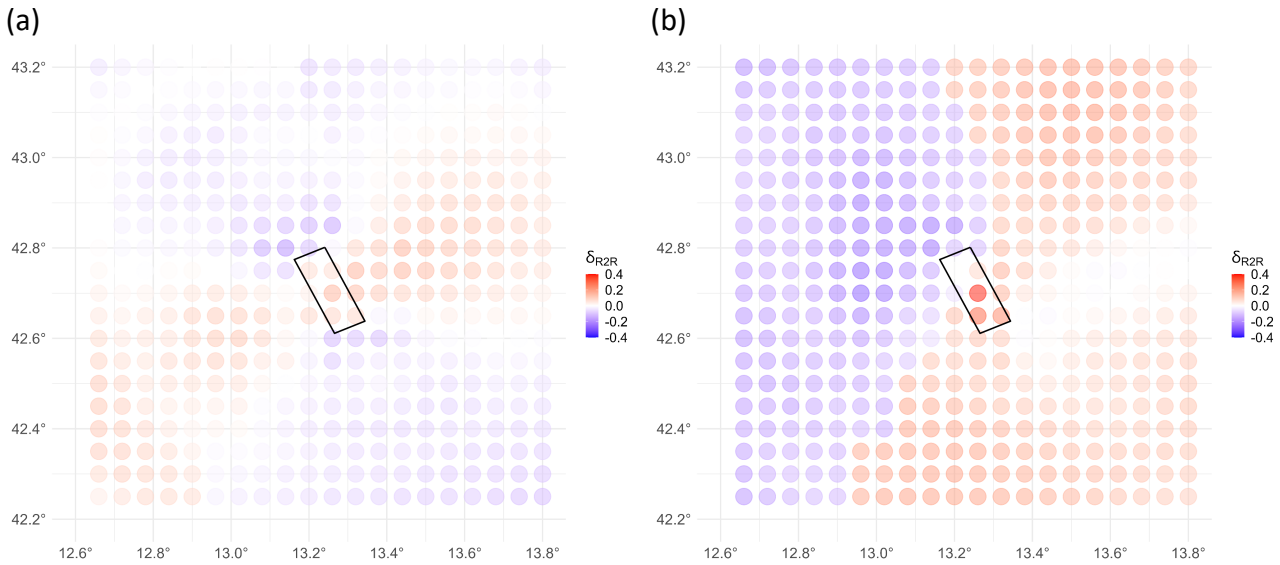

Fig. 2 – Receiver-to-receiver residual terms (log10-units) for (a) 0.5 Hz and (b) 5 Hz. Circles show δ_{R2R} at the virtual receivers; the black rectangle indicates the surface projection of the fault plane.

References

Al-Atik, L. A., Abrahamson, N., Bommer, J. J., Scherbaum, F., Cotton, F., & Kuehn, N.; 2010: The variability of ground-motion prediction models and its components. Seismological Research Letters, 81(5), 794-801, https://doi.org/10.1785/gssrl.81.5.794

Anderson, J. G., & Brune, J. N.; 1999: Probabilistic seismic hazard analysis without the ergodic assumption. Seismological Research Letters, 70(1), 19-28, https://doi.org/10.1785/gssrl.70.1.19

Bommer, J. J., & Abrahamson, N. A.; 2006: Why do modern probabilistic seismic-hazard analyses often lead to increased hazard estimates?. Bulletin of the Seismological Society of America, 96(6), 1967-1977, https://doi.org/10.1785/0120060043

Boore, D. M.; 2010: Orientation-independent, nongeometric-mean measures of seismic intensity from two horizontal components of motion. Bulletin of the Seismological Society of America, 100(4), 1830-1835, https://doi.org/10.1785/0120090400

Čejka, F., Sgobba, S., Pacor, F., Felicetta, C., Valentová, Ľ., & Gallovič, F.; 2024: Constraining between-event variability of kinematic rupture scenarios by empirical ground-motion model: A case study in central Italy. Bulletin of the Seismological Society of America, 114(4), 2138-2150, https://doi.org/10.1785/0120230251

Gallovič, F., & Brokešová, J.; 2007: Hybrid k-squared source model for strong ground motion simulations: Introduction. Physics of the Earth and Planetary Interiors, 160(1), 34-50, https://doi.org/10.1016/j.pepi.2006.09.002

Corresponding author: marta.freddi@unicam.it

Characterization of the Arena of Verona and Its Subsoil using a Non-Invasive Geophysical Approach

M.R. Gallipoli[1], S. Lucente[1], V. Serlenga[1], N. Tragni[2], G. Gangone[1] & NEW AGE Working Group

[1] National Research Council of Italy, CNR-IMAA (Italy)
[2] ITALFERR SPA (Italy)

Current Italian guidelines for the preservation of monumental heritage do not adequately address the integrated characterization of structures, foundation systems, and buried urban features such as archaeological layers. Seismic microzonation protocols, meanwhile, focus primarily on the seismotectonic, lithostratigraphic, and geotechnical properties of surface soils, overlooking their interaction with the built environment. Separating ground motion analysis from structural response evaluation is particularly limiting in historic centres, where monuments often rest on complex subsoils containing archaeological remains.

Within this framework, the NEW AGE Project (PRIN 2022, "NEW integrated approach for seismic protection and valorisation of heritAGE buildings on historical soil deposits") aims to bridge these gaps by developing a multiscale, multi-resolution geophysical methodology for the integrated investigation of geological subsoils, archaeological layers, soil-foundation systems, and heritage structures. This approach, based on a holistic perspective, has been tested on two prestigious monuments: the Roman Arena of Verona (northern Italy) and the Santa Sofia bell tower in Benevento (southern Italy).

This study presents the first results of the geophysical investigation carried out on the Arena of Verona and its subsoil. An extensive seismic survey campaign was carried out (MASW, ESAC, and 17 single-station seismic noise measurements) aimed at the seismo-stratigraphic and mechanical characterization of the subsoil. In addition, 21 seismic array configurations were performed inside the structure to estimate the main vibrational modes, mode shapes, and wave propagation velocities at various points of the monument.

The adopted approach proved highly effective due to its rapidity, full non-invasiveness, and adaptability, enabling large-scale assessments of heritage structures without affecting normal tourist operations.

Urban Soil and Building Characterisation for Advanced Seismic Risk Assessment: the city of Potenza (southern Italy)

G. Gangone[1,2], M.R. Gallipoli[1], M. Vona[2]

[1] National Research Council of Italy (CNR-IMAA), Tito Scalo (PZ), Italy
[2]Department of Structures, Geotechnics and Geology Applied to Engineering, University of Basilicata, Potenza, Italy

This study presents a new assessment of the seismic risk of the city of Potenza (Basilicata, southern Italy) by integrating seismic evaluations on all urban soils and overlying buildings by using experimental data and non-linear structural modelling through a holistic approach.

The experimental characterisation was carried out through 453 single-station ambient noise measurements analysed using the Horizontal-to-Vertical Spectral Ratio (HVSR) technique (Nakamura, 1989). Of these, 300 measurements were collected on the main lithological units of the urban soils, while 153 were performed on buildings selected as representative of the city in terms of structural typology, construction period, height, and foundation lithology. The fundamental soil frequencies (f_s) range from 1.1 to 9.5 Hz, with a median value of 3.5 Hz. The point measurements were interpolated using the Kriging method to generate iso-frequency maps and the associated uncertainty maps, providing a continuous spatial representation of the variability in soil characteristic frequencies across the investigated area.

The fundamental frequencies of the monitored buildings (f_b), ranging between 1.2 and 6.5 Hz, show a clear dependence on building height, structural typology, and plan area. This evidence enabled the derivation of an empirical relationship, which was subsequently used to estimate the fundamental frequency of the entire building stock of the city. A comparison between building frequencies and those of the underlying soils allowed the identification and mapping, at the urban scale, of areas potentially affected by soil–structure resonance in the linear elastic range, providing a first spatial indicator of possible seismic damage amplification. Based on the degree of overlap between building and soil frequency bands, a graphical representation was produced using a traffic-light colour scheme, in which red indicates a high likelihood of double resonance, while dark green denotes conditions under which resonance is virtually negligible (Fig. 1).

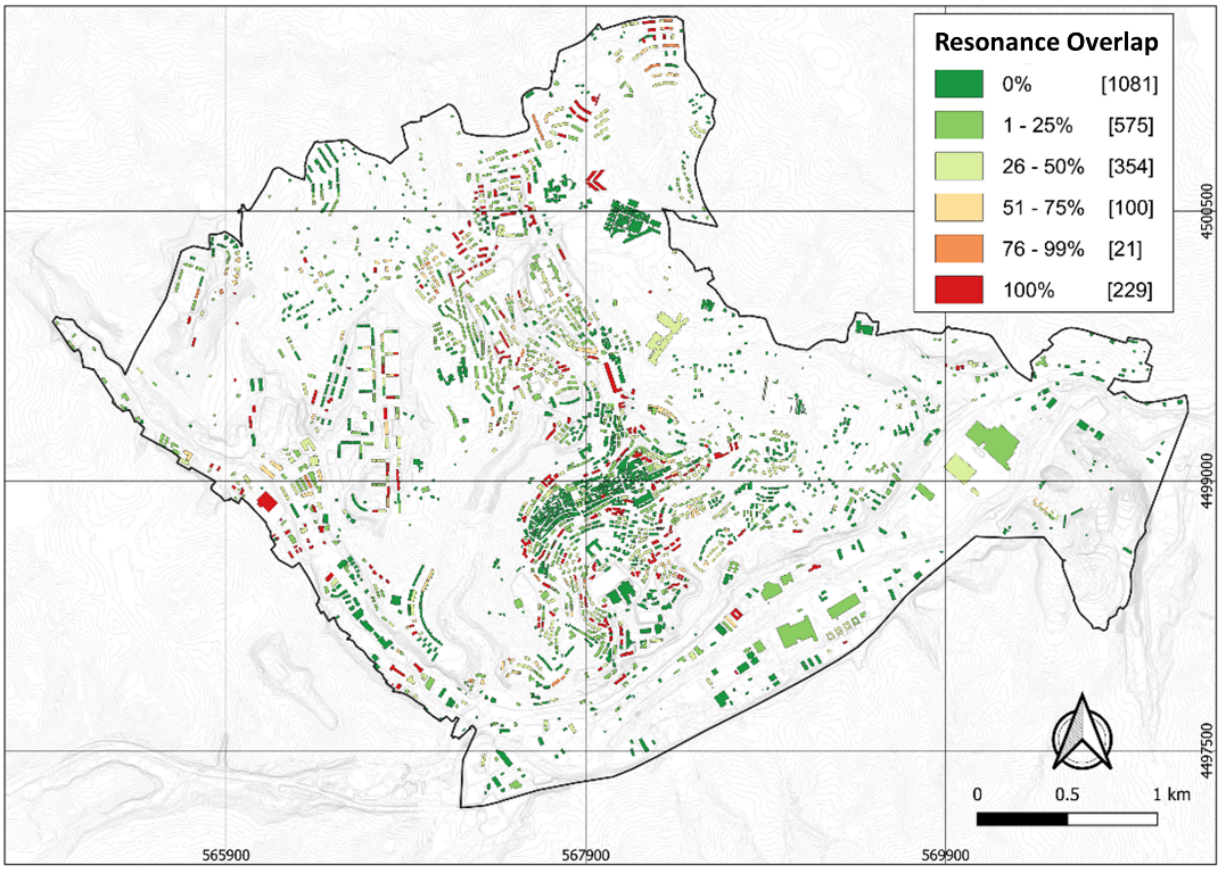

Fig. 1 – Soil–structure resonance map. The probability of resonance between buildings and soils are represented using a traffic-light colour scale: green indicates negligible resonance potential, whereas red highlights a high probability of occurrence of the resonance effect.

The assessment of structural performance focused on reinforced concrete buildings classified into eight typological classes based on construction period (pre- and post-1971), structural typology (infill frame and pilotis frame), and height (mid-rise and high-rise). Non-linear dynamic analyses (NLDA) were performed for each typological class using numerical models and procedures developed in previous studies (Masi & Vona, 2012). The analyses were carried out using 50 different seismic inputs, including both natural and synthetic accelerograms (Masi et al., 2011), and the structural response was interpreted in terms of damage levels according to the EMS-98 scale.

The dynamic characteristics and structural performance were summarized using trilinear elastoplastic capacity curves, which describe the global force-displacement relationship from elastic behaviour to collapse. To enable comparison across buildings of different scales, base shear force was normalized by total building weight, and displacement was expressed in dimensionless form relative to building height.

The first branch of the curve, corresponding to elastic behaviour, was constrained using the experimentally measured fundamental vibration periods. The subsequent branches—yielding, maximum displacement, and collapse—were defined based on force and displacement percentiles derived from NLDA and associated with damage limit states DL = 2, 3, and 4, respectively. Figure 2 illustrates the construction of the trilinear capacity curve for one of the eight typologies, together

with coloured crosses representing NLDA results and marking the attainment of the corresponding EMS-98 damage levels.

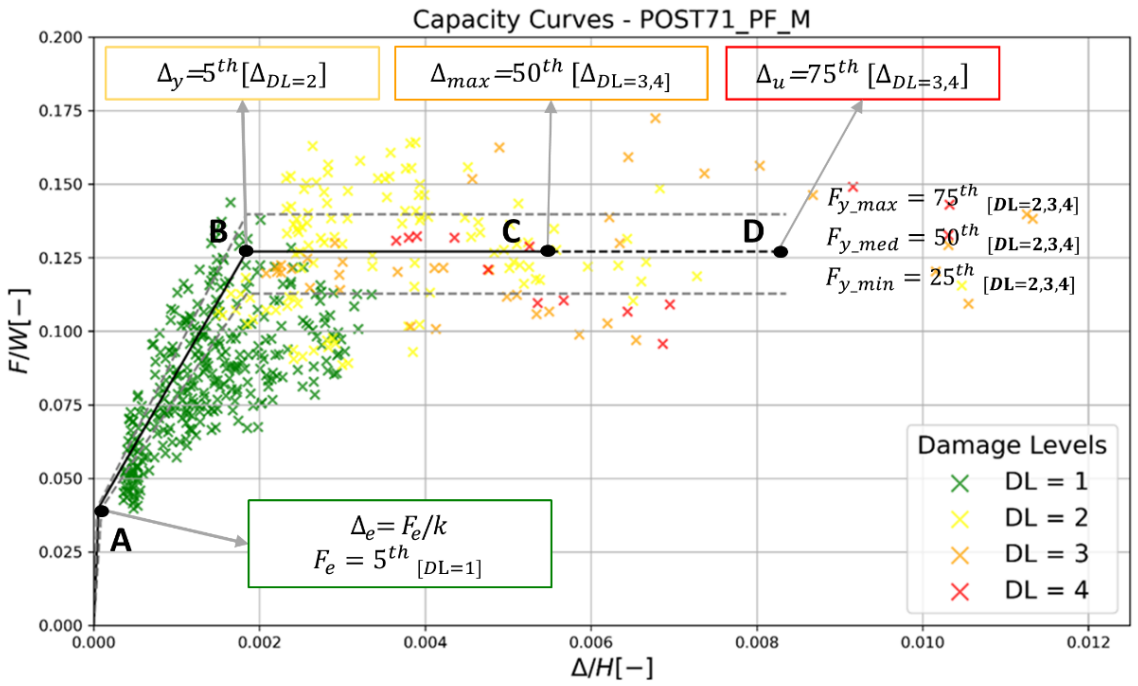

Fig. 2 Trilinear capacity curve in terms of normalized roof displacements and normalized base shear force, with coloured crosses representing NLDA results and the corresponding EMS-98 damage levels.

The final step was the construction of probabilistic fragility curves based on site-specific demand spectra, obtained by taking into account both the seismic hazard and the urban stratigraphy. The intersection between the demand spectra and capacity curves allowed for the estimation of performance points and the definition of fragility curves as the probability of exceeding damage limit states as a function of PGA, for each typological class and for each homogeneous seismic zone.

These curves form the basis for defining a synthetic seismic risk index (Vona, 2020), integrating probabilistic information on different damage levels into a single parameter. This enables the creation of urban seismic vulnerability maps that jointly consider soil dynamic characteristics, structural performance of buildings, and expected damage scenarios (Dolce et al., 2003).

Overall, integrating local seismic response, soil-structure interaction, and structural vulnerability allows for a more realistic and physically grounded assessment of urban seismic risk compared to traditional approaches, with potential applications in urban planning and risk mitigation strategies.

References

Dolce, M., Masi, A., Marino, M., & Vona, M.; 2003: Earthquake damage scenarios of the building stock of Potenza (Southern Italy) including site effects. Bulletin of Earthquake Engineering, 1(1), 115-140.

Masi, A., Vona, M., & Mucciarelli, M. (2011). Selection of natural and synthetic accelerograms for seismic vulnerability studies on reinforced concrete frames. Journal of Structural Engineering, 137(3), 367-378.

Masi, A., & Vona, M.; 2012: Vulnerability assessment of gravity-load designed RC buildings: Evaluation of seismic capacity through non-linear dynamic analyses. Engineering Structures, 45, 257-269.

Nakamura, Y.; 1989: A method for dynamic characteristics estimation of subsurface using microtremor on the ground surface. Railway Technical Research Institute, Quarterly Reports, 30(1).

Vona, M.; 2014: Fragility curves of existing RC buildings based on specific structural performance levels. Open Journal of Civil Engineering, 4(2), 120-134.

Vona, M.; 2020: A novel approach to improve the code provision based on a seismic risk index for existing buildings. Journal of Building Engineering, 28, 101037.

Corresponding author: giovannigangone@cnr.it

A new multidisciplinary study on active and capable faulting for the Seismic Microzonation of the city of L'Aquila, central Italy, enhances the legacy of the 2009, M_W 6.1 earthquake for seismic risk mitigation

S. Gori[1], E. Falcucci[1], S. D'Annibale[1], M. Francescone[2], M. Iorio[3], M. Mariani[1,2], A. Testa[2], P. Boncio[2], F. Galadini[1], A. Pizzi[2], D. Cosentino[3], F. D'Ajello Caracciolo[1], M.G. Di Giuseppe[1], G. Di Giulio[1], F. Doumaz[1], D. Famiani[1], I. Garofalo[4], S. Hailemikael[1], R. Isaia[1], V. Materni[1], A. Mercuri[1], L. Miconi[1], L. Minarelli[1], I. Nicolosi[1], V. Romano[1], V. Sapia[1], V. Sepe[1], M. Tallini[4], A. Troiano[1], M. Vassallo[1]

[1] Istituto Nazionale di Geofisica e Vulcanologia INGV (Italy)
[2] Dipartimento INGEO, Università degli Studi G. d'Annunzio Chieti e Pescara (Italy)
[3] Dipartimento di Scienze, Università degli Studi Roma tre (Italy)
[4] Dipartimento DICEAA, Università degli Studi dell'Aquila (Italy)

Introduction

The M_W 6.1 earthquake that struck the L'Aquila territory in 2009, in the central Apennines of Italy, dramatically emphasised the need to improve the preparedness of urbanised areas to earthquake-related geological hazards. Seismic Microzonation aims to address this issue by identifying zones with homogeneous seismic response in terms of ground-motion amplification. A further objective is to identify and map surficial geological instabilities that may represent critical constraints for land-use planning, preservation and urban development (Gruppo di Lavoro MS, 2008). These instabilities comprise landslides, liquefaction and differential compaction, all of which may be triggered by seismic shaking. Particular attention is devoted to surface faulting, that is, ground rupture caused by the activation of active and capable faults. This hazard, which is the focus of the present contribution, is related to the rupture of the causative earthquake fault. Italian guidelines for the management of territories affected by active and capable faults (Commissione Tecnica per la Microzonazione Sismica, 2015) prescribe the definition of specific zones across fault traces, together with land-use restrictions for urban and peri-urban areas.

Following the 2009 earthquake, an unprecedented number of studies were carried out in the epicentral area to characterise the geological framework of the L'Aquila territory for seismic microzonation purposes. Geological models of several sectors of the municipality were then proposed (e.g. Nocentini et al., 2017; Tallini et al., 2019, 2025), leading to the publication of

dedicated studies and geological maps. These investigations addressed different geological aspects of the L'Aquila region, ranging from the stratigraphy of the pre-Quaternary bedrock and Quaternary deposits (Galli et al., 2010; Cosentino et al., 2017) to the identification of active and capable faults (Boncio et al., 2010; Galli et al., 2011; Moro et al., 2013) (Fig. 1). These include the surface expression of the fault responsible for the 2009 earthquake, the Paganica fault (hereafter PF). The well-documented surface faulting along the PF became a benchmark for the definition of Italian guidelines on active and capable faults (Boncio et al., 2012).

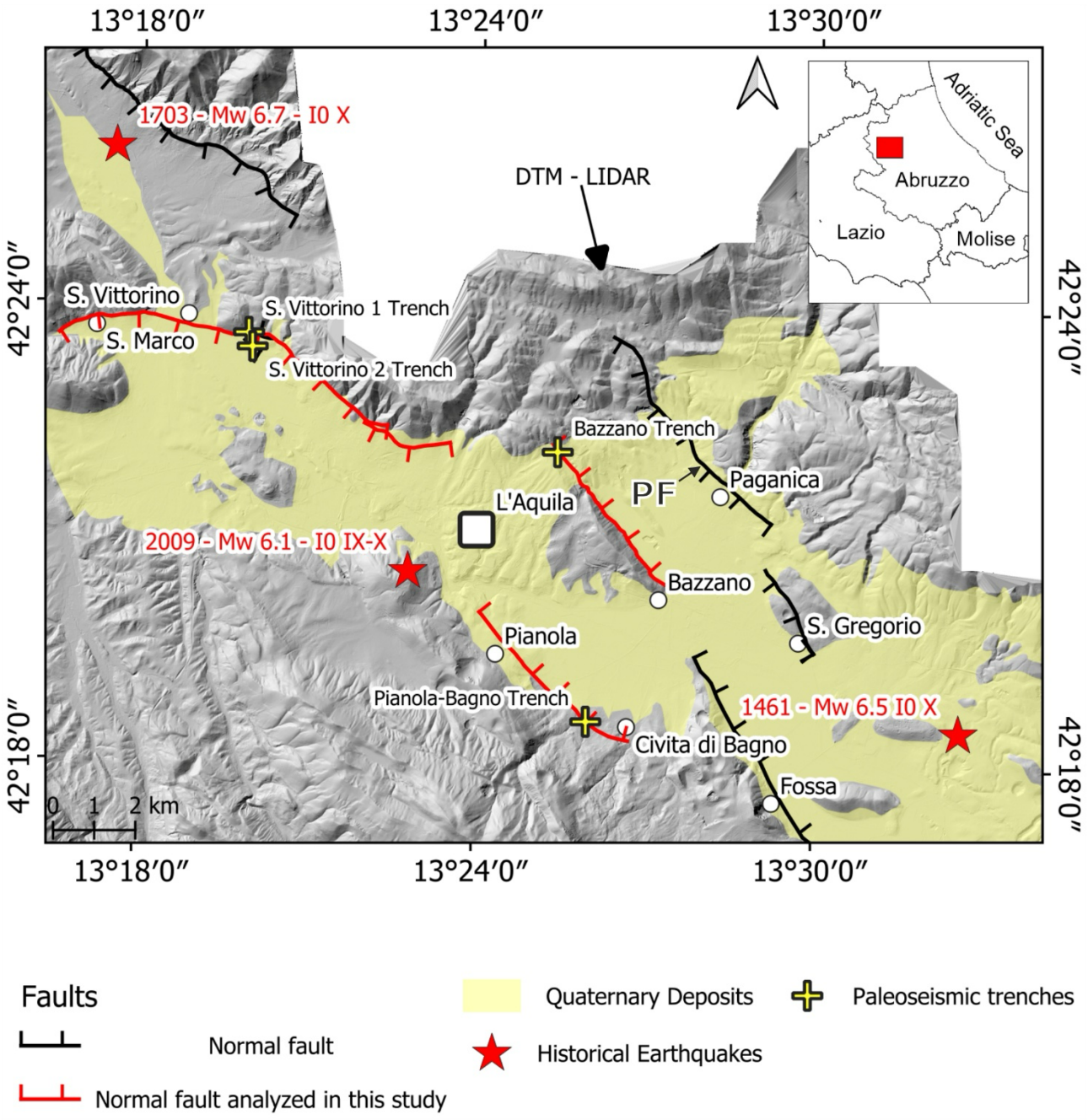

Fig. 1 – Digital Terrain Model (shaded relief) of the L'Aquila Basin. Faults in red are those active and capable analysed in this study. Yellow crosses are the trench sites. Red stars are the historical earthquakes that affected the L'Aquila region; PF, the Paganica Fault.

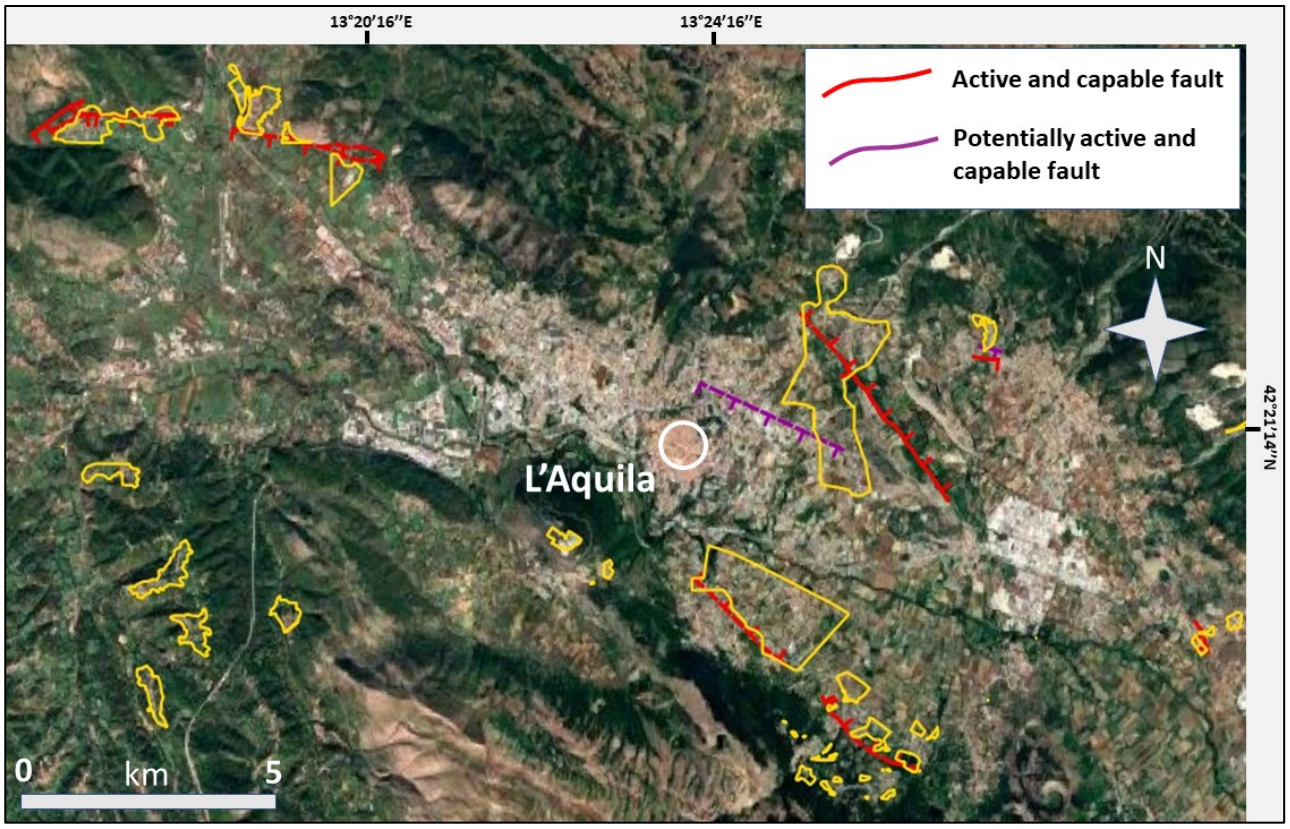

Fig. 2 – Satellite image (from Google Earth) showing the L'Aquila territory. The L'Aquila city historical centre is indicated by the with circle. The yellow polygons show the areas under investigation for Seismic Microzonation purpose.

Nevertheless, some portions of the L'Aquila territory remained comparatively poorly investigated and required further analyses. To address this gap, the L'Aquila Municipality and INGV signed a scientific agreement at the end of 2023, building on collaborations initiated shortly after the 2009 event.

Preliminary investigations suggested that these areas might be affected by active or potentially active and capable faults previously identified or hypothesised, but not mapped at a scale suitable for seismic microzonation (Fig. 2). Consequently, a multidisciplinary research group was established, involving researchers from INGV and the Universities of Chieti–Pescara, L'Aquila and Roma Tre, with expertise in Quaternary geology, structural geology, geomorphology, geophysics and seismic microzonation. The objective was to refine the characterisation of these fault structures.

Results

In a sector within L'Aquila downtown, previous studies suggested the possible presence of a normal fault responsible for the displacement of Middle Pleistocene carbonate breccias, which are one of the most surficial geological units onto which L'Aquila is built. This hypothesised fault segment might be the southern prolongation of the active and capable Pettino normal fault (APAT, 2005; Nocentini et al., 2017; Tallini et al., 2019) whose trace might reach the northern part of L'Aquila downtown. On the contrary, in the official fine-scale Seismic Microzonation maps (first and third level) this supposed fault element is not reported in the investigated area (macroarea 1) (Gruppo di Lavoro MS–AQ, 2010). Nonetheless, this supposed potentially active and capable fault should affect a

sector of the city known as Colle Sapone, where several school buildings are located. Therefore, this aspect renders the assessment of the fault presence and capability even more relevant.

We here performed geological investigations on both pre-Quaternary and Quaternary formations (based on field analyses and borehole data), paleoseismological trenching supported by geophysical investigation (specifically Electrical Resistivity Tomography), and geomorphological investigation aimed at defining the possible occurrence of morphotectonic features. We also analysed a detailed Digital Elevation Model retrieved from LiDAR data acquired in 2009 and from aerial photographs dataset taken in 1944-1945. The advantage of analysing such an old imagery of the territory is to have a view of the landscape when the urban fabric was much less developed than in the last years, and the original geomorphic features were still preserved.

The results indicate that the widespread shear planes affecting the outcropping bedrock are not related to the current extensional tectonic regime. Only reverse and transpressive faulting affecting pre-Quaternary limestones was documented, consistent with earlier compressive tectonics. In several locations, bedrock units across the presumed fault strand show no evidence of extensional displacement, being either continuous or juxtaposed by strike-slip or reverse faults. Paleoseismological trenching did not reveal displacement of the upper portion of the L'Aquila breccias. As observed in other sectors of the city, only features attributable to karst processes developed within the limestone bedrock and breccias were identified. These findings rule out the presence of an active and capable fault in the Colle Sapone school area, in agreement with Arriga et al. (2024), who proposed that displacement along the Pettino fault is transferred south-eastwards to the Paganica fault, bypassing the urban area of L'Aquila.

As for the other possible active and capable fault strands affecting the area under investigation, we confirmed the presence of an active and capable fault in the area of Pianola and Bagno, here named the Pianola-Bagno fault (hereafter PBF) south of L'Aquila. The fault has been found and investigated by previous studies (Maceroni et al., 2018). The authors defined that the tectonic feature is an antithetic fault of the Paganica fault, and that it is responsible for at least one activation episode after the 1st century AD. Geological field analyses, geophysical investigation and ambient seismic noise analyses allowed detailed mapping of the fault zone which cuts across the village of Bagno.

Another antithetic structure, the Bazzano fault (BF), was also investigated. Its activation during the 2009 earthquake was hypothesised by some authors (e.g. Vittori et al., 2011), although the observed coseismic features were alternatively interpreted as sediment compaction at the base of the fault scarp (Falcucci et al., 2009). The BF had not been investigated in detail after 2009. Analysis of historical aerial photographs suggested that its trace extends further north than the geomorphologically evident bedrock scarp. This interpretation is supported by paleoseismological trenching and geophysical data, which indicate late Holocene surface faulting events. Importantly, the BF trace intersects the A24 motorway, a major regional transport corridor. Surface faulting along the Paganica fault during the 2009 earthquake produced minor vertical displacement (5–10 cm) of the same infrastructure (Falcucci et al., 2009), indicating that the BF should also be considered capable of surface rupture affecting the motorway. Moreover, paleoseismological data from both the Paganica fault (e.g. Boncio et al., 2010; Moro et al., 2013) and the BF trench suggest that pre-

2009 events produced significantly larger surface displacements, increasing concern regarding surface faulting hazard for critical infrastructure.

Finally, paleoseismological and geophysical investigations confirm late Quaternary activity of the Pettino fault in the San Vittorino area, where synthetic and antithetic branches define a fault zone several metres wide.

Concluding remarks

Overall, this study provides an updated and detailed definition and mapping of active and capable faults affecting the L'Aquila territory, highlighting potential interactions with critical infrastructure. The results emphasise the need for an integrated approach to fault characterisation that considers not only recent activity but also the long-term geological and structural evolution of fault systems. From a seismotectonic perspective, beyond applications to seismic microzonation, the collected data contribute to improved assessment of seismic potential and fault segmentation within the L'Aquila Basin and the central Apennines.

Acknowledgments

The present work has been made in the framework of the INGV-L'Aquila Municipality Scientific Agreement 2023-2026 (Protocollo INGV n. 0024313 del 19/09/2023).

References

APAT; 2005: Geological map of Italy at 1:50,000 scale, sheet n°359 L'Aquila. S.EL.CA. Firenze, doi: https://doi.org/10.15161/oar.it/212295. Available online at: https://www.openaccessrepository.it/records/212295

Arriga G., Marchegiano M., Peral M., Hu H.-M., Cosentino D., Shen C.-C. et al.; 2024: Long-term tectonostratigraphic evolution of a propagating rift system, L'Aquila Intermontane Basin (central Apennines). Tectonics, 43, e2024TC008548, https://doi.org/10.1029/2024TC008548

Boncio P., Galli P., Naso G., Pizzi A.; 2012: Zoning surface rupture hazard along normal faults: insight from the 2009 M_W 6.3 L'Aquila, Central Italy, earthquake and other global earthquakes. Bull. Seismol. Soc. Am. 102 (3), 918–935, doi: 10.1785/0120100301

Boncio P., Pizzi A., Brozzetti F., Pomposo G., Lavecchia G., Di Naccio D. et al.; 2010: Coseismic ground deformation of the 6 april 2009. L'Aquila earthquake (central Italy, M_W 6.3). Geophys Res. Lett. 37, L06308, doi: 10.1029/2010GL042807

Commissione tecnica per la microzonazione sismica; 2015: Linee guida per la gestione del territorio in aree interessate da Faglie Attive e Capaci (FAC), versione 1.0 Conferenza delle Regioni e delle Province Autonome –Dipartimento della protezione civile, Roma, 2015.

Cosentino D., Asti R., Nocentini M., Gliozzi E., Kotsakis T., Mattei M. et al.; 2017: New insights into the onset and evolution of the central Apennine extensional intermontane basins based on the

tectonically active L'Aquila Basin (central Italy). Bull. Geol. Soc. Am. 129, 1314–1336, doi: 10.1130/B31679.1.

Falcucci E., Gori S., Peronace E., Fubelli G., Moro M., Sarol, M., et al.; 2009: The Paganica fault and surface coseismic ruptures caused by the 6 april 2009 earthquake (L'Aquila, Central Italy). Seismol. Res. Lett. 80, 940–950, doi: 10.1785/gssrl.80.6.940

Galli P., Giaccio B., Messina P.; 2010: The 2009 central Italy earthquake seen through 0.5 Myr-long tectonic history of the L'Aquila faults system. Quat. Sci. Rev. 29, 3768–3789, doi: 10.1016/j.quascirev.2010.08.018

Galli P. A. C., Giaccio B., Messina P., Peronace E., Zuppi G.M.; 2011: Palaeoseismology of the L'Aquila faults (central Italy, 2009, M_W 6.3 earthquake): implications for active fault linkage. Geophys J. Int. 187, 1119–1134, doi: 10.1111/j.1365-246X.2011.05233.x

Gruppo di lavoro MS; 2008: Indirizzi e criteri per la microzonazione sismica. Conferenza delle Regioni e delle Province autonome - Dipartimento della protezione civile, Roma, 3 vol. e Dvd.

Gruppo di Lavoro MS–AQ; 2010: Microzonazione sismica per la ricostruzione dell'area aquilana. Regione Abruzzo – Dipartimento della Protezione Civile, L'Aquila, 3 vol. e Cd-rom.

Maceroni D., Racano S., Falcucci E., Gori S., Galadini F.; 2018: Application of quaternary studies for the assessment of active and capable faults in the central Apennines: Implications for microzonation and seismotectonic analyses. Alpine and Mediterranean Quaternary, ISSN: 2279-7327.

Moro M., Gori S., Falcucci E., Saroli M., Galadini F., Salvi S.; 2013: Historical earthquakes and variable kinematic behaviour of the 2009 L'Aquila seismic event (central Italy) causative fault, revealed by paleoseismological investigations. Tectonophysics 583, 131–144, doi: 10.1016/j.tecto.2012.10.036

Nocentini M., Asti R., Cosentino D., Durante F., Gliozzi E., Macerola L., et al.; 2017. Plio-quaternary geology of L'Aquila-Scoppito basin (Central Italy). J. Maps 13, 563–574, doi:10.1080/17445647.2017.1340910

Tallini M., Maceroni D., Falcucci E., Galadini F., Gori S., Guerriero V., Spadi M., Moro M. Saroli M.; 2025: Multi-methodological approach for assessing surface faulting and paleoliquefaction history in central Italy: applicative implications for seismic microzonation studies in the Quaternary L'Aquila basin. Front. Earth Sci. 13:1523730, doi: 10.3389/feart.2025.1523730.

Tallini M., Spadi M., Cosentino D., Nocentini M., Cavuoto G., Di Fiore V.; 2019: High-resolution seismic reflection exploration for evaluating the seismic hazard in a Plio-Quaternary intermontane basin (L'Aquila downtown, central Italy). Quat. Int. 532, 34–47, doi: 10.1016/j.quaint.2019.09.016

Vittori E., Di Manna P., Blumetti A.M., Comerci V., Guerrieri L., Esposito E., Michetti A.M., Porfido S., Piccardi L., et al.; 2011: Surface faulting of the 6 april 2009 M_W 6.3 L'Aquila earthquake in central Italy. Bull. Seism. Soc. Am., 101 (4), 1507-1530, https://doi.org/10.1785/0120100140.

Corresponding author: emanuela.falcucci@ingv.it

Exploring the regional differences of ground motion in Italy through the non-ergodic modelling

G. Lanzano[1], S. Sgobba[1], D. Bindi[2]

[1] Istituto Nazionale di Geofisica e Vulcanologia, Sezione di Milano, Italy
[2] GFZ Helmholtz Centre for Geosciences, Potsdam, Germany

Data and methods

Recently, significant methodological advances have been made in ground motion modeling, moving from ergodic GMMs (Ground Motion Models) to partially or fully non-ergodic GMMs, thanks to the identification of systematic effects and the estimation of the epistemic uncertainty associated with these terms. The observable repeatable effects can be manifold and vary according to specific cases. In the most common formulation, however, they refer to the event, the station/instrument, the causative source, and the source-site path. This scheme is very useful for constructing prediction models that incorporate corrections to describe the local characteristics of seismic motion that differ from the median model, without the need to calibrate separate GMMs.

This brief note illustrates the application of this modeling approach to active crustal earthquakes in Italy. The reference dataset is ITACAext 2.0 (Lanzano et al. 2025), which collects regional earthquake recordings of Mw>=3.0 from 1972 to 2022. The parameters investigated are the spectral ordinates of the Fourier spectrum (FAS), calculated for both the entire signal and the strong signal phase (from the arrival of the S waves onwards, considering the strongest part of the waveform). Details on the FAS calculation are given in Lanzano et al. (2025). Reference is made to the horizontal motion, obtained as a vectorial combination of the two horizontal components of the seismic recordings.

The proposed model is based on the original ITA18 function (Lanzano et al. 2019), which calibrates a partially non-ergodic GMM, with random terms for events and sites. In this case, the model is completely non-ergodic and is described by the following equation:

$$log_{10}Y_{FNE}(IM) = log_{10}Y_{PNE}(IM) + \delta L2L|source + \delta c_3\left(\sqrt{R^2 + h^2} - R_{ref}\right)|path \quad [1]$$

Where Y_{FNE} is the "full non-ergodic" prediction and Y_{PNE} is the "partially non-ergodic" prediction adopting the ITA18 functional form. In addition, there is a random correction term for the source, δL2L, and one for the coefficient of the anelastic attenuation function of the original model, δc_3. In this term, R is a distance metric that can be either Joyner-Boore or distance for the rupture plane, h is the pseudo-depth, and R_{ref} is the reference distance equal to 1 km. The predicted intensity measures (IM) are the FAS amplitudes at 81 equispaced frequencies on a logarithmic scale from 0.1 to 28Hz.

The new repeatable source and path terms are modeled according to two schemes: 1) zonations by Brunelli et al. (2023) to define homogeneous but geometrically different areas for source and path; 2) grid with 0.2x0.2° spacing to estimate corrections that vary continuously in space.

Main findings

Although the GMM calibrations were performed at all frequencies, the results are shown for a high-frequency FAS ordinate, corresponding to approximately 16 Hz, where significant local differences in seismic ground motion are observed. Figure 1 shows the correction values δL2L for the source areas derived from the zonation of Brunelli et al. (2023), obtained by appropriately modifying the seismogenic zone of Visini et al. (2022). The amplitude of seismic motion is approximately twice as high for events occurring in the northwest, Puglia, and the southern Ionian Sea. However, it is approximately half as great along the Ionian coast of Calabria and on the mainland of Sicily. In other cases, the differences are smaller.

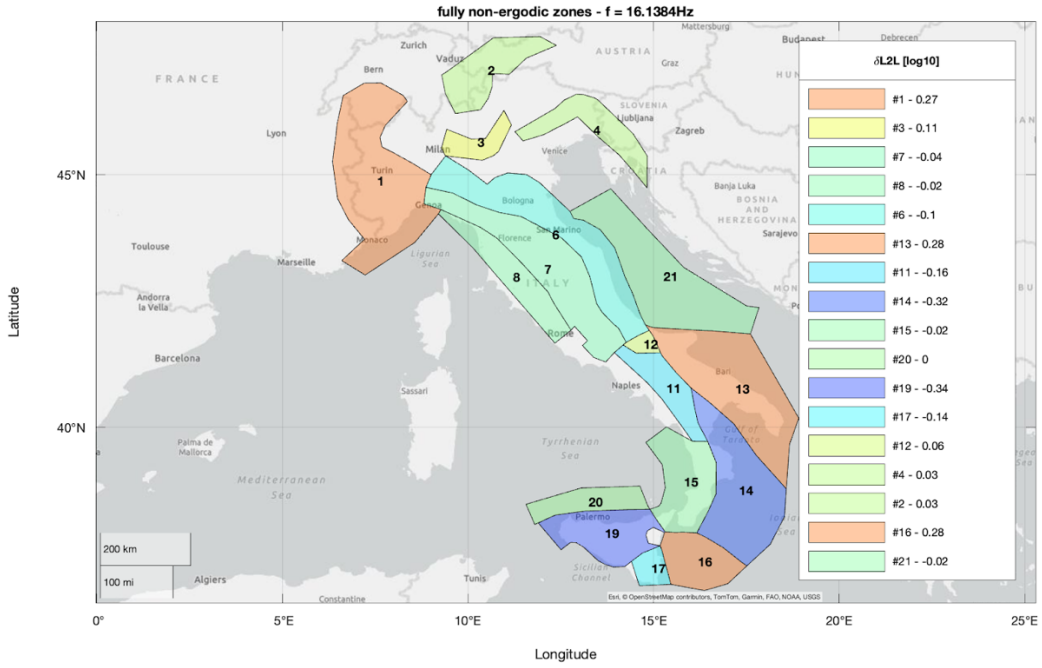

Fig. 1 – δL2L corrective terms for FAS ordinates at f=16Hz for the entire signal.

In the case of path correction, the result of calibration with the grid at the same frequency is reported (Figure 2), which proves to be very advantageous for highlighting propagation differences in a data-driven approach. Red cells indicate areas where seismic motion attenuates faster than the reference motion (Y_{PNE} in Eq. 1), while blue cells indicate the opposite. There are clear lines separating the red areas (the entire Apennines chain, Calabria, and northern Sicily) from the blue areas (the Po Valley, Puglia, and Iblei Massif). The differences in the Alps are more complex, partly due to the smaller number of recordings.

These results are extremely promising for inclusion in a ground motion model for engineering parameters (acceleration response spectrum ordinates), enabling the reconstruction of shaking scenarios that are much more accurate than those of traditional models.

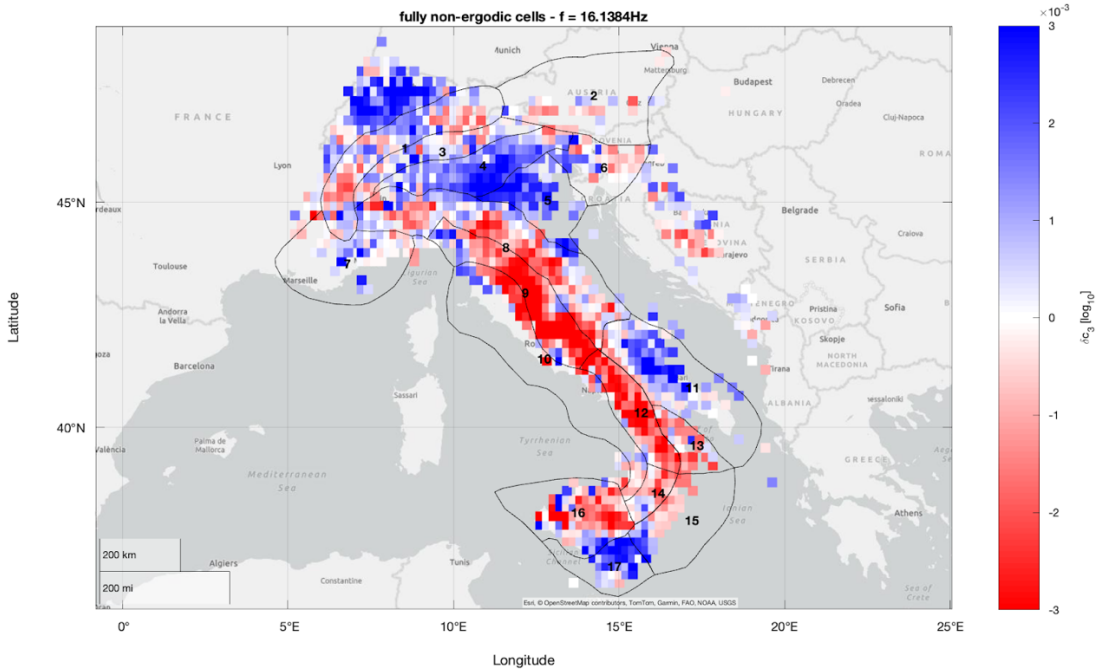

Fig. 2 – δc_3 coefficient correction for FAS at f=16Hz for the entire signal.

References

Brunelli, G., Lanzano, G., Luzi, L., Sgobba, S.; 2023. Data-driven zonations for modelling the regional source and propagation effects into a Ground Motion Models in Italy. Soil Dynamics and Earthquake Engineering, Vol. 166, 107775.

Lanzano, G., Luzi, L., Pacor, F., Felicetta, C., Puglia, R., Sgobba, S., D'Amico, M.; 2019. A revised ground-motion prediction model for shallow crustal earthquakes in Italy. Bulletin of the Seismological Society of America, Vol. 109, n. 2, pp. 525-540.

Lanzano, G., Vitrano, L., Bindi, D., Felicetta, C., Sgobba, S., Luzi, L., Pacor, F.; 2025. ITACAext 2.0: A High-Quality Parametric Table of Strong-to-Weak Motion Recordings for Seismological and Engineering Research in Italy. Seismological Research Letters. Vol. 96, n. 5, pp. 3295–331.

Visini, F., Meletti, C., Rovida, A., D'Amico, V., Pace, B., Pondrelli, S.; 2022. Updated area-source seismogenic model for seismic hazard of Italy. Natural Hazards and Earth System Sciences, Vol. 22, pp. 2807–2827.

Corresponding author: giovanni.lanzano@ingv.it

Construction of seismic fragility curves for reinforced concrete frame buildings in Cuba

Kenia Mercedes Leyva Chang[1], Grisel Morejón Blanco[1], Eduardo Rafael Álvarez Deulofeu[2]

[1] Centro Nacional de Investigaciones Sismológicas (CENAIS), Santiago de Cuba, Cuba
[2]Universidad de Oriente, Santiago de Cuba, Cuba

Is presented the first comprehensive procedure to generate specific seismic fragility curves for reinforced concrete frame buildings in Cuba. A total of 297 structural variants designed under NC 46:1999 and NC 46:2017 regulations were analyzed, incorporating mechanical properties of Cuban reinforcing steels (G-40, A44) and local seismic conditions. Using Nonlinear Dynamic Analysis with representative accelerograms scaled to match the Cuban Uniform Hazard Spectrum, damage thresholds were quantified based on maximum inter-story drift. Results show reductions of up to 60.3% in drift for complete damage state in NC 46:2017 structures, demonstrating significant improvements in seismic performance. Empirical validation using international data confirmed high accuracy (R^2 = 0.976). The resulting curves constitute a robust probabilistic tool for the technical evaluation of seismic vulnerability and the revision of design codes in Cuba.

References

Aguiar, R. y Bobadilla, D.; 2005: Curvas de fragilidad para estructuras de H/A de Ecuador menores a siete pisos. Revista Ciencia, Vol. 8, No. 2, pp. 81-88, Quito, Ecuador.

Álvarez, L., Lindholm, C.y Villalón, M.; 2016: Seismic hazard for Cuba: A new approach. Bulletin of the Seismological Society of America, 107 (1): 1-11, doi: 10.1785/0120160074.

American Concrete Institute; 2019: Building code requirements for structural concrete (ACI 318-2019) and commentary. Farmington Hills, MI: Author.

American Society of Civil Engineers; 2017: ASCE/SEI 41-17: Seismic evaluation and retrofit of existing buildings. Reston, VA: Author.

American Society of Civil Engineers; 2022: ASCE/SEI 7-22: Minimum design loads for buildings and other structures. Reston, VA: Author.

Applied Technology Council; 1985: Earthquake damage evaluation data for California (Report No. ATC-13). Redwood City, CA: Author.

Applied Technology Council; 1996: ATC-40: Seismic evaluation and retrofit of concrete buildings. Report No. ATC–40, Redwood City, CA: Author.

Arco, B., Morejón, G. y Vidau, I.; 2023: Evaluación del desempeño sísmico de la variante 3 modificada del sistema constructivo E-14. Ciencia en su PC, 1(1), 99-115.

Computers and Structures, Inc.; 2020: SAP2000 (Versión 22) [Software de análisis estructural].

European Committee for Standardization; 2004: Eurocode 8: Design of structures for earthquake resistance—Part 1: General rules, seismic actions and rules for buildings (EN 1998-1). Brussels, Belgium: Author.

FEMA; 1999: HAZUS®99 Earthquake Loss Estimation Methodology, User Manual. Federal Emergency Management Agency. Washington, DC: Author.

FEMA; 2003: Multi-hazard loss estimation methodology (HAZUS-MH). Washington, DC: Author.

FEMA: 2005: Improvement of Nonlinear Static Seismic Analysis Procedures (FEMA 440). Washington, DC: Author.

FEMA; 2012: Multi-hazard loss estimation methodology, Earthquake model (HAZUS-MH MR5). Washington, DC: Author.

FEMA; 2018: Seismic Performance Assessment of Buildings, Volume 1 - Methodology, Second Edition. FEMA P-58-1. Washington, DC: Author.

FEMA; 2020: HAZUS-MH 2.1: Earthquake model technical manual. Federal Emergency Management Agency. Washington, DC: Author.

Frómeta, Z.; 2009: Caracterización y evaluación de los aceros de refuerzo producidos por ACINOX Las Tunas para su empleo en zona sísmica. [Tesis doctoral, Universidad Politécnica de la Habana].

Leyva, K., Morejón, G.y Candebat, D.; 2018: Construcción de las curvas de fragilidad para edificaciones sin información estructural en Cuba. Ciencia en su PC, volumen 1, No.1, pp 86-95.

Leyva Chang, K.M., Diez Zaldívar, E.R. y Villalon Semanat, M.; 2025: Vulnerabilidad sísmica estructural y estimación de daños en dos iglesias de la ciudad Santiago de Cuba. Revista de Estudios Latinoamericanos sobre Reducción del Riesgo de Desastres REDER, 9(1), 232-242. https://doi.org/10.55467/reder.v9i1.188.

Morejón, G., Leyva, K. y Arco, B.; 2017: Evaluación de la seguridad estructural de edificaciones postterremotos. Ciencia en su PC No.4 octubre-diciembre 2017 pp 78-90.

Morejón, G., Leyva, K.y Candebat, D.; 2021: Atlas de tipologías representativas en la ciudad Santiago de Cuba con fines de gestión de riesgo sísmico. Ciencia en su PC, volumen 1, No.1 pp 25-45.

Oficina Nacional de Normalización NC.; 2017: Norma Cubana NC 46:2017: Construcciones Sismorresistentes. Requisitos Básicos para el Diseño y Construcción. La Habana, Cuba.

Corresponding author: keniamerecedesleyvachang@gmail.com

Investigating Soil–Structure Interaction at the Santa Sofia Bell Tower (Benevento, southern Italy)

S. Lucente[1], M.R. Gallipoli[1], V. Serlenga[1], B. Petrovic[2], S. Parolai[3]

[1] National Research Council of Italy, CNR-IMAA (Italy)
[2] GFZ German Research Centre for Geosciences (Germany)
[3] University of Trieste (Italy)

Introduction

Within the PRIN NEW AGE ("NEW integrated approach for seismic protection and valorisation of heritAGE buildings on historical soil deposits") project framework, we tested Ambient Noise Deconvolution Interferometry (ANDI) as a suitable method for assessing soil-structure interaction effects between the Santa Sofia bell tower of Benevento (southern Italy) and its foundation soil. We recorded two hours of seismic noise simultaneously on the bell tower and the surrounding soil using velocimeter arrays. This study presents the first results of wave propagation velocity of the bell tower, of its foundation soil and the wave propagation from the bell tower to the soil.

Test site

The geophysical surveys were performed on June 13th and 14th, 2024 by the IMAA – CNR geophysical group within the 2022 PRIN NEW AGE project. The Santa Sofia bell tower is part of a monumental complex listed since 2011 in the UNESCO World Heritage. From a structural point of view, the original bell tower was constructed in the 11th Century but was destroyed during the 1688 earthquake and then reconstructed in the 1703 as an isolated edifice 26 m high with a square base.

Experimental setup and data acquisition

The surveys were performed by installing a set of 29 SentinelGEO seismic stations composed of triaxial 85dB MEMS accelerometers and 4.5 Hz geophones. The instruments were placed at different level in the bell tower and on the surrounding soil, following two directions (NS and EW) aligned with the bell tower and defining 2 L-shaped configurations (Fig. 1). We acquired about 2 hours of ambient noise for each configuration.

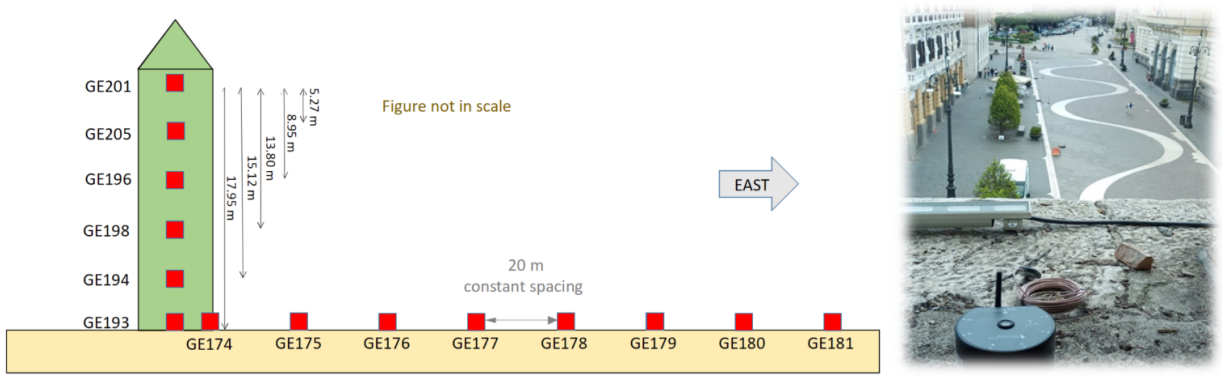

Fig. 1 – On the left: sketch of the sensor layout on the bell tower and on the soil for the second configuration (EW); on the right: picture of sensor placed on the bell tower.

Methods and analysis

First, we estimated the eigenfrequencies of the bell tower using the Standard Spectral Ratio method by analysing seismic noise recorded simultaneously at the top and at the base of the structure. The analysis identified two eigenfrequencies at 3.2 Hz and 12 Hz, consistent with those previously reported by De Angelis et al. (2022).

The pre-processing for ambient noise deconvolution interferometry (ANDI) method consists of: i) synchronization of all tracks; ii) removal of the mean, linear trends, and noise transients using a STA-LTA method specifically adapted to the noise context; iii) filtering between 0.01 and 20 Hz. Using stacked windows of about 20 s, we performed the ANDI analysis consisting in the seismic spectral ratio between the signal acquired by a fixed reference station and the signal of an *i-th* station (Lacanna et al., 2019; García-Macías & Ubertini, 2019; Petrovic et al., 2019; Skłodowska et al. 2023). The inverse Fourier transform of the deconvolved signal returns an impulse response function (IRF), which represents the travel time of the signal from the reference to the *i-th* station. We fixed the reference station on the top of the bell tower and carried out the deconvolution with respect all the other stations of the structure and the soil. We repeated the analysis for each of two configurations.

To better follow the seismic pulse released by the bell tower and interpret the obtained soil IRFs, we developed a model which simulates the Green's function of a spike-shaped waveform propagating from the bell tower to the soil. The model allowed us to identify the reflections at different sensors.

Results

The wave propagation velocities for both horizontal components, retrieved using the ANDI method, are approximately 300 m/s within the bell tower. These values are consistent with those reported for other bell towers and similar monumental structures (García-Macías & Ubertini, 2019). The velocities obtained for the soil are on the order of 400 m/s, in agreement with the ESAC and MASW velocity profiles measured at the foundation soil.

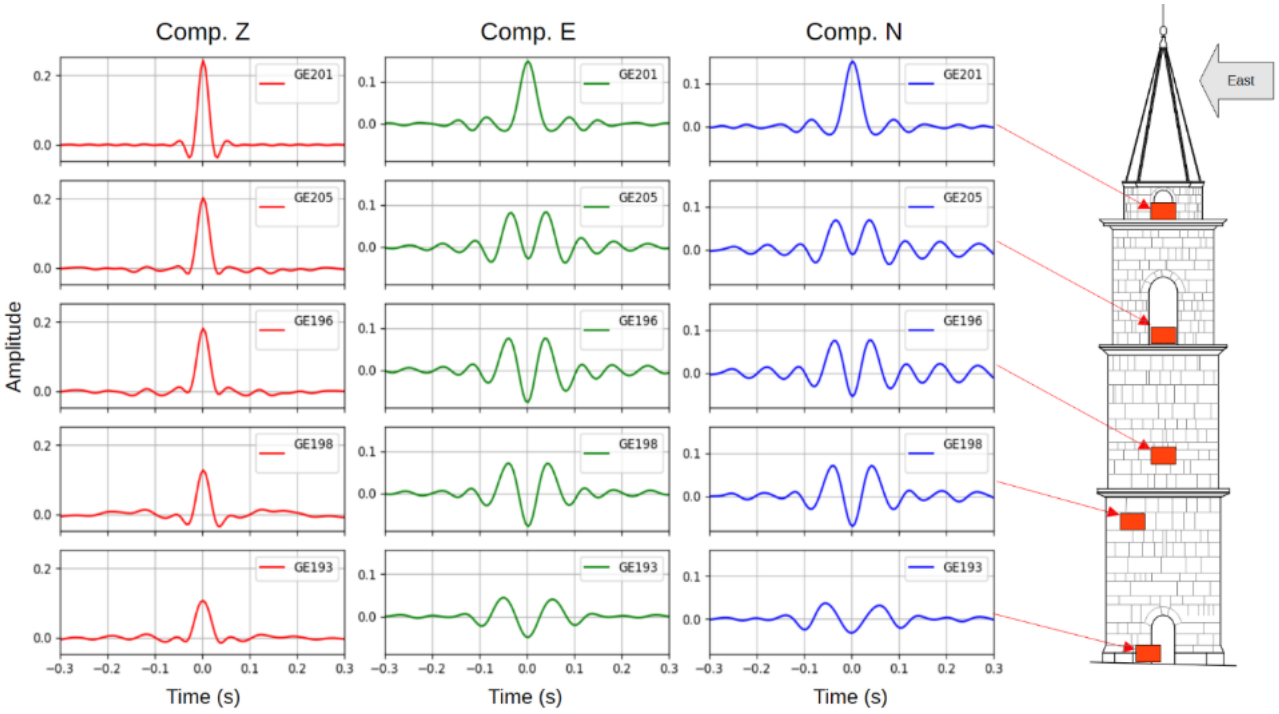

Fig. 2 – Impulse Response Functions (IRFs) obtained through ANDI analysis evaluated in the bell tower. The location of the sensors is reported in the right side of the figure. The waveforms of the horizontal components show impulse propagation symmetrically well picked both in the acausal and causal parts. In the vertical component, the two impulses are not well resolved, due to the high velocity of propagation of signal in this direction. The reference station was selected at the top of the tower (sensor GE201).

While the waveform recorded within the bell tower is well defined, yielding reliable and stable velocity estimates, the energy peak radiated from the structure is more difficult to track in the surrounding soil due to noise disturbances, primarily related to vehicular traffic. These perturbations persist even after transient noise removal. For this reason, we implemented a model that simulates the Green's function to track pulse propagation from the bell tower into the soil (Fig. 3). The model allowed us to more effectively track the wavefield transmitted into the soil and to infer that the contribution of the tower remains detectable in the soil up to approximately 80 m.

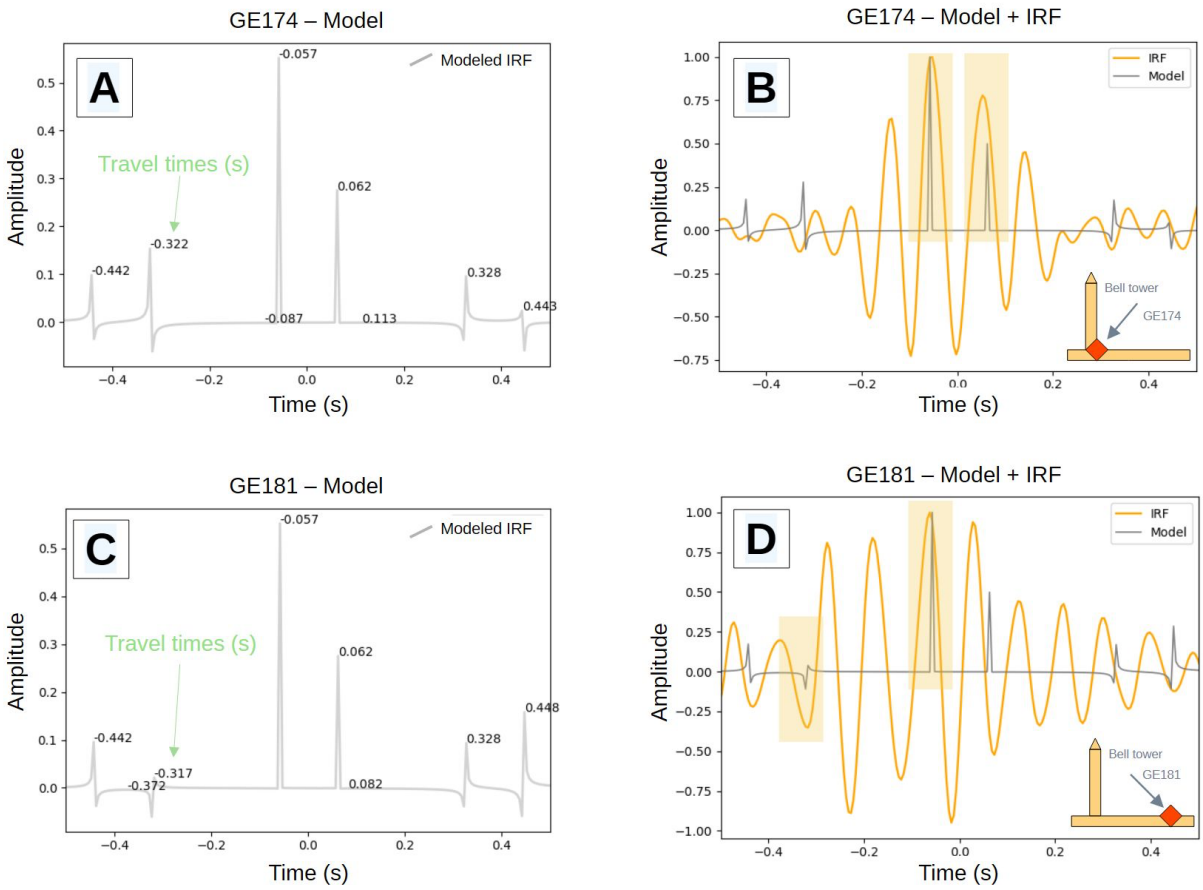

Fig. 3 – Modelled IRFs evaluated for the sensor GE174, placed at the base of the bell tower (A) and for the sensor GE181 (C), located 140 m from the monument. (B) and (D) show the comparison between modelled and experimental IRFs. The amplitude in the right graphs is normalised to better compare the real and simulated waveforms. The best fit of the peaks is highlighted with yellow bands.

References

De Angelis, A., Lourenço, P. B., Sica, S. & Pecce, M. R.; 2022: Influence of the ground on the structural identification of a bell-tower by ambient vibration testing. Soil Dynamics and Earthquake Engineering, 155, 107102.

García-Macías, E. & Ubertini, F.; 2019: Seismic interferometry for earthquake-induced damage identification in historic masonry towers. Mechanical Systems and Signal Processing, 132, 380–404. https://doi.org/10.1016/j.ymssp.2019.06.037.

Lacanna, G., Ripepe, M., Coli, M. et al.; 2019: Full structural dynamic response from ambient vibration of Giotto's bell tower in Firenze (Italy), using modal analysis and seismic interferometry. NDT & E International 102:9–15. https://doi.org/10.1016/j.ndteint.2018.11.002.

Petrovic, B., Parolai, S., Romanelli, M., Affatato, A., Petronio, L., Barbagallo, A., Sorgo, D., Stefani & M., Caputo, R.; 2019: An innovative approach for a better understanding of the seismic interaction

between soil and structures: The Ferrara test site. Bollettino di Geofisica Teorica ed Applicata, 60, pp.140–147.

Skłodowska, A.M., Parolai, S., Petrovic, B. & Romanelli, F.; 2023: Soil-structure interaction assessment combining deconvolution of building and field recordings with polarization analysis: application to the Matera (Italy) experiment. Bullettin of Earthquake Engineering, 21, 5867–5891, https://doi.org/10.1007/s10518-023-01750-7.

Corresponding author: salvatorelucente@cnr.it

Integrating Seismic, Landslide, and Flood Hazards Through an AHP-Based Multi-Hazard Framework: The Marche Region Case Study

Pietro Marincioni[1], Tiziano Volatili[1], Emanuele Tondi[1,2]

[1] Affiliation (School of Science and Technology– Geology Division, University of Camerino, Camerino, Italy)
[2] Affiliation (Seismology and Tectonophysics Division, National Institute of Geophysics and Volcanology, Camerino, Italy)

Multi-hazard assessments that integrate seismic, landslide, and flood susceptibilities are critical for regional-scale risk reduction in tectonically active and geomorphologically heterogeneous areas. The present study proposes a multi-hazard framework for the Marche region (central Italy) by integrating physics-based ground-motion scenarios, geomorphological and hydrological indicators, and a structured multi-criteria weighting procedure based on the Analytic Hierarchy Process (AHP). The analysis employs the ground-motion simulations and seismogenic source hypotheses presented by Gironelli et al. (2023), with particular emphasis on the Fabriano (1741, Mw 6.1) event.

The methodological workflow (Fig. 1) comprises three main stages: The generation of thematic single-hazard layers for seismic, landslide, and flood hazards constitutes the initial phase of the process. Following this, the next phase involves the normalisation and ranking of indicators within each hazard class. The third and final phase of the process is the hierarchical weighting and integration of the single-hazard layers by AHP. Seismic hazard layers incorporate scenario magnitude, proximity, and orientation relative to mapped active faults, Vs30-based site-condition estimates, regional lithology, macroseismic intensity distribution and PGA fields from scenario simulations. The landslide hazard is integrated with IFFI inventory typologies, land-use/land-cover, slope derived from a high-resolution digital elevation model (DEM), lithology, distance to faults, and modelled permanent displacements. These are computed via a Newmark-type sliding-block formulation following Jibson et al. (2007).

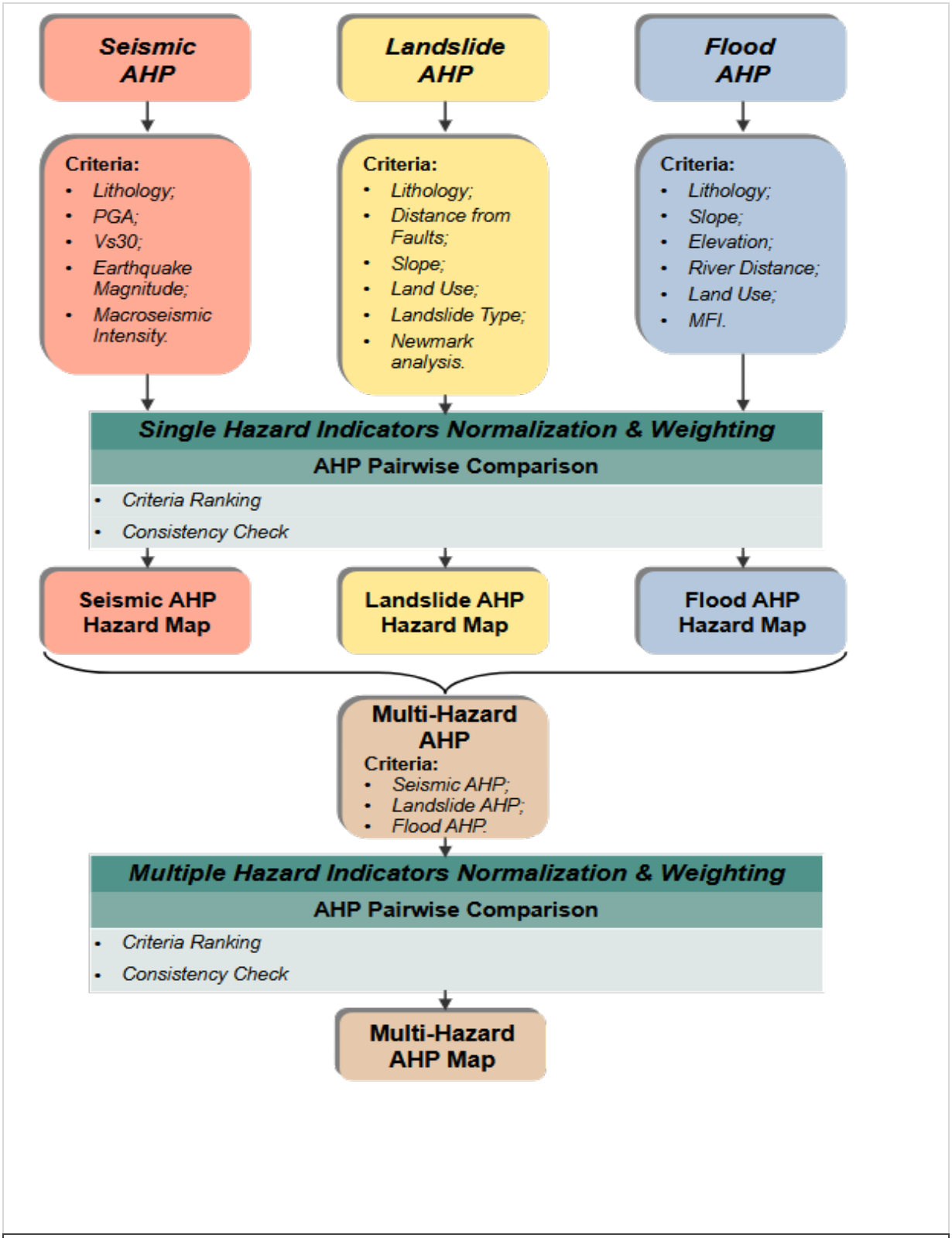

Fig. 1 – Single- and Multi-hazard Analytic Hierarchy Process workflow.

The estimates of permanent displacement were obtained using a bespoke Python implementation that was developed for the purposes of this study. This implementation is derived from and extends the open-source pyNewmarkDisp framework (Montoya-Araque et al., 2024) and was adapted for regional-scale raster processing, direct ingestion of scenario-dependent PGA fields, and tailored lithotechnical parameterization. The combination of flood-hazard layers involves the integration of

the Modified Fournier Index (MFI) as proposed by Ferro et al. (1991), the distance to hydric networks, the regional Digital Elevation Model (DEM), land-use patterns, and slope to encompass the climatic and topographic influences on runoff and accumulation.
Within each hazard class, indicators were standardised and weighted via pairwise AHP comparisons, with consistency ratios computed to validate judgments. The three hazard components were then integrated to produce a composite multi-hazard map.

The composite map delineates spatially coherent multi-hazard hotspots and identifies areas where seismic loading markedly increases landslide and flood susceptibility. The two Fabriano sources exhibit significant variations, particularly in upland regions adjacent to the inferred sources. This observation underscores the impact of source-model uncertainty on the reliability of regional multi-hazard assessments.

References

Al-Dogom, D., Schuckma, K., & Al-Ruzouq, R.; 2018: Geostatistical seismic analysis and hazard assessment; United Arab Emirates. *The International Archives of the Photogrammetry, Remote Sensing and Spatial Information Sciences*, *42*, 29-36.

Aydın, M. C., Birincioğlu, E. S., Büyüksaraç, A., & Işık, E.; 2024: Earthquake risk assessment using GIS-Based analytical hierarchy process (AHP): the case of Bitlis Province (Türkiye). *International Journal of Environment and Geoinformatics*, *11*(1), 1-9.

Bucci, F., Santangelo, M., Fongo, L., Alvioli, M., Cardinali, M., Melelli, L., & Marchesini, I.; 2022: A new digital lithological map of Italy at the 1: 100 000 scale for geomechanical modelling. *Earth System Science Data*, *14*(9), 4129-4151.

Choine, M. N., O'Connor, A., Gehl, P., D'Ayala, D., García-Fernández, M., Jiménez, M. J., ... & Power, R.; 2015: A multi hazard risk assessment methodology accounting for cascading hazard events.

Ferro, V., Porto, P., & Yu, B. (1999). A comparative study of rainfall erosivity estimation for southern Italy and southeastern Australia. *Hydrological sciences journal*, *44*(1), 3-24.

Gironelli, V., Volatili, T., Luzi, L., Brunelli G., & Tondi, E.; 2024: Dual-proxy estimation of Vs30: the case study of the Marche Region (central Italy), Journal of Maps, 20:1, 2349787, DOI: 10.1080/17445647.2024.2349787;

Han, L., Ma, Q., Zhang, F., Zhang, Y., Zhang, J., Bao, Y., & Zhao, J.; 2019: Risk assessment of an earthquake-collapse-landslide disaster chain by Bayesian network and Newmark models. *International journal of environmental research and public health*, *16*(18), 3330.

Jibson, R. W.; 2007: Regression models for estimating coseismic landslide displacement. *Engineering geology*, *91*(2-4), 209-218.

Ma, S., & Xu, C.; 2019: Assessment of co-seismic landslide hazard using the Newmark model and statistical analyses: a case study of the 2013 Lushan, China, Mw6. 6 earthquake. *Natural Hazards*, *96*(1), 389-412.

Materazzi, M., Bufalini, M., Dramis, F., Pambianchi, G., Gentili, B., & Di Leo, M.; 2022: Active tectonics and paleoseismicity of a transverse lineament in the Fabriano valley, Umbria-Marche Apennine (central Italy). *International Journal of Earth Sciences*, *111*(5), 1539-1549.

Mokhtari, E., Mezali, F., Abdelkebir, B., & Engel, B.; 2023: Flood risk assessment using analytical hierarchy process: A case study from the Cheliff-Ghrib watershed, Algeria. *Journal of Water and Climate Change*, *14*(3), 694-711.

Nwe, Z. Z., & Tun, K. T.; 2016: Seismic hazard Analysis using AHP-GIS. *Int. J. Res. Chem. Metallurg. Civ. Eng*, *3*, 1442-1450.

Rehman, A., Sajjad, M., Song, J., Riaz, M. T., Mehmood, M. S., & Ahamad, M. I.; 2025: Integrated frequency ratio-analytical hierarchy and geospatial techniques-based earthquake risk assessment in mountainous cities: a case from the Northwestern Himalayas. *Georisk: Assessment and Management of Risk for Engineered Systems and Geohazards*, *19*(2), 389-409.

Sar, N., Ryngnga, P. K., & De, D. K.; 2025: Application of the analytical hierarchy process (AHP) for flood susceptibility mapping using GIS techniques in lower reach of Keleghai River Basin, West Bengal, India. *Geohazard Mechanics*.

Skilodimou, H. D., Bathrellos, G. D., Chousianitis, K., Youssef, A. M., & Pradhan, B.; 2019: Multi-hazard assessment modeling via multi-criteria analysis and GIS: a case study. *Environmental Earth Sciences*, *78*(2), 47.

Stucchi, M., Monachesi, G., & Mandrelli, F. M.; 1991: Investigation of 18th century seismicity in central Italy in the light of the 1741 Fabriano earthquake. Tectonophysics, 193(1-3), 65-82.

Corresponding author: pietro.marincioni@unicam.it

Supporting regional risk reduction through archetype building analysis

M.G. Masciotta[1,2], G. Cianchino[1], G. Brando[1,2]

[1] Department of Engineering and Geology, University ''G. d'Annunzio'' of Chieti-Pescara, Pescara, Italy
[2] UdA-TechLab, Research Center, University "G. d'Annunzio" of Chieti-Pescara, Chieti, Italy.

This paper presents an integrated large-scale methodology to assess the seismic vulnerability of masonry residential buildings and to support the optimization of seismic risk mitigation strategies. The proposed approach aims to bridge the gap between empirical large-scale methods, which are suitable for regional assessments but often lack mechanical rigor, and detailed numerical analyses, which provide higher accuracy but are impractical for application to extensive building stocks.

The study focuses on the masonry building assets of the Abruzzi region, Central Italy, and uses data and information collected through the CARTIS database. CARTIS is a structured building inventory based on expert surveys that compiles key structural and typological characteristics of Italian residential buildings. Based on this database, a semi-automated MATLAB procedure was employed to identify representative masonry building archetypes (Basaglia et al., 2021). By filtering and clustering buildings according to eight key parameters (masonry type, number of storeys, construction period, slab and roof typology, presence of tie rods, wall thickness, and distance between walls), deemed as the most impacting on the buildings seismic response, 26 archetypes were identified. These archetypes represent approximately 86% of the unreinforced masonry (URM) residential stock in the region. As an example, the geometric configuration and main characteristics of Archetype 1 are shown in Fig.1.

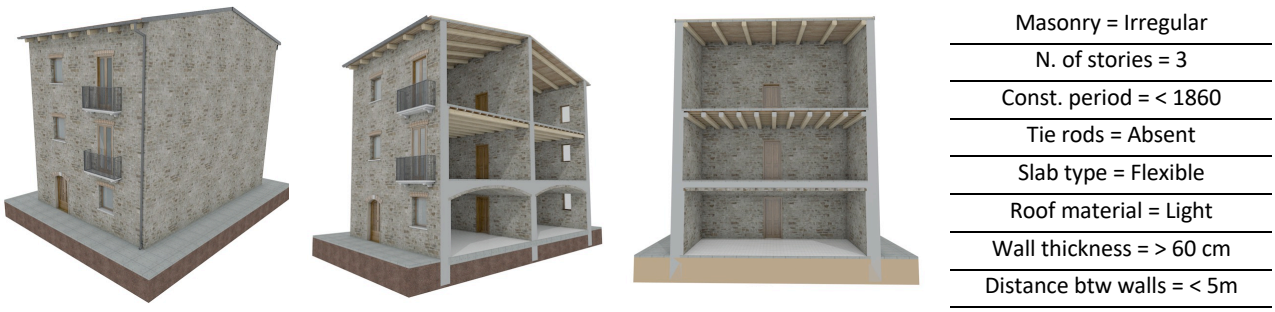

Masonry = Irregular
N. of stories = 3
Const. period = < 1860
Tie rods = Absent
Slab type = Flexible
Roof material = Light
Wall thickness = > 60 cm
Distance btw walls = < 5m

Fig. 1 – Geometric configuration and major features of one of the building archetypes (Archetype 1) identified in the Abruzzo region based on CARTIS data.

The seismic vulnerability of each archetype was evaluated by combining two complementary approaches. Local out-of-plane behaviour was assessed through linear and nonlinear kinematic analyses, focusing on typical collapse mechanisms such as façade overturning and flexural bending (Casapulla et al., 2017). For each mechanism, capacity curves were derived and converted into acceleration–displacement format. Global in-plane behaviour was instead analysed using nonlinear static (pushover) analyses based on the Equivalent Frame Model approach, implemented through the Midas commercial finite element environment (Camata et al., 2022). This allowed the evaluation of shear and flexural failure mechanisms in masonry piers and spandrels under horizontal seismic loads. Seismic demand was represented by a set of 125 natural ground motion records, grouped into nine PGA-based intensity levels, thereby accounting for record-to-record variability as the main source of uncertainty. For both local and global mechanisms, capacity curves were compared with seismic demand spectra to identify performance points and corresponding damage states (from D1 to D5, according to the European Macroseismic Scale, EMS-98). Damage thresholds were defined consistently with EMS-98 criteria and national code provisions. Finally, fragility curves were derived for each archetype and damage grade, assuming lognormal distributions. Figure 2a and 2b show the capacity curves of Archetype 1- obtained from kinematic analyses and nonlinear static analyses respectively, compared with the seismic demand and the corresponding fragility curves, obtained by the probability of exceeding each damage grade.

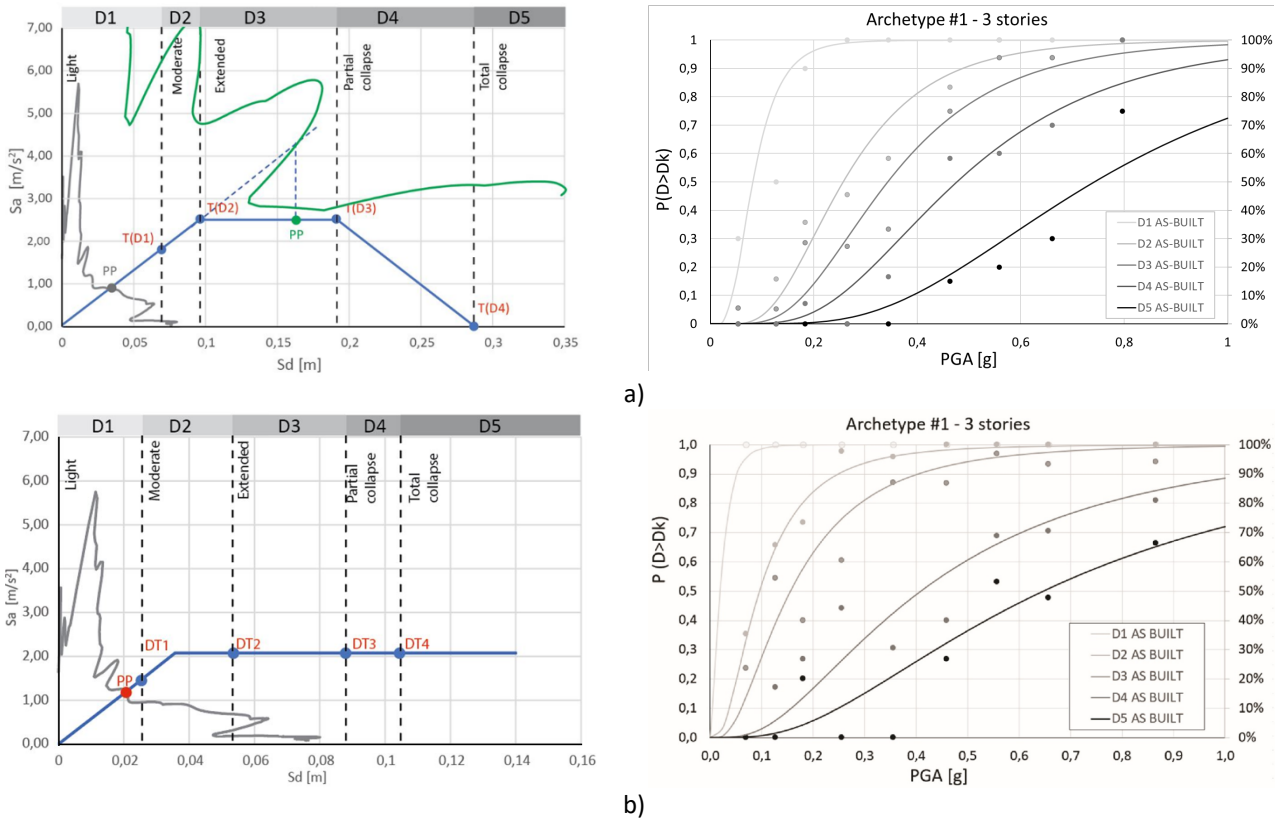

Fig. 2 – Analytical (a) and numerical (b) capacity curves and fragility curves for Archetype #1. Points are interpolated by a lognormal function.

The analytical (out-of-plane) and numerical (in-plane) fragility curves were subsequently integrated to capture the combined effect of local and global failure mechanisms. When one mechanism

governed across all intensity levels, the corresponding curve was adopted; otherwise, an integrated curve was derived through statistical fitting.

Finally, the methodology was applied to evaluate the effectiveness of seismic retrofitting strategies. Two interventions were considered: the installation of steel tie rods to reduce out-of-plane vulnerability, and the application of natural fabric–reinforced cementitious matrix (NFRCM) systems to enhance in-plane strength and ductility (De Carvalho Bello, et al., 2019). Updated analyses demonstrated significant reductions in damage probabilities, quantified through an improvement factor based on the probability of exceeding extensive damage (Fig.3).

The results highlight that relatively simple and low-invasive retrofitting solutions can lead to substantial improvements in seismic performance, particularly when interventions are specifically targeted at the most vulnerable mechanisms identified for each archetype. Moreover, the comparison between different strengthening configurations shows that the effectiveness of a retrofitting measure strongly depends on both the structural typology and the adopted intervention layout, emphasizing the importance of tailored mitigation strategies at the building-class level.

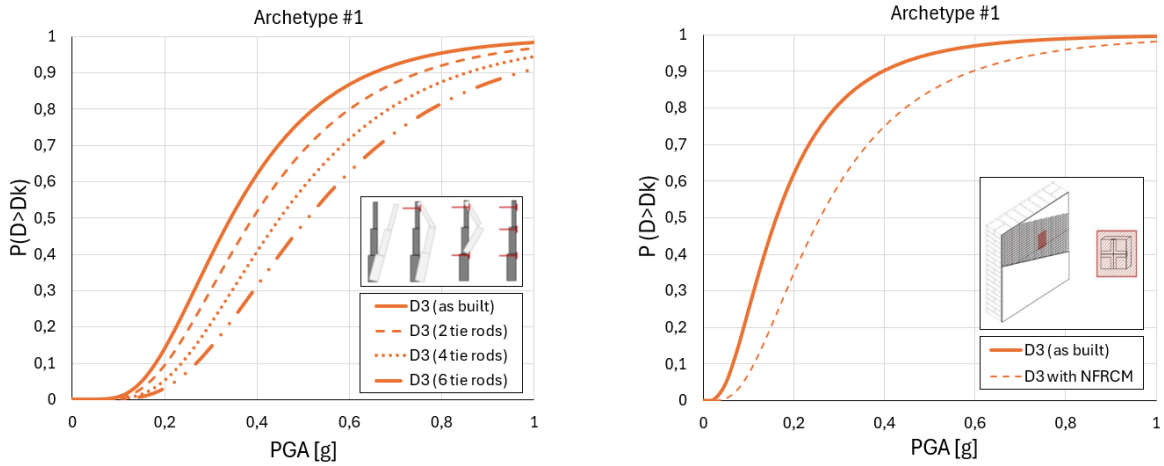

Fig. 3 – Fragility curves of Archetype #1 obtained from kinematic and numerical analyses in their as-built and retrofitted configurations.

Overall, the proposed methodology represents an effective and scalable tool for seismic vulnerability assessment at regional scale, combining the robustness of mechanical modelling with the computational affordability required for large building stocks. In fact, by relying on a limited, yet representative, set of archetypes derived from a structured inventory, the methodology allows capturing both local and global failure mechanisms while maintaining a reasonable computational effort. The results confirm that integrating analytical and numerical approaches leads to a more realistic representation of expected damage and provides a sound basis for comparing alternative retrofitting strategies. As such, the proposed approach can support informed decision-making in seismic risk mitigation planning, enabling the prioritization of interventions and the efficient allocation of resources, and it can be readily extended to other regions characterized by similar masonry building stocks.

Acknowledgments

This study was carried out as part of the IDPC-ReLuis joint project. The Authors gratefully thank all the researchers who worked on the development of the CARTIS form.

References

Basaglia, A., Cianchino, G., Cocco, G., Rapone, D., Terrenzi, M., Spacone, E., & Brando, G.; 2021: An automatic procedure for deriving building portfolios using the Italian "CARTIS" online database. Structures, 34(June), 2974–2986. Tratto da https://doi.org/10.1016/j.istruc.2021.09.054

Camata, G., Marano, C., Sepe, V., Spacone, E., Siano, R., Petracca, M., Roca, P., Pelà, L.; 2022: Validation of non-linear equivalent-frame models for irregular masonry walls. Engineering Structures, 253(February 2022), 113755. Tratto da https://doi.org/10.1016/j.engstruct.2021.113755

Casapulla, C., Giresini, L., & Lourenço, P.; 2017: Rocking and Kinematic Approaches for Rigid Block Analysis of Masonry Walls: State of the Art and Recent Developments. Buildings, 3(69), 7. Tratto da https://doi.org/10.3390/buildings7030069.

De Carvalho Bello, C., Baraldi, D., Boscato, G., Cecchi, A., Mazzarella, O., Meroi, E., Aldreghetti, I., Costantini, G., Massaria, L., Scafuri, V., Tofani, I.; 2019: Numerical and Theoretical Models for NFRCM-Strengthened Masonry. Key Engineering Materials (817), 44–49. Tratto da https://doi.org/10.4028/www.scientific.net/kem.817.44

Corresponding author: giuseppe.brando@unich.it

On the choice of the q-behaviour factor for Light-Frame Timber buildings

Alessandro Mazelli[1], Chiara Bedon[1], Antonino Morassi[2]

[1] University of Trieste, Department of Engineering and Architecture, Trieste, Italy
[2] University of Udine, Polytechnic Department of Engineering and Architecture, Udine, Italy

Introduction

Despite the large use of new wood-based engineered products such as Cross Laminated Timber (CLT), Light-Frame Timber (LFT) structures still represent a valid alternative for low and medium rise buildings, since it is possible to save material (studs and sheathing instead of solid wood panels) and have rather good ductile capacity, which is mostly ensured by dissipation of each sheathing-to-framing nailed connection.

Such a dissipation capacity has a key role for LFT design, given that current standards and codes provide seismic force reduction factors based on the structural dissipation capacity and on its over-strength, such as the q-behaviour factor by Eurocode 8 (2013) (or the R-factor by US codes). Moreover, specific provisions for seismic design of LFT buildings are still not covered by current European codes, pending the promulgation of the new Eurocodes and some uncertainties regarding the value of expected q-behaviour factor (Faggiano et al. 2022), for which only few data are available in literature (Rossi et al. 2019; Schwendner et al. 2018). In the last year, several new studies analysed the necessity of recalibrating the q-factors.

In Schwendner et al. (2018), a simple LFT building was used to derive the q-behaviour factor via non-linear dynamic analysis. Each wall element was represented by an elastic cantilever beam and a non-linear spring. The non-linear deformation of the fasteners was described with the SAWS cyclic model included in the spring (Folz and Filiatrault 2001). A pre-design was performed according to Eurocode 8 (2013), setting q=1.00, and three wall types were chosen to keep the demand-capacity ratio close to one, thus avoiding overdesign. Seven accelerograms were used to individuate the PGA at collapse, defined at 2% of inter-storey drift ratio. Mean values of the q-factor varying between 2.61 and 3.34 were found, considering hold-downs and angle brackets elastic. However, it is worth to note that only one reference floorplan was used, and that the ductility of the nailed connection was not declared. Moreover, only seven accelerograms were used to evaluate the q-factor.

Rossi et al. (2019) evaluated the q-behaviour factor for LFT buildings by means of non-linear static analysis. Four case study buildings were used, varying the number of storeys from 2 to 4. Moreover, six ductility classes were chosen, imposing a displacement ductility from 4 to 14 to the sheathing-to-framing connection, increasing the value by 2 at each step. All the structures were designed

according to different peak ground acceleration and q-behaviour factors, taking into account the Capacity Design approach by Casagrande et al. (2014), with an overstrength factor equal to 1.6. Under these hypotheses and applying pushover analysis to the structures, the authors obtained a mean q-factor between 3.0 and 3.3 for a ductility class of the sheathing-to-framing connection equal to 4 (corresponding to the minimum requirement for Low-Ductility LFT structures according to the Italian Building Code NTC18 (2018)), and between 3.5 and 4.2 for ductility class 6 (minimum for High-Ductility LFT buildings according to NTC18 (2018)). Higher classes were proposed by the authors only for numerical comparison purposes. However, it is worth noticing that a non-linear static analysis was used, rather than a dynamic approach. Thus, the hysteretic behaviour of the LFT wall was not considered, and the influence of ground motion characteristics and higher modes was neglected. Moreover, hold-down and angle brackets were kept elastic.

Evaluation of the q-behaviour factor via Incremental Dynamic Analysis

To obtain reliable ranges for the q-behaviour factor of LFT buildings, a parametric study was developed, based on six case study buildings (three regular and three non-regular, see Fig. 1) (Mazelli et al. 2025). Each building was designed according to Eurocode 5 (2005) and 8 (2013), considering a q=3 and a peak ground acceleration of 0.35g.

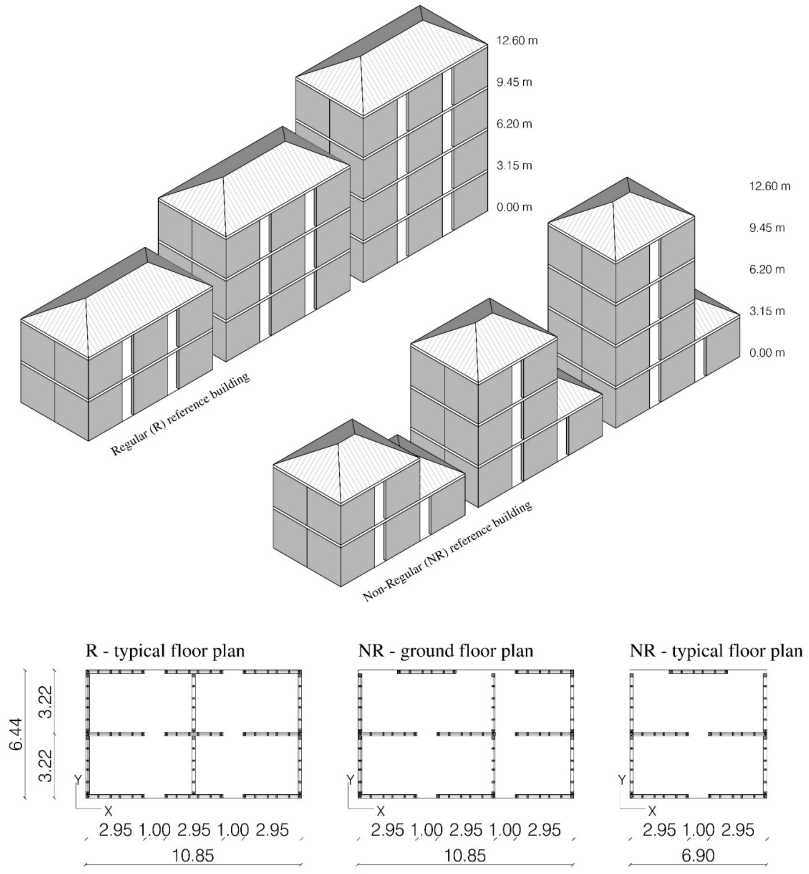

Fig. 1 – Regular (R) and Non-Regular (NR) case study buildings (First published in Bulletin of Earthquake Engineering, 1573-1456, 2025 by Springer Nature – Mazelli et al. 2025).

In order to overcome some limitations detected in earlies studies (only 7 ground motions and non-linear static approach), an Incremental non-linear Dynamic Analysis (IDA) approach was implemented (Vamvatsikos and Cornell 2002), considering a set of 20 accelerograms. Signal couples were applied simultaneously to 3D models of the buildings, and scaled up to reach the collapse of the structure.

Different set of LFT walls were generated starting from a laboratory test in order to match the design requirement of the buildings, and displacement ductility of the nailed connection (4, 6 and 8), number of OSB layers (1 or 2) and resistance of the single nailed connection (0.72, 1.00 and 1.40 kN) were varied.

Moreover, the cyclic behaviour of the walls was properly modelled by means of diagonal non-linear springs, and the hysteresis parameters were calibrated on the laboratory test (Fig. 2).

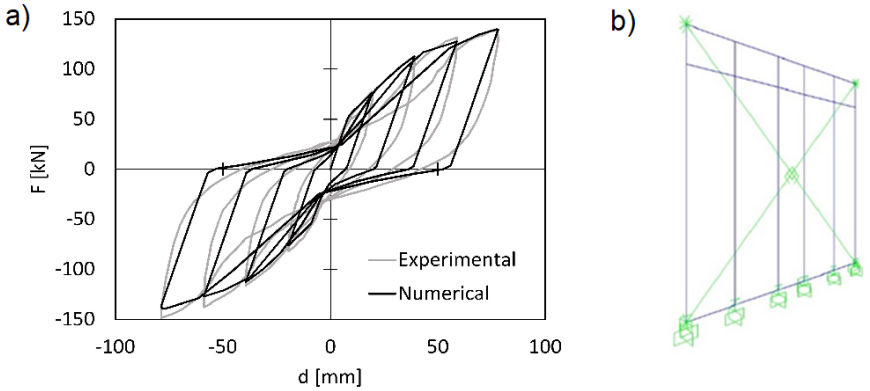

Fig. 2 – Calibration of the cyclic behaviour of the LFT wall (a) and FEM model with diagonal non-linear spring (b) (First published in Bulletin of Earthquake Engineering, 1573-1456, 2025 by Springer Nature – Mazelli et al. 2025).

To evaluate the q-behaviour factor, 360 single IDA studies were carried out, for a total of more than 7000 single non-linear dynamic analysis. For a ductility class of the sheathing-to-framing connection equal to 4 (Low-Ductility structures according to NTC18 (2018)), mean values of the q-factor equal to 2.9 and 3.4 were obtained for the regular and irregular cases respectively, with an average global q=3.2. On the other hand, the mean values 3.6 (regular) and 3.7 (non-regular) were obtained for a ductility class of 6 (High-ductility minimum requirement proposed by NTC18 (2018)), and therefore the global mean q-factor equal to 3.7 was calculated. It is worth to note that, in the proposed evaluation method the dissipation linked to hold-down and angle-brackets was neglected, since a Capacity Design approach was applied (Casagrande et al. 2014). Considering all source for energy dissipation and the rocking behaviour of tallest walls can lead to higher q values.

Results and discussion

In Table 1, a summary of the mean q-factors is reported, referred to the aforementioned literature works and to the proposed method of evaluation. According to the Italian Building Code NTC18 (2018), a displacement static ductility equal to 4 is the minimum requirement for the connections to design low-ductility structures, while a ductility equal to 6 is necessary for high-ductility class. Thus, Table 1 reports the results from sheathing-to-framing connection ductility classes 4 and 6.

Tab. 1 – Structural q-behaviour factor for the seismic design of low- and high-ductility class LFT buildings according to different authors and Italian Building code.

Authors	Low Ductility	High Ductility
Schwendner et al. (2018)	2.6 – 3.3	–
Rossi et al. (2019)	3.0 – 3.3	3.5 – 4.2
Mazelli et al. (2025)	2.9 – 3.4	3.6 – 3.7
Italian Building Code (2018)	3.0	5.0

It is worth to note that in Schwendner et al. (2018) no sheathing-to-framing connection ductility was declared. However, the results suggest a low ductility class.

Current Italian regulation provide a q-behaviour factor of 3.0 for low ductility class, and a value of 5.0 for the high class. Recent results highlighted the necessity of a further calibration of the q-factor, in order to design LFT structures reflecting the actual dissipation capacity of the connections.

The q-behaviour factors found in the literature were almost validated by the IDA approach. Moreover, the value q=3.0 proposed by the Italian code can be confirmed. On the other hand, high-ductility LFT walls did not reach q=5, and values from 3.5 and 4.2 were found. Furthermore, the more refined approach via IDA showed that mean values below 4.0 are present, thus highlighting the necessity of an upgrade of code provisions.

Conclusions

In this abstract, several indications for the correct choice of the q-behaviour factor for the seismic design of LFT building were proposed. Preliminary work present in the literature showed limitations regarding the number of analysed cases or the type of analysis performed. Thus, a more complete procedure was considered, enlarging the analysed cases and the seismic input. Furthermore, non-linear IDA were performed on 3D complete structural models. Based on the results, the value q=3.0 represents a reliable choice for low-ductility LFT buildings. On the other hand, a maximum value of 3.7 should be chosen for high-ductility structures according to IDA procedure, even if literature approaches showed that a slight increment to 4.0 can be considered. However, a slightly higher value should be chosen only when taking into account rocking behaviour and dissipation linked to hold-downs and angle brackets.

Acknowledgments

This work was carried out as part of the DPC-ReLUIS 2022-2024 project financed by the Department of Civil Protection.

References

Casagrande, D., Sartori, T., Tomasi, R.; 2014: Capacity design approach for multi-storey timber-frame buildings, in: 1st. INTER Meeting 1, Bath

EN 1995-1-1:2005. Eurocode 5: design of timber structures—part 1-1: general—common rules and rules for building, Brussels, Belgium, CEN, European Committee for Standardization, 2005

EN 1998-1:2013. Eurocode 8: design of structures for earthquake resistance part 1: general rules, seismic actions and rules for buildings. Brussels, Belgium, CEN, European Committee for Standardization, 2013

Faggiano, B., Sandoli, A., Iovane, G., Fragiacomo, M., Bedon, C., Gubana, A., Ceraldi, C., Follesa, M., Gattesco, N., Giubileo, C., Pio Lauriola, M., Podestà, S., Calderoni, B.; 2022: The Italian instructions for the design, execution and control of timber constructions (CNR-DT 206 R1/2018). Engineering Structures, vol. 253, Art. no. 113753, doi: 10.1016/j.engstruct.2021.113753

Folz, B., Filiatrault, A.; 2001: Cyclic analysis of wood shear walls. Journal of Structural Engineering, 127:433-441

Italian Building Code NTC 2018, Ministerial Decree of 17th January 2018, M.I.T., Rome, 2018 (in Italian).

Mazelli, A., Bedon, C., Morassi, A.; 2025: Sheathing-to-framing connection ductility role in the q-behaviour factor of Light Frame Timber buildings. Bulletin of Earthquake Engineering https://doi.org/10.1007/s10518-025-02308-5

Rossi, S., Giongo, I., Casagrande, D., Tomasi, R., Piazza, M.; 2019: Evaluation of the displacement ductility for the seismic design of light-frame wood buildings. Bulletin of Earthquake Engineering, vol. 17, no. 9, pp. 5313 – 5338, doi: 10.1007/s10518-019-00659-4

Schwendner, S., Hummel, J., Seim W.; 2018: Evaluation of the behaviour factor q for light-frame buildings – a comparative study. WCTE 2018 Seoul, Korea

Vamvatsikos, D., Cornell, C.A.; 2002: Incremental dynamic analysis. Earthquake Engineering and Structural Dynamics, vol. 31, no. 3, pp. 491–514

Corresponding author: alessandro.mazelli@phd.units.it

A 3D Subsoil Model to Enhance Near Real-Time Earthquake Impact Assessment in Northeastern Italy

Ileana E. Monsalvo Franco[1], Elisa Zuccolo[2], Chiara Scaini[2], Valerio Poggi[2], Carla Barnaba[2], Chiara Smerzini[1]

[1] *Politecnico di Milano, Italy*
[2] *Istituto Nazionale di Oceanografia e di Geofisica Sperimentale – OGS, Italy*

Rapid earthquake impact assessment is essential for supporting emergency response. In the Friuli–Venezia Giulia region of Northeastern Italy, the National Institute of Oceanography and Applied Geophysics (OGS) operates the Rapid Damage Scenario Assessment (RDSA) system (Poggi et al., 2021), which provides near-real-time damage scenarios based on empirical ground-motion estimates from the ShakeMaps software(Wald et al., 1999; Worden et al., 2020), combined with exposure data and literature-based fragility models. To improve the accuracy of ground-motion predictions, OGS has developed UrgentShake (Zuccolo et al., 2025), a system designed to complement ShakeMaps and provide physics-based ground-motion input to RDSA. The system performs near-real-time physics-based simulations of seismic wave propagation using various numerical codes, including the spectral-element code SPEED (Mazzieri et al., 2013), and has been developed within OGS institutional activities aimed at supporting the Regional Civil Protection of Friuli–Venezia Giulia by providing advanced ground-motion information for emergency response.

UrgentShake is currently under testing, with active development and continuously updates to improve the accuracy, level of detail, and timeliness of the ground-motion estimates. In this context, this work focuses on the update of the regional-scale 3D subsoil model for the Friuli–Venezia Giulia region, designed for use in SPEED simulations within UrgentShake. The model was constructed by integrating geological and geophysical datasets to include the 3D geometry associated with the Friuli plain, depth-dependent velocity model for the sediments, and a representative regional crustal structure. Preliminary validation against available recordings for selected earthquakes indicates that the modelling is capable to reproducing the main characteristics of observed ground motion.

The developed model was also used offline to derive physics-based intensity measures for region-specific empirical fragility curves calibration. This approach follows methodologies explored in previous studies (Monsalvo Franco et al., 2025; Rosti et al., 2023) and is applied to damage data from the Mw 6.4 May 6, 1976 Friuli earthquake, for which preliminary calibration results are presented. Overall, these developments represent a significant step toward improving the accuracy of physics-based ground-motion estimates and, ultimately, damage assessments for operational earthquake response.

Acknowledgments

This work is funded by the National Recovery and Resilience Plan project TeRABIT (Terabit network for Research and Academic Big data in Italy—IR0000022—PNRR Missione 4, Componente 2, Investimento 3.1 CUP I53C21000370006) and supported by the National Plan of Research Infrastructures (PNIR) 2021–2027. It is also supported by National Institute of Oceanography and Applied Geophysics (OGS) and CINECA under Italian High-Performance Computing Training and Research for Earth Sciences (HPC-TRES) program Award Number 2019-03 and the Italian SuperComputing Resource Allocation (ISCRA) type C Project NUMERA (Numerical Modeling for Multi-Hazard and Risk Assessment).

References

Mazzieri, I., Stupazzini, M., Guidotti, R., Smerzini, C.; 2013: SPEED: SPectral Elements in Elastodynamics with Discontinuous Galerkin: a non-conforming approach for 3D multi-scale problems. International Journal for Numerical Methods in Engineering Vol. 95, n. 12, pp. 991–1010, https://doi.org/10.1002/nme.4532

Monsalvo Franco, I.E., Smerzini, C., Rosti, A., Rota, M., Paolucci, R., Penna, A.; 2025: Seismic fragility curves with unconventional ground motion intensity measures from physics-based simulations. Bulletin of Earthquake Engineering, Vol. 23, n.5, pp. 1885–1915, https://doi.org/10.1007/s10518-025-02104-1

Poggi, V., Scaini, C., Moratto, L., Peressi, G., Comelli, P., Bragato, P.L., Parolai, S.; 2021: Rapid Damage Scenario Assessment for Earthquake Emergency Management. Seismological Research Letters Vol. 92, n. 4, pp. 2513–2530, https://doi.org/10.1785/0220200245

Rosti, A., Smerzini, C., Paolucci, R., Penna, A., Rota, M.; 2023: Validation of physics-based ground shaking scenarios for empirical fragility studies: the case of the 2009 L'Aquila earthquake. Bulletin of Earthquake Engineering Vol. 21, n.1, pp. 95–123, https://doi.org/10.1007/s10518-022-01554-1

Wald, D.J., Quitoriano, V., Heaton, T.H., Kanamori, H., Scrivner, C.W., Worden, C.B.; 1999: TriNet "ShakeMaps": Rapid Generation of Peak Ground Motion and Intensity Maps for Earthquakes in Southern California. Earthquake Spectra Vol. 15, n. 3, pp. 537–555, https://doi.org/10.1193/1.1586057

Worden, C.B., Thompson, E.M., Hearne, M., Wald, D.J.; 2020: ShakeMap Manual Online: Technical Manual, User's Guide, and Software Guide. U.S. Geological Survey, https://doi.org/10.5066/F7D21VPQ

Zuccolo, E., Bolzon, G., Pitari, F., Rodríguez Muñoz, L., Scaini, C., Vanini, M., Poggi, V., Salon, S.; 2025: Advancing Rapid Response to Earthquakes with Tiered Physics-Based Ground-Shaking Simulations: The UrgentShake System. Seismological Research Letters Vol. 96, n. 5, pp. 2995-3011, https://doi.org/10.1785/0220240472

Corresponding author: ileanaelizabeth.monsalvo@polimi.it

Research for the Update of the Cuban Seismic-Resistant Standard

Grisel Morejón Blanco[1], Kenia Mercedes Leyva Chang[1], Darío Candebat Sánchez[1] , Zulima Rivera Alvarez[1], Javier Sánchez Arce[1]

[1] *Centro Nacional de Investigaciones Sismológicas (CENAIS), Santiago de Cuba, Cuba*

The current Cuban seismic-resistant construction standard, approved in 2017, does not fully address the necessary requirements to ensure adequate structural design in Cuba. Aiming to contribute to the improvement of this standard and directly influence disaster risk management, this work presents proposed changes for updating NC 46:2017. The key aspects focus on: scope, application, and exclusions; reference regulations; building classification; seismic zoning; new design spectra; structural system analysis methodology (including an empirical equation for calculating the fundamental vibration period, coefficients and factors for seismic-resistant system design, and soil-structure interaction); maximum tolerable ultimate drifts; performance-based design guidelines; building instrumentation; and a methodology for evaluating and intervening in existing structures. The proposal for updating NC 46:2017 is based on the minimum content document of the reference seismic code for Latin America and the Caribbean, which considers a wide range of regional scenarios and summarizes current state-of-the-art knowledge in seismic design from across the region. These reference guidelines were adapted to Cuban conditions and characteristics to ensure safe constructions that safeguard human lives and, in the future, progress toward the challenge of resilient constructions and cities.

References

American Concrete Institute; 2019: Building code requirements for structural concrete (ACI 318-2019) and commentary. Farmington Hills, MI: Author.

American Society of Civil Engineers; 2017: ASCE/SEI 41-17: Seismic evaluation and retrofit of existing buildings. Reston, VA: Author.

American Association of State Highway and Transportation Officials [AASHTO] ; 2020: LRFD Bridges. Design specifications (9th edition). Washington, DC, USA.

American Society of Civil Engineers; 2022: ASCE/SEI 7-22: Minimum design loads for buildings and other structures. Reston, VA: Author.

Álvarez L., Lindholm C., Villalón M; 2017: Seismic Hazard for Cuba: A New Approach. Bulletin of the Seismological Society of America, Vol. 107, doi: 10.1785/0120160074. Estados Unidos.

Applied Technology Council; 1996: ATC-40: Seismic evaluation and retrofit of concrete buildings. Report No. ATC–40, Redwood City, CA: Author.

BSSC (Building Seismic Safety Council); 2001: NEHRP recommended provisions for seismic regulations for new building and other structures. Part 1 – Provisions, 2000 edition. BSSC, Washington D.C., 374 pp.

Computers and Structures, Inc.; 2020: SAP2000 (Versión 22) [Software de análisis estructural].

European Committee for Standardization; 2004: Eurocode 8: Design of structures for earthquake resistance—Part 1: General rules, seismic actions and rules for buildings (EN 1998-1). Brussels, Belgium: Author.

FEMA; 1997: NEHRP guidelines for the seismic rehabilitation of buildings (FEMA 273). Washington, DC: Author.

FEMA; 2006: Next-Generation Performance-Based Seismic Design Guidelines (FEMA 445). Washington, DC: Author.

FEMA; 2018: Seismic Performance Assessment of Buildings, Volume 1 - Methodology, Second Edition. FEMA P-58-1. Washington, DC: Author.

Mander, J. B., Priestley, M. J. N., Park, R.; 1988: Theoretical Stress-Strain Model for Confined Concrete. Journal of Structural Engineering, 114(8), 1804-1826. Recuperado de http://www.asce.org/

Messlem, A. y Lang, D. ; 2014: Seismic Vulnerability Assessment. Development of Numerical Model for Nonlinear Static Analysis in SAP2000. Kjeller, Norway: NORSAR.

Morejón, G., Llanes, C., Frometa, Z. ; 2014: Realidades del Código Sísmico vigente en Cuba. Retos para su actualización. Revista Ciencia en su PC, №1, enero-marzo, 2014, p. 74-86. ISSN: 1027-2887.

Morejón Blanco, G.; Llanes Burón C. y Frómeta Salas, Z.; 2018: Estimación del factor de reducción de las fuerzas sísmicas en edificaciones aporticadas de hormigón armado. Revista de Obras Públicas ROP. 2018, Vol 1630. ISSN: 1695-4408.

Oficina Nacional de Normalización NC.; 2009: Norma Cubana NC 733:2009. Carreteras—puentes y alcantarillas—requisitos de diseño y método de cálculo. ICS: 91.140.80; 93.040. La Habana. Cuba.

Oficina Nacional de Normalización NC; 2017: Norma Cubana NC 46:2017: Construcciones Sismorresistentes. Requisitos Básicos para el Diseño y Construcción. La Habana. Cuba.

Rivera Z., Slejko D., Caballero L., Álvarez J. y Santulin M.; 2015: Soil amplification in Santiago de Cuba. Journal: Atti del 34° Convegno Nazionale del Gruppo Nazionale di Geofisica della Terra Solida.

Corresponding author: griselmorejonblanco@gmail.com

Improving Decentralized On-Site Earthquake Early Warning by rapid estimation of drift and inter-storey drift

Roselena Morga[1], Stefano Parolai[2], Valerio Poggi[3], Fabio Romanelli[2]

[1] Università degli Studi di Bari Aldo Moro, Dipartimento di Scienze della Terra e Geoambientali, Italy
[2] Università degli Studi di Trieste, Dipartimento di Matematica, Informatica e Geoscienze, Italy
[3] Istituto Nazionale di Oceanografia e di Geofisica Sperimentale – OGS Centro di Ricerche Sismologiche, Italy

The goal of an earthquake early warning system (EEWS) is to send rapid alert after detecting an earthquake, in order to mitigate the risks associated with strong seismic events. Most of EEW systems work using two types of configurations: regional and on-site. Regional systems (network-based) are focused on the prediction of ground shaking at target sites by estimating in real time source parameters (e.g. location and magnitude); on the other hand, on-site systems (OSEWS) infer the expected severity of incoming ground shaking by exploiting early ground-motion parameters recorded at the site, typically during the initial phase of the event. We decided to focus on on-site approach (and in particular on the decentralized one) that is particularly useful for target areas (like in most of Europe) where dense strong-motion networks are not available, or for industrial facilities (Parolai et al., 2015).

The idea is to implement an OSEWS for infrastructures aimed at rapidly estimating the expected structural response and damage potential during the early phase of an earthquake, e.g. by improving the system developed by Parolai et al. (2015). The occurrence of damage can be estimated by the observation of relative displacement and, in particular, inter-storey drift, which is a key engineering parameter providing critical information on the structural response during seismic loading.

Here, we propose an approach that directly estimates the probability of exceeding structural damage thresholds based on the total and/or inter-storey drifts, using the peak ground displacement (PGD) observed at the base of the buildings during the early stages of an earthquake, within the first few seconds (maximum 3 s after P-wave arrival). The first step is to model the probabilistic relationship between the maximum drift or interstorey drift and the early PGD observed at the base of the selected buildings. The model is calculated through regression analysis, using Bayesian regression models that explicitly quantify the uncertainty in the model parameters and in the resulting drift estimates. This step is important to evaluate statistical parameters (e.g. mean and standard deviation) that characterize the probability of exceeding literature drift and inter-storey drift limits. The probability thresholds that must characterize the alarm system are

selected for different building types, height-class and damage state, by evaluating the optimal trade-off between Precision, Recall and Accuracy. Then, the performance of the selected thresholds is tested to estimate the percentage of false and missed alarms as well as in terms of achievable lead time with respect to the arrival of damaging ground motion. The method is applied to the strong-motion recordings of medium and strong seismic events (magnitude > 4.0) obtained from Italian structural seismic monitoring network (OSS), which is a network of permanent seismic monitoring systems installed in public buildings (Dolce et al., 2017). The network is composed of more than 120 public buildings (mostly reinforced concrete and masonry structures) equipped with a complete monitoring system, where sensors are located at least at the top and the bottom of the buildings.

References

Dolce, M., Nicoletti, M., De Sortis, A., Marchesini, S., Da Spina, D., Talanas, F.; 2017: Osservatorio sismico delle strutture: The Italian structural seismic monitoring network. Bulletin of Earthquake Engineering Vol. 15, pp. 621-641, https://doi.org/10.1007/s10518-015-9738-x.

Parolai, S., Bindi, D., Boxberger, T., Milkereit, C., Fleming, K., Pittore, M.; 2015: On-site early warning and rapid damage forecasting using single stations: Outcomes from the REAKT project. Seismological Research Letters Vol. 86, n. 15, pp. 1393–1404, http://doi.org/10.1785/0220140205 .

Corresponding author: roselena.morga@uniba.it

Site effects characterisation for the city of Trieste

F. Parentelli[1] , C. Beltrame[1], S. F. Fornasari[1] , G. Costa[1]

[1] *Università degli Studi di Trieste, Dipartimento di Matematica, Informatica e Geoscienze, Italia*

This study focuses on site effect characterisation for the city of Trieste, specifically using new data from the under-development Urban Accelerometric Network (RAU, or ”Rete Accelerometrica Urbana di Trieste” in Italian) and noise measurements from previous field campaigns. The network has been established to investigate site effects in the urban environment, mainly in university buildings, by repurposing decommissioned accelerometric instruments, which configures it as an almost total low-cost network.

These data were used to investigate site effects at the stations. The methods used are: HVSR (Horizontal to Vertical Spectral Ratio) of ambient noise, HVSR of the event recordings and SSR (Standard Spectral Ratio), using a reference station on rock. The results have been compared with the available geological information and the outcome of some ambient noise campaigns.

The Trieste central area, known as Borgo Teresiano (in Fig.1), is characterised by sediments and artificial materials (Fizko et al., 2007), with a simplified 1-D geometry, but most of the city is located on the flysch, a strongly heterogeneous material (Busetti et al., 2012). Under the flysch there are the carbonatic rocks, visible in the Karst Plateau behind the city.

Although there have been no major earthquakes in the city recently, there are many potentially active faults nearby, linked to the Dinaric system. These faults were also responsible for the 1511 earthquake, the strongest event that hit the city (Ribaric, 1979), as reported by many historical documents.

The central area of Borgo Teresiano also corresponds to the highest thickness of sediments, estimated from the fundamental frequency of HVSR curves (and the shear velocity of the sediments), and validated with available well data logs. This part of the city centre along the seaside is also, as expected, the sector showing the greatest amplification in the city (Fitzko et al., 2007). Indeed, Borgo Teresiano presents a horizontally layered nature because it was constructed by the Austrians at the mouth of a river converted into salt pans (Panjek, 2007). The amplification frequency of the site is not very different from the natural resonance frequency of the historical buildings, which would not exclude resonance phenomena. The first level of microzonation (Marish and Zavagno, 2016) pointed out that this zone is also an area of instability, with the possible occurrence of liquefaction phenomena, in case of strong motion. Also, this site, despite being close

to the sea, shows a lack of directivity of the seismic noise (as shown by the yellow peaks in the polar plots within Fig.1), analysing HVSR measurements, and this may allow to identify and restrict the part of the centre of Trieste characterised by horizontally layered stratigraphy.

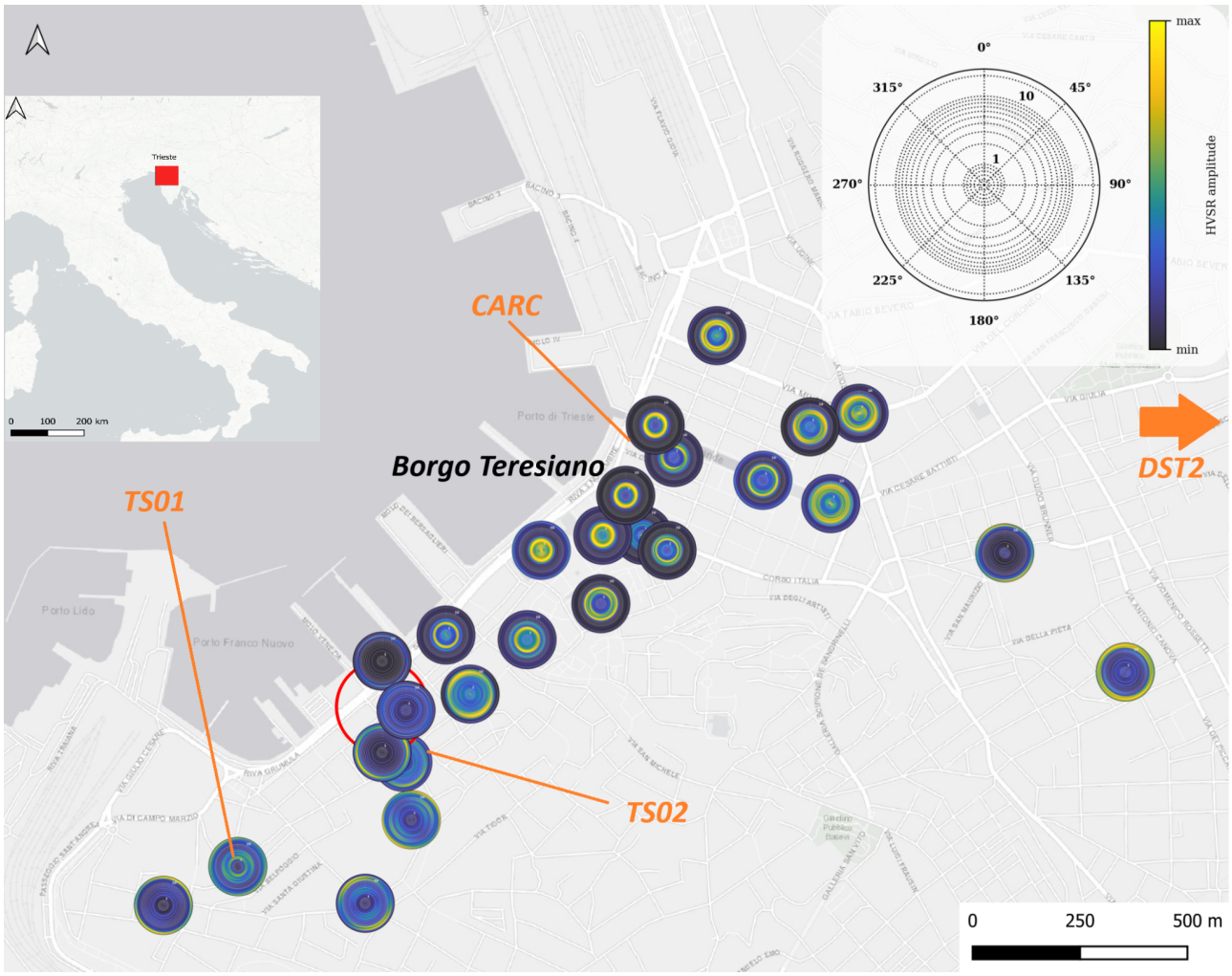

Fig. 1 – Directivity of HVSR measurements for the city centre of Trieste. The area characterised by 1D geometry, despite its proximity to the sea, also shows a lack of directivity. The position of the seismic stations are indicated in orange.

Interpreting TS01 and TS02 stations data (part of the RAU network), located in the southwest part of the centre (position indicated in Fig.1), and the data from Palazzo Carciotti station (CARC, part of the RAF network -Rete Accellerometrica Friuli Venezia Giulia- in Fig.1), in the heart of Borgo Teresiano, the part of the centre susceptible to strong amplification seems to remain limited and confined to Borgo Teresiano.

Although the amplification is considerable in the vicinity of Palazzo Carciotti, with amplifications on the order of 10 times around 2 Hz (Fitzko et al., 2007), TS01 and TS02, by contrast, do not display such evident signs of site amplification. The data analysis has been carried out using HVSR to earthquake events at the stations and HVSR of ambient noise, and applying the SSR reference method (Borchedt, 1970), using DST2 (an other station of the RAF, out of Fig. 1), located on flysch (in this case we can consider as rock), as a reference station. In Fig.2, the summary results for TS02 characterisation are shown. Even if the HVSR of noise and events show some common patterns,

with a peak around 4 Hz more visible in the HVSR of noise, and a peak at 6 Hz highlighted in the HVSR of events. As expected, the SSR of the vertical component is almost flat, whereas the SSR of the two horizontal components shows higher energy in the 4–7 Hz frequency range. The amplification in this part of the city is not completely negligible, but it is still much smaller compared to Borgo Teresiano.

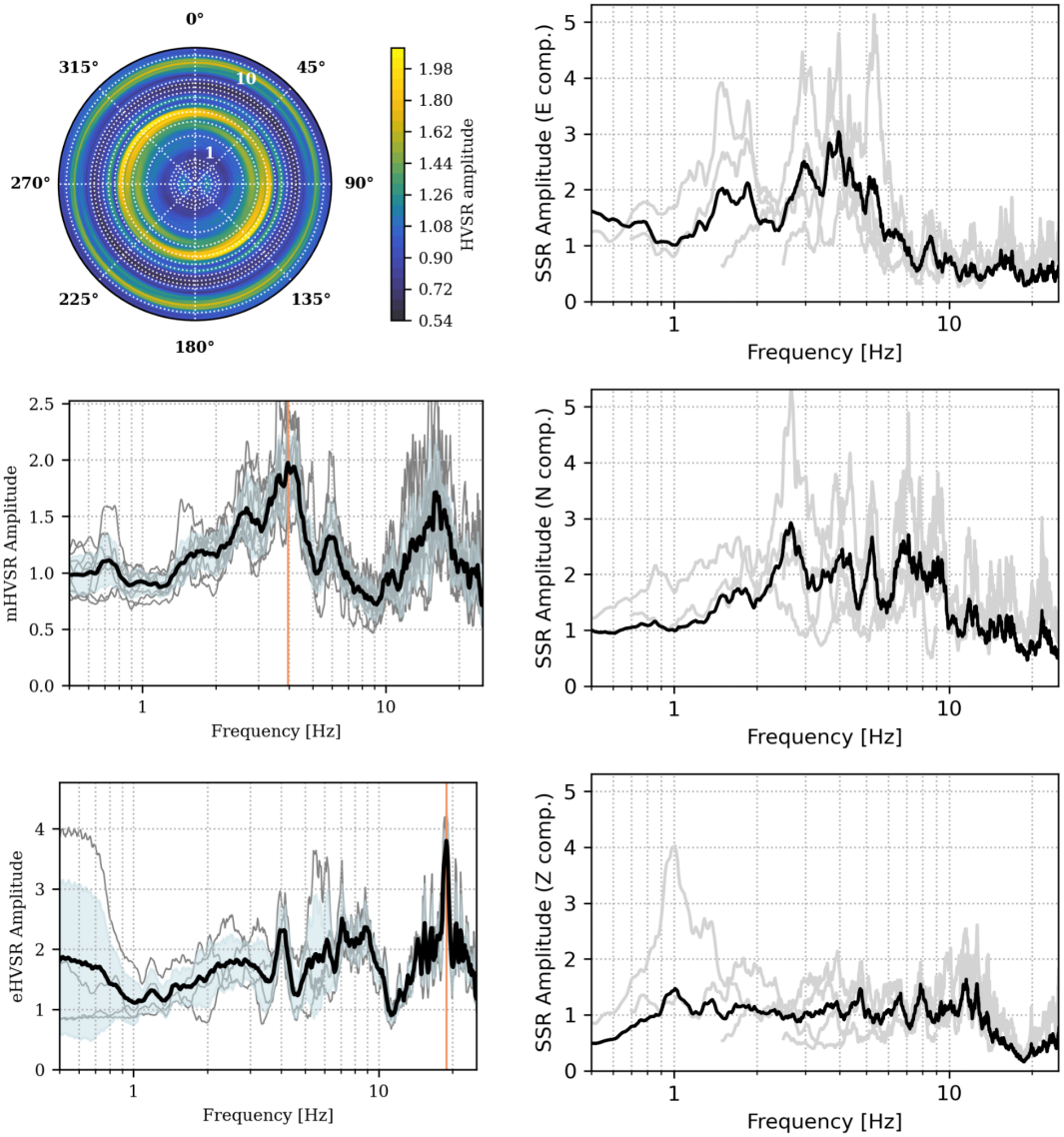

Fig. 2 – TS02 station characterisation summary analysis. Amplification is not negligible but smaller than Borgo Teresiano.

A bedrock depth model of the city centre (Fig. 3) has been computed, using the data from wells and the HVSR measurements with a lack of directivity.

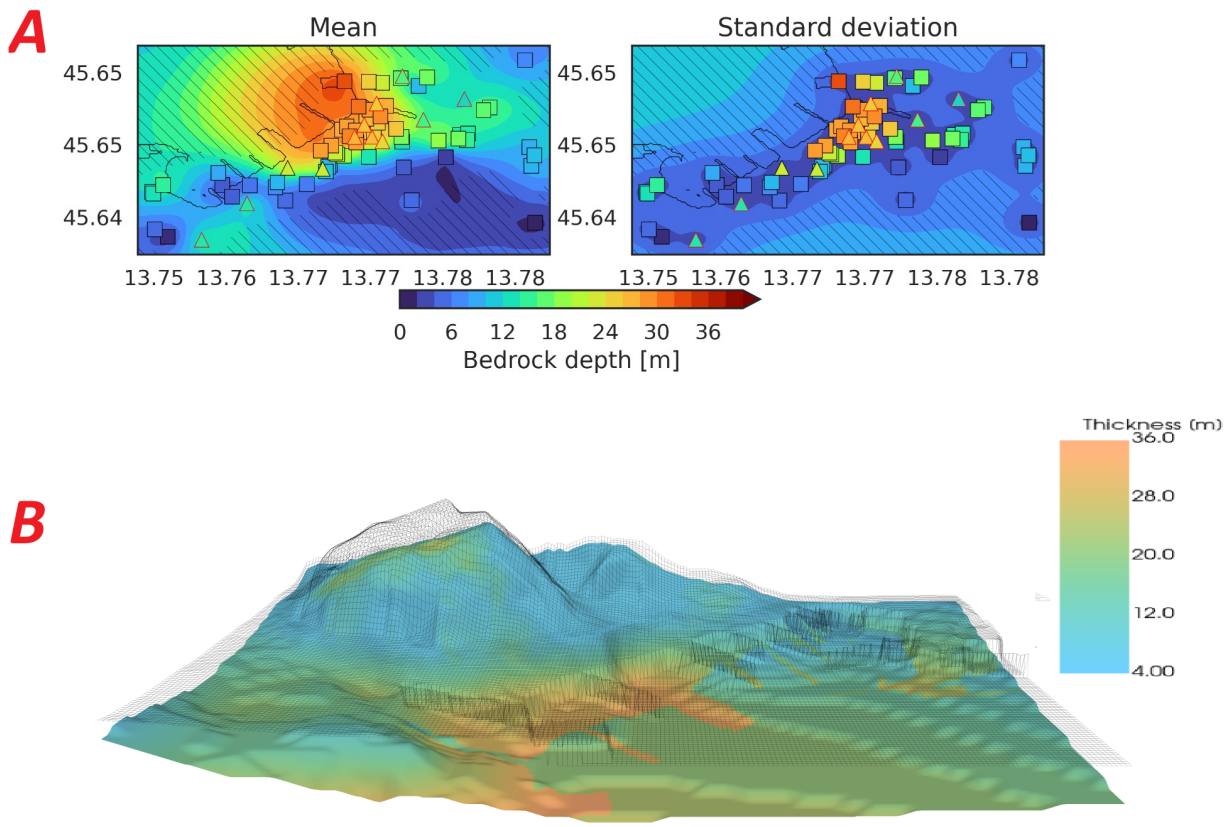

Fig. 3 – A: Bedrock depth in Trieste centre; B: 3D sediments model of Trieste city centre; the vertical dimension is exaggerated.

The subsoil model of the city of Trieste has been developed with the idea to be a base for seismic wave simulations in sensitive areas of the city.

The outcomes of the study confirmed that Borgo Teresiano presents strong amplifications, but other parts of the centre have lesser site effects. Nevertheless, for the municipality of Trieste amplification is not negligible, and the presence of active faults close to Trieste suggests it would be useful to obtain a better knowledge of site effects and the behaviour of the wavefield pattern.

Developing an urban seismic network plays a key role in the seismic monitoring of the city and the territory, which improves knowledge of site effects, with implications for forward-looking urban planning, resilient urban planning, seismic retrofitting of buildings, and for the selection of effective CLE (“Condizioni Limite per l'Emergenza") plans (used in case of a natural disaster to organize rescue operations and relief efforts). Observing Fig.3, even though the subsurface of Borgo Teresiano is approximately horizontally layered, it is evident that the geometry of Trieste is strongly 3D. In other parts of the city there are also heavily populated small valleys filled with sediments that also require a precise and quantitative evaluation of site effects. The next step will be to develop seismic wave models to assess the seismic wave propagation and also understand the role of the complex geometry and heterogeneous material in the propagation through the city.

REFERENCES

Borcherdt, R. D.; 1970: 'Effects of Local Geology on Ground Motion near San Francisco Bay'. *Bulletin of the Seismological Society of America* 60, no. 1 29–61. https://doi.org/10.1785/BSSA0600010029.

Busetti, M., Zgur, F., Romeo, R., Sormani, L., Pettenati, F. and others.; 2012: 'Caratteristiche Geologico-Strutturali Del Golfo Di Trieste'. *Contributi al Meeting Marino. Progetto CARG. Cartografia Geologica Delle Aree Marine. Roma 25-26 Ottobre 2012*, 2012, 65–70.

Fitzko, F., Costa, G., Delise, A., Suhadolc, P.; 2007: 'Site Effects Analysis in the Old City Center of Trieste (NE Italy) Using Accelerometric Data'. *Journal of Earthquake Engineering* 11, no. 1: 33–48. https://doi.org/10.1080/13632460601123123.

Marsich, P., Zavagno E.; 2016: 'Microzonazione sismica relazione illustrativa, regione autonoma Friuli Venezia Giulia, comune di Trieste'

Panjek A.; 2007: 'Buildings and Economy in the Hapsburg Port City of Trieste (1760-1809)'. École Française de Rome, 119-2 pp.543-557.

Ribarič, V.; 1979: 'The Idrija Earthquake of March 26, 1511 —a Reconstruction of Some Seismological Parameters'. *Tectonophysics* 53, nos 3–4: 315–24. https://doi.org/10.1016/0040-1951(79)90076-3.

Corresponding author: federico.parentelli@phd.units.it

GA-OGS-ARSO Transfrontier CE3RN AdriaArray Seismicity Experiment (GOAT-CASE) installations and results

Damiano Pesaresi[1], Nikolaus Horn[2], Jurij Pahor[3]

[1] *Istituto Nazionale di Oceanografia e di Geofisica Sperimentale - OGS, Italy*
[2] *Geosphere Austria (GA), Austria*
[3] *Slovenian Environment Agency (ARSO), Slovenia*

The GOAT-CASE experiment aims to evaluate the expected improvement in automatic earthquake localisation in the joint area of NE Italy, Austria and Slovenia, performed by the respective authoritative agencies, also members of AdriaArray experiment (AdriaArray, 2022) and virtual network CE^{3}RN (Central and Eastern Europe Earthquake Research Network; CE^{3}RN, 2014; Lenhardt et al., 2021): Geosphere Austria (GA), National Institute of Oceanography and Applied Geophysics (OGS) and Slovenian Environment Agency (ARSO). We re-picked P-wave arrival onsets on the seismometer channels of permanent seismic stations of the three agencies, additional AdriaArray stations and other additional permanent stations in the joint area plus a 50 km surrounding belt. The onset detections were performed by each member agency of the experiment for stations within its authoritative area while the detection association was performed centrally. The resulting catalogue was compared against the joint catalogue of manually revised locations as the reference. Only the location parameters were compared in this experiment, while the magnitudes were taken from manual catalogues. We used the Antelope software (Antelope, 2024) for analysis in a similar way as in the regular real-time monitoring procedures of the three agencies, but with commonly agreed parameters. The comparison of procedures and parameters used by the three agencies was also one of the goals of the experiment. After reviewing the results of the comparison for the first two years of the experiment for events with local magnitude $M_L > 1.5$ we concluded that there was observable improvement in earthquake locations (Fig. 1). This is reflected by the median distance between automatic and manual locations with the GOAT-CASE result being better than the results of any of the individual agencies.

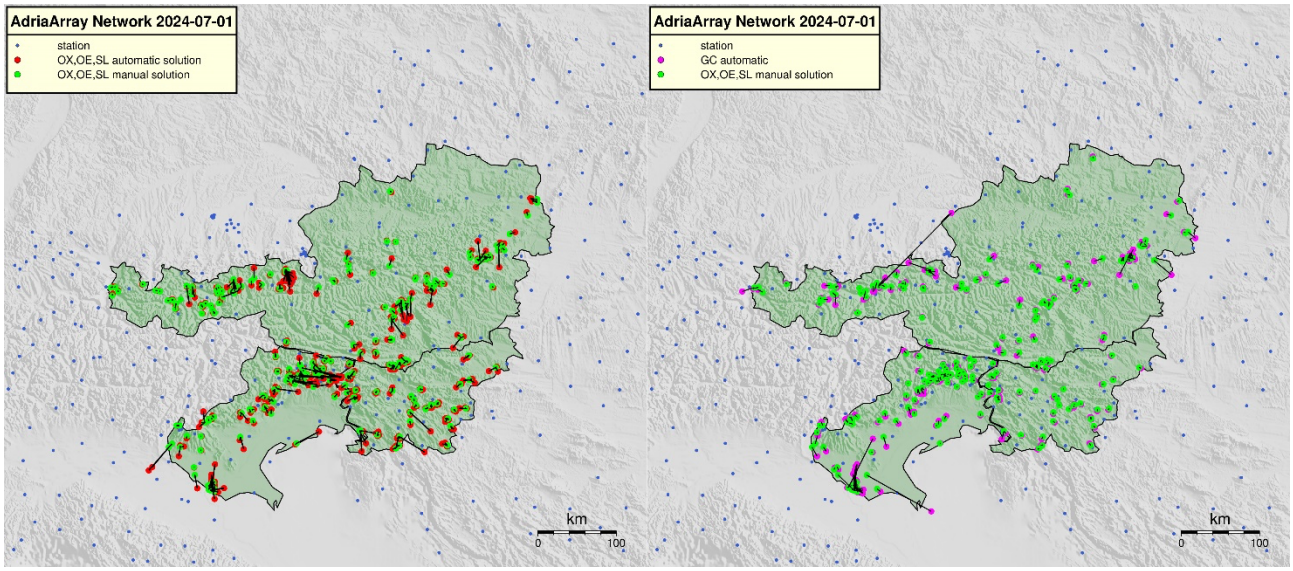

Fig. 1 – (left) For the individual institutions, comparison between automatic real-time locations (red dots) and manual locations of the individual institutions (green dots). (right) Comparison between GOAT-CASE earthquake locations (pink dots) and manual locations of the individual institutions (green dots).

Additionally, we discuss the installation by OGS of six temporary seismic stations in sites already used by the previously successful AlpArray project (Hetényi et al., 2018; Molinari et al., 2016; Govoni et al., 2017) (Fig. 2).

Fig. 2 – Components of an OGS seismic station for the AdriaArray project: (top left) the Nanometrics Centaur acquisition system; (centre left) the mobile internet router with switches; (top right) both integrated in a closed metal cabinet; (bottom left) the Nanometrics Trillium Compact 120 sec broadband seismometer, installed on a marble plate; (bottom right) the sensor covered with plastic thermal insulation.

References

AdriaArray; 2022: https://orfeus.readthedocs.io/en/latest/adria_array_main.html.

Antelope; 2024: https://brtt.com/software/.

CE^{3}RN; 2014: https://www.ce3rn.eu/.

Govoni A., Bonatto L., Capello M. et al.; 2017: AlpArray-Italy: Site description and noise characterization. Advances in Geosciences.

Hetényi G., Molinari I., Clinton J. et al.; 2018: The AlpArray Seismic Network: A Large-Scale European Experiment to Image the Alpine Orogen. Surveys in Geophysics.

Lenhardt W. A., Pesaresi D., Živčić M. et al.; 2021: Improving cross border seismic research: The Central and Eastern Europe Earthquake Research Network (CE^{3}RN). Seismological Research Letters.

Molinari I., Clinton J., Kissling E. et al.; 2016: Swiss-AlpArray temporary broadband seismic stations deployment and noise characterization. Advances in Geosciences.

Corresponding author: dpesaresi@ogs.it

A structured GIS-based workflow for identifying priority investigation sites in Level 3 Seismic Microzonation

A. Porchia[1], G. Tortorici[2], A. D'Agostino[1], E. Peronace[2], G. Ortolano[2], S. Catalano[1,2]

[1] Department of Biological, Geological and Environmental Sciences (DBGES) – Section of Earth Science, University of Catania, Catania, Italy;
[2] Institute of Environmental Geology and Geoengineering of the Italian National Research Council, Monterotondo, Italy;

Seismic Microzonation (SM) at Level 3 (SM3) requires a robust, spatially coherent characterization of the subsurface geological framework based on the integrated interpretation of geognostic and geophysical data. The effectiveness of SM3 studies largely depends on the density, spatial homogeneity and geological representativeness of available investigations. In volcanic areas and in structurally complex geological contexts, the distribution of data is often clustered, irregular or incomplete.

This condition may hinder the construction of reliable subsoil geological-geotechnical models and challenges both the technical–scientific efficiency (i.e., allocating investigations where geological uncertainty is highest) and the economic efficiency required for sustainable large-scale Microzonation programs (Dolce, 2012; Albarello & Moscatelli, 2021).

In this framework, tools capable of objectively analysing the spatial distribution, representativeness and quality of existing investigations are essential to support evidence-based planning of new SM3 campaigns. To address this focus, we present a GIS-based workflow designed to optimize the planning of SM3 investigations through a structured, reproducible Control Point (CP)–centered approach. The workflow is implemented through four modular Python scripts, each of which can be executed independently within the QGIS environment and adjusted through user-defined parameters.

The execution of the GIS-based tool requires the availability of a minimal set of input datasets, structured in accordance with the national standards for Seismic Microzonation studies (Technical Commission for Seismic Microzonation, 2020). These datasets are loaded into the QGIS Table of Contents (TOC) through the MZSTools plugin (Cosentino et al., 2024; 2025), which enables the import of SM1 datasets into the GIS environment, ensuring a consistent field structure, a uniform coordinate reference system and standardized naming conventions.

Module 1 builds harmonized point and linear investigation layers by merging geometric information, Level-1 zonation attributes and quality indicators. Module 2 generates and refines the Control Point

network (Types 1 and 2) through customizable grid spacing, spatial filters and checks ensuring coverage of all the SM1 zones (stable and instable zones). Type-1 CPs, developed on a coarser grid, are typically associated with investigations that directly support the construction and validation of the geological–geotechnical subsoil model, such as boreholes, MASW and Down-Hole tests. Conversely, Type-2 CPs, built on a finer grid, are linked to HVSR measurements, which are low-cost, easy-to-acquire data particularly suitable for capturing lateral geological variations and estimating the depth of the resonant layer. Module 3 assigns existing investigations to CPs by applying configurable criteria such as (i) search radius; (ii) geological consistency (the investigation and the associated CP are located within the same SM1 zone); (iii) quality thresholds of data; (iv) investigation-type selection.

Final outputs (Module 4) include CP-based maps of investigation density, aggregated statistics at the scale of MOPS types, and thematic layers supporting the identification of data gaps and priorities for new SM3 campaigns. The modular structure and the presence of adjustable parameters allow the workflow to be adapted to different study areas, investigation densities and geological complexities.

The complete set of Python modules is openly available through a dedicated Zenodo repository (Porchia et al., 2026), providing full access to the source code and documentation.

The workflow was applied to the municipality of Acireale, in frame of the ETNA FAC+MS project (ETNA FAC+MS Working Group, 2022). The study area is located on the southern flank of Mt. Etna, a volcanic context characterized by strong lateral heterogeneity and stratigraphic complexity. Figure 1 illustrates the distribution of boreholes assigned to Type-1 CPs (grid spacing 1000 m), highlighting the lack of direct geognostic control in wide portions of the study area. Figure 2 shows the distribution of HVSR measurements around Type-2 CPs (grid spacing 500 m), showing their irregular spatial coverage. Figure 3 presents the aggregated MOPS-level synthesis, which reveals that only a limited subset of geological contexts is currently supported by adequate stratigraphic data.

These results demonstrate that the surroundings of each CP - defined by a search radius consistent with the grid spacing - represent objective zones where additional data recovery or the acquisition of new SM3 investigations has to be evaluated. CPs with few or no associated investigations therefore delineate priority areas for targeted field campaigns, enabling more efficient and technically informed planning the acquisition of new data.

The approach offers methodological homogeneity, reduces operator-dependent bias, and provides a transparent and reproducible procedure suitable for Seismic Microzonation in volcanic or geologically complex settings at national scale.

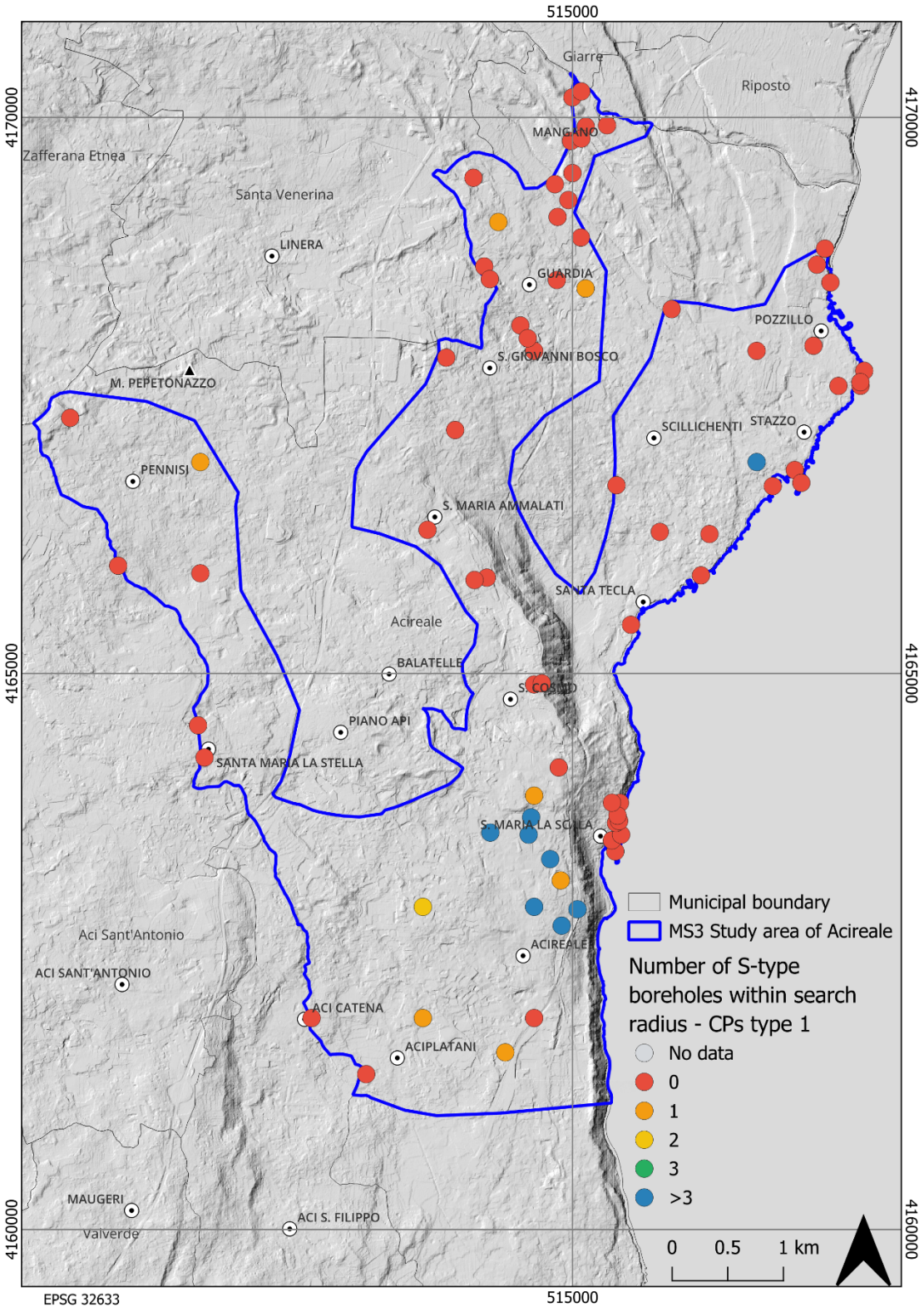

Fig. 1 – *Type-1 Control Points classified by the number of boreholes (S-type) located within their surroundings.*

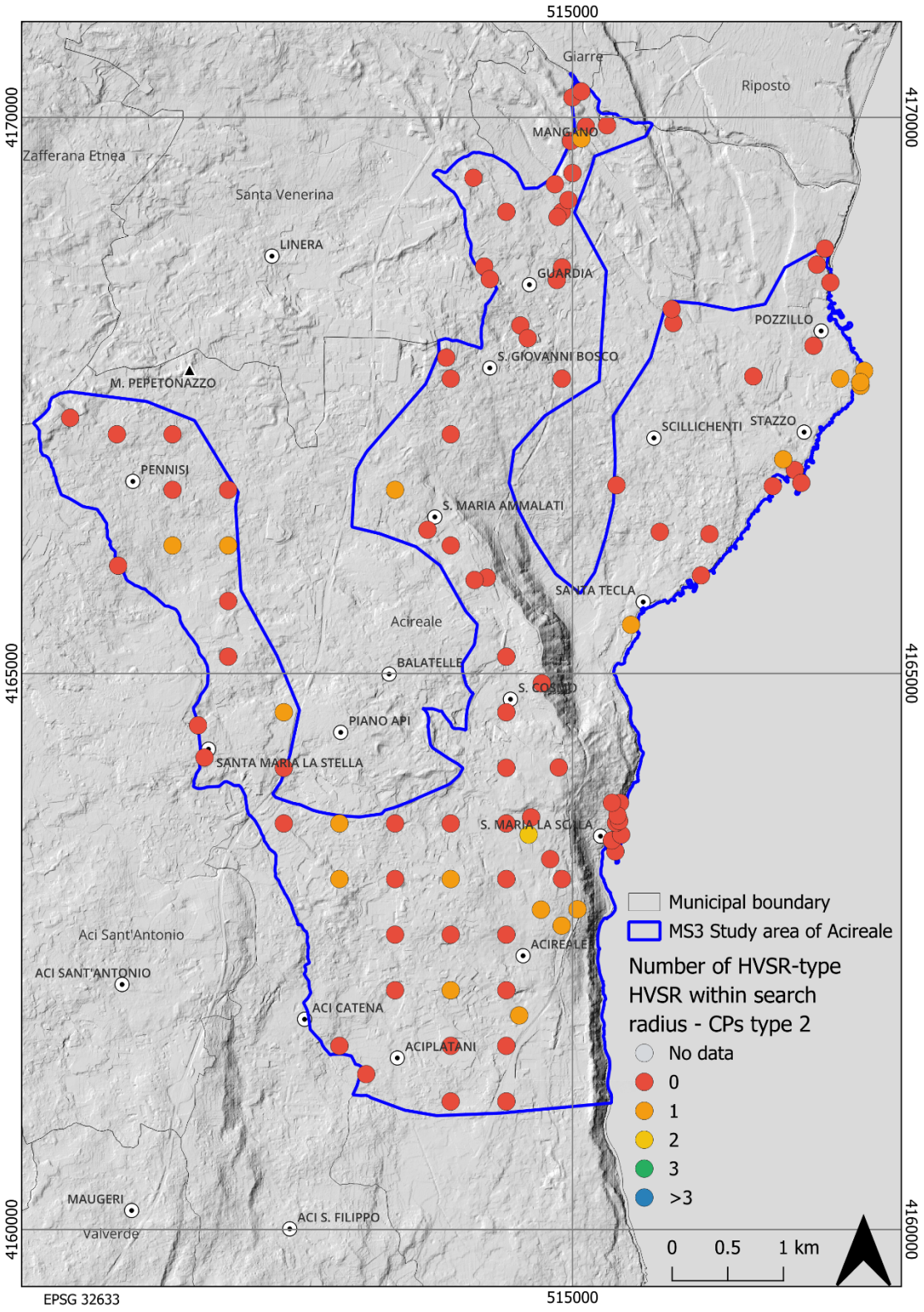

Fig. 2 – *Type-2 Control Points classified by the number of HVSR measurements located within their surroundings.*

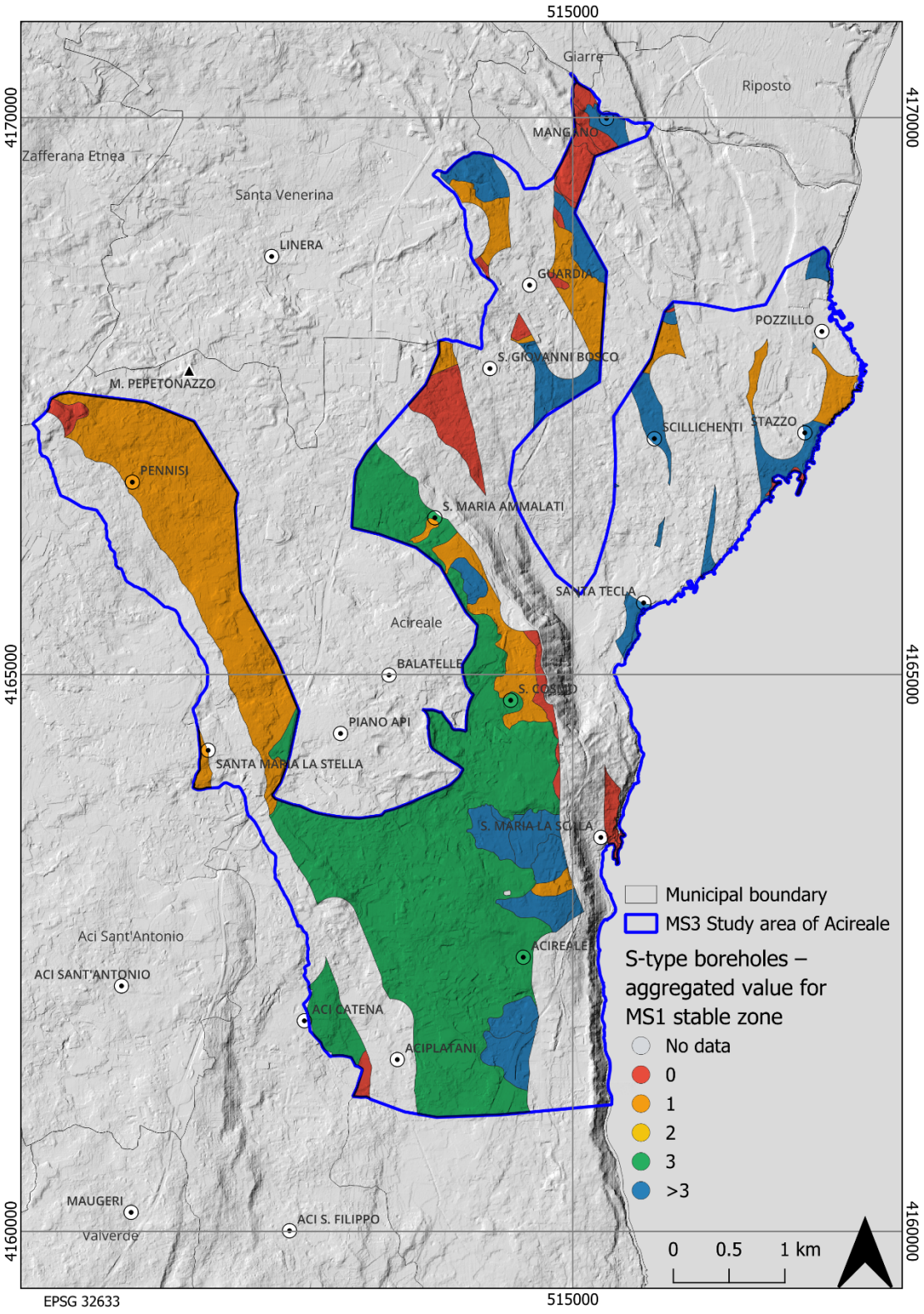

Fig. 3 - Aggregated count of boreholes (S-type) for each SM1 stable zone, derived from the CP-based analysis.

References

Albarello, D., Moscatelli, M.; 2021: Extensive Microzonation as a Tool for Seismic Risk Reduction: Methodological and Political Issues. In Building Knowledge for Geohazard Assessment and Management in the Caucasus and other Orogenic Regions (pp. 329-341). Berlin : Springer (10.1007/978-94-024-2046-3_18).

Cosentino, G., Pennica, F., Tarquini, E.; 2025: MzS Tools (2.0.4). Zenodo. https://doi.org/10.5281/zenodo.17202163

Cosentino, G., Pennica, F., Tarquini, E.; 2024: MzS Tools. doi:10.5281/zenodo.15691566. https://explore.openaire.eu/search/result?pid=10.5281%2Fzenodo.17202163

Dolce, M.; 2012: The Italian national seismic prevention program. In: Proceedings of 15th world conference on earthquake engineering. Lisbon, September, pp. 24–28, https://www.civil.ist.utl.pt/~mlopes/conte udos/SISMOS/DOLCE.pdf

ETNA FAC+MS Working Group, 2022: R2 - Relazione tecnico-scientifica di progetto. Accordo ai sensi dell'art. 15 della legge 241/1990 e del decreto legislativo 50/2016 e ss.mm.ii. tra il Dipartimento Regionale della Protezione Civile della Presidenza della Regione Siciliana e il C.N.R. Istituto di Geologia Ambientale e Geoingegneria. CUP: B75F21002880002, 113 pp.

Porchia, A., D'Agostino, A., Tortorici, G., Peronace, E., Ortolano, G., & Catalano, S.; 2026: Python modules for GIS-based planning of Level 3 Seismic Microzonation investigation campaigns (Version 1.0.0). Zenodo. https://doi.org/10.5281/zenodo.18214590

Technical Commission for Seismic Microzonation 2020: Graphic and data archiving standards. Version 4.2. Department of Civil Protection of the Presidency of the Council of Ministers. Rome.

Corresponding author: attilio.porchia@igag.cnr.it

Seismic Waveforms Envelopes Analysis for Stochastic Simulations

Ramadan F. [1], Mazloum Z.[2] , Lanzano G.[1], Sgobba S.[1], Pacor F.[1], Seif El Dine B[2], Jradi L.[2], Traversa P.[3]

[1] *Istituto Nazionale di Geofisica e Vulcanologia*
[2] *Lebanese University- Faculty of Engineering*
[3] *Électricité de France*

This work aims to enhance the time-domain characterization of seismic input by proposing a framework for the development of envelope prediction models. The resulting models are specifically designed for integration into stochastic simulations following Boore (2003) methodology. To achieve this aim, this work investigates the characteristics of three-component seismic waveform envelopes for Italian shallow crustal events, using the ITA18 dataset (https://shake.mi.ingv.it/ita18-flatfile/, Lanzano et al. 2022) which consists of 5439 records of earthquakes having Mw ranging from 3.0 to 7.5 where each record has 2 horizontal components and one vertical. All along with trimming of waveforms based on Arias intensity to get rid of noise.

The method for preprocessing waveforms, includes component selection, filtering, baseline correction, and Arias intensity-based trimming. To preserve the portion of the signal that contains most of the seismic energy, trimming is done as a function of cumulative energy percentage, and a distance-dependent trimming relationship is obtained. Empirical envelopes were computed applying Root Mean Square (energy-based) approach (see Fig.1).

A simplified Gaussian-type functional form:

$$f(x) = \mathrm{a}.\exp\left(-\left(\frac{[\![log10(t-b)]\!]}{2c}\right)^2\right) \quad \text{[eq.1]}$$

was used to fit the empirical envelopes. The model is dependent on three parameters to characterize the signal in the time **t** domain: **a** controls the maximum amplitude of the envelope; **b** represents the time at peak energy release; and **c** describes the temporal spread of the signal. The amplitude evolution and energy distribution of ground motion are compactly and physically described by these parameters.

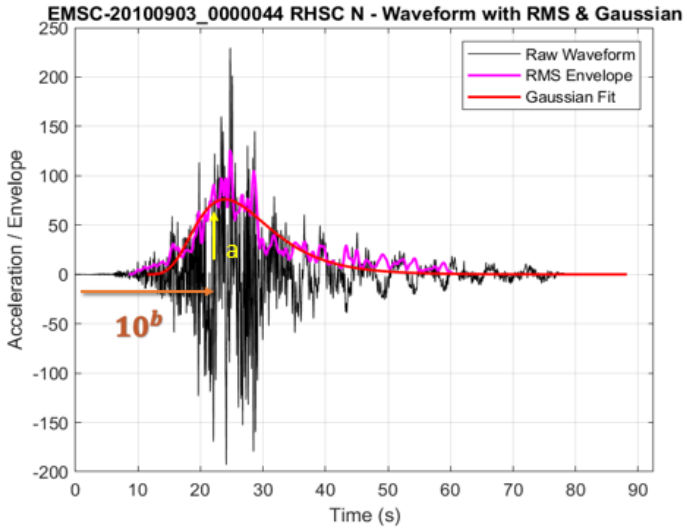

Fig. 1 raw waveform fitted into empirical 'RMS' and functional form.

A comprehensive analysis is performed to investigate the dependence of the envelope parameters on explanatory variables commonly used in ground-motion characterization, including magnitude, distance, peak ground acceleration (PGA), and site conditions (see Fig.2). A clear and systematic

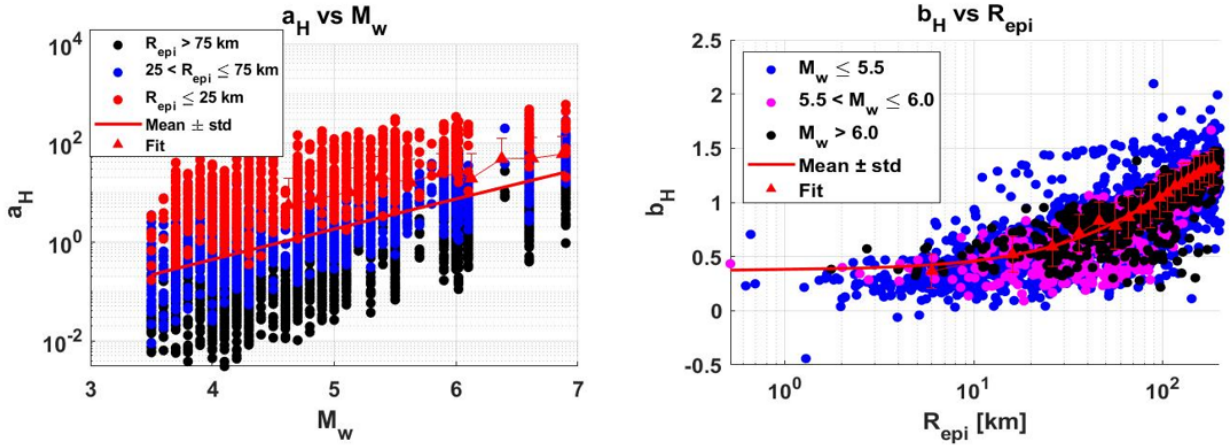

Fig. 2 variation of a and b parameters wrt to Mw and Repi respectively showing obvious dependance on explanatory variables.

correlation is observed between PGA and parameter a, highlighting the physical link between the fitted envelope shape and this ground-motion intensity measures. Differences between near-source and far-field records, as well as between high-amplitude short-duration and low-amplitude long-duration signals, are also explored.

References

Lanzano, G.; Luzi, L.; Pacor, F.; Felicetta, C.; Puglia, R.; Sgobba, S.; D'Amico, M.; 2019: A Revised Ground-Motion Prediction Model for Shallow Crustal Earthquakes in Italy. Bulletin of the Seismological Society of America Vol. 109, n. 2, pp. 525–540, https://doi.org/10.1785/0120180210

Lanzano, G.; Ramadan, F.; Luzi, L.; Sgobba, S.; Felicetta, C.; Pacor, F.; D'Amico, M.; Puglia, R.; Russo, E.; 2022: Parametric table of the ITA18 GMM for PGA, PGV and Spectral Acceleration ordinates. Istituto Nazionale di Geofisica e Vulcanologia (INGV), https://doi.org/10.13127/ita18/sa_flatfile

Luzi, L.; Lanzano, G.; Puglia, R.; Russo, E.; D'Amico, M.; Felicetta, C.; Pacor, F.; Cantore, L.; 2020: Italian Accelerometric Archive (ITACA) and Italian Accelerometric Archive version 2.0. Istituto Nazionale di Geofisica e Vulcanologia, https://itaca.mi.ingv.it/

Boore, D. M.; 2003: Simulation of ground motion using the stochastic method. Pure and Applied Geophysics Vol. 160, n. 3, pp. 635–676

Stafford, P. J.; Sgobba, S.; Marano, G. C.; 2009: An energy-based envelope function for the stochastic simulation of earthquake accelerograms. Soil Dynamics and Earthquake Engineering Vol. 29, n. 7, pp. 1123–1133

Corresponding author: fadel.ramadan@ingv.it

A building footprint segmentation dataset from the Friuli Venezia Giulia region

Claudio Rota[1], Flavio Piccoli[1], Rajesh Kumar[1], Gianluigi Ciocca[1], Chiara Scaini[2] and the SMILE team[3]

[1] University of Milano-Bicocca, Dept. of Informatics, Systems and Communication, Milano, Italy
[2] OGS, National Institute of Oceanography and Applied Geophysics, Italy
[3] OGS, CNR-IMATI Milano, and University of Florence

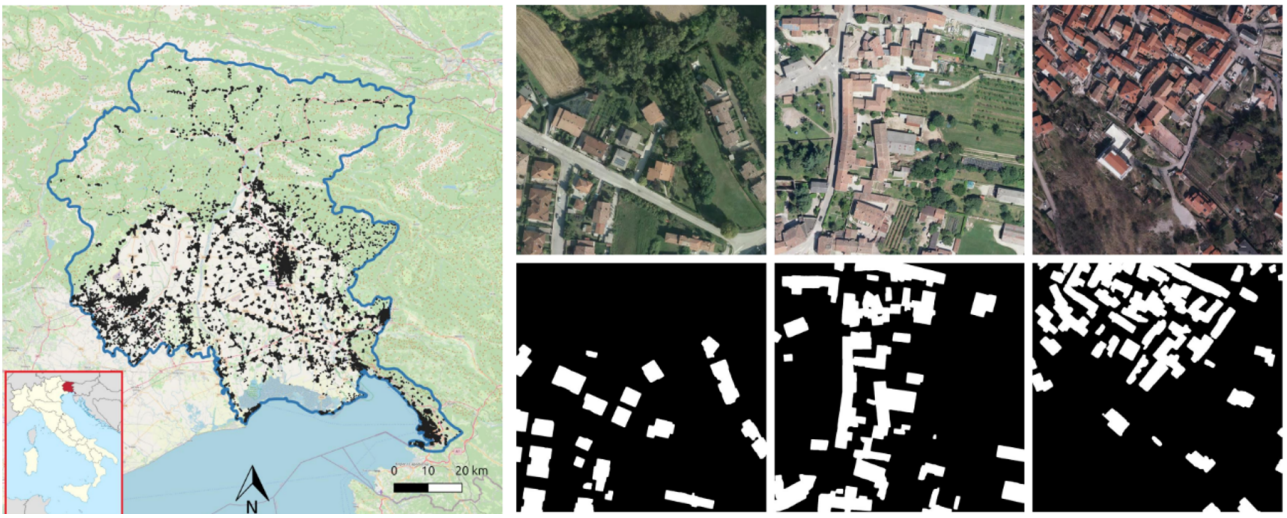

Fig. 1. Spatial distribution of the image in the dataset across the Friuli Venezia Giulia region and samples of their annotation.

Accurate and up-to-date information on the spatial distribution and characteristics of the built environment is a fundamental component of exposure assessment, which in is turn is paramount for disaster risk reduction (DRR). Building footprints and associated geometric information are useful for land use planning and risk assessment and mitigation strategies. Building footprint segmentation (i.e. detect building footprint area) from aerial and satellite imagery is a thus a key component of numerous geospatial applications. Despite the rapid progress enabled by deep learning, the performance and generalization capability of modern segmentation models remain limited by the availability of large, diverse, and high-resolution annotated datasets. Existing resources typically lack one or more of these characteristics, constraining their utility for training robust models across heterogeneous geographical contexts.

In this work, we introduce Segmentation Friuli Venezia Giulia (SegFVG), a large-scale dataset containing 15,403 aerial tiles at 0.1 m ground sampling distance, each with precise pixel-level building footprint annotations. Covering 616 km² of the Friuli Venezia Giulia region in northeastern Italy, SegFVG encompasses a wide variety of landscapes, including alpine rural zones, agricultural

plains, suburban environments, and densely populated coastal areas, resulting in approximately 357,000 annotated buildings. This geographic and environmental diversity makes SegFVG a representative and challenging benchmark for evaluating building footprint segmentation models. Fig. 1 shows the spatial distribution of the images within the region and some examples of buildings annotation.

We use SegFVG to build ML algorithms for automatic building footprint segmentation. We tested multiple deep learning architectures and achieve high performance, with 0.943 precision, 0.975 recall, 0.959 F1-score, and 0.921 IoU, demonstrating the dataset's suitability for training accurate building segmentation models.

Beyond enabling benchmarking and model development, SegFVG can be useful for a wide range of practical applications, including (1) automated building detection, (2) comparison with official cadastral data to identify discrepancies, (3) detection of unauthorized constructions, and (4) multi-temporal analysis for monitoring changes in the built environment.

Acknowledgments

This research contributes to the PRIN 2022 PNRR project SMILE "Statistical Machine Learning for Exposure development" (code P202247PK9, CUP B53D23029430001) within the European Union-NextGenerationEU program. We warmly acknowledge our colleagues from the SMILE team: Chiara Scaini, Antonella Peresan, Piero Brondi, Hazem Badreldin, and Hany Mohammed Hassan Elsayed (OGS), Elisa Varini and Maria Teresa Artese (CNR-IMATI Milano), Matteo Del Soldato, Silvia Bianchini, and Olga Nardini (University of Florence).

Corresponding author: claudio.rota@unimib.it

Simulation of cumulative damage scenarios: three case studies

R.M. Sava[1,2], R. Arcoraci[3], A. Greco[3], A. Pluchino[1,2], A. Rapisarda[1,2,4]

[1] *Department of Physics and Astronomy "Ettore Majorana", University of Catania, Catania, Italy*
[2] *INFN Sezione di Catania, Catania, Italy*
[3] *Department of Civil Engineering and Architecture, University of Catania, Catania, Italy*
[4] *Complexity Science Hub, Vienna, Austria*

We present an extension and application of a methodology for simulating seismic damage scenarios at an urban scale. This approach focuses on the effects of seismic sequences, by accounting for the damage accumulation and the vulnerability evolution of buildings affected by multiple subsequent shocks.

The methodology was initially applied and calibrated to the 2009 L'Aquila seismic sequence (Sava et al., 2025), using the ShakeMaps generated by the INGV (Michelini et al., 2008,2020) to reproduce the sequence (Fig. 1), and information from the Da.D.O. (Dolce et al., 2019) to characterize the building stock and define vulnerability classes and as a reference dataset for comparing simulated and observed damage scenarios.

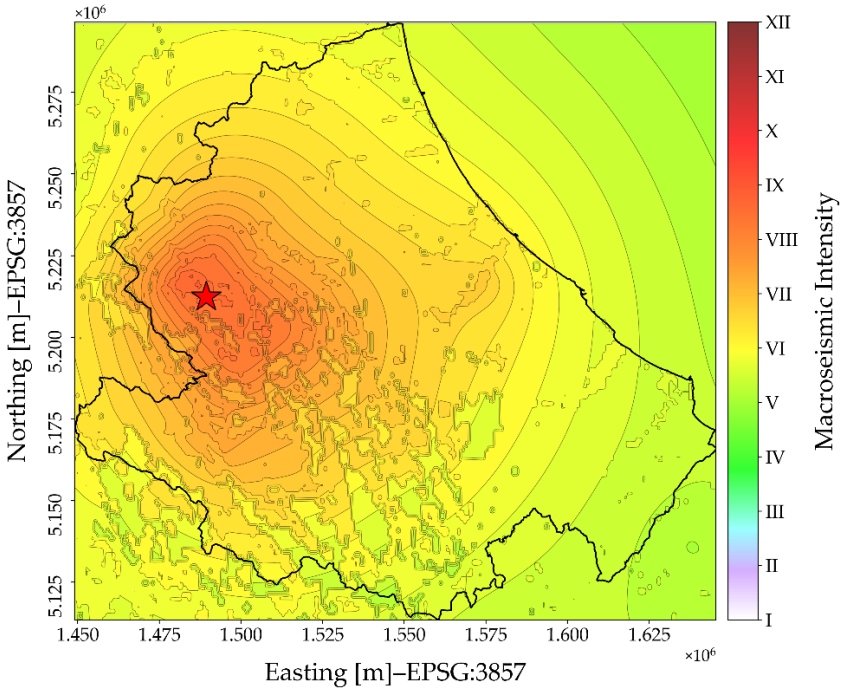

Fig. 1 – Macroseismic intensity ShakeMap generated by the INGV for the L'Aquila 2009 mainshock (available on the INGV ShakeMap Archive, https://shakemap.ingv.it). The administrative boundaries of the Abruzzo region (data from ISTAT) are outlined in black. The red star marks the epicenter of the mainshock. (From Sava et al., 2025).

The results (see Fig. 2) show that the method is able to reproduce the distribution of observed damage across vulnerability classes, taking into account not only the mainshock but also the events of magnitude greater than a chosen threshold.

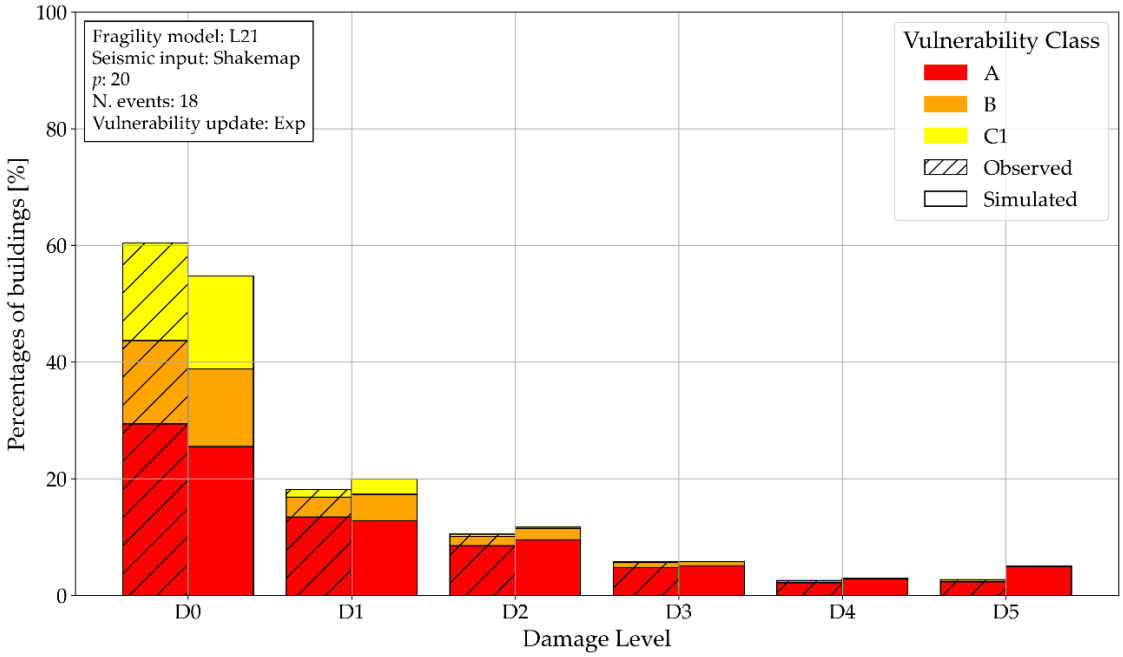

Fig. 2 – Comparison between the distribution of simulated (solid bars) and observed (diagonally hatched bars) final total damage levels for the L'Aquila 2009 sequence. For each damage level, stacked bars also illustrate the distribution of the initial vulnerability classes of the buildings: A (red), B (orange), and C1 (yellow). (From Sava et al., 2025).

Here we further investigate the methodology by applying it to two additional seismic sequences: the 2013 Garfagnana-Lunigiana and the 2016-2017 Central Italy sequences. A comparative study of the results allows the assessment of damage accumulation across different seismic sequences and urban contexts, analysing the influence of the sequences' characteristics and of the building stocks' properties on damage scenarios. This comparison also serves to evaluate the generalizability of the approach and its potentialities and limitations as a tool to analyse damage data for risk mitigation. Finally, future research will test the applicability of the approach to new urban areas, employing both real and synthetic sequences (Greco et al., 2019; Fisher et al., 2023).

References

Sava, R.M., Arcoraci, R., Greco, A., Pluchino, A., Rapisarda, A.; 2025: Simulations of damage scenarios in urban areas: the case of the seismic sequence of L'Aquila 2009. Buildings, 15, 3980, https://doi.org/10.3390/buildings15213980

Michelini, A., Faenza, L., Lauciani, V., Malagnini, L.; 2008: Shakemap implementation in Italy. Seismological Research Letters, 79, 688–697, https://doi.org/10.1785/gssrl.79.5.688

Michelini, A., Faenza, L., Lanzano, G., Lauciani, V., Jozinović, D., Puglia, R., Luzi, L.; 2020: The new ShakeMap in Italy: Progress and advances in the last 10 years. Seismological Research Letters, 91, 317–333, https://doi.org/10.1785/0220190130

Dolce, M., Speranza, E., Bocchi, F., Conte, C., Giordano, F., Borzi, B., Faravelli, M., Di Meo, A., Pascale, V.; 2019: Observed damage database of past Italian earthquakes: the Da.D.O. WebGIS. Bollettino di Geofisica Teorica ed Applicata, 60, 141–164, https://doi.org/10.4430/bgta0254

Greco, A., Pluchino, A., Barbarossa, L., Barreca, G., Caliò, I., Martinico, F., Rapisarda, A.; 2019: A New Agent-Based Methodology for the Seismic Vulnerability Assessment of Urban Areas. ISPRS International Journal of Geo-Information, 8, 274, https://doi.org/10.3390/ijgi8060274

Fischer, E., Barreca, G., Greco, A., Martinico, F., Pluchino, A., Rapisarda, A.; 2023: Seismic risk assessment of a large metropolitan area by means of simulated earthquakes. Natural Hazards, 118, 117–153, https://doi.org/10.1007/s11069-023-05995-y

Corresponding author: rosa.sava@phd.unict.it

Systematic analysis of the components of ground motion variability from physics-based simulations

C. Smerzini[1], S. Sgobba[2], M. Vanini[1], A. Bazrafshan[1], G. Lanzano[2]

[1] Department of Civil and Environmental Engineering, Politecnico di Milano, Italy
[2] Istituto Nazionale di Geofisica e Vulcanologia (INGV), Sezione di Milano, Italy

Introduction

Empirical ground motion models (GMM) represent the reference tool for seismic hazard analyses and generation of ground shaking scenarios, but, in spite of their considerable evolution and ease of use, they still suffer from the paucity of recordings in peculiar conditions, such as in the proximity of the earthquake source (near-field) and in peculiar seismotectonic (e.g. volcanic) and geologic (e.g. deep soft alluvial basins). Such lack of observational evidences may prevent an accurate and robust prediction of the ground motion (and of its variability) in the variety of source-to-site conditions which are of practical interest. With the advancement of high-performance computing (HPC) resources, physics-based numerical simulations (PBS) have emerged as a valuable approach to complement recordings where they are insufficient, by providing validated ground motions in realistic source and source-to-site configurations and with features apt for engineering applications. In spite of the increasing consideration of PBS, the issues related to the integration of recorded and simulated data in the frame of ground motion modelling and seismic risk applications is still at the frontier of research.

In this contribution, we aim at advancing the research related to the integration of recorded and simulated data in the frame of ground motion modelling, which is still subject of debate (Liu et al. 2025). For this purpose, BB-SPEEDset, a dataset of broadband simulated accelerograms from 3D PBS, validated from both a seismological and engineering point of view (Paolucci et al. 2021; Smerzini et al. 2024), is analyzed systematically to identify the repeatable source, site and path effects through residual decomposition. The systematic components of residuals, between-event, site-to-site and single-site within-event, and the corresponding variability are quantified by means of the linear mixed-effect analysis for various intensity measures and compared with the ones obtained from a recorded near-source dataset (NESS2, Sgobba et al. 2021).

Datasets: empirical (NESS) and simulations (BB-SPEEDset)

BB-SPEEDset is a dataset of near-source broadband earthquake ground motions from 3D PBS obtained through the HPC code SPEED (http://speed.mox.polimi.it/, Mazzieri et al. 2013), developed at Politecnico di Milano. The dataset is assembled by processing a large number of simulated waveform scenarios through a homogeneous workflow and converting low-frequency simulation outputs into broadband time histories using an artificial neural-network-based technique trained on recorded strong-motion data (Paolucci et al. 2018). The current version 2.3 comprises over 20,000 three-component accelerograms from simulated earthquakes with moment magnitudes (Mw) ranging approximately from 4.9 to 7.4 and Joyner–Boore distances up to about 110 km, encompassing various faulting styles and site conditions.

BB-SPEEDset has undergone successfully validation tests against recorded datasets on the statistical distribution of several ground motion intensity measures, such as Peak Ground Acceleration (PGA), Peak Ground Velocity (PGV) and Spectral Acceleration (SA) (see Paolucci et al. 2021), as well as on that of selected Engineering Demand Parameters (e.g. ductility demand) of simplified inelastic structural models (see Smerzini et al. 2024). In the present study, BB-SPEEDset is further compared with the empirical dataset NESS to provide additional checks on the distribution of the systematic components of residuals and their variability. The NESS (NEar-Source Strong-motion) is a globally compiled dataset of near-source earthquake ground-motion records and related metadata that focuses on moderate-to-large earthquakes with moment magnitude Mw ≥ 5.5 and hypocentral depths shallower than 40 km. Version NESS2.0 (the current release) contains ground-motion parameters and comprehensive metadata from 81 events and 1,189 three-component waveforms selected worldwide, distributed in flat-file format. Fig. 1 shows the distribution of the BB-SPEEDset data against the NESS one, in terms of magnitude M_W and Joyner and Boore distance R_{JB}.

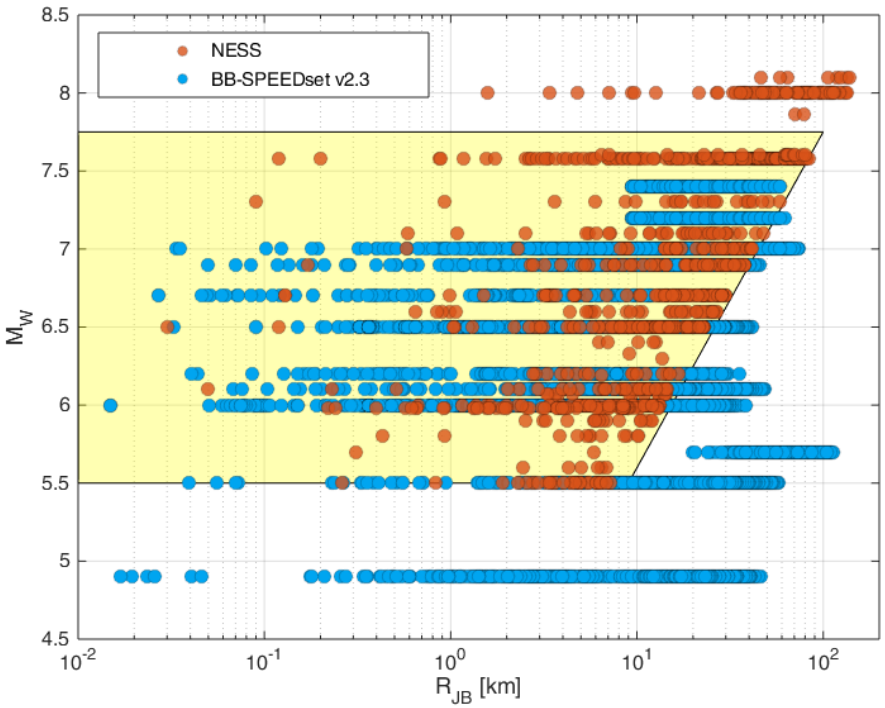

Fig. 1. Distribution of data from BB-SPEEDset (blue circles) and NESS dataset (red dots, after Sgobba et al., 2021). The yellow shaded region highlights the data in comparable ranges of magnitude M_w and distance R_{JB}.

Methodology and Results

In this study, residuals are calculated as the (base 10) logarithmic difference between observed (or simulated) ground-motion intensities and the corresponding prediction from a reference GMM and decomposed according to the partially non-ergodic approach (Al Atik et al. 2010), as follows:

$$R_{es} = y_{es} - \mu_{es} = \delta_0 + \delta B_e + \delta S2S_s + \delta WS_{es} \quad (1)$$

in which y_{es} is the logarithm of the ground-motion parameter observed at site *s* during earthquake *e*, and μ_{es} is the logarithmic median ground motion predicted by the GMM. According to eq. (1), total residuals R_{es} are separated into the median bias δ_0, between-event residual δB_e, site-to-site residual $\delta S2S_s$, and single-site within-event residual δWS_{es}. If the standard deviation of δB_e, $\delta S2S_s$ and δWS_{es} is represented by τ, ϕ_{S2S} and ϕ_{SS}, respectively, the total standard deviation of the model can be written as:

$$\sigma_T = \sqrt{\tau^2 + {\phi_{S2S}}^2 + {\phi_{SS}}^2} \quad (2)$$

In this analysis, the reference GMM is the one by Lanzano et al. (2019) calibrated on records from Italian crustal earthquakes, and adjusted for a near-source correction factor based on NESS dataset (Sgobba et al., 2021), referred to as ITA18$_{\text{NESS}}$.

Figure 2 summarizes the residual analysis results for PGA and SA(1s) from BB-SPEEDset and NESS with respect to the ITA18$_{\text{NESS}}$ ground-motion model. In this figure, between-event residuals (δB_e) are shown as a function of moment magnitude, site-to-site residuals ($\delta S2S_s$) as a function of V_{S30}, and the single-site within-event (δWS_{es}) as a function of R_{JB}. The mean residuals for each dataset are indicated with larger circles, and the vertical lines represent the 16th and 84th percentiles of the residuals within each bin.

For the NESS dataset, δB_e for both PGA and SA(1s) remain centered around zero for Mw between about 5.5 and 7.0, while a systematic negative deviation becomes apparent at larger magnitudes, likely influenced by the limited number of large-magnitude events. For the BB-SPEEDset, while the overall scatter of δB_e is comparable to that of NESS, the binned mean values exhibit a more pronounced magnitude-dependent deviation. It is worth noting that the NESS consists of 77 events compared to the 37 events available in BB-SPEEDset. This reflects the different nature of the two datasets: empirical datasets contain many events, each sampled in most cases by few records, while simulated datasets consist typically of relatively few events but each sampled by an optimal number of records. The trend of $\delta S2S_s$ indicates that the median site-to-site residuals for BB-SPEEDset are very close to zero across the entire V_{S30} range, indicating no systematic bias in predicting PGA and SA(1s) at individual stations. In contrast, NESS exhibits slightly greater scatter for PGA, with noticeable negative deviations for values of V_{S30} below 200 m/s and above 800 m/s, most likely influenced by the scarcity of data. For the SA(1s) the deviation only can be seen particulary at very stiff sites. Therefore, while the BB-SPEEDset reproduces the mean station-to-station response well, it underestimates the site-to-site variability, in line with recent studies on the CybarShake dataset (Liu et al. 2025). The third plot shows the comparison of single-site within-event for the two datasets. Once again, the mean residuals for both BB-SPEEDset and NESS are close to zero, and the

variability is moderate and well-behaved, indicating that the PGA predictions are generally reliable across stations for both datasets.

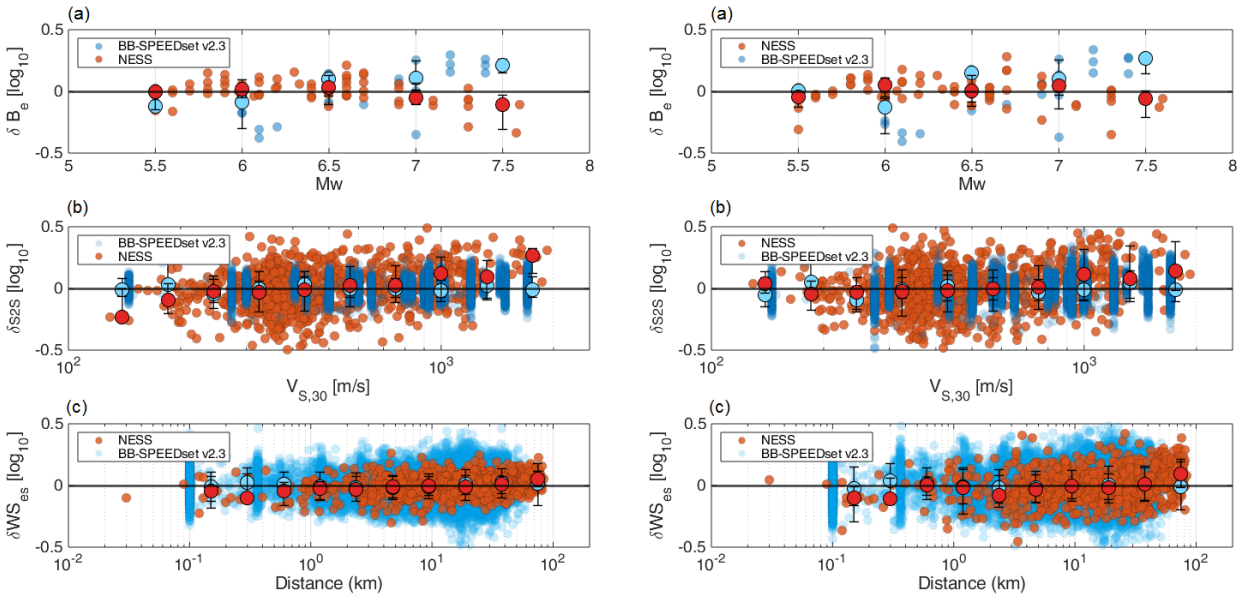

Fig. 2 – Residual analysis of the GMM for PGA (left) and SA(1s) (right) across different databases. a) Between-event residuals as a function of M_W, b) Site-to-site residuals versus V_{S30} and c) single-site within-event against R_{JB}

Conclusions

This work has addressed the systematic analysis of the components of ground motion variability from a validated dataset of physics-based simulated accelerograms from multiple regions and styles of faulting, in comparison with those from a recorded dataset. The results indicate that the simulated dataset is able to provide unbiased residuals, in their different components, apart from some deviations related to the scarcity of data samples. As a matter of fact, for the between-event residual, this bias is somewhat more pronounced, since the number of events in the simulated dataset is limited. In contrast, the simulated dataset shows a more stable performance in estimating the site-to-site component, whereas real dataset often suffer from a lack of sufficient records and therefore exhibit some distinct deviations. Nevertheless, the site-to-site variability obtained from simulations would be inherently smaller than the corresponding values observed in reality, as even sophisticated models may not fully represent the heterogeneous and variable conditions of real sites. This limitation becomes even more pronounced when simplified, often nearly homogeneous, velocity models are employed, which ultimately leads to an underestimation of the variability.

References

Al Atik, L., Abrahamson, N., Bommer, J.J., Scherbaum, F., Cotton, F., Kuehn, N.; 2010: The variability of ground motion prediction models and its components. Seismol Res Lett 81(5): pp. 794‑801

Lanzano, G., Luzi, L., Pacor, F., Felicetta, C., Puglia, R., Sgobba, S., D'Amico, M.; 2019: A revised ground-motion prediction model for shallow crustal earthquakes in Italy. Bulletin of the Seismological Society of America, 109(2), pp.525-540.

Liu, X., Cotton, F., Fu, L., Chen, S., Li, X.; 2025: Advancing ground-motion modeling through data fusion? Insights combining NGA-West2 data and CyberShake simulations. Bulletin of Earthquake Engineering, pp.1-22.

Mazzieri, I., Stupazzini, M., Guidotti, R., Smerzini, C.; 2013: SPEED: SPectral Elements in Elastodynamics with Discontinuous Galerkin: A non-conforming approach for 3D multi-scale problems. International Journal for Numerical Methods in Engineering, 95(12), pp.991-1010.

Paolucci, R., Gatti, F., Infantino, M., Smerzini, C., Güney Özcebe, A., Stupazzini, M.; 2018: Broadband ground motions from 3D physics-based numerical simulations using artificial neural networks. Bulletin of the Seismological Society of America, 108(3A), pp.1272-1286.

Paolucci, R., Smerzini, C., Vanini, M.; 2021:. BB-SPEEDset: A validated dataset of broadband near-source earthquake ground motions from 3D physics-based numerical simulations. *Bulletin of the Seismological Society of America*, *111*(5), pp.2527-2545.

Sgobba, S., Felicetta, C., Lanzano, G., Ramadan, F., D'Amico, M., Pacor, F.; 2021: NESS2. 0: An updated version of the worldwide dataset for calibrating and adjusting ground-motion models in near source. Bulletin of the Seismological Society of America, 111(5), pp.2358-2378.

Smerzini, C., Amendola, C., Paolucci, R., Bazrafshan, A.; 2024: Engineering validation of BB-SPEEDset, a data set of near-source physics-based simulated accelerograms. *Earthquake Spectra*, *40*(1), pp.420-445.

Corresponding author: chiara.smerzini@polimi.it

Preliminary validation of a Physics-based Simulated Ground-Motion Database

Giovanni Smiroldo[1], Marco Fasan[1], Fabio Romanelli[2], Chiara Bedon[1]

[1] *University of Trieste – Department of Engineering and Architecture*
[2] *University of Trieste – Department of Mathematics, Informatics and Geoscience*

Introduction

The study focuses on the limited availability of recorded ground motions that are truly representative of strong seismic shaking, especially for large-magnitude events in near-fault conditions and for specific combinations of source, path, and site characteristics. This lack of suitable recordings directly affects advanced applications such as nonlinear time-history analyses, seismic fragility and risk assessments, and detailed site-response studies. Although strong-motion databases have grown over time, they still do not adequately cover high-intensity scenarios with the required geological and seismotectonic consistency.

Within this context, the study proposes the use of Physics-Based Simulated (PBS) ground motions as a physically sound alternative to recorded accelerograms (Graves et al., 2011; Panza et al., 2001; Paolucci et al., 2018). Unlike empirical approaches, PBS explicitly models the physical processes governing seismic wave generation and propagation. However, for PBS ground motions to be reliably used in engineering practice, they must undergo rigorous validation against observed data (Bradley et al., 2017; Galasso et al., 2012; Petrone et al., 2021; Smerzini et al., 2024). The validation strategy adopted in this work is based on energy-related intensity measures, which are particularly relevant for structural response and damage assessment.

Physics-based simulation methodology

The PBS framework used in the study explicitly accounts for source, path, and site effects (Fasan, 2017; Magrin, 2012; Panza et al., 2012). Seismic wave generation is modeled using an Extended Source (ES) model, where the fault plane is represented as a finite surface discretized into multiple sub-sources. The rupture process is simulated stochastically, allowing different realizations of slip distribution, rupture propagation, and nucleation point (Gusev, 2011). This approach captures key features of near-fault ground motions, such as rupture directivity, broadband frequency content, and realistic time-domain characteristics, while also accounting for intra-event variability.

Wave propagation from the source to the site is simulated using the Discrete Wavenumber (DWN) technique, assuming laterally homogeneous but vertically layered viscoelastic media (Pavlov, 2009;

Vaccari & Magrin, 2022). This method allows for the full seismic wavefield, including body waves and near-field terms, to be modelled consistently. Path effects are defined through deep geological structures derived from regional tomography studies, while local site effects are incorporated by adding real, site-specific shallow stratigraphies. These stratigraphies are classified according to Eurocode 8 soil categories (A, B, and C) and are selected from the Engineering Strong Motion database (Luzi et al., 2020). Figure 1 shows the velocity profiles of the B soil category:

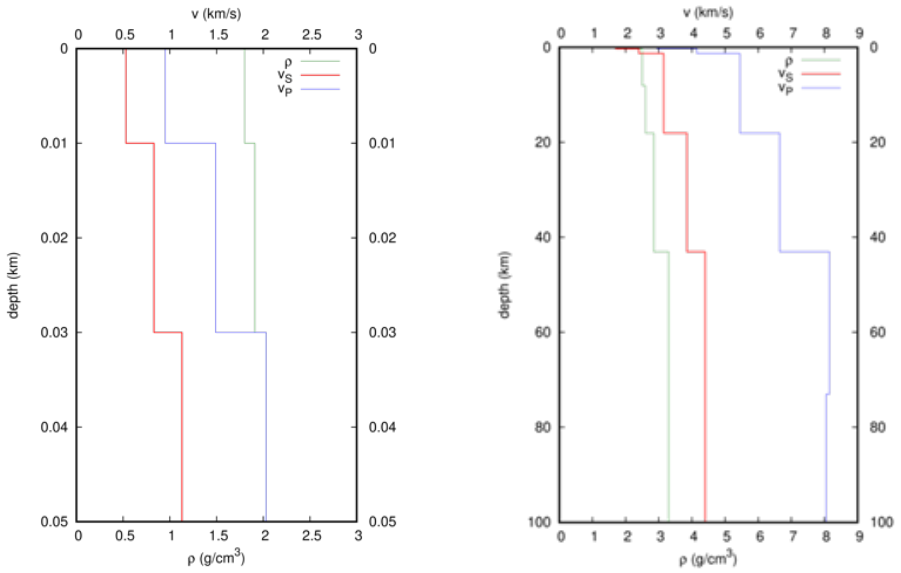

Figure 1 - Velocity (a) deep structure and (v) shallow structure adopted

PBS database

Using this modelling framework, a large PBS database is constructed, comprising 6300 simulated earthquake scenarios. The simulations cover a wide range of controlling parameters, including moment magnitude (M_w 5.5–7.5), source-to-site distance, source–receiver azimuth, focal mechanism, and local soil conditions. For each configuration, multiple stochastic rupture realizations are generated, ensuring a statistically meaningful representation of variability related to the rupture process. The adopted parameters are shown in the following Table 1 and Table 2:

Table 1 - Range of investigated parameters

Parameter	Range
Moment Magnitude (Mw)	5.5, 6.0, 6.5, 7.0, 7.5
Distance R (km)	5, 10, 15, 20, 30, 50, 100
Local soil category (EC8)	A, B, C (real stratigraphy, different for each fault)
Source-Receivers angles (°)	0, 60, 120, 180, 240, 300
Number of rupture processes	10, random (different random seed)

Table 2 - Parameters of the simulated fault geometries (DISS Working Group, 2021)

DISS – ID	ITIS120
Name	Gemona sud
Faulting Style	Thrust
Length [km]	16
Width [km]	9
Min depth [km]	2
Strike [deg]	290
Dip [deg]	30
Rake [deg]	105

Energy-based validation

The validation of the database is carried out using an energy-based approach. The selected intensity measure is the Relative Energy Input Velocity (V_{EIr}) (Decanini & Mollaioli, 2001), which represents the equivalent velocity associated with the elastic relative input energy (Eq. (1), Eq. (2) and Eq. (3)):

$$m\ddot{x} + c\dot{x} + kx = -m\ddot{x_g} \tag{1}$$

$$E_{Ir} = -\int m\ddot{x}_g dx = \frac{m\dot{x}}{2} + \int (c\dot{x})dx + \frac{kx^2}{2} \tag{2}$$

$$V_{EIr} = \sqrt{2E_{Ir}/m} \tag{3}$$

V_{EIr} is particularly suitable for validation purposes because it correlates with the energy demand imposed on structures and with hysteretic energy dissipation during seismic response. The V_{EIr} values computed from the PBS accelerograms are compared with predictions from an empirical energy-based Ground Motion Prediction Equation (or GMPE) (Cheng et al., 2014).

The comparison is performed through both direct and statistical analyses. Simulated V_{EIr} values are plotted against the GMPE median predictions for different soil categories and distances, allowing a direct assessment of consistency. In addition, residuals are computed as normalized differences between simulated and GMPE-predicted values, making it possible to identify systematic trends or biases with distance (Eq. (4)).

$$Res(D) = \frac{\log\big(obs(D)\big) - \log\left(sim(D)\right)}{\sigma_{GMPE}} \tag{4}$$

Both comparisons are illustrated for the B soil category by the following Figure 2:

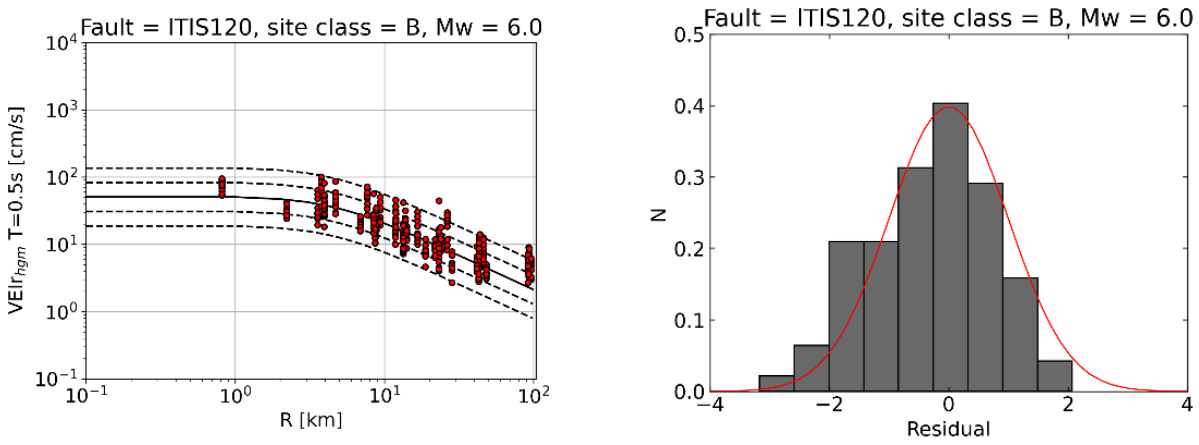

(a) (b)

Figure 2 - Equivalent Velocity of Relative Energy Input V_{Elr} for fault ITIS120, Mw = 6.0, R as distance metric and soil category (EC8) B. Comparison with GMPE (Cheng et al. 2014) (a) and distribution of the residuals (b)

Results

The results show that, for all considered soil classes and magnitudes, most simulated values lie within ±1 standard deviation of the GMPE, and no significant distance-dependent bias is observed.

Overall, the results indicate that the PBS database reproduces the energy content of real ground motions in a statistically consistent manner. Although detailed results are shown mainly for M_w = 6.0 for clarity and B soil category, similar behaviours are observed for the other magnitudes and shallow soils considered. The study therefore concludes that the proposed PBS database is suitable for engineering applications, particularly in cases where recorded ground motions are scarce or not representative (Smiroldo, 2025). Further developments are expected to include the use of additional intensity measures and GMPEs, as well as an expansion of the variability of the simulated scenarios, to strengthen and extend the validation framework.

References

Bradley, B. A., Pettinga, D., Baker, J. W., & Fraser, J.; 2017: Guidance on the Utilization of Earthquake-Induced Ground Motion Simulations in Engineering Practice. *Earthquake Spectra*, *33*(3), 809–835. https://doi.org/10.1193/120216eqs219ep

Cheng, Y., Lucchini, A., & Mollaioli, F.; 2014: Proposal of new ground-motion prediction equations for elastic input energy spectra. *Earthquakes and Structures*, *7*(4), 485–510. https://doi.org/10.12989/eas.2014.7.4.485

Decanini, L. D., & Mollaioli, F.; 2001: An energy-based methodology for the assessment of seismic demand. *Soil Dynamics and Earthquake Engineering*, *21*(2), 113–137. https://doi.org/10.1016/S0267-7261(00)00102-0

DISS Working Group.; 2021: *Database of Individual Seismogenic Sources (DISS), Version 3.3.0: A compilation of potential sources for earthquakes larger than M 5.5 in Italy and surrounding areas. Istituto Nazionale di Geofisica e Vulcanologia (INGV)*. https://doi.org/https://doi.org/10.13127/diss3.3.0

Fasan, M.; 2017: *Advanced seismological and engineering analysis for structural seismic design*. University of Trieste.

Galasso, C., Zareian, F., Iervolino, I., & Graves, R. W.; 2012: Validation of Ground-Motion Simulations for Historical Events Using SDoF Systems. *Bulletin of the Seismological Society of America*, *102*(6), 2727–2740. https://doi.org/10.1785/0120120018

Graves, R., Jordan, T. H., Callaghan, S., Deelman, E., Field, E., Juve, G., Kesselman, C., Maechling, P., Mehta, G., Milner, K., Okaya, D., Small, P., & Vahi, K.; 2011: CyberShake: A Physics-Based Seismic Hazard Model for Southern California. *Pure and Applied Geophysics*, *168*(3–4), 367–381. https://doi.org/10.1007/s00024-010-0161-6

Gusev, A. A.; 2011: Broadband Kinematic Stochastic Simulation of an Earthquake Source: a Refined Procedure for Application in Seismic Hazard Studies. *Pure and Applied Geophysics*, *168*(1–2), 155–200. https://doi.org/10.1007/s00024-010-0156-3

Luzi, L., Lanzano, G., Felicetta, C., D'Amico, M. C., Russo, E., S., S., Pacor, F., & 5, & O. W. G.; 2020: Engineering Strong Motion Database (ESM) (Version 2.0). *Istituto Nazionale Di Geofisica e Vulcanologia (INGV)*. https://doi.org/https://doi.org/10.13127/ESM.2

Magrin, A.; 2012: *Multi-scale seismic hazard scenarios*. University of Trieste.

Panza, G. F., Mura, C. La, Peresan, A., Romanelli, F., & Vaccari, F.; 2012: *Seismic Hazard Scenarios as Preventive Tools for a Disaster Resilient Society* (pp. 93–165). https://doi.org/10.1016/B978-0-12-380938-4.00003-3

Panza, G. F., Romanelli, F., & Vaccari, F.; 2001: Seismic wave propagation in laterally heterogeneous anelastic media: Theory and applications to seismic zonation. *Advances in Geophysics*, *43*(0), 1–95. https://doi.org/10.1006/ageo.2001.0001

Paolucci, R., Gatti, F., Infantino, M., Smerzini, C., Özcebe, A. G., & Stupazzini, M.; 2018: Broadband Ground Motions from 3D Physics-Based Numerical Simulations Using Artificial Neural Networks. *Bulletin of the Seismological Society of America*, *108*(3A), 1272–1286. https://doi.org/10.1785/0120170293

Pavlov, V. M.; 2009: Matrix impedance in the problem of the calculation of synthetic seismograms for a layered-homogeneous isotropic elastic medium. *Izvestiya, Physics of the Solid Earth*, *45*(10), 850–860. https://doi.org/10.1134/S1069351309100036

Petrone, F., Abrahamson, N., McCallen, D., & Miah, M.; 2021: Validation of (not-historical) large-event near-fault ground-motion simulations for use in civil engineering applications. *Earthquake Engineering and Structural Dynamics*, *50*(1), 116–134. https://doi.org/10.1002/eqe.3366

Smerzini, C., Amendola, C., Paolucci, R., & Bazrafshan, A.; 2024: Engineering validation of BB-SPEEDset, a data set of near-source physics-based simulated accelerograms. *Earthquake Spectra*, *40*(1), 420–445. https://doi.org/10.1177/87552930231206766

Smiroldo, G.; 2025: *Validation of physics-based ground-motion simulations for structural engineering purposes* [PhD, University of Trieste]. https://doi.org/https://hdl.handle.net/11368/3104780

Vaccari, F., & Magrin, A.; 2022: A user-friendly approach to NDSHA computations. In *Earthquakes and Sustainable Infrastructure* (pp. 215–237). Elsevier. https://doi.org/10.1016/B978-0-12-823503-4.00016-6

Corresponding author: giovanni.smiroldo@dia.units.it

Recent developments and applications of STATION, a dynamic webservice for seismic site characterisation across Europe

G. Tarchini[1], D. Spallarossa[1], D. Scafidi[1], L. Colavitti[1], S. Parolai[2], M. Picozzi[3], D. Bindi[4]

[1] *University of Genoa, Department of Earth, Environmental and Life Sciences, Italy*
[2] *University of Trieste, Department of Mathematics, Informatics and Geosciences, Italy*
[3] *National Institute of Oceanography and Applied Geophysics – OGS, Trieste, Italy*
[4] *GFZ Helmholtz Centre for Geosciences, Potsdam, Germany*

We present an updated overview of STATION (Seismic sTATion and sIte amplificatiON – https://distav.unige.it/rsni/station.php; Tarchini et al., 2024), a service designed to provide updated information on specific seismological characteristics of more than 3,500 seismic stations distributed across Italy and Europe. The system integrates data from permanent and temporary networks and exploits recordings from over 150,000 earthquakes collected between 2005 and 2024.

STATION delivers a suite of standardised products – including local magnitude residuals, horizontal-to-vertical spectral ratios (HVSRs), and mean noise spectra – made accessible through both a user-friendly web interface and direct station-based queries. These features enable rapid retrieval of site-specific information and associated metadata, supporting several scientific and operational applications, from network characterisation to post-event analyses.

Building on the framework previously presented, this work highlights recent advancements and ongoing developments aimed at enhancing the robustness and scope of the service. In particular, we report on the recent inclusion into the database of new stations and stations for which data access has become unrestricted. We also explore statistical properties of the existing dataset, including preliminary assessments of HVSR variability and distribution, with the aim of identifying systematic patterns related to site conditions or environmental effects. In addition, we discuss seasonal analyses conducted on long-term HVSR and noise datasets, investigating whether subtle fluctuations are observable at regional or station scale. Furthermore, we outline the expansion of STATION to several broadband and strong-motion seismic networks in Türkiye and Northern Europe, where HVSRs and local magnitude residuals have been computed for hundreds of velocimetric and accelerometric stations. These tests provide a valuable benchmark for evaluating

the transferability of the methods and services offered by STATION beyond the Italian national borders.

Overall, the results and prospects presented underscore the potential of STATION as a scalable, interoperable platform capable of supporting large-scale site characterisation studies and fostering cross-network harmonisation within the broader seismological community.

References

Tarchini G., Scafidi, D., Parolai, S., Picozzi, M., Bindi, D., and Spallarossa, D.; 2024: The Seismic Station and Site Amplification Service: Continuously Updated Information on Italian Seismic Stations, Seismol. Res. Lett., 96, 2027–2038, https://doi.org/10.1785/0220240291.

Corresponding author: gabriele.tarchini@edu.unige.it

Characterization of the Net4Fer seismic station network

P. Taverna[1,2], A. Bazzanella[2], F. Brighenti[2], C. Barnaba[1], R. Caputo[2]

[1] *Istituto Nazionale di Oceanografia e di Geofisica Sperimentale – OGS Centro di Ricerche Sismologiche, Italy*
[2] *Dipartimento di Fisica e Scienze della Terra, Università di Ferrara, Italy*

In June 2025, a geophysical acquisition based primarily on ambient seismic noise measurements was carried out in the provinces of Ferrara and Rovigo, within the alluvial plain surrounding the Po River. The aim of the survey was to characterize the seismic stations managed by the University of Ferrara and to assess near-surface properties, with a particular focus on shear-wave velocity (Vs).

The monitoring network (Fig. 1) has recently been expanded through the installation of 10 new seismic stations by Enel GreenPower and HERA concessionaires during 2021–2022 and all stations are equipped with a 150 m-deep borehole drilled from ground level, completed with a steel casing of 3-inch nominal diameter.

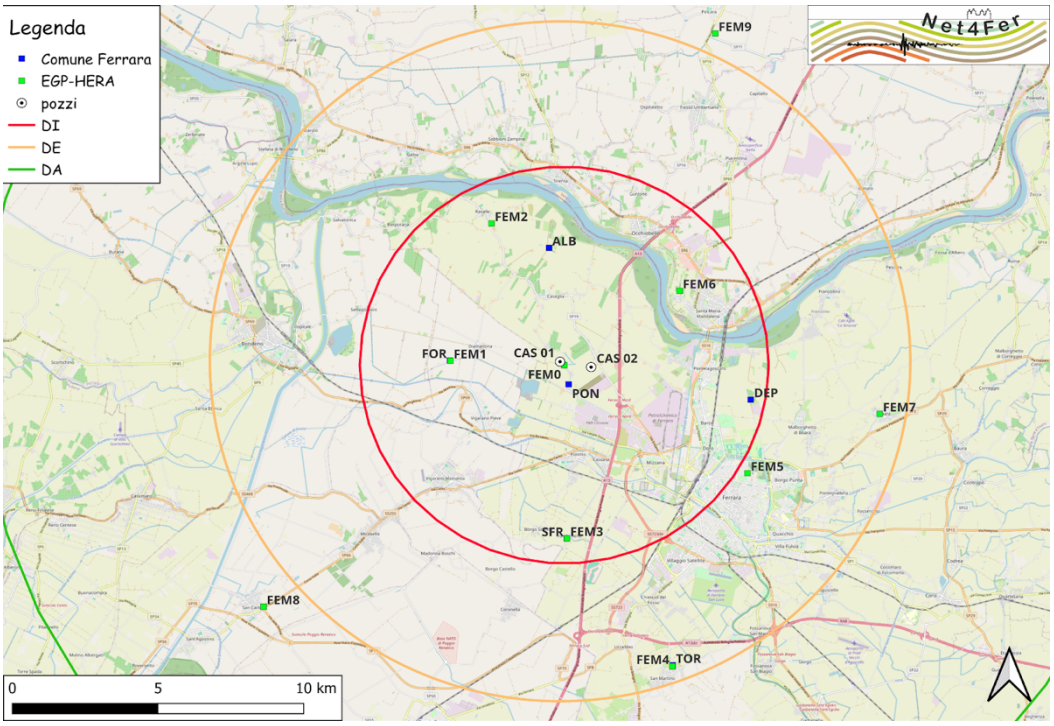

Fig. 1 – Current location of the microseismic network stations of the Net4Fer network in the alluvial plain. The stations in blue are those managed by the Municipality of Ferrara since 1990, while the more recent ones are in green (https://net4fer.unife.it/index.php/it/monitoraggio/monitoraggio-sismico).

The study area is located in the Po Plain near the city of Ferrara, an area characterized by almost flat topography with weak morphological variations mainly related to the occurrence of ancient and present river system. Generally, there are an extensive Quaternary fluvial deposits which represent only the shallowest portion of a very thick sedimentary succession filling the Padano–Adriatic foredeep. The investigated area within the Po Plain actually lies in correspondence of the buried sector of the Northern Apennines fold-and-thrust belt, which recently manifested its activity with the 2012 seismic sequence (Caputo et al. 2015).

In summer 2012 a seismic sequence affected the area with a ML 5.9 mainshock on May 20, near the towns of Ferrara and Modena. The largest aftershock occurred on May 29, approximately 12 km west of the first mainshock, with a ML 5.8 magnitude. The two earthquakes, occurring at depths of about 6.3 km and 10.2 km, respectively, activated two distinct roughly E–W–trending fault segments approximately 15 km-long (Scognamiglio et al., 2012). The earthquakes that occurred in the area in 2012 are the strongest events recorded during the instrumental period. Slightly east of the 2012 epicentral area another seismic sequence occurred in historical time (1570-1575) associated to an MW 5.5 mainshock (Rovida et al. 2022). Regarding recent seismicity, several earthquakes with ML < 3 occurred in the area during the current year. Two events with ML greater than 3 were located near the study area: on July 9, 2025 (07:43:21 UTC), an ML 3.5 earthquake at a depth of 3 km (latitude 44.86° N, longitude 11.19° E), and on January 15, 2025 (15:34:49 UTC), an ML 3.5 earthquake at a depth of 8 km with latitude 44.86° N, longitude 11.26° E (INGV, https://terremoti.ingv.it).

The aim of the measurements is to define the shear wave velocity (Vs) profile at each seismic station and to collect all available information in the area to better constrain the local seismic response. This is the starting point for defining the soil's mechanical properties, in terms of Vs and densities, to better constrain the geological model necessary for numerical modeling.

To this purpose, we adopted the ESAC (Extended Spatial Autocorrelation) method, an extension of the SPAC (Spatial Autocorrelation) technique originally proposed by Aki (1957) and later developed by Ohori et al. (2002). In each site, we deployed an array of at least 15 measuring points, using 15 seismic stations. In two sites the measuring points were 20. Each station was equipped with Lunitek Sentinel-Geo sensors, consisting of an integrated triaxial velocimeter, with an eigen frequency of 1 Hz. Each site of the Net4Fer network had a specific geometry, according to the on-site logistic condition. In some site (FEM5 and FEM9) the acquisition was performed in two times: a first one, with short interstation distances; a second one, with larger interstation distances, with a common central station. In addition to the application of the ESAC method, at the same sites we acquired ambient noise following the HVSR (Horizontal-to-Vertical Spectral Ratio) method proposed by Nakamura (1989). This approach allows to identify resonance frequencies and provide further constraints on the shallow subsurface. Ambient noise acquisition was performed with the triaxial 5-second Lennartz LE-3D/5S sensor, connected to a high-resolution datalogger (RefTek RT130).

The processing of the array data was then subdivided into three steps: pre-processing, extraction of the dispersion curve and inversion. The pre-processing consists in re-formatting the data, set the station position and for the sites with two-time acquisitions, the definition of the sub-arrays. The

extraction of the Rayleigh-wave dispersion curve was obtained by Geopsy software (Wathelet et al., 2008). A window of minimum 30 minutes of synchronous recording was chosen and analysed with the high-resolution beam forming frequency-wave number (F-k) method. The dispersion curve was determined by the maximum energy within the F-k spectrum. For sites where two arrays are present, we repeated the processing and we merged the curves: the array with short distances between stations define the dispersion curve at higher frequencies, and describes the shallow soil part, while the array with longer distances defines the lower frequencies and it is related to the deeper part of the soil. We tested the software parameters to detect as good as possible dispersion curves. Finally, we picked the dispersion curves and used these values as input for inversion with Dinver, another tool provided in the Geopsy software package. We constrain the inversion with the additional geological and geophysical information from several earlier researches, included also the outcome of Microzonation studies and the recently published results of the CARG sheet 185-Ferrara (Caputo et al., 2025), in order to produce a more detailed inversion.

The preliminary results show that most dispersion curves are reliable in the frequency range between 1 and 4 Hz; however, in some cases where the dispersion pattern is clearer (e.g. FEM9; Fig. 2), the minimum frequency reaches about 0.8 Hz and the maximum extends up to 10 Hz. Based on these preliminary analyses, the investigation depth associated with the dispersion curves was estimated. Since lower frequencies are related to larger wavelengths, they correspond to greater investigation depths. Using the minimum reliable frequency and the corresponding phase velocity, a first-order estimate of the investigation depth can be obtained (Foti et al., 2014). According to these estimates, all Net4Fer sites reached investigation depths of at least 100 m.

The HVSR measurements were processed using the open-source Python-based software “hvsrpy” (Vantassel et al., 2021). The results indicate that some station located at the center of the study area (FEM2, FEM0 and FEM9) exhibits a well-defined resonance peak at approximately 0.8 Hz, which is indicative of the presence of a deeper and mechanically stiffer subsurface layer.

These results are preliminary and currently undergoing further refinement, but they already provide valuable constraints for the characterization of station sites and for future seismic response studies in the Ferrara–Rovigo area.

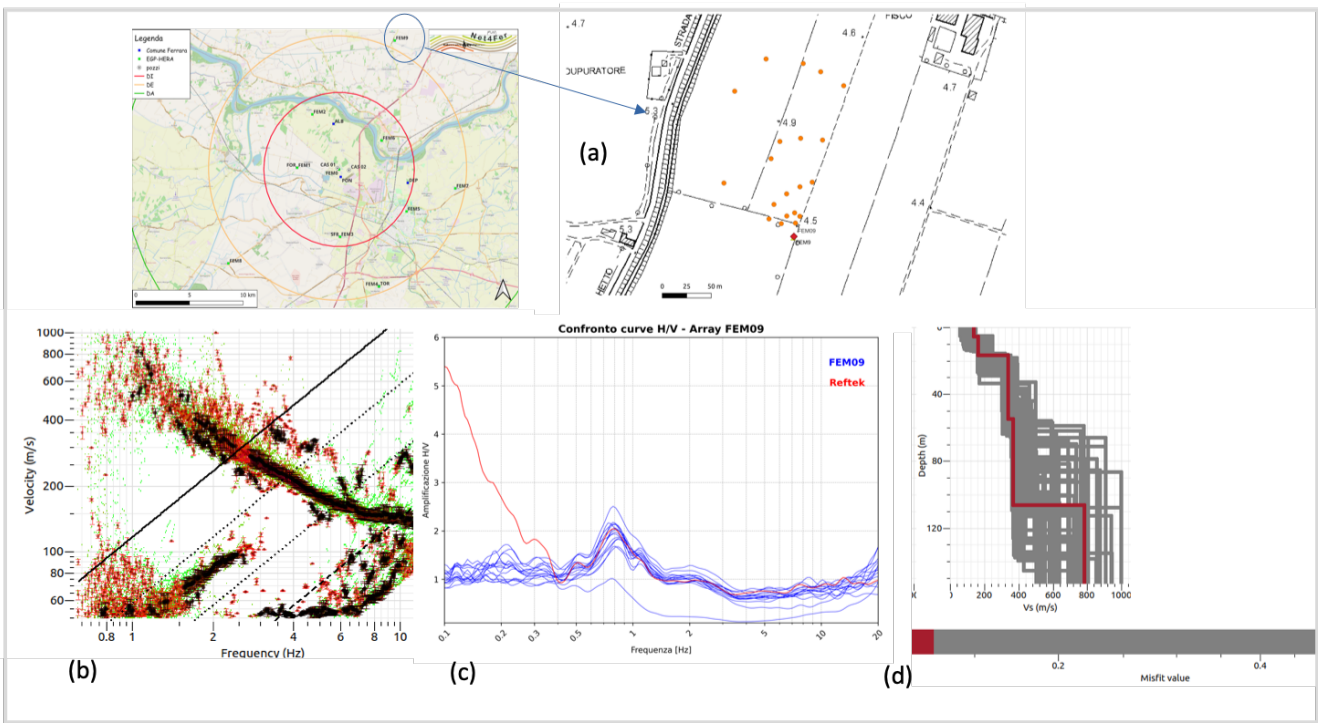

Fig. 2 – FEM9 site near Rovigo: (a) array geometry; (b) dispersion curve obtained using Geopsy software; (c) HVSR results, with blue curves representing recordings from the stations and the red curve representing the 5-s sensor; (d) shear-wave velocity (Vs) profile of the site, with a misfit lower than 0.2.

References

Aki, K.; 1957: Space and time spectra of stationary stochastic waves, with special reference to microtremors, Bull. Earthquake Res. Inst. Tokyo Univ., 35, 415-456

Caputo, R., Pellegrinelli, A., Bignami, C., Bondesan, A., Mantovani, A., Stramondo, S., & Russo, P.; 2015: High-precision levelling, DInSAR and geomorphological effects in the Emilia 2012 epicentral area. Geomorphology, 235, 106-117, doi: 10.1016/j.geomorph.2015.02.002

Caputo, R., Caggiati, M., Amorosi, A., & Rapti, D.; 2025: Note Illustrative della Carta geologica d'Italia alla scala 1:50.000, F. 185 Ferrara, Servizio Geologico d'Italia - ISPRA. ISPRA. https://doi.org/10.15161/oar.it/c2s5n-23h51

Foti, S., Lai, C. G., Rix, G. J., & Strobbia, C.; 2014: *Surface wave methods for near-surface site characterization*. CRC press.

Nakamura, Y.; 1989: A method for dynamic characteristics estimation of subsurface using microtremor on the ground surface. Railway Technical Research Institute, Quarterly Reports, 30(1).

Ohori, M., Nobata, A., & Wakamatsu, K.; 2002: A comparison of ESAC and FK methods of estimating phase velocity using arbitrarily shaped microtremor arrays. Bulletin of the Seismological Society of America, 92(6), 2323-2332.

Rovida A., Locati M., Camassi R., Lolli B., Gasperini P., Antonucci A.; 2022: Catalogo Parametrico dei Terremoti Italiani (CPTI15), versione 4.0 [Data set]. Istituto Nazionale di Geofisica e Vulcanologia (INGV). https://doi.org/10.13127/cpti/cpti15.4

Vantassel, J. P., Cox, B. R., & Brannon, D. M.; 2021: HVSRweb: an open-source, web-based application for horizontal-to-vertical spectral ratio processing. In *IFCEE 2021* (pp. 42-52).

Wathelet, M.; 2008: An improved neighborhood algorithm: parameter conditions and dynamic scaling. Geophysical Research Letters, 35, L09301, doi: 10.1029/2008GL033256

Corresponding author: perla.taverna@unife.it

Hybrid Geotechnical Digital Twins: A Validation Framework for Seismic Risk (HGDT-SR)

Teresa Tufaro

Istituto Nazionale di Geofisica e Vulcanologia, Sezione Roma 1, Italia

Introduction

The presented research originates from this fundamental question: "Why do we know our buildings better than the ground on which they stand?" This question has guided the entire study: the existence of sophisticated digital twins for built structures contrasts with the lack of reliable quantitative models for the subsurface—an open, heterogeneous system subject to significant uncertainties (Phoon & Kulhawy, 1999), despite its determining role in local seismic response (Kramer, 1996). To address this challenge, a "Soil Digital Twin" was conceived and developed. Its reliability was validated through a rigorous approach based on synthetic data (Oberkampf & Roy, 2010). The development of three virtual models of increasing complexity (A, B, C) enabled the testing and calibration of the entire computational workflow, from data input to shaking prediction. The final objective is a scalable methodology capable of integrating national geoscientific databases (ISPRA, INGV, Microzonation) and transforming seismic planning in Italy, shifting from a sectoral and static logic to a systemic, dynamic one founded on quantitative knowledge of the subsurface.

Philosophy and Strategy for Validation with Synthetic Data

To ensure the reliability and robustness of the proposed methodology, a "synthetic-first" approach was adopted, following best practices for validating complex numerical models (Oberkampf & Roy, 2010). The process was fully tested and calibrated using fictitious hybrid models of increasing complexity, named Model A (simple), Model B (intermediate), and Model C (complex). This enables the validation of each individual computational step and the quantification of how uncertainties in input data or geometric simplifications propagate into final outputs, such as response spectra. The methodology adopted in this research is illustrated in Figure 1.

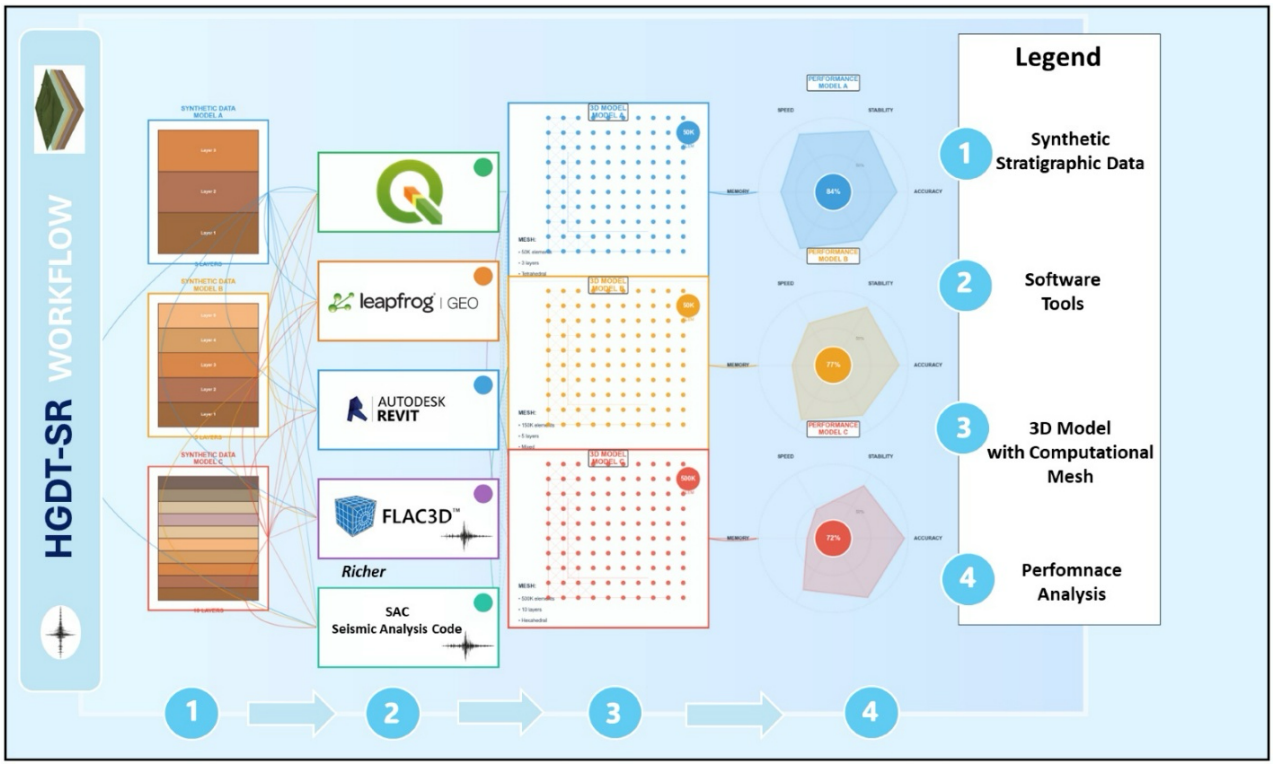

Fig. 1 – Workflow: From data collection to processing for the validation of synthetic hybrid geotechnical digital twins.

Phase 0: Generation of Synthetic Data and Parameterization

The starting point is synthetic datasets. For each of the three models (A, B, C), a series of virtual "boreholes" were generated at defined spatial positions, simulating different densities of in-situ investigation (Phoon & Kulhawy, 1999). For each borehole, parametric tables in CSV format were created containing all the geotechnical and geophysical properties needed for subsequent simulations. These parameters include: geometric properties (thickness and depth of each layer); fundamental dynamic properties (density ρ, shear wave velocity Vs Poisson's ratio ν) essential for seismic site characterization (Kramer, 1996); and strength parameters for non-linear analyses (cohesion c' and friction angle ϕ').

Phase 1: Geological and Geospatial 3D Modeling

The synthetic CSV tables are imported into a GIS environment (QGIS) and georeferenced onto an equally synthetic Digital Terrain Model (DTM). This step simulates the creation of an initial geospatial database. The data are then exported in the .DXF exchange format and converted to .STL (Stereolithography) by CAD software (AutoCAD), thus testing a first critical step of interoperability, a common challenge in building integrated digital workflows (Tao et al., 2018). The STL file is finally imported into 3D geological modeling software (Seequent Leapfrog Geo). Here, starting from the discrete points of the "virtual boreholes," the contact surfaces between layers are interpolated and constructed, giving life to the 3D volumetric solids representing the geological units of each model.

Phase 2: Model Preparation for Finite Elements - The Critical Distinction between Geometric and Computational Mesh

The 3D geological model is transferred to an engineering modeling environment (Autodesk Revit) for a crucial phase that requires a clear conceptual distinction between representative geometric mesh and computational mesh. This distinction is fundamental because a geometrically perfect mesh can be numerically unstable, while an optimized computational mesh may accuracy and stability in dynamic simulations of seismic wave propagation (Itasca, 2023).

Phase 3: Geostatic and Dynamic Numerical Analysis

The final computational mesh is imported into the finite difference code FLAC3D (Itasca, 2023). The simulation proceeds with two sequential steps. First, a geostatic analysis is performed, where the model is subjected only to gravity to reach natural equilibrium and develop a realistic initial stress state. Subsequently, the dynamic analysis is executed: a synthetic seismic input is applied at the base of the model (bedrock). For each of the three models the analysis was repeated using two different constitutive laws for soil behavior: a linear elastic law and an elasto-plastic law (Kramer, 1996; Boulanger & Ziotopoulou, 2017).

Phase 4: Post-Processing and Quantitative Validation

The raw results from FLAC3D (time histories of accelerations and displacements at various points in the model) are exported and processed with the Seismic Analysis Code (SAC) (Goldstein et al., 2003). The main objective is to calculate the Spectral Amplification Ratios (FAS), which quantify, as a function of frequency, how much the seismic motion at the surface is amplified compared to the input at bedrock.

Hybrid Architecture

To address the complexity of the problem, a family of three models was designed and developed, based on a purpose-conceived hybrid architecture. This methodological choice allowed the fusion of the rigor of controlled synthetic data with the realism of physically based simulations, creating a progressive validation system aimed at systematically isolating and quantifying the influence of topography, a critical factor in the analysis of local seismic response. The geometric and geotechnical differences between the models were defined and organized in Tables 1, 2 and 3. The 3D models were then subjected to advanced numerical analysis using the FLAC3D code are illustrated in Figure 2.

Tab. 1 – Geometrical and geotechnical parameters for defining Model A.

Layer	Description	Depth (m)	γ (kN/m³)	Vs (m/s)	c' (kPa)	ϕ' (°)
1	Surface	0 - 20	17.5	180	15	28
2	Alluvial	20 - 35	19.0	350	1	33
3	Bedrock	>35 (down to 50)	22.0	800	-(*)	-(*)

Tab. 2 – Geometrical and geotechnical parameters for defining Model B.

Layer	Description	Depth (m)	γ (kN/m³)	Vs (m/s)	c' (kPa)	ϕ' (°)
1	Anthropogenic Fill	0 - 5	17.0	150	10	28
2	Soft Clays	5 - 15	18.0	200	20	25
3	Medium-Dense Sands	15 - 35	19.0	280	1	32
4	Gravels	35 - 65	20.0	400	1	36
5	Basal Bedrock	>65 (down to 100)	22.5	850	- (*)	-(*)

Tab. 3 – Geometrical and geotechnical parameters for defining Model C.

Layer	Description	Depth (m)	γ (kN/m³)	Vs (m/s)	c' (kPa)	ϕ' (°)
1	Surface Layer	0 - 3	17.0	150	10	28
2	Clayey Silts	3 - 5	17.5	180	15	25
3	Loose Sands	5 - 15	18.0	220	1	30
4	Stiff Clays	15 - 25	18.5	280	25	22
5	Dense Sands	25 - 38	19.0	350	2	33
6	Gravels and Sands	38 - 55	19.5	420	1	35
7	Cemented Gravels	55 - 75	20.0	520	50	38
8	Conglomerates	75 - 90	21.0	620	100	40
9	Weathered Rock	90 - 100	22.0	730	- (*)	- (*)
10	Competent Bedrock	> 100	22.5	850	- (*)	- (*)

Consequently, a table focusing on geometric and numerical modeling parameters (Tab. 4) is presented to describe the three models.

Tab. 4 – Geometric and modeling parameters for Models A, B, C.

PARAMETER	Model A	Model B	Model C
Total Elements	96	192	192
Grid (XYZ)	60×80×20	60×80×40	60 × 80 × 40
Nodes	103,761	201,201	206,451
Dimensions	2,676×3,625× 50 m	2,676×3,625× 100 m	2676.20 m × 3624.99 m × 150 m
Resolution	44.6×45.3×2.5 m	44.6×45.3×2.5 m	44.60 m × 45.31 m × 3.75 m
Mesh Type	Strutturata Brick	Strutturata Brick	Structured Brick (Hexahedral)
Geol. Layers	3	5	10
Elem./Layer Ratio	40:30:30 %	5:10:20:30:35 %	~19,200
Element Density	0.000198 elem/m³	0.000198 elem/m³	0.186 elements/m³
Interfaces	2	4	10
Average Performance	Media	Medio-Alta	RAM: ~2 GB, Time: 5-15 min

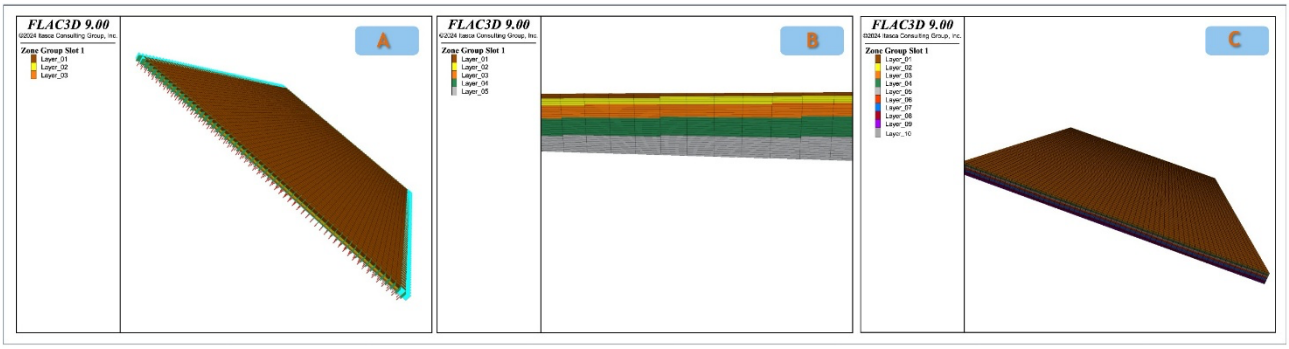

Fig. 2 – Illustration of the 3D numerical models A, B, and C. In a) Model A with a 3-layer geometry, total depth of 50 m. In b) Model B with a 5-layer geometry, total depth of 100 m, showing a detail of the stepped topography that reproduces the discontinuity and non-linearity of the actual ground. In c) Model C with a 10-layer geometry, total depth of 100 m.

Results and Discussion

The comparative dynamic analysis based on a "synthetic-first" approach on three geotechnical models of increasing complexity (A, B, C) has demonstrated that the local seismic response is deterministically governed by the level of detail of the subsoil digital twin. The methodology utilized a standardized seismic input, a Ricker pulse applied to the base of the models, characterized by significant energy content in the 0-30 Hz band. Surface accelerations were extracted from the simulations and analyzed in the frequency domain to calculate the key site-effect evaluation:

$$\mathrm{FAS}(f) = \frac{|\ \mathrm{FFT}[a_{\mathrm{surface}}(t)]\ |}{|\ \mathrm{FFT}[a_{\mathrm{input}}(t)]\ |} \qquad (1)$$

where FFT indicates the Fast Fourier Transform algorithm, a fundamental tool for converting signals from the time domain to the frequency domain and quantifying amplification for each frequency component.

Response in the Linear-Elastic Regime

Tab. 5 – Response in the linear-elastic regime for Models A, B, C.

PARAMETER	Model A	Model B	Model C	Trend A→C
Peak FAS [-]	4.0	4.5	5.0	↗ Increases (+25%)
Peak Period, T0 [s]	0.25	0.50	1.10	↗ Increases (+180%)
Amplification Bandwidth (FAS>2) [s]	<0.5	0.3 - 1.2	0.2 - >1.5	↗ Expands (>+200%)
Number of Principal Modes	Unimodal	Bimodal	Multimodal	↗ Complexity increases
Spectral Coverage	Limited to high freq.	Medium	Complete (0-30 Hz)	↗ Improves

The progression from a simple model (A) to a complex one (C) in the linear regime leads to a systematic increase in maximum amplification, a shift of the peak towards longer periods, and a significant expansion of the period band in which the soil amplifies the seismic motion. Model C, with its detailed 3D geometry, is the only one capable of capturing a multimodal response and complete coverage of the spectrum of interest.

Effects of Plasticity (Mohr-Coulomb Law)

Tab. 6 – Response effects of plasticity (Mohr-Coulomb law) for Models A, B, C.

PARAMETER	Model A	Model B	Model C	Trend A→C
Peak FAS Reduction [%]	-2.5%	-5.6%	-10.0%	↘ Reduction increases (x4)
Permanent Displacement [cm]	+0.5	+1.2	+2.8	↗ Increases drastically (+460%)
Equivalent Damping ξ [%]	~5%	~12%	~18%	↗ Increases (+260%)
Extent of Plastic Zones	Limited	Moderate	Extensive	↗ Increases significantly
Physical Realism (Scale 1-5)	2.5	3.5	4.8	↗ Improves

The introduction of plastic behavior highlights effects proportional to the model's complexity. Model C shows the greatest energy dissipation (FAS reduction -10%) and the widest mobilization of permanent deformations (+2.8 cm). This indicates that detailed geotechnical models not only

provide a richer response in the elastic field but are also more susceptible to realistic non-linear and dissipative effects under strong excitations. The analysis demonstrates that the FAS parameter, calculated through Fourier analysis (FFT), is a sensitive and quantitative tool for discriminating model performance. The results confirm that the geometric and stratigraphic complexity of the digital twin is the main driver for a realistic and complete prediction of the seismic response, both in linear and non-linear fields.

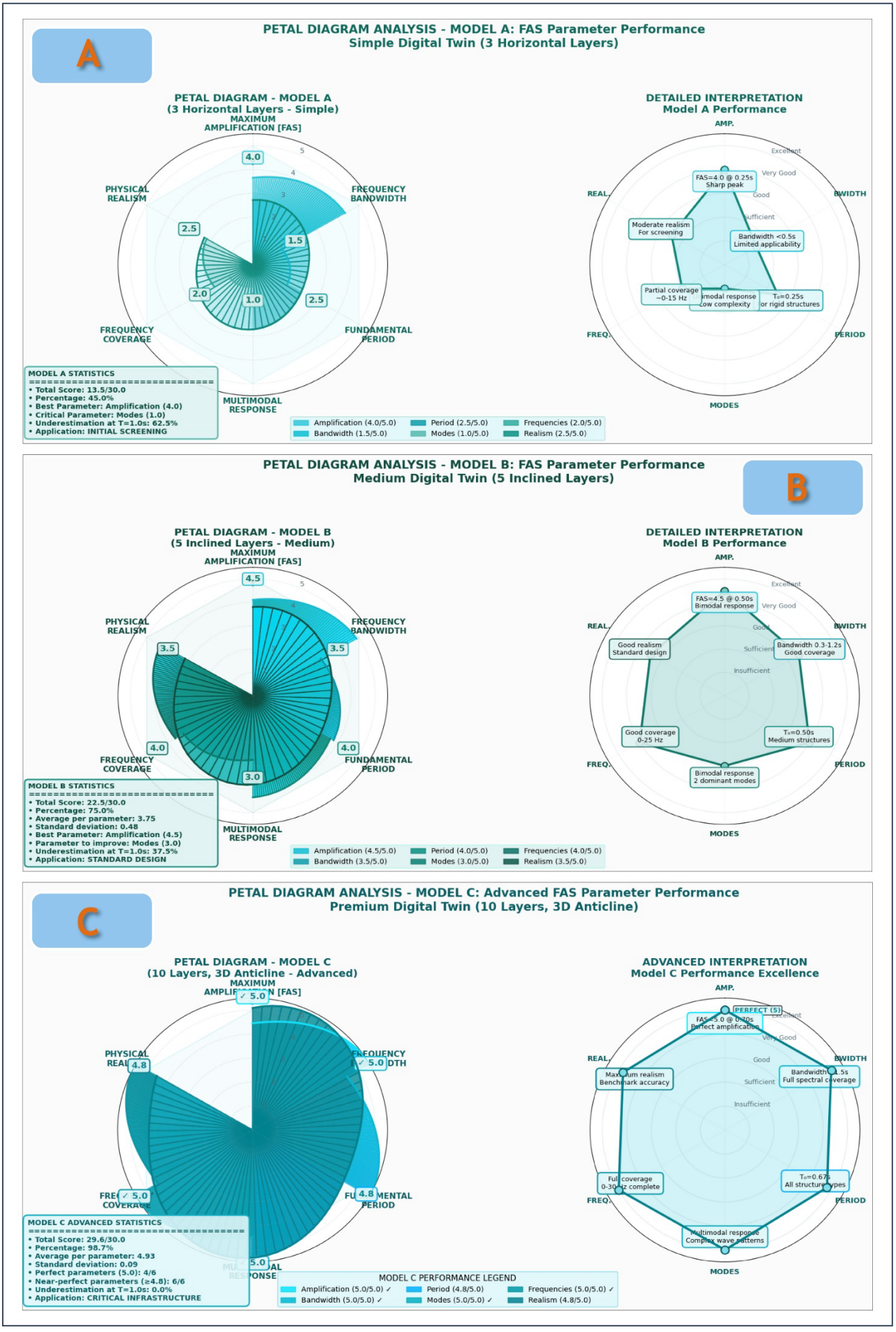
A
PETAL DIAGRAM ANALYSIS - MODEL A: FAS Parameter Performance
Simple Digital Twin (3 Horizontal Layers)
PETAL DIAGRAM - MODEL A
(3 Horizontal Layers - Simple)
MAXIMUM
AMPLIFICATION [FAS]
FREQUENCY
BANDWIDTH
FUNDAMENTAL
PERIOD
MULTIMODAL
RESPONSE
FREQUENCY
COVERAGE
PHYSICAL
REALISM
4.0
1.5
2.5
1.0
2.5
2.0
MODEL A STATISTICS
• Total Score: 13.5/30.0
• Percentage: 45.0%
• Best Parameter: Amplification (4.0)
• Critical Parameter: Modes (1.0)
• Underestimation at T=1.0s: 62.5%
• Application: INITIAL SCREENING
DETAILED INTERPRETATION
Model A Performance
AMP.
BWIDTH
PERIOD
MODES
FREQ.
REAL.
Excellent
Very Good
Good
Sufficient
FAS=4.0 @ 0.25s
Sharp peak
Bandwidth <0.5s
Limited applicability
Tₙ=0.25s
or rigid structures
Multimodal response
Low complexity
Partial coverage
~0-15 Hz
Moderate realism
For screening
Amplification (4.0/5.0)
Period (2.5/5.0)
Frequencies (2.0/5.0)
Bandwidth (1.5/5.0)
Modes (1.0/5.0)
Realism (2.5/5.0)
B
PETAL DIAGRAM ANALYSIS - MODEL B: FAS Parameter Performance
Medium Digital Twin (5 Inclined Layers)
PETAL DIAGRAM - MODEL B
(5 Inclined Layers - Medium)
MAXIMUM
AMPLIFICATION [FAS]
FREQUENCY
BANDWIDTH
FUNDAMENTAL
PERIOD
MULTIMODAL
RESPONSE
FREQUENCY
COVERAGE
PHYSICAL
REALISM
4.5
3.5
3.5
4.0
4.0
3.0
MODEL B STATISTICS
• Total Score: 22.5/30.0
• Percentage: 75.0%
• Average per parameter: 3.75
• Standard deviation: 0.48
• Best Parameter: Amplification (4.5)
• Parameter to improve: Modes (3.0)
• Underestimation at T=1.0s: 37.5%
• Application: STANDARD DESIGN
DETAILED INTERPRETATION
Model B Performance
AMP.
BWIDTH
PERIOD
MODES
FREQ.
REAL.
Excellent
Very Good
Good
Sufficient
Insufficient
FAS=4.5 @ 0.50s
Bimodal response
Bandwidth 0.3-1.2s
Good coverage
Tₙ=0.50s
Medium structures
Bimodal response
2 dominant modes
Good coverage
0-25 Hz
Good realism
Standard design
Amplification (4.5/5.0)
Period (4.0/5.0)
Frequencies (4.0/5.0)
Bandwidth (3.5/5.0)
Modes (3.0/5.0)
Realism (3.5/5.0)
C
PETAL DIAGRAM ANALYSIS - MODEL C: Advanced FAS Parameter Performance
Premium Digital Twin (10 Layers, 3D Anticline)
PETAL DIAGRAM - MODEL C
(10 Layers, 3D Anticline - Advanced)
MAXIMUM
AMPLIFICATION [FAS]
FREQUENCY
BANDWIDTH
FUNDAMENTAL
PERIOD
MULTIMODAL
RESPONSE
FREQUENCY
COVERAGE
PHYSICAL
REALISM
✓ 5.0
4.8
✓ 5.0
4.8
✓ 5.0
5.0
MODEL C ADVANCED STATISTICS
• Total Score: 29.6/30.0
• Percentage: 98.7%
• Average per parameter: 4.93
• Standard deviation: 0.09
• Perfect parameters (5.0): 4/6
• Near-perfect parameters (≥4.8): 6/6
• Underestimation at T=1.0s: 0.0%
• Application: CRITICAL INFRASTRUCTURE
ADVANCED INTERPRETATION
Model C Performance Excellence
AMP.
BWIDTH
PERIOD
MODES
FREQ.
REAL.
PERFECT (5)
Excellent
Very Good
Good
Sufficient
Insufficient
Bandwidth 0.1-5s
Full spectral coverage
Tₙ=0.67s
All structure types
Multimodal response
Complex wave patterns
Full coverage
0-30 Hz complete
Maximum realism
Benchmark accuracy
MODEL C PERFORMANCE LEGEND
Amplification (5.0/5.0) ✓
Period (4.8/5.0)
Frequencies (5.0/5.0) ✓
Bandwidth (5.0/5.0) ✓
Modes (5.0/5.0) ✓
Realism (4.8/5.0)

Fig. 2 – The sequential petal diagram series quantitatively demonstrates the deterministic relationship between stratigraphic complexity and seismic response prediction accuracy in digital soil twins. The models show a clear progression in performance based on the increasing model complexity: Model A (3 Layers - Simple): Score of 13.5/30.0 (45.0%). It exhibits a peak Amplification [FAS] at 4.0/5.0 but has low performance in Bandwidth (1.5/5.0) and Multimodal Response (1.0/5.0). It is suitable only for the initial screening of rigid structures. Model B (5 Layers - Medium): Score of 22.5/30.0 (75.0%). It offers a good and balanced performance, with Amplification [FAS] at 4.5/5.0. It is ideal for Standard Design of medium structures, thanks to good coverage (0-25Hz) and bandwidth. Model C (10 Layers Advanced): Near-perfect score of 29.6/30.0 (98.7%). It achieves a Perfect (5.0/5.0) score for many parameters, including Amplification [FAS]. It demonstrates maximum realism and full spectral coverage. It is designated for the most critical application: Critical Infrastructure. In summary, the three models highlight how increasing stratigraphic complexity leads to an increase in predictive accuracy, transitioning from a simple model for screening to an advanced model essential for critical infrastructure.

Conclusions and Future Developments

This research has validated an innovative framework for Hybrid Geotechnical Digital Twins (HGDT-SR), demonstrating that extending digital twin technology to the subsurface is feasible and crucial for accurate seismic risk assessment. The principal goals of the research:

- A Robust Workflow Pipeline: An integrated eight-phase workflow has been established and tested, ensuring interoperability between specialized software platforms (QGIS → SAC) to transform geological data into validated seismic predictions.
- The Critical Role of Soil Behavior: A comparative analysis between linear-elastic and Mohr-Coulomb constitutive laws demonstrates that only advanced models can capture essential non-linear effects.

The validated HGDT-SR framework enables concrete implementation pathways:

- Towards National Digital Twins for Italy: Creation of three regional reference models for the most critical geological contexts: the deep alluvial plains of the Po Valley, the clay-sand sequences of the Apennines, and the volcanic and coastal terrains of Southern Italy and the Islands.
- Validation with Seismic History: The operational reliability of the models can be further strengthened through calibration with records from major Italian earthquakes (e.g., Friuli 1976, Central Italy 2016, Irpinia 1980).

The current validation intentionally excludes highly complex and evolving geomorphological scenarios, such as actively degrading slopes or dynamic coastal systems. This delineation of scope, however, establishes a clear trajectory for the framework's evolution. Future development will advance HGDT-SR into a collaborative hybrid platform, designed to systematically integrate process-based geomorphological models with a continuous validation cycle. This evolution will ensure the framework's robust application to extreme real-world contexts and enhance its utility for next-generation.

References

https://www.protezionecivile.gov.it/it-attivita/rischio-sismico/microzonazione-sismica

https://www.isprambiente.gov.it/it/attivita/suolo-e-territorio/rischio-sismico

QGIS Development Team 2024: QGIS Geographic Information System (Version 3.34) [Computer software]. QGIS Association. http://www.qgis.org.

AutoCAD (Version 2024) 2024: [Computer software]. Autodesk. https://www.autodesk.com/products/autocad.

Leapfrog Geo (Version 2024:1) [Computer software]. Seequent Ltd. https://www.seequent.com/products-solutions/leapfrog-geo/.

Goldstein P.; Dodge D.; Firpo M.; Lee Minner.; 2003: "SAC2000: Signal processing and analysis tools for seismologists and engineers, invited contribution to "The IASPEI International Handbook of Earthquake and Engineering Seismology", Edited by WHK Lee, H. Kanamori, P.C. Jennings, and C. Kisslinger, Academic Press, London.

Itasca Consulting Group, Inc, 2019: FLAC3D-Fast Lagrangian Analysis of Continua in Three-Dimensions, Ver. 7.0. Minneapolis: Itasca.

Kramer S.L.; 1996: Geotechnical Earthquake Engineering.

Oberkampf W L.; Roy C J.; 2010: Verification and validation in scientific computing. Cambridge University Press.

Phoon K-K. ; Kulhawy F H.; 1999: Characterization of geotechnical variability. Canadian Geotechnical Journal, *36*(4), 612-624. https://doi.org/10.1139/t99-038.

Stewart J P.; Klimis N.; Savvaidis A.; Theodoulidis N.; Zargli E.; Athanasopoulos G.; Pelekis P.; Mylonakis G.; Margaris B.; 2017: Compilation of a local soil classification model and typical profiles for Greece and the broader Hellenic region for the improvement of ShakeMap. National Observatory of Athens; University of Thessaly; Aristotle University of Thessaloniki; University of Patras; Earthquake Planning and Protection Organization (EPPO).

Oberkampf W. L.; Roy C. J.; 2010: Verification and validation in scientific computing. Cambridge University Press.

Boulanger R. W. ; Ziotopoulou K. ; 2017 : Nonlinear deformation analyses of liquefaction effects on earth structures. In R. W. Boulanger & K. Ziotopoulou (Eds.), Soil liquefaction during earthquakes (pp. 1-46). Earthquake Engineering Research Institute.

Tao F.; Cheng J.; Qi Q.; Zhang M.; Zhang H.; Sui F.; 2018: Digital twin-driven product design, manufacturing and service with big data. The International Journal of Advanced Manufacturing Technology, *94*(9–12), 3563–3576. https://doi.org/10.1007/s00170-017-0233-1.

Corresponding author: teresa.tufaro@ingv.it

SYNTPLASM: An Integrated Framework Probabilistic Multi-Hazard Assessment, Operational Planning and Risk Communication in Mountain Infrastructures

Teresa Tufaro[1], Lorenzo Biagini[2], Alessandra Iaiza[3], Michela Romano[4]

[1] *Istituto Nazionale di Geofisica e Vulcanologia, Sezione Roma 1, Italia 1*
[2] *Corpo Nazionale Vigili del Fuoco, Comando VV.F. Livorno, Italia*
[3] *Return Academy - 1st Edition, Università Federico II di Napoli, Italia*
[4] *Università Federico II di Napoli, Dipartimento di Scienze Sociali e statistiche, Italia*

The Systemic Challenge of Multi- Risk in Mountainous Communities

The beating heart of the research we present is SYNTPLASM (SYNthetic Probabilistic Assessment of Mountain Systems) a "hybrid" methodology between theoretical research and practical action, conceived for a radical transformation in the management of multi-hazard risk in Italian mountain areas. It is not a static solution, but a dynamic and continuously evolving compass, designed to navigate the growing complexity of interdependent risks and their ever-different manifestations. The necessity for this paradigm shift emerges with dramatic evidence from the mountain context in which we live and work. Our mountains embody the very definition of systemic and multi-hazard risk. They are a fragile ecosystem in which earthquakes, landslides, wildfires, and extreme climatic events coexist, trigger and amplify each other, creating cascading and synergistic threats that render traditional sectoral approaches obsolete (ISPRA, 2023) (Figure 1). The crisis is structural, and the data confirms it: 94% of mountain municipalities are exposed to hydrogeological risk, over 10.600 km of our road network is vulnerable to landslides, approximately 3.800 bridges require urgent intervention (ANAS, 2022), while the climate crisis exacerbates vulnerabilities and isolates communities (IPCC, 2022). SYNTPLASM, however, is born from our deepest awareness: behind every risk there is a community, and behind every statistic, a human story. When a bridge collapses, it is not just infrastructure that fails: the path of children to school is severed, an entire town remains isolated, the social and economic fabric of a valley unravels. Recognizing the indirect and far-reaching consequences that a single event can have, this project was conceived with the ambitious goal of building an operational bridge between the most advanced science and human action on the territory. To give a tangible signal of this change, we start with a fundamental objective: to translate complex predictive models into clear and immediately usable decision-making tools, functional both for long-term strategic planning and for critical choices during emergencies.

Fig. 1 – Infrastructural Disruption: Case Studies of the Domino Effect.

Philosophy, Genesis and Development

We chose the acronym SYNTPLASM because it encapsulates our operational philosophy, our vision of risk, and our ambition for the Italian mountains. SYNTPLASM embodies a dual foundational principle:

- SYNT (Synthetic) represents our principle of integrated knowledge: the commitment to synthesize diverse data, disciplines, and perspectives, from seismic engineering to sociology, from climatology to economics, to build a unified diagnosis of the territory. It is the methodological response to the question: "What is really happening within the system?"
- PLASM (Plastic Modeling) is instead our principle of adaptive action: the vision of the territory as a malleable organism, whose reactions to crises we can simulate, whose vulnerabilities we can test, and, above all, for which we can actively design resilience pathways. It is the transformative response to the question: "How can we shape a safer future?"

This dual vision was born from a direct experience in Terranova of Pollino (October 2022) where the disruption of a road left an entire community isolated. From there emerged the driving question: how do we move from detecting isolation to systematically preventing it? SYNTPLASM aims to be our response framework, designed to shift the paradigm from emergency management to the proactive prevention of community. SYNTPLASM has developed through two complementary phases that define its hybrid nature: quantitative scientific formalization and qualitative multidisciplinary integration. Thie firsts initial phase involved translating empirical observations into a rigorous technical-probabilistic core, using advanced models to operationally quantify resilience

outlined in Tufaro et al. (2023) and validated by Vona et al. (2024). The second phase broadened the framework's perspective through a multidisciplinary dialogue involving 40 experts during the first Return Academy. This iterative exchange reshaped SYNTPLASM from a technical tool into a holistic framework. This two-phase development process is what forges SYNTPLASM's hybrid identity, enabling it to bridge the gap between precise scientific analysis and the complex reality of communities at risk. SYNTPLASM has taken shape and been tested in three permanent territorial laboratories: Terranova of Pollino, Tobbiana of Montale, and Tolmezzo. This first testing phase demonstrates that SYNTPLASM already represents an effective operational model, capable of translating a precise philosophy into concrete actions.

Computational and Operational Architecture of SYNTPLASM

The computational architecture integrates three methodological pillars, seven operational phases, and a modular technical implementation flow in Python into a circular path that moves from theory to action. The computational pillars on which SYNTPLASM is based are illustrated in Table 1.

Tab. 1 – The Three Computational Pillars.

PILLAR	DESCRIPTION
(SYNT Core)	This is our integration principle. We transform disparate data into a unified digital representation of the territory as a dynamic graph-network.
(PLASM Engine)	This is our principle for exploring the future. The heart of the system is a Monte Carlo simulator that we run for tens of thousands of iterations, propagating uncertainty through specific statistical distributions.
(CORE Interface)	This is our principle for action synthesis, translating complex results into immediately usable decision-support tools while integrating the socio-perceptual dimension.

The sequential operational phases are: (Phase 1) System Characterization: Multidisciplinary data collection and harmonization. (Phase 2) Network Modeling: Formal representation of the territory as a functional graph-network. (Phase 3) Multi-Risk Interaction Analysis: Quantitative assessment of hazard correlations and cascading effects. (Phase 4) Probabilistic Scenario Generation: Execution of Monte Carlo simulations to create a library of future scenarios. (Phase 5) Resilience Quantification: Calculation of system robustness metrics, such as Weibull survival curves for infrastructure. (Phase 6) Socio-Perceptual Integration. (Phase 7) Operational Response Modeling (CORE): Final synthesis into actionable plans, decision tools, and deployable protocols (Figure 2).

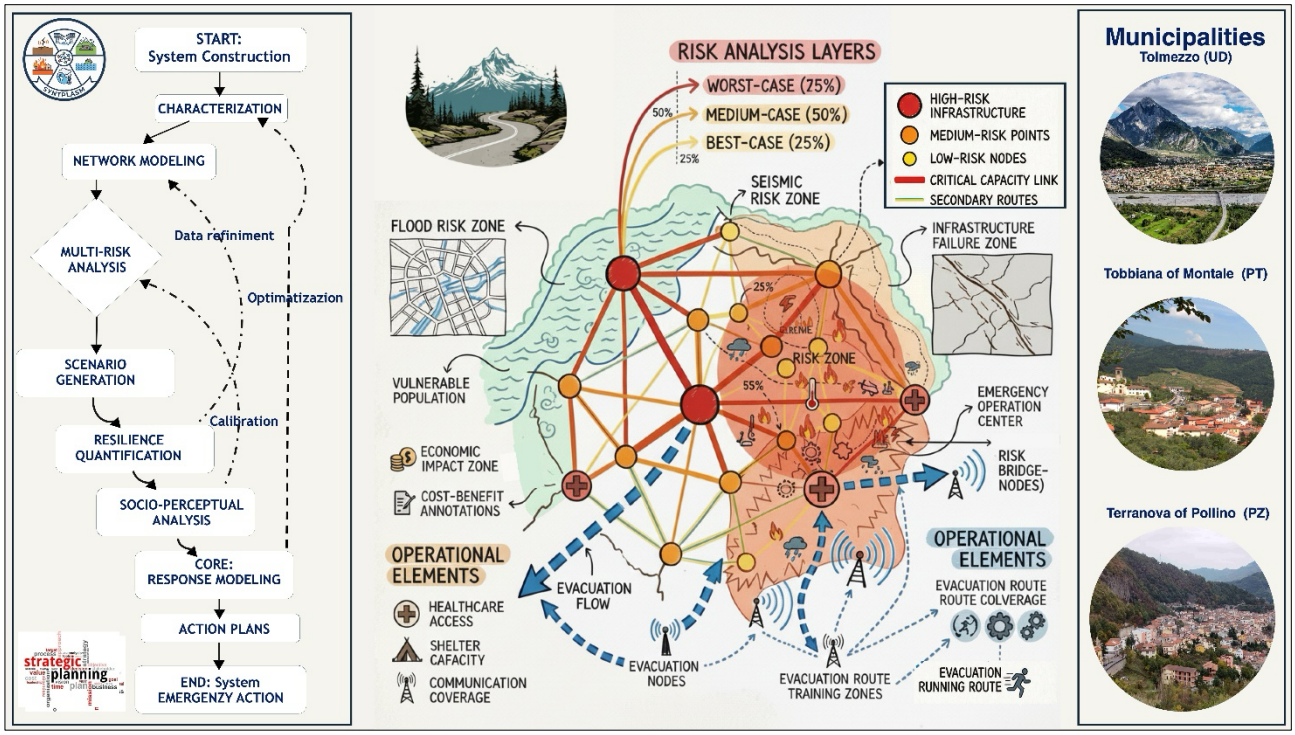

Fig. 2 – SYNTPLASM Framework: Operational Workflow.

The implementation is divided into four main modules of Python scripts (Table 2).

Tab. 2 – Technical Implementation: The Python Modules.

PYTHON MODULES	DESCRIPTION
Block 1: System Diagnosis (Phases 1-4)	Environment configuration, model construction, and Monte Carlo simulations.
Block 2: Strategy & Planning (Phases 5-6)	Resilience quantification and strategic plan development.
Block 3: Operational Action (Phase 7, Part 1)	Generation of control room dashboards and real-time support tools.
Block 4: Specialist Response (Phase 7, Part 2)	Dedicated module for intervention priorities and evacuation plans.

The strength of our approach lies in its end-to-end methodological coherence. The uncertainty captured in Phase 4 by the Monte Carlo simulator is propagated and tracked through all subsequent blocks in Python. This ensures that each of our final operational recommendations is accompanied by a quantified statistical confidence level (e.g., a 95% confidence interval). The result is a dynamic decision-making ecosystem: a set of over 50 integrated visualizations in high-resolution outputs. In this way, our computational architecture fully enacts the theoretical framework, positioning itself as a robust bridge between the science of complexity and human decision-making, and offering a holistic support system in Python for the entire risk management cycle in mountain areas.

Results and Discussions

In this session, we present a synthesis of the hybrid and probabilistic results obtained from the application of the SYNTPLASM framework to the three mountainous case study areas. The integrated analyses reveal a robust comparative picture that highlights shared vulnerabilities and local specificities, which must necessarily inform differentiated and robust emergency plans. The main results for each municipality are summarized in Table 3.

Tab. 3 – Comparative summary of the main results for the three case study contexts (Mean values and 95% confidence interval).

CRITICAL PARAMETER	Tobbiana of Montale (PT)	Tolmezzo (UD)	Terranova of Pollino (PZ)
Population (Census 2023)	852	9,691	967
Risk of Main Bridge Collapse	95.0% ± 0.5% (Ponte Agna)	96.0% ± 0.8% (Ponte Tagliamento)	98.0% ± 0.5% (Ponte Sinni)
Isolated Population (Worst Scenario)	74.5% ± 16.9%	82.3% ± 12.5%	68.4% ± 18.2%
Ageing Index (2023)	235.1	210.5	248.3
Effectiveness of Primary Communication Channel	SMS (92% ± 4%)	Radio Carnia (95% ± 3%)	SMS (95% ± 3%)
Trust in Institutions Index	0.62 ± 0.08	0.71 ± 0.06	0.58 ± 0.09
4x4 Vehicle Requirement (Worst Scenario)	10 ± 2	18 ± 3	15 ± 2

From the integrated analysis of data in Table 5.1 and of visual outputs, such as those presented in Figure 3, developed for the municipality of Terranova of Pollino, several fundamental considerations emerge:

- The Multiplicative Factor of Mountain Complexity: The case of Tolmezzo (UD) is paradigmatic. Although its population is only ten times larger than that of Tobbiana of Montale (PT), the requirement for 4x4 vehicles in the worst-case scenario is almost double (+80%). This gap, quantified for the first time so clearly, is the synergistic result of three elements: the physical isolation of hamlets (raising the percentage of isolable population to 82.3%), severe seasonal climate, and the vulnerability of the primary road network (88.5% risk of inoperability).
- Social Vulnerability as a Risk Amplifier: The comparison between Terranova of Pollino (PZ) and Tolmezzo shows how social parameters can overturn expectations based solely on physical data. Despite the estimated risk of population isolation being lower in Terranova (68.4% vs. 82.3%), the combination of the highest aging index in Italy (248.3) with the lowest trust in institutions index (0.58) configures an operational scenario of extreme criticality.

- The Need for Hyper-Local Communication Strategies: The results disprove the hypothesis of a "universal emergency communication channel". Channel effectiveness is strongly dependent on the local socio-cultural fabric. In Tolmezzo, Radio Carnia (95% effectiveness) confirms itself as a critical social infrastructure. Conversely, in Apennine and hilly municipalities, digital systems like SMS achieve maximum penetration.

From the comparison of the three investigated geographical realities emerge some immediate and medium-term operational recommendations. It is crucial to clarify that these are not definitive prescriptions, but represent a prototype of a hybrid decision-making method. We expect that, in operational reality, results may vary significantly based on local conditions and the actors involved. Their value lies in demonstrating a new pathway to justify investment priorities, including:

- Priority Structural Mitigation Interventions: Urgently initiate procedures for the seismic and hydraulic reinforcement of bridges identified at maximum risk (Ponte Sinni in Terranova of Pollino (PZ), Ponte Tagliamento in Tolmezzo (UD), Ponte Agna in Tobbiana of Montale (PT)).
- Differentiated Logistical Planning for Mountain Areas: Provincial and regional administrations must adopt scalable resource deployment models that account for the "mountain multiplicative factor".
- Communication and Community Engagement Plans: Each municipal civil protection plan must incorporate an evidence-based "communication chapter", which includes mapping effective channels, information and training campaigns (ROI >250%), and proximity contacts in isolated hamlets.

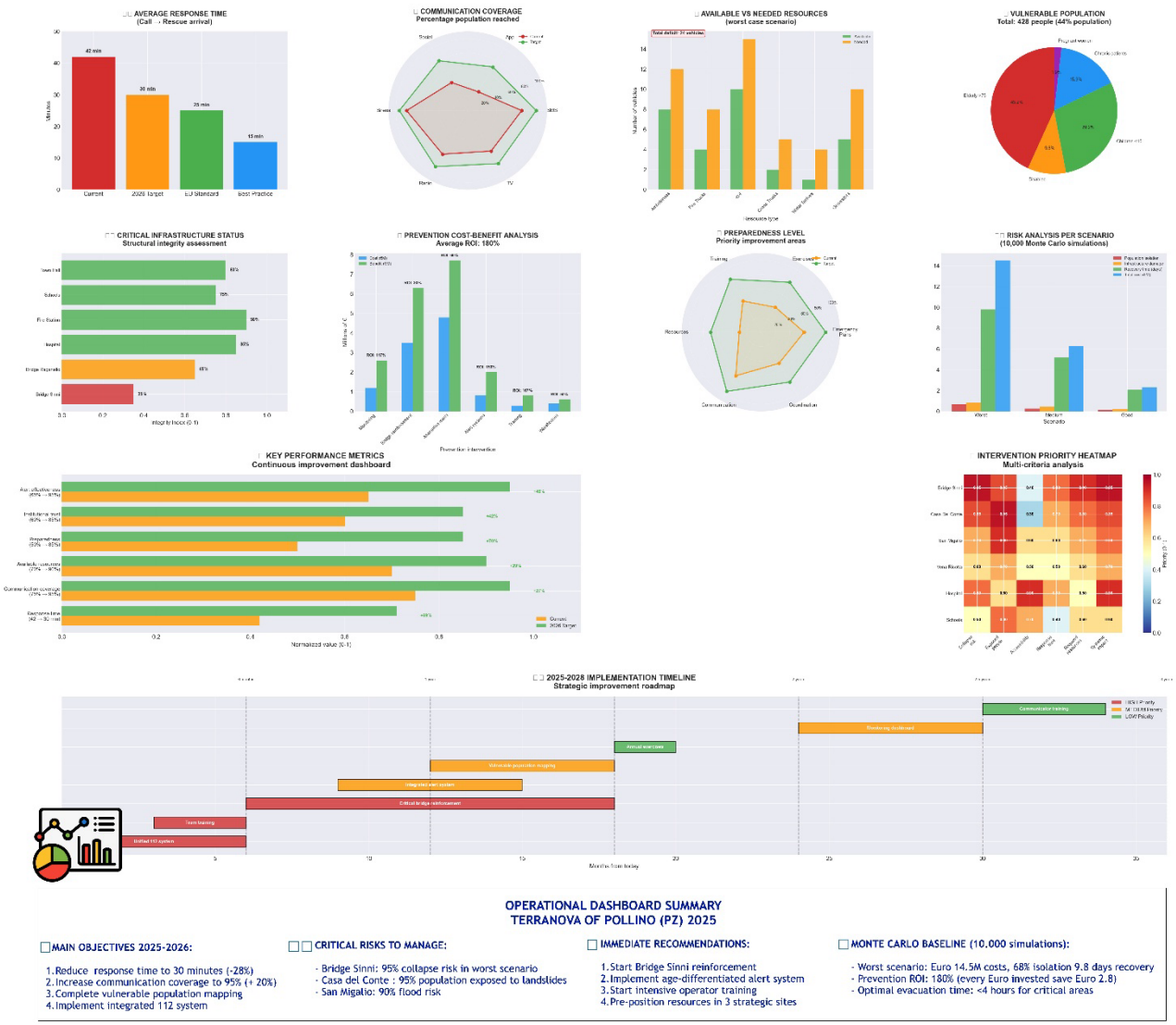

Fig. 3 – Hybrid Operational Dashboard Prototype Terranova Of Pollino (PZ) 2025. A prototypical strategic dashboard that concretely represents what emerges from the integration of real data, advanced simulations, and human evaluation. It visualizes: a) Critical operational metrics (response times; communication coverage; resource deficit); b) Priority heatmap (red/yellow/green matrix) for intervention areas, alongside the status of critical infrastructure and mapping of vulnerable populations; c) Scenario simulations (Worst/Medium/Good) derived from 10000 Monte Carlo runs, with quantified impacts on isolation, damage, recovery days, and costs, d) Operational timeline 2025-2028 and highlighted immediate recommendations.

Conclusions and Future Developments

SYNTPLASM represents our continuously evolving methodological starting point, designed for multi-hazard risk management in mountain regions. Its central innovation: translating the complexity of multi-hazard risk into quantitative answers to critical command center questions, with the objective of ensuring output of emergency protocols that are immediately applicable on the territory. The results converge in demonstrating that the greatest criticality lies in the dangerous synergy between physical vulnerability, geographic isolation, and socio-demographic fragility. However, the full realization of the framework encounters intrinsic limitations: dependence on often lacking quality data, the inevitable simplification of multi-risk simulations, and computational barriers for small

municipalities. Our true strength lies precisely in recognizing these boundaries, configuring ourselves as a hybrid system by definition. The computational architecture, necessarily requires the integration of expert judgment and local qualitative knowledge. It is precisely this awareness that defines our future development path, which aims to:

- More accessible and modular computational tools, to break down technical barriers in multi-hazard risk management.
- Integration of real-time data from sensors and platforms, to increase responsiveness in multi-hazard analysis.
- Development of tools on risk perception, to bridge the gap between calculated risk and lived risk in multi-risk contexts.

SYNTPLASM provides a concrete methodological response to the challenge of multi-hazard risk management and to the value of not leaving behind the most vulnerable communities. Protecting human life requires operational strategies calibrated on the specific combination of risks and resources of each territory.

Acknowledgments

This work benefited from the expert and multidisciplinary contribution of all professionals at the Return Academy. Special thanks are extended to Dr. Lorenzo Biagini, Firefighter, for his decisive contribution as an expert in Emergency Governance. SYNTPLASM framework is the tangible result of a collective knowledge that unites academic theory with hands-on operational experience.

References

ANAS 2022: This reference was cited in your text but was not found in the search results you provided. You would need to locate and provide the full bibliographic details for this source.

IPCC 2022: Climate Change 2022: Impacts, Adaptation and Vulnerability. Contribution of Working Group II to the Sixth Assessment Report of the Intergovernmental Panel on Climate Change. Cambridge University Press.

ISPRA 2023: Hydrogeological Instability in Italy: Hazard and Risk Indicators. Italian Institute for Environmental Protection and Research.

Tufaro, T.; 2023: Valutazione del Rischio Sismico di un Modello di Rete Stradale per la Regione Friuli Venezia Giulia (NE) PhD Thesis https://arts.units.it/handle/11368/3059812.

Vona, M.; Anelli A.; Tufaro, T.; Harabaglia, P.; Mori, F.; Manganelli, B.; 2024: Seismic resilience-based strategies for prioritization of interventions on a subregional area. Bulletin of Earthquake Engineering. https://doi.org/10.1007/s10518-024-02072-y.

Corresponding author: teresa.tufaro@ingv.it

Regional High-Quality Ambient Noise Models for Italy

F. Varchetta[1], M. Massa[1], R. Puglia[1] , P. Danecek[1], D. Galluzzo[2]

[1] INGV, sezione di Milano, Italia
[2] INGV, OV, Osservatorio Vesuviano, Napoli,Italia

Characterizing seismic background noise is fundamental for evaluating station performance, optimizing network design, and estimating detection capabilities. While the New High- and Low-Noise Models (NHNM/NLNM) by Peterson (1993), derived from a sparse set of stations, serve as global benchmarks, these often fail to capture the variability of modern, dense national networks. In Italy, specific regional factors—including complex topography, geology, and intense anthropogenic activity—limit the applicability of global references.

In this work, we present the New Italian Seismic Noise Model (NISNM), developed to accurately characterize ambient noise across the Italian territory. Following the approach of McNamara and Buland (2004), we analyzed Probability Density Functions (PDF) of Power Spectral Density (PSD) computed from continuous recordings of the Italian National Seismic Network (RSN), operated by INGV. The dataset comprises approximately 340 broadband stations, covering the period from January 1, 2024, to February 28, 2025.

A key methodological aspect of this study is the implementation of a rigorous data selection procedure to ensure that the derived models represent true background noise. We systematically exclude time windows contaminated by station malfunctions (identified via the ISMDq database; Massa et al., 2022) and transient seismic events, applying conservative empirical exclusion thresholds based on earthquake magnitude and hypocentral distance. The NISNM boundaries are defined by the 5th and 95th percentiles of the stacked PDFs. Compared to previous Italian noise models (e.g., D'Alessandro et al., 2021), the NISNM exhibits narrower percentile ranges, proving the efficacy of the earthquake-exclusion criteria.

To account for Italy's geological diversity, we further derived region-specific noise models. These sub-models highlight significant spectral differences, specifically for the Po Plain tectonic basin and for volcanic districts (Campi Flegrei, Etna, and Stromboli).

Finally, the reliability of the NISNM was validated using an independent dataset of 60 broadband stations not included in the model construction. We applied a binomial statistical test to verify whether the median PSDs of these independent stations fell within the NISNM confidence bounds. The Harmonic Mean p-value (HMP) method by Wilson (2019) confirmed the null hypothesis with high statistical significance and demonstrated that the NISNM provides a robust and representative characterization of seismic noise in Italy.

References

D'Alessandro, A., Greco, L., Scudero, S., Lauciani, V.; 2021: Spectral characterization and spatiotemporal variability of the background seismic noise in Italy. Earth and Space Science Vol. 8, n. 4, e2020EA001579, https://doi.org/10.1029/2020EA001579

Massa, M., Scafidi, D., Mascandola, C., Lorenzetti, A.; 2022: Introducing ISMDq—A Web Portal for Real-Time Quality Monitoring of Italian Strong-Motion Data. Seismological Research Letters Vol. 93, n. 1, pp. 241–256, https://doi.org/10.1785/0220210178

McNamara, D. E., Buland, R. P.; 2004: Ambient noise levels in the continental United States. Bulletin of the Seismological Society of America Vol. 94, n. 4, pp. 1517–1527.

Wilson, D. J.; 2019: The harmonic mean p-value for combining dependent tests. Proceedings of the National Academy of Sciences Vol. 116, n. 4, pp. 1195-1200, https://doi.org/10.1073/pnas.1814092116

Peterson, J. R.; 1993: Observations and modeling of seismic background noise, *U.S. Geol. Surv. Tech. Rept.* 93-322.

Corresponding author: fabio.varchetta@ingv.it

Exposure and vulnerability characterization for reliable seismic risk assessment: the case study of Bologna

G. Yazici[1], F. Ferretti[1], G. Salamida[1], N. Buratti[1], L. Pozza[1]

[1] Department of Civil, Chemical, Environmental and Materials Engineering, University of Bologna, Bologna, Italy

Relevant seismic risk characterizes the Italian territory, given the high seismic hazard and densely populated regions. In the framework of territorial seismic risk assessment, assessing the vulnerability of existing buildings and defining the exposed assets are crucial and multiple data sources should be consulted for proper characterization of these risk elements. In this work, the city of Bologna was selected to perform seismic risk assessments and examine the impacts of seismic events in Bologna by analyzing the vulnerability and exposure through physical, social, and economic parameters.

In Italy, ISTAT (National Institute of Statistics) provides a wide range of datasets that are commonly used for seismic risk studies for the entire Italian territory. These datasets are available at the census tract scale as aggregated data about the characteristics of the buildings – such as construction material, age, number of floors, and occupancy – and the characteristics of the population – such as age, gender, education level, unemployment, rented dwellings, housing density, single parent families – which allow the exposure and vulnerability characterization at the territorial level.

The main aim of this study is to evaluate the impacts of different seismic events, in terms of building damages and human losses, within the Saragozza district of the city of Bologna. To achieve this goal, firstly, data collection was performed and the reliability of the ISTAT data was controlled by performing on-site visits in the Saragozza district. Later, masonry and reinforced concrete building typologies in the zone were defined to be able to select appropriate fragility models (Salamida et. al. 2023 & Salamida et. al. 2023 & Monteferrante et al. 2025). To evaluate the impacts of seismic events, social vulnerability and occupancy rate factor were also taken into account within different seismic scenarios (Salamida et al. 2023).

Methodology

Historical analysis of the evolution of the city of Bologna was performed by analysing old maps and cartography, and different satellite images from different periods. Later, detailed analyses were

carried out in the Saragozza district to understand the construction period of the investigated zone. After historical analysis, the data about characteristics of existing buildings – such as address, construction material, age, number of floors, etc. - were collected through on-site surveys. Data collection was carried out according to RETURN (Multi-risk science for resilient communities under a changing climate) building taxonomy which is designed for multi-hazard assessments. When the data comparison is performed between the survey dataset and the ISTAT dataset, a small discrepancy was detected (Fig.1). The reason for the difference was mainly related to the way of collecting the data: ISTAT collects the data by civic number, but during the survey, the data was collected on a building scale.

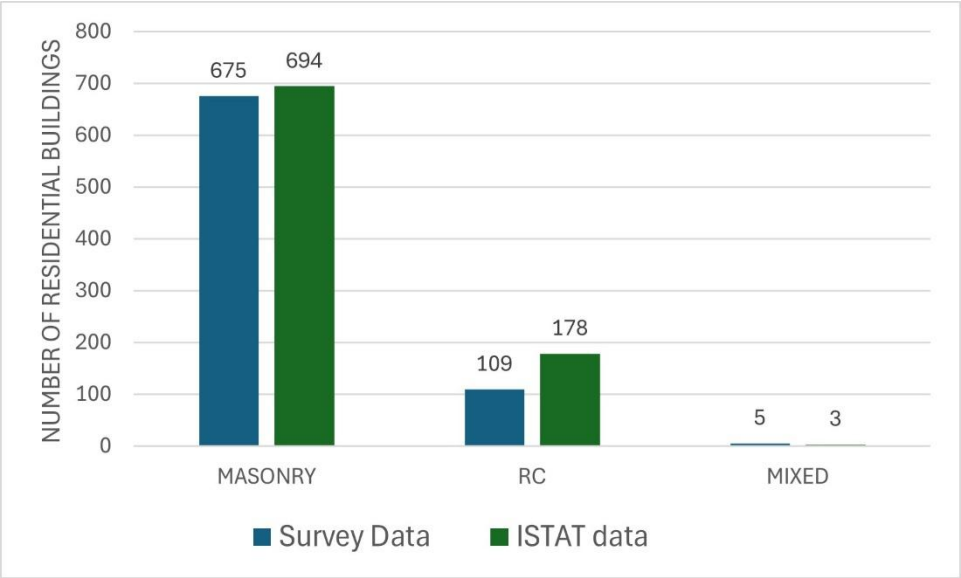

Fig. 1 – Comparison between on-site survey and ISTAT data in terms of construction material

Due to the extensive data gathered during the on-site investigations, the structural typologies were identified (Fig. 2) based on building characteristics such as construction material, construction age, number of floors, and surface of the buildings. The majority of the structures within the zone were masonry that are mid-rise buildings constructed before 1945. As for the reinforced concrete buildings, the most common typology was medium-rise buildings, with large surface areas and built after 1945. The building typologies were utilized to select proper fragility models, which describe the probability of structural damage to a certain degree at a level when subject to a ground motion intensity measure (Salamida et. al. 2023 & Monteferrante et al. 2025). The use of the fragility model helps to classify the possible damage grades of the buildings from D0 to D5. The damage levels help to estimate the number of lost human lives and the number of injuries (Salamida et. al. 2023).

To assess the social vulnerability (Fig. 3*a*), the deprivation index was calculated by using the 2011 ISTAT data at the census tract scale. The deprivation index expresses the level of relative social disadvantage through the combination of various characteristics of the resident population. For the calculation of the index, five indicators were selected that describe the concept of social deprivation: low education, unemployment, rented dwellings, housing density, and single-parent families. The index was calculated as the sum of the standardized indicators and then categorized into five different vulnerability classes (i.e., low to very high social vulnerability).

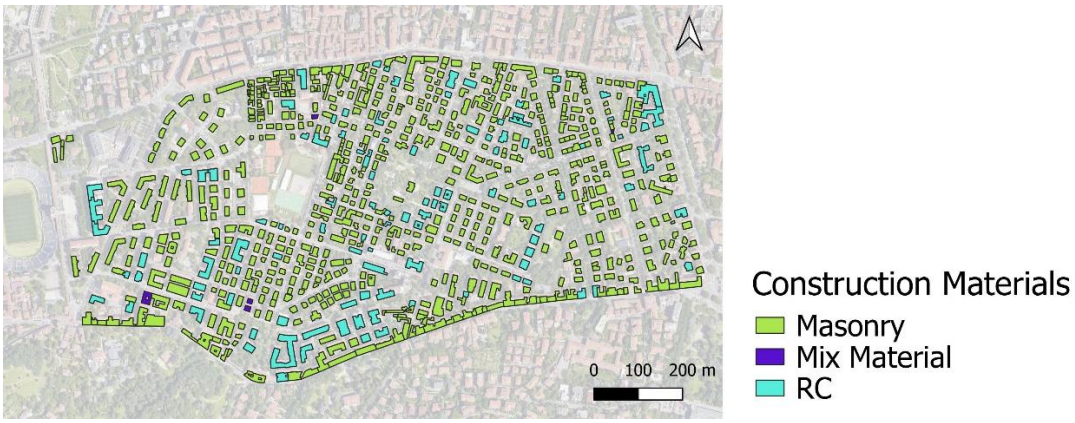

Fig. 2 – Building typologies in the Saragozza district

The occupancy rate is related to the number of people inside the building in specific time of the day, which obviously have a relevant impact on the human losses, mainly depending on the time when the event occurs (Manfredi et al. 2023). To analyze the occupancy rate, different seismic events and various timing scenarios are proposed. The evaluation of the number of deaths and injuries (Fig. 3*b,c*) is also based on the expected number of buildings affected by different damage levels. According to this, the expected numbers of deaths and injuries were calculated by combining the distribution of occupants in buildings that reached damage levels D4 and D5, since casualty rates are associated with these damage levels.

Fig. 3 – Evaluation of vulnerability and impacts: a) Social Vulnerability based on the deprivation index, b) Human losses-number of deaths, c) Human losses-number of injured people

References

Salamida G.; Buratti N.; 2023: Fragility models for RC frames with masonry infills and analysis of the efficiency of different IMs. Procedia Structural Integrity.

Salamida G.; Buratti N.; Mazzotti C.; 2023: Ground Motion Analysis Toolbox and Seismic Scenarios Toolbox: software tools for seismic damage scenarios assessment in the Emilia-Romagna Region. Procedia Structural Integrity.

Monteferrante et al.; 2025: Observational Seismic Fragility Models for Unreinforced Masonry Buildings Based on Building-by-Building Damage Data From the 2012 Emilia Earthquakes. Earthquake Engineering & Structural Dynamics

Manfredi et al.; 2023: Estimation of Human Casualties Due to Earthquakes: Overview and Application of Literature Models with Emphasis on Occupancy Rate. Safety

Corresponding author: gunseli.yazici2@unibo.it